Prediction of Fire Test Performance Based on Varying FRP Resin/Fire Retardant Additive Ratios

A Major Qualifying Project Report
submitted to the Faculty of
WORCESTER POLYTECHNIC INSTITUTE
in partial fulfillment of the requirements for the
Degree of Bachelor of Science
By:

_____
Jerome Anaya

_____
Rocio Cristina Herrera

_____
Daniel Morgan

May 2014
Project number: FQ13

_____
Professor Nicholas A. Dembsey, Advisor

Table of Contents

List of Tables

List of Figures

Authorship

Jerome Anaya

- Introduction

Cristina Herrera

- Flammability Parameter
- ASTM E84 Screening Tool
- Comparison of Kreysler Composites with Commercial FRPs

Daniel Morgan

- Cone Testing
- NFPA 285 Screening Tool
- Conclusion

Authorship for Appendices is listed under the title for each Appendix

Organization of the Report

This MQP report consists of a 20 page conference paper in which fire test performance of FRP's with varying amounts of fire retardant ratios where compared using a flammability parameter. The flammability parameter is then followed by two screening tools that can be used to predict a materials fire performance within an ASTM E84 and NFPA 285 fire tests. This is then followed by multiple briefs included within the appendices where more in depth information regarding the flammability parameter and screening tools can be found. All results and data collected from the cone and various calculations can also be found in the appendices.

Abstract

The use of Fiber Reinforced Polymers (FRPs) for architectural applications in the construction industry is subjected to several requirements of the International Building Code: ASTM E84 and NFPA 285. These large scale tests can be costly and failure can be detrimental for the development of new FRP systems. These FRP systems use differing ratios of resin and fire retardant additives. How these differing ratios affect performance in ASTM E84 and NFPA 285 is investigated by further developing a set of screening tools based on flame extension and flame spread models to predict fire performance. These tools use data from the bench scale Cone Calorimeter to measure material fire characteristics. These characteristics are then used as input for the screening tools to estimate ASTM E84 and NFPA 285 performance. The predicted changes in performance based on changes in resin to fire retardant additive ratios is reported for each FRP tested.

Acknowledgements

The team would like to acknowledge Professor Nicholas Dembsey for his continuous guidance throughout the completion of this project and for his unconditional support.

The team would also like to acknowledge Kreysler & Associates for providing test specimens for all cone calorimeter tests.

Last but not least, the team would also like to thank Randy Harris, the fire lab manager, for instructing the group in the proper use of the cone and performance of ASTM E1354 Standard.

Prediction of Fire Test Performance Based on Varying FRP Resin/Fire Retardant Additive Ratios

Introduction

The use of fiber reinforced polymers (FRPs) in nowadays construction industry has increased due to the material's corrosive resistant properties, low manufacturing costs, and ease of molding for architectural applications. As an interior finish or exterior wall assembly, it is subjected to several requirements of the International Building Code (IBC) [1]. The IBC is often referenced in the United States to establish safety requirements for new constructions. Chapter 8 of the IBC requires interior wall and ceiling finishes to be classified by standardized test: ASTM E84[2] commonly referred at the Steiner Tunnel Test. It classifies the materials by flame spread and smoke production. This classification will determine where the material can be used inside the building. The IBC also requires all materials that contain combustible components (i.e. FRPs) to pass NFPA 285[3], the Multi-Story Building test. These tests are both time consuming and costly for the company. If the desired result is not attained, the material developer must make changes and submit the material for retesting. The additional testing imposes a potentially significant economic penalty for material development.

Currently, there are a number of correlations and models developed to assess performance in full-scale tests based on economical bench-scale standardized tests such as the Cone Calorimeter (ASTM E 1354)[4]. However these models are limited because they were developed to for specific types of products. To help address this problem, this project further develops a set of bench scale screening tool to predict the thermal behavior of several Fiber Reinforced Polymers (FRP) samples varying in composition ratios of aluminum trihydrate (ATH) and Sand. Specifically, this project further develops models to determine modifying the additive ratios in the composite will affect the performance in the full-scale assembly test based on the Cone Calorimeter results.

A flame length screening tool is used to determine the class rank from the Tunnel Test. The screening tool uses the equations developed by *Acosta et al*[5] to determine the flame spread. For the smoke developed index, the tool adapts Janssens' model[6] to find the transmission percentage to relate cone results to the Tunnel Test. A flame height equation for wall fires is

derived based on research done on small pool fires. This model is able to use input parameters derived from cone calorimeter to calculate the length of flame spread in the NFPA 285 test. This Exterior Screening Test will provide data to determine whether or not a material will pass or fail NFPA 285. The success of both models would allow material developers to run multiple bench-scale tests to refine their materials before spending time, money, and resources on a both large-scale test.

Materials Description:

Fiber Reinforced Polymers (FRP) are composite materials based on thermoplastic and thermoset resins in a heterogeneous mixture of two or more compounds bonded together with fillers, additives and fibers that enhance the mechanical, electrical and thermal properties as shown in Appendix MS. Given the multifunctional properties of FRPs with lightweight and high strength, FRPs are extremely attractive for architectural applications. This project analyzes the fire characteristics of two fire retardant composites described in

Table ***1***: Hetron 650 T20 developed by *Ashland Performance Materials* which is an unsaturated polyester resin that contains different percentages by weight (wt%) of Aluminum Trihydrate (ATH) in different mixtures with varying glass content. ATH is a crystalline, water-insoluble powder obtained chiefly from bauxite, an aluminum ore.

The second FRP is Fireblock gel-coat manufactured by *Composites Creating Progress*, which has a polymer concrete coating based on Fireblock resin and a sand aggregate over a FRP substrate; the Fireblock resin and sand ratios are varied as shown in Table 2**.** Concrete polymers have some special features that are described in Appendix CP.

Table 1: Composition of Hetron Systems

Composite	ATH Ratio (wt%)	Glass %	Assigned Name
Hetron 650 T20	100:00	41.86	HR-0
Hetron 650 T20	100:33	51.11	HR-33
Hetron 650 T20	100:66	60.37	HR-66
Hetron 650 T20	100:100	67.32	HR-100
Hetron 650 T20	100:130	71.65	HR-130

Table 2: Composition of Fireblock Systems

Composite	Sand Ratio %	Glass %	Assigned Name
CCP Fireblock Gelcoat	100:00	30.95	FB-0
CCP Fireblock Gelcoat	70:30	36.5	FB-30
CCP Fireblock Gelcoat	60:40	36.5	FB-40
CCP Fireblock Gelcoat	50:50	36.5	FB-50
CCP Fireblock Gelcoat	40:60	36.5	FB-60

Cone Testing

To get all the information that was needed from each of the FRP sample, a cone calorimeter was used to test each sample. The Cone Calorimeter is a device that is used to study the fire behavior of small samples around a maximum size of 100 mm by 100 mm. The cone calorimeter works by inducing an incident heat flux onto the samples surface and recording a variety of information on the various analyzers on the machine during the burning of the sample.
In order for the cone calorimeter to determine the heat release rate, it uses the principle of oxygen consumption calorimetry.

The principle of oxygen consumption calorimetry is the backbone of the cone calorimeter. Oxygen consumption calorimetry is the determination of the heat release rate of a material based on the amount of oxygen that is being burned during the test. By measuring the depletion of oxygen in the exhaust gases, this information can be used along with a general assumption of the amount of heat that is released during the burning of oxygen to determine the heat release rate from a specific material. Full information about the cone calorimeter and how it works can be found in Appendix Cone.

To allow for the best representation of our data within the ASTM E84 and the NFPA 285 tests, the samples would have to be run at a range of heat fluxes. An initial heat flux of 50 kW/m^2 was used in order to develop a baseline data set for the materials. Additional tests were conducted at incident heat flux of 75 kW/m^2 along with additional tests being run at incident heat fluxes of 25 and 40 kW/m^2. Typical results from the cone testing for heat release rate and specific extinction area are shown below in Figure 1. All other cone testing results can be seen in Appendix Graphs.

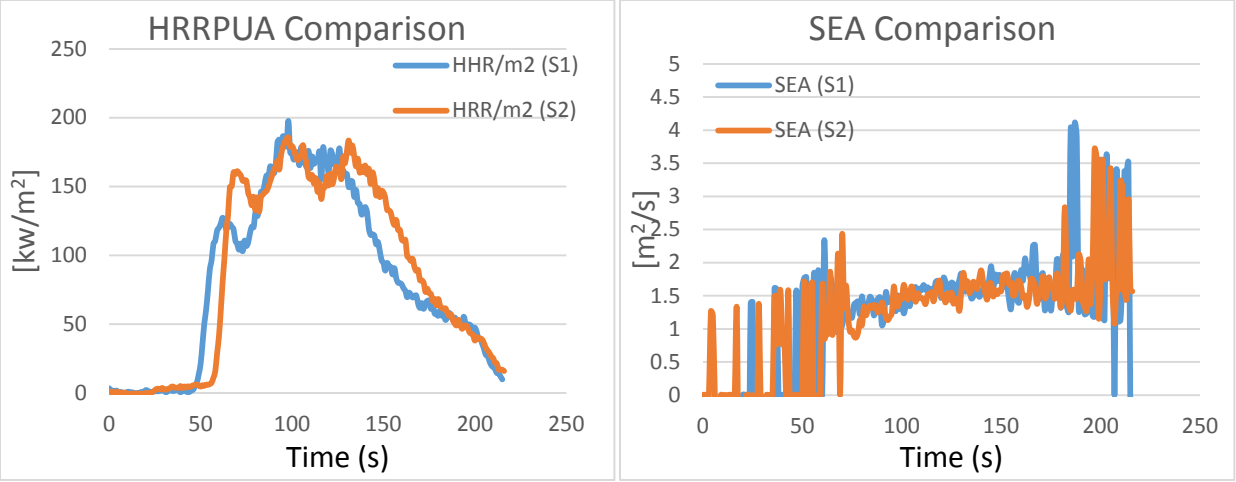

Figure 1: HRRPUA and SEA for hetron 100:0 at IHF of 40 kW/m^2

Flammability Parameter

In order to compare the basic fire characteristic of each Kreysler system when the addictive ratio changes, one of the most relevant indicators is the potential for propagating flame spread. The flammability parameter indicates how easily the material will burn or ignite based on key constraints that control the flame spread. This analysis uses the theoretical considerations of Mowrer and Williamson[7] that evaluates the flammability parameter from small-scale heat release measurements. Mowrer and Williamson used a model based on the upward flame spread theory developed by Cleary and Ouintiere[8] which describes the concurrent flame spread model where the flame spreads in the same direction as the flow; this is the behavior seen in the ASTM E84 test and the NFPA 285 test. The schematic of the model is shown in Figure 2.

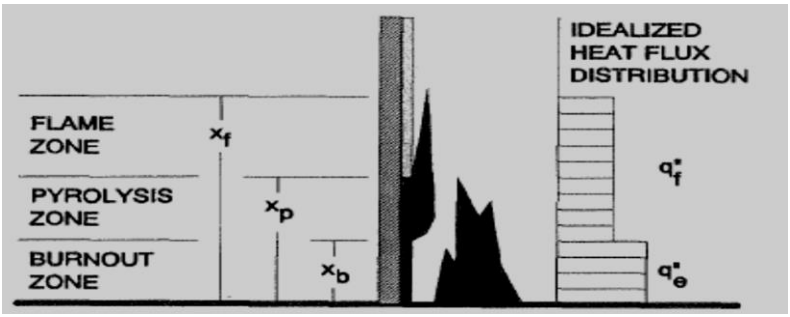

Figure 2: Schematic of flame spread mode1[7]

According to Mowrer and Williamson and based on Cleary and Quintiere model, the net rate flame propagation equals the difference between the pyrolysis front velocity and the burnout front velocity, defined by the following equation:

(1) $$V_p = \frac{dx_p}{dt} = \frac{x_f(t) - x_p(t)}{t_f}$$

As result, after various integrations before and after burnout commences, the potential for acceleratory spread depends on three major parameters:

- Heat release rate per unit area $\dot{Q}''$
- Flame spread time t_f
- Burning duration t_{bo}

According to this model, acceleratory spread is predicted when:

(2) $$k_f \dot{Q}'' - \frac{t_f}{t_{bo}} > 1$$

For simplicity, the above inequality can be represented and rearranged as:

(3) $$Flammability\ parameter = k_f \dot{Q}'' - \frac{t_f}{t_{bo}} - 1$$

Where t_f is the time the material takes to heat to the point where ignition is possible. It is measured directly in the cone as the time when the test sample ignites under the imposed heat flux. The complete derivation of the model can be found in Appendix FP.

Flammability parameter calculations

Since the flammability parameter is in terms of the heat release rate per unit area from the Cone testing, a simple use of equation (3) can yield the flammability behavior of each system. The first set of tests was run at an incident heat flux of 50 kW/m^2 and three to four tests were performed for each Hetron and each Fireblock system. This study used three different approaches for the inputs in equation (3) using different interpretations for the Heat Released Rate and the burnout time, as shown in Appendix AVG. Each method was used to compute the flammability parameter for each test run to obtain systematic results. From these calculations, an average was computed for each system and the uncertainty of the calculations was computed using the pooled variance theory[9] to account for the possible error of each measurement, as shown in Appendix AVG.

Negative values for the flammability parameter show decelerating spread, while positive values show an accelerating flame spread behavior. Table 33 shows the results for the ten systems evaluated with an uncertainty level of ±0.403. A first screening suggests all Hetron samples are

not expected to have an acceleratory flame spread behavior while two Fireblock samples registered positive values which might suggest an acceleratory flame spread behavior. However, those positive values are really small, closer to zero than to 1 which in principle means Fireblock Systems are not expected to have an accelerator behavior either.

Table 3: Average Flammability Parameter values

Composite	Average Flammability Parameter
Hetron 100:00	-0.442 ± 0.403
Hetron 100:33	-0.561 ± 0.403
Hetron 100:66	-0.577 ± 0.403
Hetron 100:100	-0.667 ± 0.403
Hetron 100:130	-1.478 ± 0.403
Fireblock 100:00	0.441 ± 0.403
Fireblock 70:30	0.123 ± 0.403
Fireblock 60:40	-0.146 ± 0.403
Fireblock 50:50	-0.332 ± 0.403
Fireblock 40:60	-0.345 ± 0.403

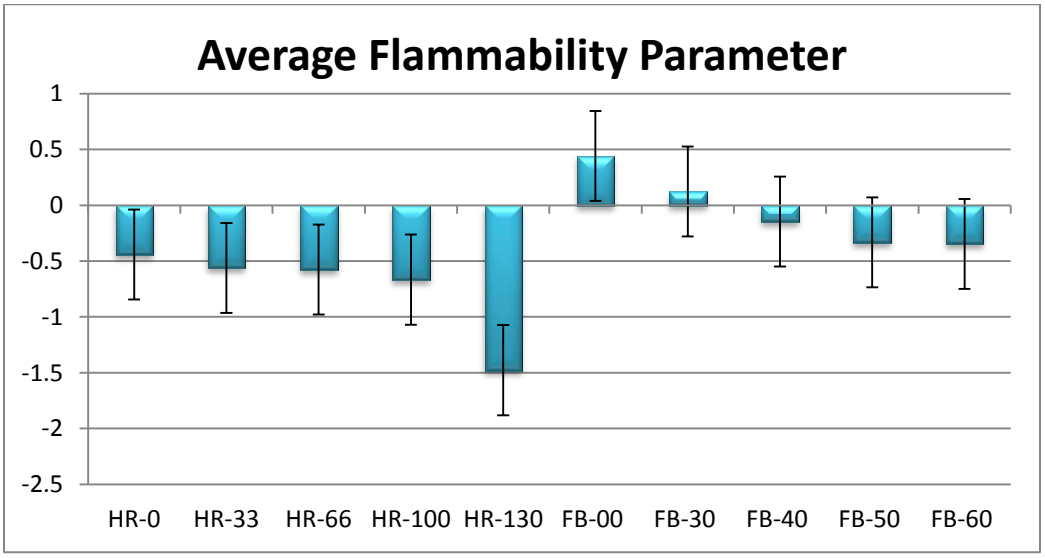

Figure 3: Average flammability parameter per composite

From Figure 3, looking at the data for Hetron Systems and taking into account the uncertainty level which is represented by the error bars, the flammability parameter for Hetron samples tends to be the same at approximately -1 for an ATH ratio from 0 to 100. When the ATH ratio increases to 130, there is a significant drop in the parameter to approximately twice

the value. On the other hand, Fireblock Systems do not show any visible trend in terms of what happens when the ratio of the sand additive decreases. At Fireblock 50:50 it seems that the flammability parameter reaches a steady value of -0.7.

Flammability parameter under different incident heat fluxes:

The same procedure used in the previous section was used to compute the flammability parameter for selected Hetron and Fireblock systems under 25, 40 and 75 kW/m^2. The results obtained for each system are summarized in Table 4.

Table 4: Flammability parameter for different incident heat fluxes

Composite	25 kW/m2	40 kW/m2	50 kW/m2	75 kW/m2
Hetron 100:00	-1.346	-0.397	-0.442	0.235
Hetron 100:100	-3.015	-2.594	-0.666	-1.171
Hetron 100:130	-4.800	-3.273	-1.477	-1.021
Fireblock 100:00	-2.131	-0.008	0.440	0.465
Fireblock 60:40	-1.748	-0.027	-0.146	0.645
Fireblock 40:60	-1.996	-0.172	-0.346	0.587

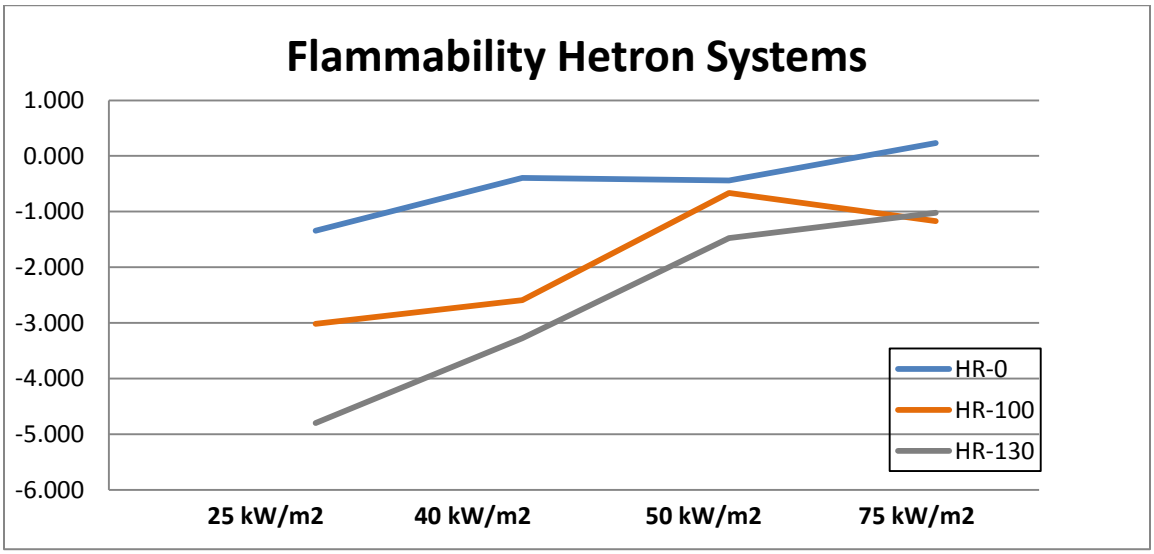

Figure 4: Flammability parameter for different incident heat fluxes

Figure 4, shows a direct relationship between the flame spread behavior and an increasing incident heat flux, which is expected that a higher incident heat flux the material tends to exhibit an acceleratory behavior. Similarly, this graph confirms the initial suggestion that after a ratio of

100:130 ATH there is a significant non-acceleratory flame spread behavior under all incident heat fluxes applied.

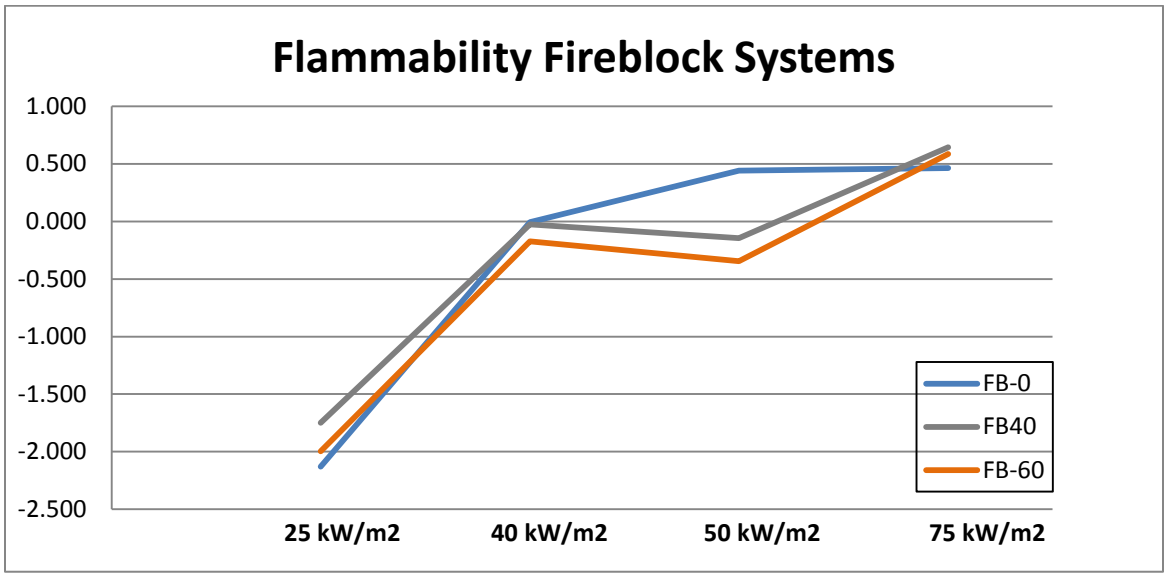

Figure 5: Flammability Parameter for Fireblock Systems

Figure 5, shows the flame spread behavior of Fireblock Systems which show a direct relationship between the incident heat flux and the flame spread behavior which increases with a higher IHF. Other than this, there is not a difference between the amount of sand in the composite and its flame spread behavior. For all three systems, the values for the flammability parameter yields values extremely close at all IHF. These results confirm the initial suggestion that the variation of sand does not seem to have a significant influence in the fire performance of the composite.

ASTM E84 Screening Tool

ASTM E84 is an assembly test that provides flame spread and smoke production data form wall and ceiling lining materials. Commonly referred to as the "Tunnel Test," ASTM E84 determines the flame spread and the smoke production of the material tested. ASTM E84 test requires the test chamber to be approximately 25 feet long and a chamber that is approximately 17 inches wide and 12.5 inches in-depth. This test is only used for screening or ranking purposes that classifies materials into:

- Class A: flame spread index from 0 to 25 and smoke developed index less than 450

- Class B: flame spread index from 26 to 75 and smoke developed index less than 450
- Class C: flame spread index from 76 to 200 and smoke developed index less than 450

Flame length screening tool

The flame spread index is an integration over time of the flame extension produced by the material, which was found using the model developed by Acosta et al. The basic assumption for this model states that the heat release rate per unit area of the specimen and the burners in the tunnel act as a line fire point source that also accounts for a point source that moves as the specimen burns in the tunnel.

Based on this model, the authors developed two set of equations for flame length screening tool, one that uses multiple incident heat fluxes and one that uses a single incident heat flux. For more information please refer to Appendix FLST.

The flame length screening tool used in this analysis is based on the single incident heat flux model from Acosta et al, which yields two main equations for an incident heat flux of 40 kW/m^2. The two equations are:

$$Concrete\ Polymer\ L_f = \left(0.2322 * \left(\frac{0.6\dot{Q}'' + 88}{0.43}\right)^{0.6494}\right) - 4.5 \quad (4)$$

$$Noncoated\ Hetron\ L_f = \left(0.1574 * \left(\frac{0.6\dot{Q}'' + 88}{0.43}\right)^{0.6494}\right) - 4.5 \quad (5)$$

Where $\dot{Q}''$ is heat release rate per unit area from the cone data, for which it is necessary to multiply it by 0.6 which would represent the pyrolysis area at the tunnel. The constant 88 (kW) accounts for the heat release by the burners and implies a flame extension of zero before ignition. The uncertainty of this model was reported to be ±30 by Acosta et al. The following graph, Figure 6, shows the typical curve obtained for flame extension of Fireblock samples.

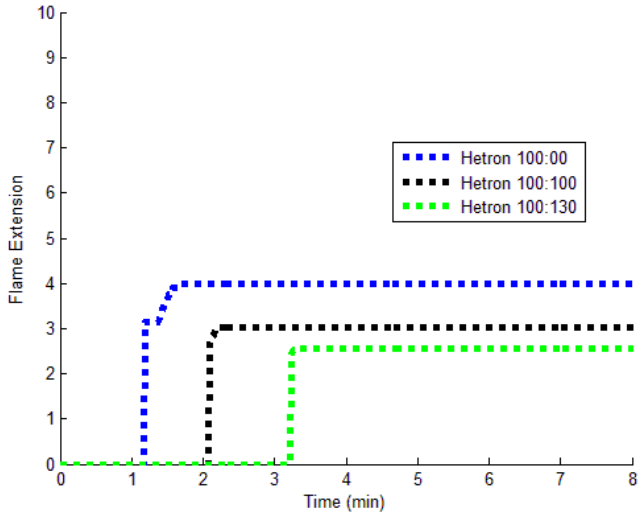

Figure 6: Flame Extension Hetron Samples for an IHF of 40 kW/m2

Data interpretation:

In order to use equations (11) and (12), an aggregate heat release rate per unit area was obtained by averaging the heat release rate for each second of the test of each when there was more than one trial per composite. The procedure followed to find the flame length and the curves obtained for each composite is shown in Appendix FLST. The flame spread index was computed for an incident heat flux of 50 kW/m^2 for all of the Kreysler composites, and for the optimal incident heat flux of 40 kW/m^2 for a selected number of systems. The results obtained are summarized in Table 5.

Table 5: Flame Spread Index predicted values

Composite	FSI (50 kW/m2)	FSI (40 kW/m2)	Classification
Hetron 100:00	23	18	A
Hetron 100:33	18	---------	A
Hetron 100:66	14	12	A
Hetron 100:100	13	---------	A
Hetron 100:130	16	9	A
Fireblock 100:00	41	41	B
Fireblock 70:30	46	---------	B
Fireblock 60:40	43	39	B
Fireblock 50:50	39	---------	B
Fireblock 40:60	46	46	B

As Table 5 shows, all Hetron Systems have a flame spread index less than 25, which means that based on this model the composites will be classified as Class A indicating that they will not spread the fire beyond the vicinity of the origin. On the other hand, for Fireblock Systems the model predicts that they would be classified as Class B which is associated with a flame spread at a relatively low rate. Some small variance between the values estimated for an IHF of 50 and for a 40 IHF is noticeable, but it can be justified by the fact that the model used was developed for an IHF of 40 kW/m^2 which simulates better the thermal environment in the tunnel test. Nevertheless, the values obtained are in right range.

Smoke developed Index

From the ASTM E84 standard, the smoke developed index is a ratio of the area under the curve of the light transmission versus time of the sample being tested and a standard reference of red oak light transmission, defined by the following equation:

$$SDI = \frac{\left(\int_0^{10\ min}(100 - T\%)dt\right)_{Test\ specimen}}{\left(\int_0^{10\ min}(100 - T\%)\right)_{Red\ Oak}} \times 100 \quad (6)$$

In order to be able to use the heat release rate per unit area obtained from the cone in a model that predict the smoke developed index in the tunnel test some correlations needed to be done, shown in Appendix SDI. These correlations used the light transmission model presented by Janssens and adapted to predict the heat release rate in the tunnel described by the following equation:

$$\dot{Q}_{tunnel} = \left(0.6 * \dot{Q}''_{cone}\right) + 88 \quad (7)$$

The heat release rate per unit area from the cone needs to be multiplied by 0.6 which is the exposed pyrolysis area in the tunnel. Finally, it needs to account for the heat generated by the burners in the tunnel so 88 kW are added.

Then, by using and adapting Janssens model the light transmission in the tunnel is defined by:

$$T\%_{(t)} = \frac{100}{\exp\left(\frac{22.268 * k}{(0.645 * Q_{cone}) + 125.6}\right)} \quad (8)$$

The transmission percentage curve obtained from Fireblock systems under an incident heat flux of 40 kW/m2 is displayed in Figure 7.

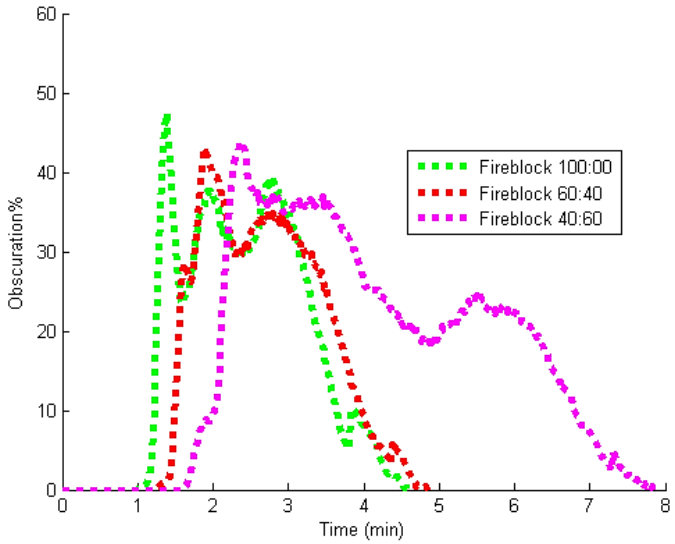

Figure 7: Light Transmission percent of Fireblock samples under an IHF of 40 kW/m^2

Data interpretation:

Similar to the procedure followed for the flame spread index, in order to find the aggregate heat release rate per unit are, all the data points each second of the test. In this case, an aggregate of the specific extension coefficient (k) was also found following the same approach, which is described in Appendix SDI. The smoke developed index was compute for an incident heat flux of 50 kW/m^2 for all Kreysler composites, and for an optimum incident heat flux of 40 kW/m^2 for a number of selected systems.

Table 6: Smoke Developed Index for 50 kW/m^2 and 40 kW/m^2

Composite	SDI (50 kW/m2)	SDI (40 kW/m2)	Class
Hetron 100:00	153	234	A
Hetron 100:33	201	-------	A
Hetron 100:66	217	105	A
Hetron 100:100	130	-------	A
Hetron 100:130	48	40	A
Fireblock 100:00	96	145	B
Fireblock 70:30	122	-------	B
Fireblock 60:40	98	140	B
Fireblock 50:50	213	-------	B
Fireblock 40:60	226	242	B

As Table 6 shows, all the values obtained from the smoke developed index for Hetron Systems and Fireblock Systems are under the maximum possible value of 450. Based on this screening tool, all Kreysler composites will pass the ASTM E84 standard with values for smoke transmission under the maximum limit. The results obtained are also subject of some level of uncertainty which was found to be ±17 by using the theory of propagation of uncertainty because the transmission percentage is dependent of other two equations as described in Appendix UNC. It is also possible to visualize a decrease in the smoke generated by Hetron samples as the ATH and glass content increases (Fiber Reinforced Polymers (FRP) are composite materials based on thermoplastic and thermoset resins in a heterogeneous mixture of two or more compounds bonded together with fillers, additives and fibers that enhance the mechanical, electrical and thermal properties as shown in Appendix MS. Given the multifunctional properties of FRPs with lightweight and high strength, FRPs are extremely attractive for architectural applications. This project analyzes the fire characteristics of two fire retardant composites described in

Table ***1***: Hetron 650 T20 developed by *Ashland Performance Materials* which is an unsaturated polyester resin that contains different percentages by weight (wt%) of Aluminum Trihydrate (ATH) in different mixtures with varying glass content. ATH is a crystalline, water-insoluble powder obtained chiefly from bauxite, an aluminum ore.

The second FRP is Fireblock gel-coat manufactured by *Composites Creating Progress*, which has a polymer concrete coating based on Fireblock resin and a sand aggregate over a FRP substrate; the Fireblock resin and sand ratios are varied as shown in Table 2. Concrete polymers have some special features that are described in Appendix CP.

*Table **1***). On the other hand, there is an increment in the smoke developed in Fireblock samples as the sand ratio increases; referring back to the composition of Fireblock, the glass content remains the same as the sand ratio increases. This suggests a further analysis of the influence of glass content in the fire characteristics of Fireblock samples.

Limitations of the screening tool

The major limitation of this screening tool relies on the fact that the tunnel test is designed to last 10 minutes. The flame spread index and smoke developed index are time dependent integrals with limits from time equals zero minutes to time equals 10 minutes.

Nevertheless, most of the tests performed did not last up to ten minutes, and in case they did, the useful data was taken only until edge burning. Therefore, the time integrals were computed using the data available and not until 10 minutes as the standard defines. Similarly, for light transmission calculations, some values for the specific extinction coefficient were recorded as negative values; these negative values were ignored and taken as zero. A negative value for the extinction coefficient means that the beam intensity with smoke is greater than the beam intensity without smoke, and since the beam intensity without smoke is assumed to be an intensity of 100%, a negative value means that the beam intensity with smoke is somehow greater than 100%, which is physically inconsistent. An extinction coefficient of zero will represent an obscuration percentage of zero assuming that there is no smoke produced. As a result, the values obtained might not be a perfect representation of the performance of these composites in the tunnel test, but they serve as a solid prediction of the possible values that Hetron and Fireblock Systems will tend to produce.

Comparison of Kreysler Composites with Commercial FRPs

Hetron 650-T20 was presented in winter 2012 as a new strategy for Fiber Reinforced materials presented by Ashland Inc. It was introduced as a high strength fire retardant resin with less volatile pricing. It belongs to the Hetron family that share many characteristics with the Modar family of fire retardant resins. From the technical datasheet[10], Modar 814A is described as an acrylic polymer resin with low viscosity which is able to achieve a flame spread index <25 and smoke generation <100. Similar to Hetron family, it also contains ATH as the fire retardant agent in a ratio of 150 and 20% glass content. Since Hetron is a halogenated polyester resin it can be rendered fire retardant through the use of additives or by grafting fire retardant materials onto the backbone of the resin.

The main reasons why modified resins are entering the market is because costs and regulations of some materials are increasing. In order to achieve the same performance level, options are typically higher in cost because without them, the performance is less effective. In cases where premium corrosion resistance and lower prices are desired, costumers are encourage to use Hetron 650 T20. The fire characteristics of Hetron samples in this analysis registered sound values compared to what commercial FRPs reported in terms of flame spread index (FSI) and smoke developed index (SDI). Modar 814 has a bigger ATH ratio than the Hetron tested in

this project, as predicted, with a ration of ATH of 130 or larger the FSI is less than 25 and the SDI is less than 100.

For Fireblock Systems, the screening tool to predict the performance in the ASTM E84 Test suggests that these composites will be ranked as Class B material with a smoke developed index between 100 and 250. Some commercially available gel-coat composites reported to have flame spread index of less than 25 and smoke developed index less than 300[11]. Comparing these values with what was obtained in this analysis, it seems that this screening tool yields similar values to what is expected from gel-coat composites. Even though, this screening tool ranked Fireblock Systems as Class B with flame spread indexes between 41 and 46 which are not significantly far from an index of 25. At this point, it is important to highlight that the glass content percentage in commercially available gel-coat composites is between 20% and 26% whereas the glass content for the Fireblock tested in this project is 36.5%. This fact suggests the future study about the glass content in this type of composites since it might be the reason why modeling predicted different values for the fire characteristics of Fireblock versus what is reported in the market.

NFPA 285 Screening Tool

Modern building codes have included requirements for fire testing of all combustible materials for decades. In recent years, similar fire testing has become a requirement for Fiber Reinforced Polymers. The use of FRP's in exterior wall systems means that it is subjected to the requirements of the Energy Conservation Code (IECC).The International Building code (IBC) requires exterior wall assembly testing in accordance with National Fire Protection Association (NFPA) 285 – Standard Fire Test Method for Evaluation of Fire Propagation Characteristics of exterior Non-Load-Bearing Wall Assemblies Containing Combustible components. NFPA 285 typically tests all combustible used in exterior wall of Types I through IV. Construction type definitions and typical wall systems are defined in the IECC and IBC regarding requirements for continuous insulation and large-scale fire testing.

To compare the results that are being obtained from the cone calorimeter to the NFPA 285 standard, this analysis looks specifically at the flame height that the specific sample might experience. Based on the NFPA 285 standard, the vertical flame height should not exceed a

height of about 3.05 meters or 10 feet. Using the flame height form proposed by Mowrer and Williamson and flame height models correlated from pool fire research, a series of flame height equations were determined that could be used to determine the dynamic flame height to compare with the NFPA 285 standard.

In order to be able to compare the results obtained from the cone calorimeter, a flame height equation for wall fires is needed to relate to the NFPA 285 standard. The problem that was determined while researching wall fires was that there was very limited research into flame heights of small fires (specifically under 100 kW/m^2). However, a large amount of research has been done on pool fires when the heat release rate per unit area is small. Research and correlations were done for small pool fires and the system of equations that roughly represents pool fires is shown below in equations (9) and (10). The full pool fire model can be seen in Appendix POOL.

(9) $\frac{Zf}{D} = 40 * {\dot{Q}_D^*}^2 ; for\ \dot{Q}_D^* < 0.1\ (Small\ Fire)$

(10) $\frac{Zf}{D} = 3.3 * \dot{Q}_D^{*\frac{2}{3}} ; for\ \dot{Q}_D^*\ between\ 0.1\ and\ 1 (Intermediate\ Fire)$

The system of equations for pool fires was used to help further develop a similar system of equations that could represent that of changing wall fires sizes. By assuming that wall fires would experience a similar flame height drop off to that of the pool fire, a system of flame height equations could be developed. To be able to assume a similar drop off in wall fires, any wall fire data that was researched had to show some signs of a drop off at the end of their data set when the heat release rate per unit area is small. By using the data sets from Delichatsios[12] and King-Mon Tu[13], a system of equations were developed for wall fires to represent small fires and large fires. The flame height equations are shown below in equations (11) and (12). The full wall fire model can be seen in Appendix WALL.

(11) $\frac{X_f}{X_p} = 6 * \left(\dot{Q}'^*_{xp}\right)^{\frac{2}{3}} ; For\ \dot{Q}'^*_{xp} > 0.1\ (Intermediate\ Flames)$

(12) $\frac{X_f}{X_p} = 130 * \left(\dot{Q}'^*_{xp}\right)^2 ; For\ \dot{Q}'^*_{xp} < 0.1\ (Small\ Flames)$

Once the system of flame height equations for wall fires had been developed, a dynamic analysis of the cone data had to be done using the above equations. In order for a dynamic analysis to be done, the flame height equations had to be reformatted into a form that could be

easily used in the Runge-Kutta 4th order method. The flame height equations were written into a form similar to that from Mowrer and Williamson. The rewriting of the equations into the Mowrer and Williamson form is shown in full detail in Appendix RK4. The reformatted equations in the Mowrer and Williamson resulted in two flame height equations and two change of the pyrolysis length equations shown below in equations (13), (14), (15), and (16).

(13) $$X_f = (6)\left(\rho_o c_{po} T_o \sqrt{g}\right)^{-\frac{2}{3}} \left(\dot{Q}''\right)^{\frac{2}{3}} \left(X_p\right)^{\frac{2}{3}} \; ; for\ \dot{Q}'^{*}_{xp} > 0.1\ (Large\ Wall\ Flames)$$

(14) $$X_f = (130)\left(\rho_o c_{po} T_o \sqrt{g}\right)^{-2} \left(\dot{Q}''\right)^{2} \; ; for\ \dot{Q}'^{*}_{xp} < 0.1\ (Small\ Wall\ Flames)$$

(15) $$\frac{dX_p}{dt} = \frac{X_f - X_p}{t_{ig}} \rightarrow \frac{dX_p}{dt} = \frac{(6)\left(\rho_o c_{po} T_o \sqrt{g}\right)^{-\frac{2}{3}} \left(\dot{Q}''\right)^{\frac{2}{3}} \left(X_p\right)^{\frac{2}{3}} - (X_p)}{t_{ig}} \; ; \; for\ \dot{Q}'^{*}_{xp} > 0.1$$

(16) $$\frac{dX_p}{dt} = \frac{X_f - X_p}{t_{ig}} \rightarrow \frac{dX_p}{dt} = \frac{(130)\left(\rho_o c_{po} T_o \sqrt{g}\right)^{-2} \left(\dot{Q}''\right)^{2} - (X_p)}{t_{ig}} \; ; \; for\ \dot{Q}'^{*}_{xp} < 0.1$$

In order to run the above equations within the Runge-Kutta method, an assumption of the pyrolysis length and limits of the small wall fire equation had to be determined. One of the first assumptions made was for the initial pyrolysis length. For solving of the Runge-Kutta, an initial pyrolysis length of 0.5 meters was chosen. The initial pyrolysis length was chosen based on the average heat flux from the calibration for the NFPA 285 test from the Kreysler Reports[14, 15]. The pyrolysis length was chosen to be 0.5 meter was based on the height above the window where the highest heat flux averages appear during the calibration of the NFPA 285 test rig. In addition, the initial pyrolysis length was also chosen based on the limits shown below, because 0.5 meters allowed for more room for the small wall fire equation to be used.

Next, the lower limits of the flame height equations had to be determined. The lowest limit of the allowable heat release rate per unit is based on the Mowrer and Williamson model. From the model, the flame height must always be greater than the pyrolysis length. Using equations (11) and (12), the dimensionless heat release rate $\dot{Q}'^{*}_{xp}$ was solved for when the flame height over the pyrolysis length is equal to one and then the heat release rate per unit area was determined from that. The full process can be seen in appendix WALL. The limits of the heat release rate per unit area based on the pyrolysis length are shown below.

Table 7: Heat Release Rate per Unit Area Limits

Xp (m)	HRRPUA (kW/m^2)
0.1	30.88507787
0.5	69.06113361
1	97.66719178

1.5	119.6173922
2	138.1222672

Once both of the equations were reformatted into the Mowrer and Williamson form and all assumptions formed, both equations (15) and (16) were run through a Runge-Kutta 4th order method that allowed for the dynamic solving of the flame height and change in pyrolysis length throughout each test. The entire Runge-Kutta 4th order process can be seen in Appendix RK4.

After running the samples through the Runge-Kutta at two different incident heat fluxes, the results are pretty conclusive. For the samples at the incident heat flux of 50 kW/m^2, the results for the pass or fail of each sample are shown in Table 8 below. Also, a typical result from running the Runge-Kutta solution is shown below in Figure 8.

Table 8: Flame Lengths at IHF of 50 kW/m^2

Results from Samples at Incident Heat Flux of 50 kW/m^2			
Sample name	**Allowable Flame height**	**Flame Height Measured**	**Pass/Fail**
Hetron 100:00	3.05 meters	0.927 meters	Pass
Hetron 100:33	3.05 meters	0.509 meters	Pass
Hetron 100:66	3.05 meters	N/A	N/A
Hetron 100:100	3.05 meters	N/A	N/A
Hetron 100:130	3.05 meters	0.949 meters	Pass
Fireblock 100:00	**3.05 meters**	**3.799 meters**	**Fail**
Fireblock 70:30	**3.05 meters**	**3.093 meters**	**Fail**
Fireblock 60:40	3.05 meters	2.949 meters	Pass
Fireblock 50:50	3.05 meters	1.648 meters	Pass
Fireblock 40:60	3.05 meters	2.334 meters	Pass
Epoxy	3.05 meters	0.854 meters	Pass

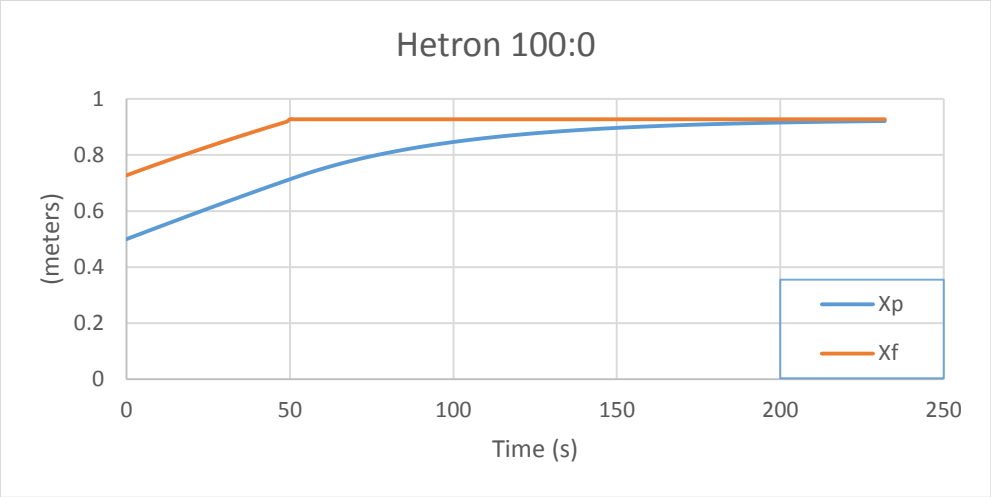

Figure 8: Hetron 100:0 Flame Height and Pyrolysis Length at IHF of 50 kW/m^2

From the results shown in Table 8, it is shown that two of the samples will fail the NFPA 285 test based on the overall flame height. The samples that fail are both Fireblock samples with ratios of 100:0 and 70:30. In addition to this, two of the Hetron samples were unable to be used in this Runge-Kutta method due to limitations of the model. Figure 8*: Hetron 100:0 Flame Height and Pyrolysis Length at IHF of 50 kW/m2*shows the flame height and the change of the pyrolysis length during the entirety of the test. The flame height reaches a certain point where the height become constant while the pyrolysis length increases until it reaches the flame height. The flame height become constant because that is the point where the flame becomes cellular due to the heat release rate per unit are becoming small. The rest of the graphical results from the Runge-Kutta are shown in Appendix RK4. The results for the incident heat flux of 40 kW/m^2 are shown in Table 9 below.

Table 9: Flame Heights at IHF of 40 kW/m^2

Results from Samples at Incident Heat Flux of 40 kW/m2			
Sample name	**Allowable Flame height**	**Flame Height Measured**	**Pass/Fail**
Hetron 100:00	3.05 meters	1.179 meters	Pass
Hetron 100:100	3.05 meters	0.877 meters	Pass
Hetron 100:130	3.05 meters	0.565 meters	Pass
Fireblock 100:0	3.05 meters	2.138 meters	Pass
Fireblock 60:40	3.05 meters	2.369 meters	Pass
Fireblock 40:60	3.05 meters	1.942 meters	Pass

From the results of the incident heat flux of 40 kW/m^2, all of the tested samples will pass the NFPA 285 test based off the flame heights. Unlike the samples at incident heat flux of 50 kW/m^2, none of the samples fail the test because of the limitation of the flame height model.

Although the results from the flame height equations look reasonable and good, the flame height model is very crude and is limited in the scope of what it can determine. There were a number of assumptions made for the development of the system of equations for wall fires and in the solving of the Runge-Kutta equations. The results shown for both incident heat fluxes could vary depending on how well refined the system of equations for the flame heights and the Runge-Kutta equations are. With our simple model, these results are the best we can get for now. The other limitation of the flame height model is that at a certain point for the lower heat release rate per unit area where the model makes no physical sense. The two Hetron Systems with additive ratios of 100:66 and 100:100 both had average heat release rate per unit area lower than the critical value.

Conclusions

Being able to predict fire test performance of FRPs with varying Fire retardant ratios is very helpful to the construction industry in decreasing the cost of material testing. With accurate predictions of fire behavior, a company can reduce the number of full scale fire tests that would be have to be performed in order to determine how the varying of the fire retardant ratios affected the material. A flammability parameter taken from the works of Cleary and Ouintiere, which was used in order to determine that for the Hetron samples, the propagation of the flame would decrease drastically when the ratio rises above 100:130, while flame propagation in the Fireblock samples remained nearly identical.

The varying of the materials fire retardant ratio means that the new material must be run through both the ASTM E84 and the NFPA 285 tests before the material is allowed for use in buildings. Having to repeat the ASTM E84 or the NFPA 285 tests can results in frustration along with large cost in repeating the tests. Two screening tools were further developed to determine how the variation of the material's fire retardant ratio would affect their performance in each of the tests. As a result of the screening tool for the ASTM E84, all of the Hetron samples would be classified as a class A material while all of the Fireblock samples would be classified as a class B material. Nevertheless, some further analysis should be performed to determine the influence of

glass content in the generation of smoke for Fireblock samples. For the NFPA 285 screening tool, all of the Hetron that fit within the limitations of the screening tool would pass the test, while the Fireblock all pass the NFPA 285 except for Fireblock 100:00 and Fireblock 70:30 at an incident heat flux of 50 kW/m^2. More research should be done into the NFPA 285 flame height model and confirmation of the result should be done before the model is confirmed.

References

1. International code council. (2011). *2012 International Building Code* Country Club Hills, III: ICC.
2. ASTM Standard e-84,2013, "Standard Test Method for Surface Burning Characteristics of Building Materials," ASTM International, West Conshohocken, PA, 2013 DOI : 10.1520/E0084-12A, www.astm.org.
3. NFPA 285, 2012, "Standard Fire Test Method for Evaluation of Fire Propagation Characteristics of Exterior Non-Load-Bearing Wall Assemblies Containing Combustible Components 2012 Edition," NFPA Catalog
4. "ASTM E1354: Cone Calorimeter | FireTEC." *Www.Firetec.umd.edu*. University of Maryland, n.d. Web. Sept.-Oct. 2013.
5. Acosta, C., Mahoney, S., Nava, N. and Wright, W. (2013). "Evaluation of Fiber Reinforced Polymer Bench Scale Specimen Sizes and Prediction of Full Scale Flame Spread Testing for Building Applications". (Undergraduate Major Qualifying Project No. NAD FM12).
6. Janssens, M., Huczek, J. and Sauceda, A. "Development of a Model of the ASTM E 84 Steiner Tunnel Test." *Fire Safety Science* 9 (2008): 279-89. Print.
7. Mowrer, F., and R. Williamson. "Flame Spread Evaluation For Thin Interior Finish Materials."*Fire Safety Science* 3 (1991): 689-98. Print.
8. Cleary, T., and J. Quintiere. "A Framework For Utilizing Fire Property Tests."Fire Safety Science 3 (1991): 647-56. Print
9. Gravetter, Frederick J., and Larry B. Wallnau. Essentials of Statistics for the Behavioral Sciences. Australia: Wadsworth, Cengage Learning, 2014. Print
10. Ashland Inc., "Modar 814 A Acrylic Modified Resin". Document 1292 V4 F2. Approved 2011. [Online] Retrieved from: http://www.ashland.com/Ashland/Static/Documents/APM/MODAR%20814%20A%20TDS.pdf Accessed: 4/23/2014.
11. CCP Composites, "NORSODYNE™ FIREBLOCK™". Document H 81269 TF. 2009-2012. [Online] Retrieved from: http://www.aircraftinteriorsexpo-us.com/__novadocuments/44357?v=635258082755670000 Accessed: 4/23/2014.
12. Delichatsios M. "Flame Heights in Wall Fires: Effects of Width, Confinement and Pyrolysis Length." *The Sixth International Symphosium* (n.d.): 729-40. Web.
13. Tu, King-Mon, and James G. Quintiere. "Wall Flame Heights with External Radiation." Fire Technology 27.3 (1991): 195-203. Print.
14. Hintz, David. Fire Performance Evalutaion of Kreysler & Associate's Kreysler Fireshield 285 Panels Tested in Accordance with NFPA 285, 2012 Edition, Standard Fire Test Method for Evaluation of Fire Propagation Characteristics of Exterior Nonloadbearing Wall Assemblies Containing Combutible Components. Rep. no. 01.17787.01.618a. San Antonio, Texas: Southwest Research Institute, 2013. Print.
15. Hintz, David. Fire Performance of a Wall Assembly Tested in Accordance with NFPA 285, 2012 Edition, Standard Fire Test Method for Evaluation of Fire Propagation Characteristics of Exterior Nonloadbearing Wall Assemblies Containing Combutible Components. Rep. no. 01.16918.01.615. San Antonio, Texas: Southwest Research Institute, 2012. Print.

Appendix

Appendix-Materials Section (MS)

Primary Author-Cristina Herrera

Secondary Author-None

Fiber Reinforced Polymers (FRP) are composite materials known as Fiber-reinforced polymers based on thermoplastics and thermoset systems. The general definition of a composite describes it as a heterogeneous mixture of two or more compounds bonded together. Typically, the composition of FRP consists of a polymer matrix or resin reinforced with fibers; these fibers are typically glass, carbon or aramid. Other materials such as fillers and additives can be added but they are not an essential part. The material for the matrix can be any plastic; in general, it is a syrupy liquid which combined with a hardener forms a cross-linked solid. The composite is ready after adding fibrous material to the matrix in the form of a cloth and letting the resin to cure. This process takes place in a closed or open mould. The addition of fibrous materials enhances the strength and elasticity of the resultant polymer. Nevertheless, the properties of the final material depend on the mechanical properties of the matrix and the fiber, their ratio, and the length and orientation of fibers in the matrix. The most common combination of polymer matrices and reinforcing fibers is shown in Figure 1.

Composites are anisotropic materials, which mean properties change according the structural configuration of each part of the material. For example, their strength is different in any region of the whole structure. In general, their stress-strain behavior is linearly elastic to the point of fracture even when the resin in the composite consists of viscous fluids and elastic. In general, composites have great mechanical properties such as high strength, fatigue endurance, light weight, material toughness, among others. Depending of the additives used in the composite, some other qualities can be achieved, such as high resistance to elevated temperature and resistance to corrosion. The properties of the final composite can be enlarged or reduced by altering the geometric shape of the material.

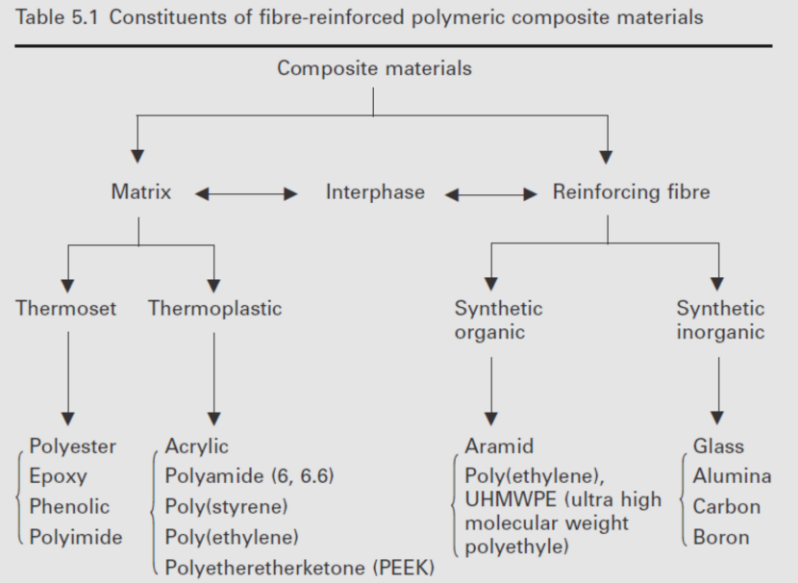

Figure 9: Common polymer matrices and fibers

Resins

There are two classes of resins, thermoplastics and thermosets; thermoplastics resins do not cure permanently because the mers in the backbone do not cross-link, this means that at room temperature it will remain a solid but melts when heated and solidifies again after cooling. On the other hand, thermosets cure permanently by an irreversible cross-link at high temperatures; this makes thermosets ideal for structural applications. Thermosets are particularly attractive to many applications since "compared with metals, they possess corrosion resistance, lighter weight, and sound and thermal insulating properties and they can be processed at lower pressures and temperatures." (ASM Desk Editions: Engineered Materials Handbook). Hetron systems and Fireblock systems are both made of polyester resins.

Polyester resins

According to the *Federal Highway administration*, polyesters are probably the most commonly used of polymeric resin materials, up to 75% of all resins. One of the main advantages of polyesters is their good compatibility with fibres due to low viscosities. In addition, polyesters are easy to manufacture, they cure over a wide range of temperatures and under moderate pressures. They are produced by the condensation polymerization of dicarboxylic acids and dihydric alcohols resulting in a relatively low molecular weight unsaturated polyester chain as shown in Figure 2. One of the less attractive characteristics of

polyesters is that during processing, curing reactions are highly exothermic with a resulting excessive heat generated.

Nevertheless, their dimensional stability and affordable cost make polyesters great candidates for composites matrices which can result high corrosion resistant and fire retardants formulations.

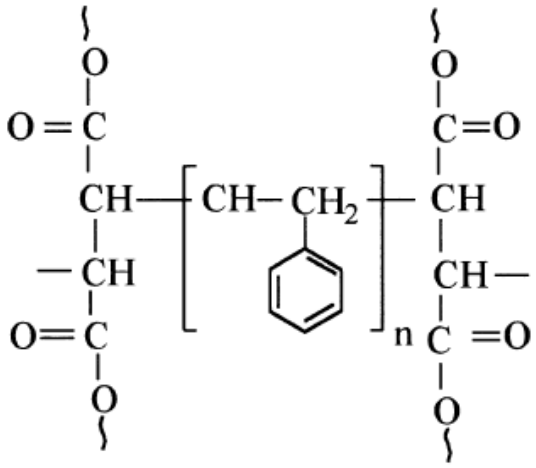

Figure 10: Polyester molecular configuration

Fibers

Fibers are the central compounds of most composites enhancing the material mechanical performance. They are fibrous materials that usually occupy from 30% to 70% of the matrix volume. They are processed with other materials such as starch, gelatin, oil or wax to improve the bonds. The main objective regarding the use of fibres is to place them in positions and orientations in which they are able to contribute efficiently to the load-carrying abilities of the final composite. Recall that FRP are anisotropic materials where the orientation of the molecular components is extremely important to determine the mechanical properties of the material. Different layers with different orientation can be used to create equal properties in all directions of the whole structure. Some of the most common fibers used in the industry are:

- Glass fibers (SiO2)
- Carbon fibers
- Aramid fibers
- Boron fibers
- Aluminia fibers

Fiberglass composites are the least expensive and carbon-fiber composites are the most expensive. In terms of fire performance, "all the fibres used for composites except Ultra High Molecular Weight PE are relatively nonflammable" (Horrocks, 187) but at high temperatures they soften or melt depending of their glass transition temperature.

Fillers

Fillers are added to lower the consumption of expensive resins for the matrix. They are a way to control the cost and slightly modify the final mechanical properties of the composite. The most common fillers used are calcium carbonate, kaolin, and alumina trihydrate (Tang, 7). Depending on how one or more fillers are added to the matrix, the use of fillers result in low shrinkage, low thermal expansion, fire and creep resistance.

Additives

When a polymer is used as the matrix of the composite, it is known that are highly flammable in comparison with metals such as aluminum or steel. That is why additives are significantly important to modify the final properties of the composite. In general, additives are used for further improvement of material properties, aesthetics, and manufacturing process. Depending on the final desirable properties there are millions of additives used in the industry. Composites are widely used in the construction and architectural fields performing many different tasks. Some of the most relevant additives used in FRP for architectural applications can be found in *the Additives Reference Guide 2013* by V, Koleske and are presented in the following list:

- Fire resistance: additives such as bromine, chlorine, borate and phosphorous are used to enhance combustion resistance of composites.
- Flame retardants: this additives retard the flame spread or flammability. These compounds should decompound by heat into nonflammable pieces, the most common are magnesium hydroxide, boric acid, phosphonic acid esters and chlorinated paraffins. There are many commercial flame retardant additives designated to specifically meet the building requirement for fire and safety.
- Air release agents: additives to improve the processability of resins. Polyesters resins tend to trap air during processing and application and using these additives insure a proper fiber wet-out.

- Viscosity control: dispersion of fillers in the resin matrix is really important, for which it is crucial to have low and workable viscosity levels.
- Electrical conductivity: in general, most composites do not conduct electricity and by adding nano metal particles, carbon particles or conductive fibers some level of conductivity can be achieved.
- Antioxidants: these additives in polymers retard the overall oxidation and degradation of the polymer.
- Antistatic agents: additives used to avoid or reduce the tendency of some polymers to attract electrical charge, especially during processing and application.
- Heat stabilizers: additives used to reduce the degradation resulted from the exposure of heat. They are commonly added to thermoplastic resins.
- Ultraviolet stabilizers: added to minimize the negative effects of UV radiation. UV absorbers are used to mitigate the loss of gloss, chalking, discoloration, change in electrical properties and disintegration due to UV radiation.
- Colorants: additives used to provide a specific color to the whole system. They can be added as part of the resin or later on in the molding process of the final product. Mostly used in decorative purposes.
- Release agents: since many FRP are manufactured by mold injection, release agents are additives that facilitate the removal of the final product from the molds. They can be applied to the resins, and the most common agent is zinc stearate. On the other hand, release agent can be applied to the surface of the molds using waxes and silicones.

References

- ASM Desk Editions: Engineered Materials Handbook 10th edition.
- Tang, B. "FIBER REINFORCED POLYMER COMPOSITES APPLICATIONS IN USA". DOT - Federal Highway Administration. USA 1997.
- Horrocks, A. Richard., and Dennis Price. Fire Retardant Materials. Boca Raton, FL: CRC, 2001. Print.
- Koleske, V. et al. Additives Reference Guide 2013. June 2013.

Appendix- Concrete Polymer (CP)

Primary Author-Cristina Herrera

Secondary Author-None

This type of composite was designed to meet most of the requirements in the construction industry without compromising the chemical durability and strength of the material. The binder in this composite is a completely synthetic organic polymer, which can be a thermoplastic or thermoset type of resin. There are five used monomers to produce concrete polymers: epoxy, carbamide, acryl metyl methacrylate, furfuryl alcohol and polyester. Similarly, there are various fillers that can be added to this resin; this includes granite, quartz, clay, expanded glass, sand and many others. "When sand is used as filler, the composite is referred to as a polymer mortar" (Figovsky, 4) where carbon or glass fibers are used to enhance the mechanical properties of the composite. The concrete polymer provided by CCP is a polyester resin that uses sand as the major binder and it reinforced with a glass content of 36%. Glass fibers are noncorrosive and nonconductive, which increases the toughness of the composite.

Concrete polymer based on polyester is a type of thermosetting resins obtained by polycondensation. According to Figovsky and Dimitri, these resins have low viscosity, high mechanical and electrical insulating properties, high resistance to acids and oil, and good adhesion to many construction materials.

Reference

- Figovsky, O. and Dimitry, B. Advanced Polymer Concretes and Compounds: *State of the Art in Polymer Concrete*. Taylor & Francis, 2013. Print.

Appendix- Cone Background and Verification (Cone)

Primary Author-Daniel Morgan

Secondary Author-None

Background

The Cone Calorimeter is a device that is used to study fire behaviors of small samples (maximum size of 100 mm x 100 mm x 50 mm).The raw data that is collected from the various parts of the cone is recorded in either a DC voltage or a temperature. The DC voltage is converted into engineering units using different conversions. The engineering units are then put through a program or macro to reduce the data and perform the calculations. The reduced data is recorded and is used to produce graphs for the different properties. The graphs show a material property versus time. The data from the cone calorimeter test are used to model fires, predict real scale fire behavior, ranking multiple materials based on their fire performance, how a material reacts to a fire (swell, shrink, melt), and to determine if a material passes or fails tests. The cone test usually lasts until the material being tested has burned out.

Oxygen consumption calorimetry measures the amount of oxygen that is consumed during the burning of the material. It determines the amount of oxygen consumed during a burn by measuring the depletion of oxygen in the exhaust gases. Using the oxygen consumption data, the cone calorimeter can determine the heat release rate and cumulative heat released. We can determine the heat released because the amount of heat that is released when burning oxygen is relatively linear.

The ASTM E1354 test is a standard to determine a material's response to controlled levels of radiant heating either with or without an external ignition source. The use for the ASTM E1354 test is to determine the materials properties (stated below), and how a material reacts to different levels of radiant heat. The scope of the ASTM E1354 test is to determine the ignitability, heat release rates, mass loss rates, effective heat of combustion, and visible smoke development of materials and products.

Data Collected

The cone calorimeter collects a large assortment of material properties and other data. The data that is collected from the cone calorimeter test include peak rate and average rate of heat released by the material, heat release rate per unit area, the total heat released from the material, the effective heat of combustion, the specific extinction area, exhaust flow rate, mass

loss rate of the material, initial and final mass of the material, time required to get a sustained ignition, the amount of carbon dioxide and carbon monoxide released from the material burning, the oxygen concentration amount, and the smoke density, etc.

Parts of the Cone

The cone calorimeter consists of six parts. The separate parts are a conical radiant electric heater, specimen holder, exhaust gas system with measuring tools, ignition spark source, data collector and analyzer, and a load cell to measure material mass. The conical radiant heater is the source of heat that will cause the material to ignite. The conical heater can provide a range of heat fluxes from 0 to 100 kW/m^2K. The specimen holder is a metal container whose job is to hold the material in place during the testing. Next is the exhaust system with the measuring tools. The measuring tools inside the duct include an oxygen, carbon monoxide, and carbon dioxide analyzers, thermocouple for measuring exhaust temperatures, orifice plate for measuring the pressure differential to determine the exhaust flow rate, and helium-neon laser for determining smoke obscuration. The ignition spark source is a spark that is placed above the material to allow for it to ignite. The data collector and analyzer is the computer and software that is used for storing and analyzing the data collected from the various components. The load cell is used to record the mass of the material during the data and that data is used to find the mass loss rate during combustion.

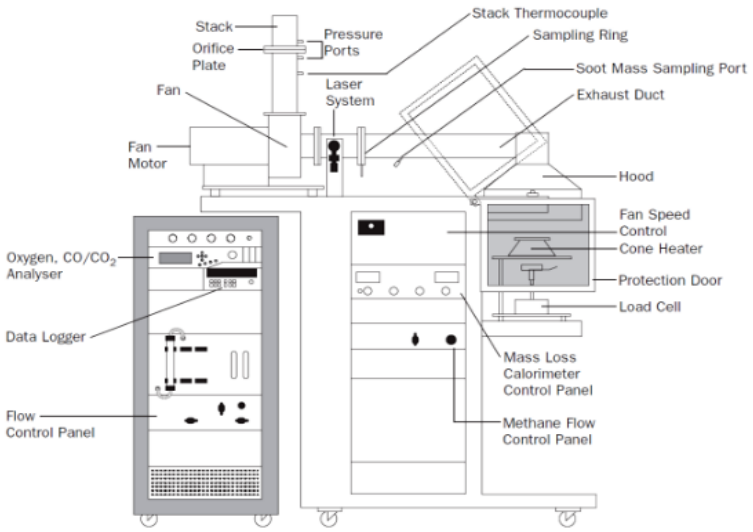

Figure 11: Cone Calorimeter

Direct/Indirect Measurements

The cone calorimeter records and determines two types of measurements, either direct or indirect measurements. Direct measurements are measurements that the cone calorimeter makes directly, such as a time or mass. The direct measurements that the cone calorimeter records during operation is the time to ignition, sample mass (load cell), oxygen, carbon monoxide, and carbon dioxide concentrations (gas analyzers), and the stack temperature (thermocouple). The other type of measurement recorded is indirect measurements. Indirect measurements are measurements that are taken that doesn't directly correlate to the property we are looking for, the measurement taken is used in a calculation to then determine the property we are looking for. The indirect measurements taken by the cone calorimeter are heat release rate, heat release rate per unit area, effective heat of combustion, specific extinction area, smoke production rate and obscuration, exhaust flow rate, mass loss rate, peak and total heat release rate, differential pressure, and the different yield amounts (oxygen, carbon monoxide, carbon dioxide, and smoke yields).

Oxygen Consumption Calorimetry (kJ/kg or MJ/kg)

Oxygen consumption calorimetry is the main backbone behind the cone calorimeter. Oxygen consumption calorimetry is based on the fact that heat released for the burning of most polymers is relatively constant. The amount of heat released for the burning of 1 kg of oxygen is roughly 13.1 MJ of heat, within plus or minus 5 percent. Using the 13.1 MJ is generally a good estimate of the heat to be released for burning of a material, unless the actual amount of heat released is known. The equation that is shown below is a way to determine the heat released for a material if the materials chemical makeup is known.

$$E = \Delta h_c \left[\frac{n_p M_p}{n_{O2} M_{O2}}\right] = \frac{\Delta h_c}{r_o}$$

Δh_c (kJ/kg) is the heat of combustion of the material that is being tested. n_p (mol) and M_p (g/mol) are the number of moles and molecular weight of the material being tested. n_{O2} (mol) and M_{O2} (g/mol) are the number of moles and molecular weight of the oxygen being consumed.

Verification

To obtain a good understanding of how a cone calorimeter works, an attempted to reproduce the data that is calculated by the cone VI. The raw data that was measured from the cone testing and attempted to reproduce the final results that were calculated by the VI as accurately as we possibly could. To reproduce the data, a wide assortment of equations was needed to reproduce the data. With the equations that were needed and the raw data that was recorded from the cone calorimeter, a reproduction of the cone data could be performed. Since the raw data is recorded only in units of voltages and temperatures, a conversion between the raw data and engineering units needed to be made. All of the conversions are laid out in the appropriate sections below. Once the equations were performed, the separate data points were graphed in excel in order to compare with the actual data. The samples that we attempted to reproduce were the FRP sample and the PMMA sample (sample 4) of thickness 23.3 mm

Heat Release Rate per Unit Area

The first reproduction that was done was for Heat Release Rate per unit area, the two equations that were needed to determine the HRR per unit area are listed below. The first equation is used to determine the Heat release rate for the material. Since the material that was being testing is small, the heat release rate per unit area needed to be used. This allows for data to be scaled up to larger sizes. The second equation is a division of equation 1 over the area testing.

$$(1)\quad \dot{Q}(t) = E1.10C\sqrt{\frac{\Delta P}{T}}\left(\frac{X_{O2}^{o} - X_{O2}}{1.105 - 1.5X_{O2}}\right)$$

$$(2)\quad \dot{q}"(t) = \frac{\dot{Q}(t)}{A_s}$$

From the two equations above, there are a total of 4 constants and 3 measured values that are taken from the raw data. The first constant is E, which is the amount of energy released from the burning of one kilogram of oxygen. The value for E is 13,100,000 Joules, unless this value is known for the material. The second constant is C, which is the C factor. The C factor is determined from calibration of the cone calorimeter, the value usually ends up around 0.042. The third constant is X^{o}_{O2}, which is the initial oxygen concentration, which is usually around 20.9%. However, this value may need adjusting depending on whether there was any drifting in the oxygen analyzer. To adjust this value, you would look at the oxygen concentration in the raw

data prior to the start of the burn and use that value. That value would need to be converted into engineering units, which will be explained in the next paragraph. The fourth constant is A_s, which is the area of the material testing, which will always be 0.01 m^2. The raw data that is needed are the differential pressure (ΔP), the stack temperature (T), and the oxygen concentration (X_{O2}).

The raw data that is measured will be in units measured in either a voltage (V) or a temperature (C). The voltages needed to be converted into engineering units so that they can be used to reproduce the calculations. The first conversion is for the differential pressure to go from volts to a pressure (Pa). To convert this, all that is needed to be done is to multiply by 100 Pa per volt. Doing so will convert the voltage into a pressure. The next conversion is for the stack temperature which needs to go from temperature in Celsius and convert into a temperature in Kelvin. For this, all you need is to add 273 to Celsius temperature. The final conversion is for the oxygen concentration, which needs to be converted from a voltage into a % concentration. To do this, a conversion factor needed to be determined to convert the voltage to a percent concentration per volt. The calibration data from the cone was taken for oxygen, which for the FRP is 0.209 at a voltage of 6.986644 volts. It was then divide by 0.209 by the voltage to obtain a conversion that would allow us to convert a voltage into a percent concentration. Using this conversion factor, it was multiplied by the oxygen voltage to get an oxygen concentration. The conversed voltages into engineering units was used in the above equations.

Graphical Comparison

Using the equations mentioned above, the equations were plotted into excel and compared it to the actual data that was directly from the cone calorimeter. The top pictures are the reproduction while the bottom ones are the actual data.

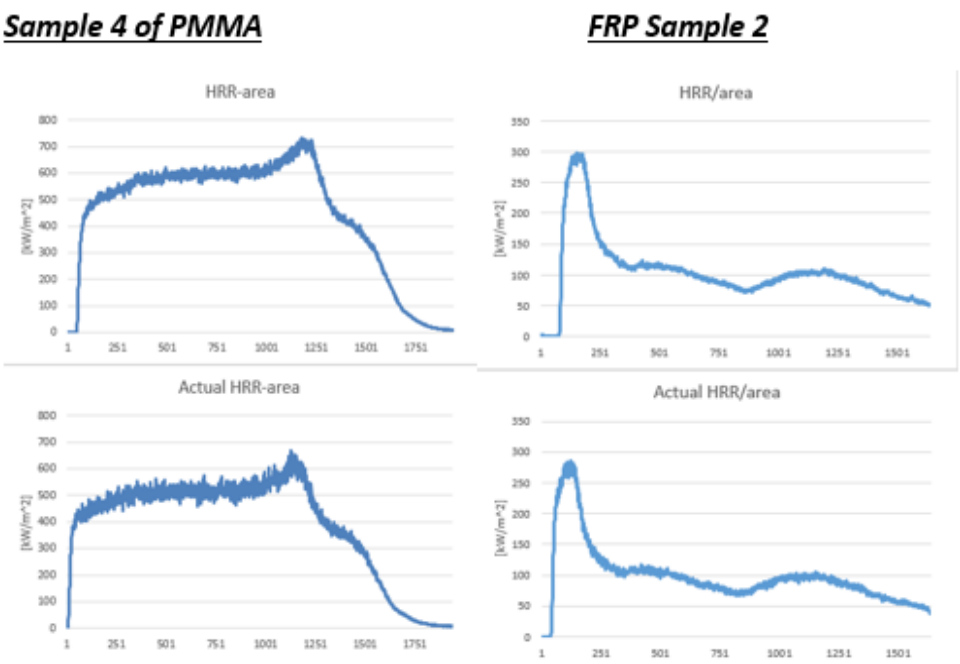

Figure 12: Heat Release Rate per Unit Area Comparison

Mass Loss Rate

The next reproduction calculation that was done was the mass loss rate calculation. The five equations below are used to determine the mass loss rate during the testing. These equations can be found in the ASTM E1354 standard for the cone calorimeter. The mass loss rate is determined from a set of scans of the material masses, the equation that is used is determined from what calculation number you are doing. The first equation is used for the very first set of data, or scan that is done. The second is used for the second, while the third is used for all other calculations up until the final two. Equations 4 and 5 are used for the second to last and the final calculations receptively.

(1) $-\left(\frac{dm}{dt}\right)_{i=0} = \frac{25m_0-48m_1+36m_2-16m_3+3m_4}{12\Delta t}$; First scan

(2) $-\left(\frac{dm}{dt}\right)_{i=1} = \frac{3m_0+10m_1-18m_2+6m_3-m_4}{12\Delta t}$; Second scan

(3) $-\left(\frac{dm}{dt}\right)_{i} = \frac{-m_{i-2}+8m_{i-1}-8m_{i+1}+m_{i+2}}{12\Delta t}$ 1<i<n-1 for scan between second and second to lass scan

(4) $-\left(\frac{dm}{dt}\right)_{i=n-1} = \frac{-3m_n-10m_{n-1}+18m_{n-2}-6m_{n-3}+m_{n-4}}{12\Delta t}$; Second to last scan

(5) $-\left(\frac{dm}{dt}\right)_{i=n} = \frac{-25m_n+48m_{n-1}-36m_{n-2}+16m_{n-3}-3m_{n-4}}{12\Delta t}$; Final scan

From the above equations, there is one constant and one measured value taken from the raw data. The only constant is the Δt, which is the time step for the data recording, which is 1 in this case. The data that is needed is mass voltages from the raw data. A conversion factor is needed to determine the mass from the voltages that are given from the cone calorimeter. To determine the conversion factor, we look at the calibration data for the mass. The calibration data was determined from a set of 5 different weights placed on the load cell and their recorded voltages. It was then took the mass that was placed on the load cell and divide it by the voltage that was recorded. We repeat this for the other mass/voltage combinations and average out all of the numbers to obtain a conversion factor. To convert the voltages to a mass, all that was needed was to multiply the conversion factor and the mass voltages that are in the raw data. The converted numbers were used in the above equations.

Once the calculations have been done, the mass loss rate graph that was produced is very noisy and jumps around a lot. This is due to noise in the recording of the mass voltages. To obtain smoother graph and smoother values, the data from the cone calorimeter was truncated and then a five point moving average was performed that smoothed out the graph. The smoothed graph is a better comparison to the actual data, and provides nicer numbers to use in the other calculations. Another five point moving average could have been used to smooth the graph even more, but was not needed in this case.

Graphical Comparison

Using the equations mentioned above, the equations were plotted into excel and compared it to the actual data that was directly from the cone calorimeter. The top pictures are the reproduction while the bottom ones are the actual data.

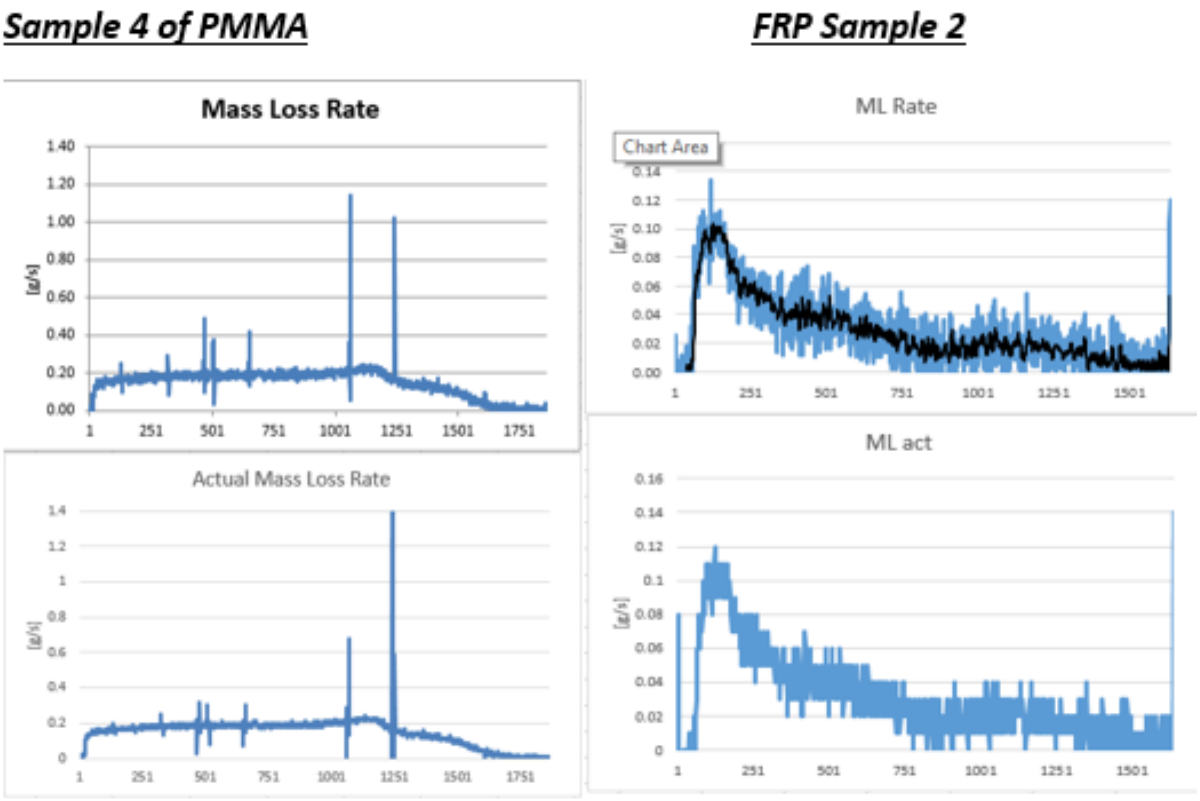

Figure 13: Mass Loss Rate Comparison

Heat Released

The next calculation that was done was to determine the heat released from the material during testing. To determine the heat released, an integral needed to be performed on the heat release rate, which is equation number (1) in the heat release rate section. The integral is being performed to determine the heat released because the heat released in just the summation of all the heat release rates at each time step. This summation ends up being the area under the curve of the heat release rate. To determine the area under the curve in excel, the trapezoid rule needs to be used, since excel does not have an integral function. The two below equations are the equations that were used to determine the heat released.

(1) $Trap = \frac{(t_2 - t_1)(\dot{Q}_2 + \dot{Q}_1)}{2}$

(2) $Heat\ Released = \sum trap$

From the equations above, there are no constants and one set of data that is taken from the determination of the heat release rate. There are also no conversion that are needed in the equation. The only data set needed for this calculation is the heat release rate ($\dot{Q}$), since t_2 minus t_1 is always 1. To determine the heat release during each time step, the two heat release rates are added together and divided by 2. This procedure is performed for all of the heat release rate values and finally, all of the traps are summed for each time step together in order to find our heat released.

Graphical Comparison

Using the equations mentioned above, the equations were plotted into excel and compared it to the actual data that was directly from the cone calorimeter. The top pictures are the reproduction while the bottom ones are the actual data.

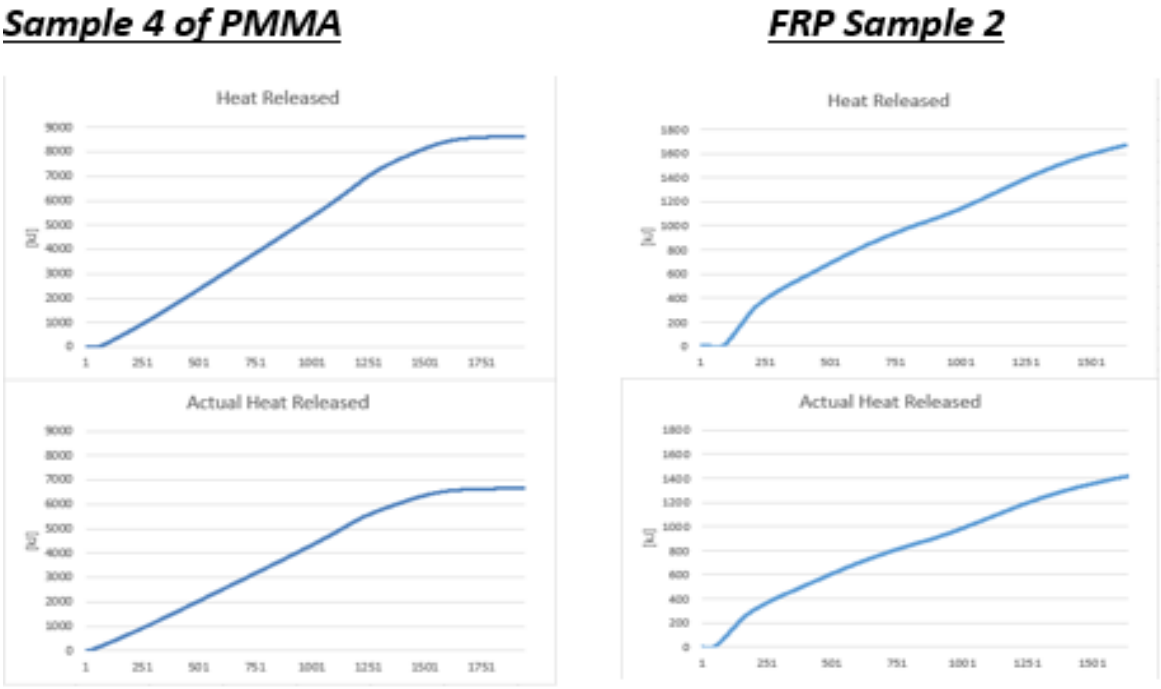

Figure 14: Heat Released Comparison

Heat of Combustion

The next calculation performed was for the heat of combustion. The only equation that is needed to determine the heat of combustion is shown below.

$$(1)\ HOC = \frac{\dot{Q}}{\dot{m}}$$

The equation for the heat of combustion has only two variables that were determined previously. The data sets needed are for this calculation are the Heat release rate ($\dot{Q}$) and the mass loss rate ($\dot{m}$) that were previously determined. There are no needed conversions for this calculation, since they were performed when determining the other data sets. Calculation the heat of combustion is just dividing the heat release rate by the mass loss rate.

Graphical Comparison

Using the equations mentioned above, the equations were plotted into excel and compared it to the actual data that was directly from the cone calorimeter. The top pictures are the reproduction while the bottom ones are the actual data.

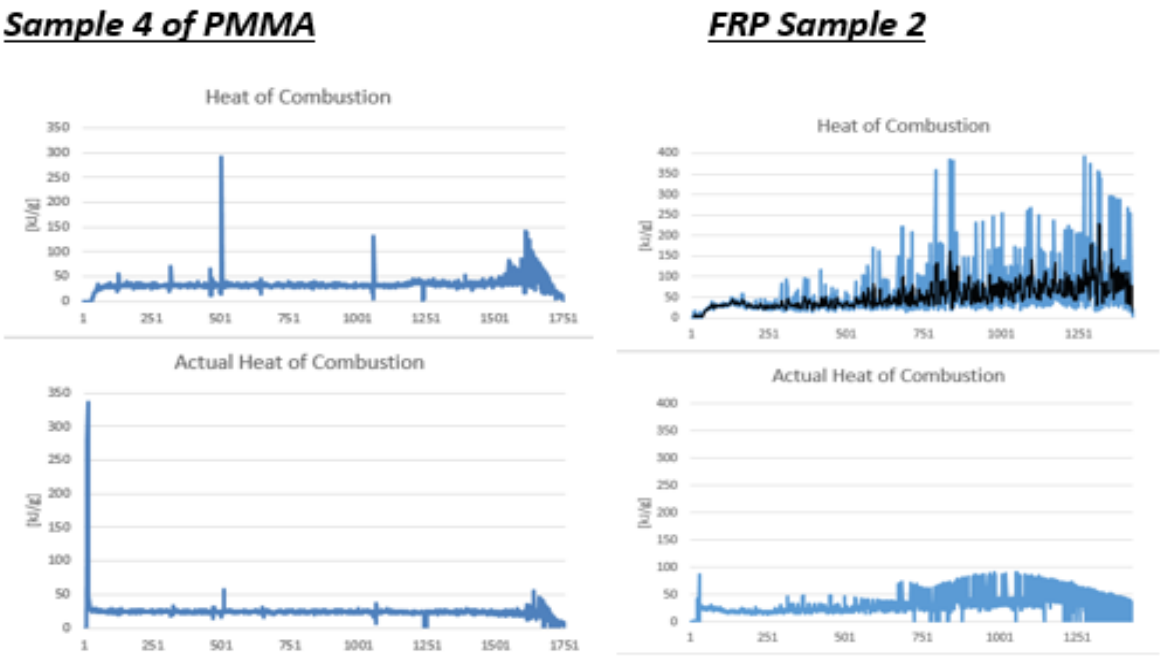

Figure 15: Heat of Combustion Comparison

Extinction Coefficient

The next equation that was used was to determine the extinction coefficient. The only equation that was needed to determine the exaction coefficient is below.

$$(1)\ k = \left(\frac{1}{L}\right)\ln\left(\frac{I_{0i}}{I_i}\right)$$

From the above equation, there is one constant and 2 sets of data that is needed from the raw data. The only constant is L, which is the exaction beam length, whose value is 0.114 meters. The two data sets that are needed are for main (I_i) and Comp (I_{oi}). In the raw data, both of these data sets are recorded in voltages, so a conversion factor needs to be determined for the data sets. To obtain the conversion factors, the calibration data for the laser is used for the determination of the calibration factor. There are 3 points of obscurity for both the main and comp diodes, and their respective voltages. The obscurity needs to be divided by the voltage to get a conversion factor. This is done for all the different obscurities for both diodes and average the conversion factors for each diode to obtain the two conversion factors needed. This is then used in the above equation to find our extinction coefficient.

Graphical Comparison

Using the equations mentioned above, the equations were plotted into excel and compared it to the actual data that was directly from the cone calorimeter. The top pictures are the reproduction while the bottom ones are the actual data.

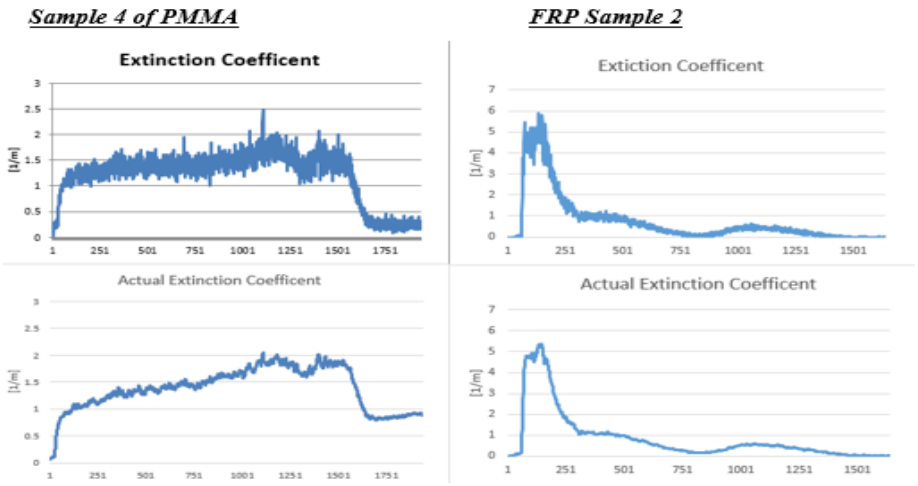

Figure 16: Extinction Coefficent Comparison

Smoke Production Rate

The next equation that was used was to determine the smoke production rate. The only equation that is used is shown below.

$$(1) \quad SPR = k\dot{V}$$

From the above equation, we have no constants and we have two variables. The first variable is the extinction coefficient (k), which was determined in the above section. The second variable is the volumetric flow rate ($\dot{V}$). The volume flow rate is found in the summary section of the data. There are no needed conversion for this calculation. Calculating the smoke production rate is multiplying the exaction coefficient by the volume flow rate.

Graphical Comparison

Using the equations mentioned above, the equations were plotted into excel and compared it to the actual data that was directly from the cone calorimeter. The top pictures are the reproduction while the bottom ones are the actual data.

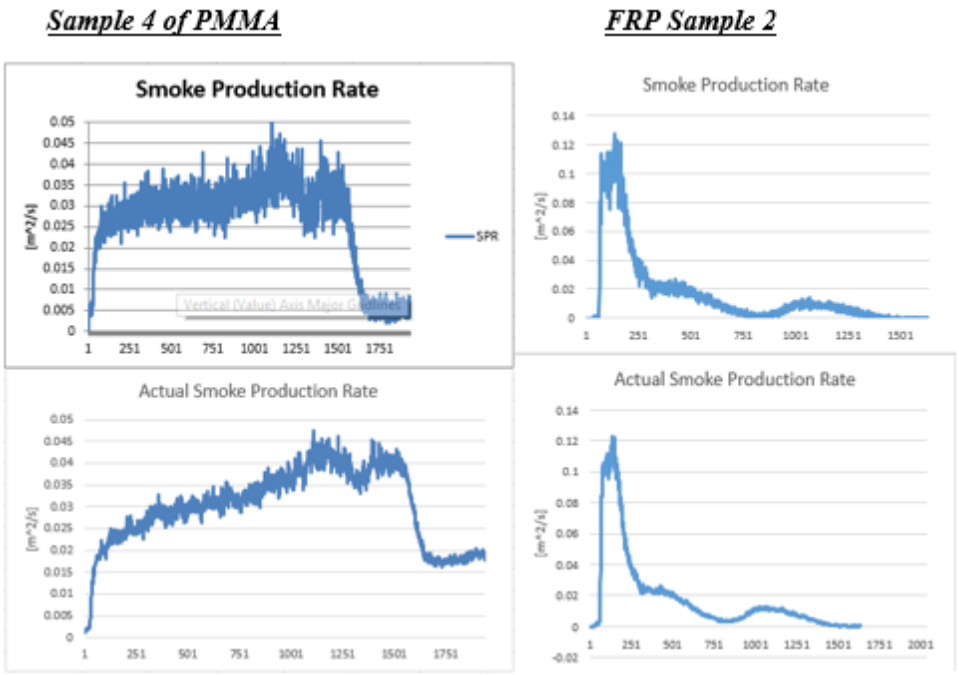

Figure 17: Smoke Production Rate Comparison

Specific Extinction Area

The next equation that was used was to determine the specific extinction area. The only equation that is needed is shown below.

(1) $SEA = \frac{SPR}{\dot{m}}$

The above equation has no constants and has only two variables. The first variable is the smoke production rate (SPR), which was calculated in the above section. The second variable is the mass loss rate ($\dot{m}$), which was determined in a previous section. Since both of the variable are already calculated, we do not need any conversion factors. Calculating the specific extinction area is just dividing the smoke production rate by the mass loss rate.

Graphical Comparison

Using the equations mentioned above, the equations were plotted into excel and compared it to the actual data that was directly from the cone calorimeter. The top pictures are the reproduction while the bottom ones are the actual data.

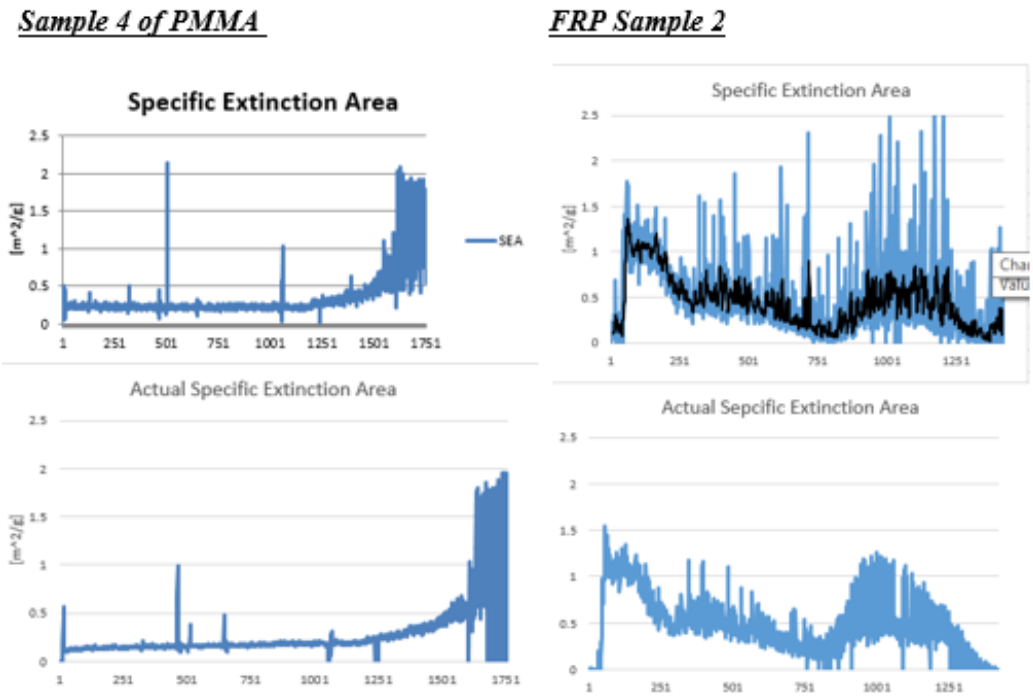

Figure 18: Specific Excitation Area Comparison

Smoke Yield

The next equation that was used was to determine the smoke yield. The only equation that was used is shown below.

$$Smoke\ Yield = SEA/SEA_{smoke}$$

The above equation has one constant and one variable. The only constant is the Specific extinction area of smoke (SEA_{smoke}), which has a value of 7.6 m^2/g. The only variable is the specific extinction area (SEA) that was determined from the above equations. There is no conversion factors that are needed for this equation. Calculating the smoke yield is just dividing the specific extinction area by the specific extinction area of the smoke.

Graphical Comparison

Using the equations mentioned above, the equations were plotted into excel and compared it to the actual data that was directly from the cone calorimeter. The top pictures are the reproduction while the bottom ones are the actual data.

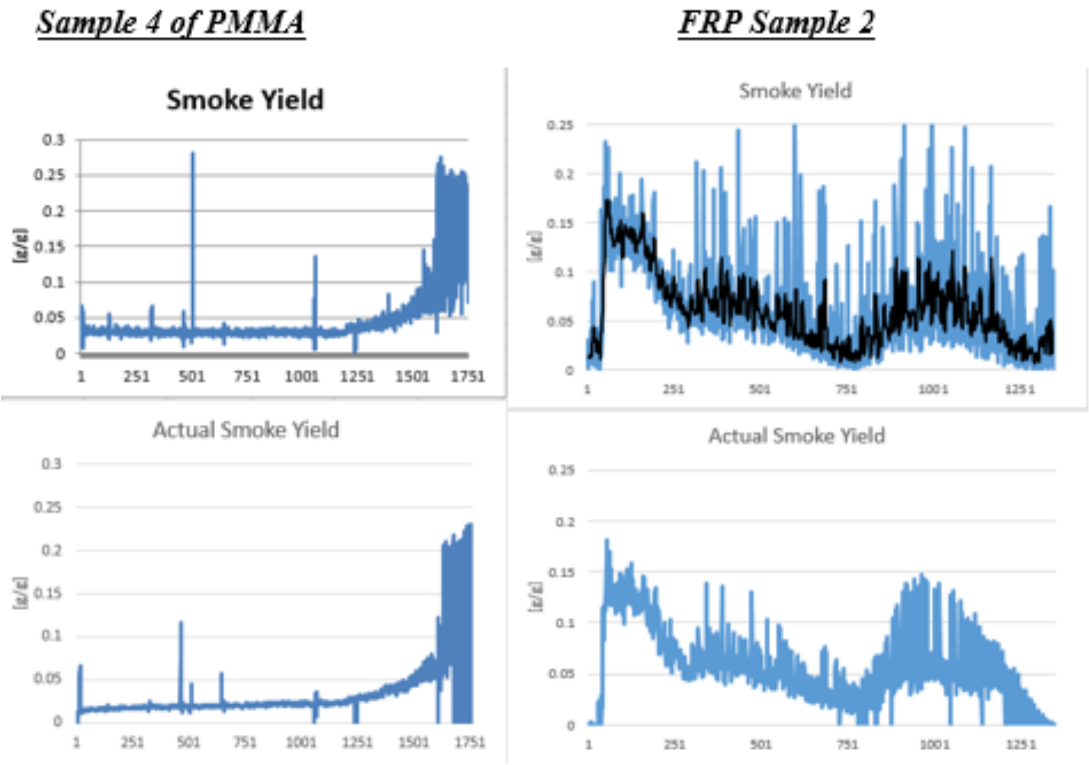

Figure 19: Smoke Yield Comparison

CO Production Rate

The next equation that was used was to determine the CO production rate. The equation that was used is shown below. The CO production rate or generation rate is taken from the SFPE handbook.

(1) $CO\ Rate = \frac{\dot{V} X_{CO} \rho}{A}$

In the above equation, there are two constants and three variables. The first constant is the density of the carbon monoxide (ρ), which is 1.15 kg/m^3. The second constant is the area of the specimen (A), which is 0.01 meters squared. The first variable is the volume flow rate ($\dot{V}$), which is taken from the summary section of the data. The second variable is the CO concentration (X_{CO}). Since the CO concentration is recorded in voltage, a conversion factor needs to be determined. To determine the conversion factor, the calibration data for the CO sensor needs to be used. The concentration is taken from the calibration (0.089 in our case) and divide it by the voltage that is given with that concentration. The converted numbers were used in the above equations.

Graphical Comparison

Using the equations mentioned above, the equations were plotted into excel and compared it to the actual data that was directly from the cone calorimeter. The top pictures are the reproduction while the bottom ones are the actual data.

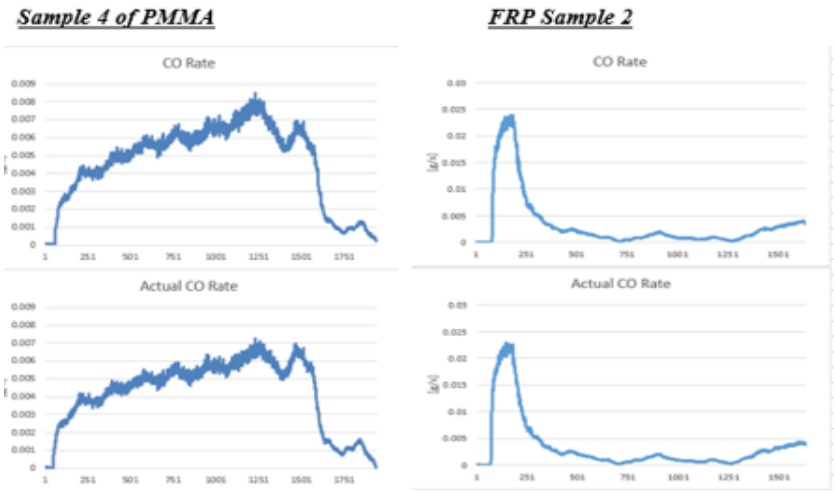

Figure 20: CO Rate Comparison

CO Yield

The next equation that was used was to determine the CO yield. The only equation that was needed is shown below.

(1) $CO\ Yield = \frac{CO\ Rate}{\dot{m}}$

The above equation has only two variables. The first variable is the CO rate, which was determined in the previous section. The second variable is the mass loss rate ($\dot{m}$), which was determined in a previous section. There are no conversion factors that are needed for the calculation of the CO yield. To calculate the CO yield, we divided the CO rate by the mass loss rate.

Graphical Comparison

Using the equations mentioned above, the equations were plotted into excel and compared it to the actual data that was directly from the cone calorimeter. The top pictures are the reproduction while the bottom ones are the actual data.

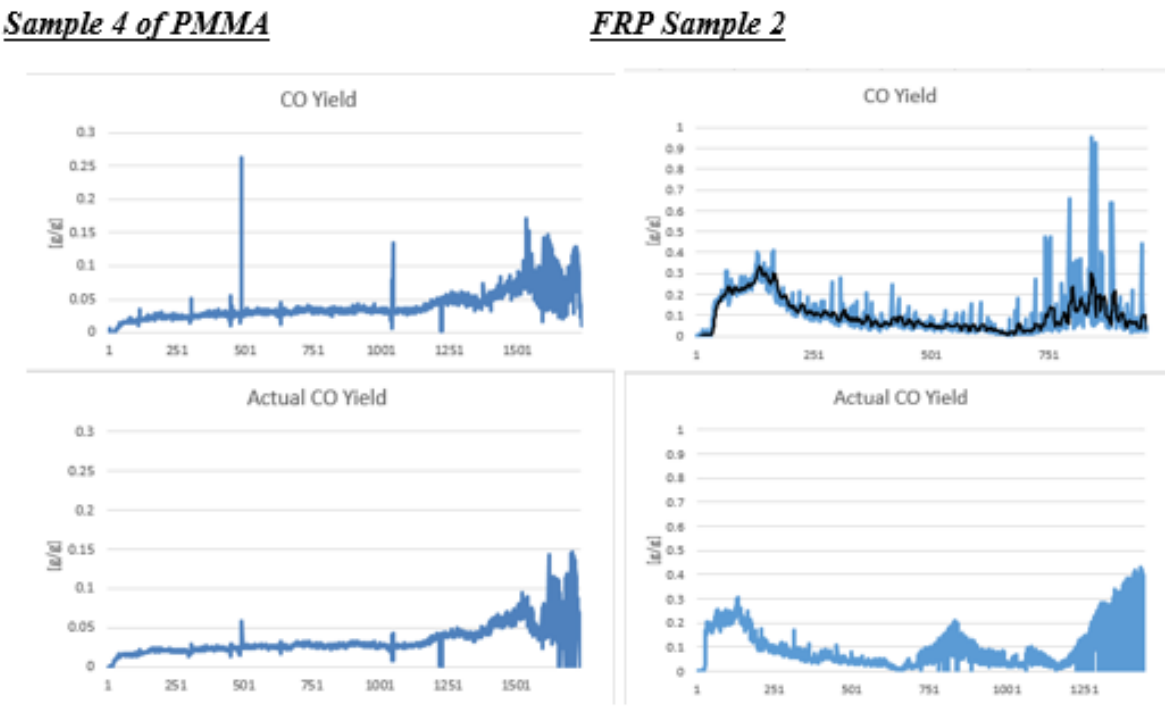

Figure 21: CO Yield Comparison

CO2 Production Rate

The next equation that was used was to determine the CO_2 production rate. The equation that was used is shown below. The CO_2 production rate or generation rate is taken from the SFPE handbook.

(1) $CO_2\ Rate = \frac{\dot{V} X_{CO2} \rho}{A}$

In the above equation, there are two constants and three variables. The first constant is the density of the carbon dioxide (ρ), which is 1.8 kg/m^3. The second constant is the area of the specimen (A), which is 0.01 meters squared. The first variable is the volume flow rate ($\dot{V}$), which is taken from the summary section of the data. The second variable is the CO_2 concentration (X_{CO}). Since the CO_2 concentration is recorded in voltage, a conversion factor needs to be determined. To determine the conversion factor, the calibration data for the CO_2 sensor needs to be used. The concentration is taken from the calibration (2214 in our case) and it is divided by one thousand times the voltage, since this voltage is given in millivolts. This will give the correct conversion factor, and then it is multiplied by the conversion factor to get the CO_2 concentration.

Graphical Comparison

Using the equations mentioned above, the equations were plotted into excel and compared it to the actual data that was directly from the cone calorimeter. The top pictures are the reproduction while the bottom ones are the actual data.

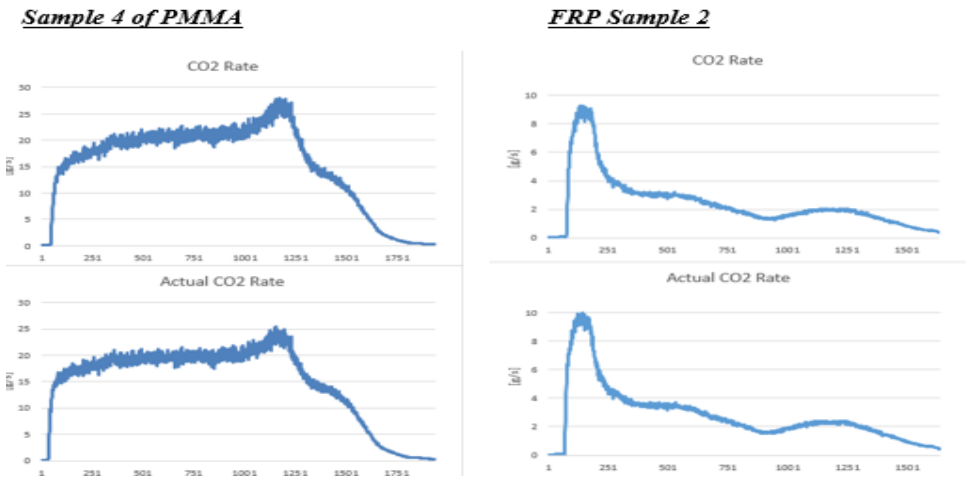

Figure 22: CO_2 Rate Comparison

CO2 Yield

The next equation that was used was to determine the CO_2 yield. The only equation that was needed is shown below.

(1) $CO_2\ Yield = \frac{CO_2\ Rate}{\dot{m}}$

The above equation has only two variables. The first variable is the CO_2 rate, which was determined in the previous section. The second variable is the mass loss rate ($\dot{m}$), which was determined in a previous section. There are no conversion factors that are needed for the calculation of the CO_2 yield. To calculate the CO_2 yield, we divided the CO_2 rate by the mass loss rate.

Graphical Comparison

Using the equations mentioned above, the equations were plotted into excel and compared it to the actual data that was directly from the cone calorimeter. The top pictures are the reproduction while the bottom ones are the actual data.

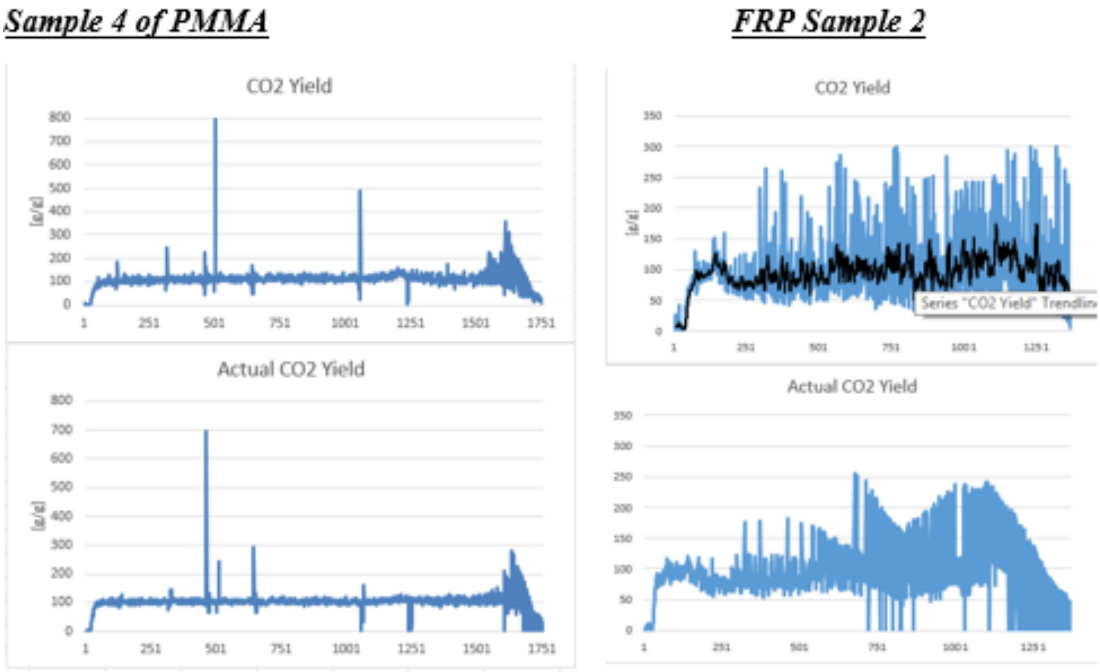

Figure 23: CO_2 Yield Comparison

Cone References

1. Ahmed, Gamal N., Mark A. Dietenberger, and Walter W. Jones. *Calculating Flame Spread on Horizontal and Vertical Surfaces*. Rep. Gaithersburg, MD: Building and Fire Research Labratory, 1994. *Fire.nist.gov*. National Institute of Standards and Technology. Web. Fall 2013.

2. "ASTM E1354: Cone Calorimeter | FireTEC." *Www.Firetec.umd.edu*. University of Maryland, n.d. Web. Sept.-Oct. 2013.
3. Babrauskas, Vytenis. "The Cone Calorimeter." SFPE Handbook of Fire Protection Engineering. 3rd ed. Quincy, MA: National Fire Protection Association, 2002. 3-63--80. Print.
4. Babrauskas, Vytenis. "Heat Release Rates." SFPE Handbook of Fire Protection Engineering. 3rd ed. Quincy, MA: National Fire Protection Association, 2002. 3-1--34. Print.
5. Babrauskas, Vytenis, and William J. Parker. *Ignitability Measurements with the Cone Calorimeter*. Rep. Vol. 11. N.p.: n.p., n.d.*Ignitability Measurements with the Cone Calorimeter*. Center for Fire Research. Web. Sept.-Oct. 2013.
6. Baroudi, Djebar. *Thermal Models for Fire Safety - Calculation of Flame Spread on Surfaces and Heating of Structures*. Rep. Helsinki University of Technology, n.d. Web. Fall 2013.
7. Chow, W.K., and S.S. Han. "Heat Release Rate Calculation in Oxygen Consumption Calorimetry." *Heat Release Rate Calculation in Oxygen Consumption Calorimetry*. N.p., n.d. Web. Sept.-Oct. 2013. <http://www.sciencedirect.com/science/article/pii/S1359431110003972>.
8. Guillaume, Eric, Damien Marquis, and Laurent Saragoza. *Calibration of Flow Rate in Cone Calorimeter Tests*. Rep. N.p., n.d. Web. Fall 2013.
9. Janssens, Marc. "Calorimetry." SFPE Handbook of Fire Protection Engineering. 3rd ed. Quincy, MA: National Fire Protection Association, 2002. 3-38--59. Print.
10. Kittle, Paul A., ed. *Flammability of Alternative Daily Cover Materials - A Summary of ASTM E1354 Cone Calorimeter Results*. Comp. Paul A. Kittle. Rusmar Incorporated, n.d. Web. <http://www.aquafoam.com/papers/tarps.pdf>.
11. Lindholm, Johan, Anders Brink, and Mikko Hupa. *Cone Calorimeter - A Tool for Measuring Heat Release Rate*. Rep. Abo Akademi Process Chemsity Cenre, n.d. Web.
12. *Reaction to Fire - Cone Calorimeter Testing*. Rep. Chiltern International Fire, n.d. Web. <http://www.chilternfire.co.uk/document/ti-1013-reaction-to-fire---cone-calorimetry-testin.pdf>.
13. *Standard Test Method for Heat and Visible Smoke Release Rates for Materials and Products Using an Oxygen Consumption Calorimeter*. Rep. ASTM International, n.d. Web. Fall 2013.
14. Walters, Richard N., Stacey M. Hackett, and Richard E. Lyon. *Heats of Combustion of High Temperature Polymers*. Rep. N.p., n.d. Web. Fall 2013. <http://large.stanford.edu/publications/coal/references/docs/hoc.pdf>.
15. Zhao, Lei. "Bench Scale Apparatus Measurement Uncertainty Effects on Measurements of Fire Characteristics of Materials Systems." Thesis. Worcester Polytechnic Institute, 2005. Print.

Appendix- Graphs (Graphs)

Primary Author-Jerome Anaya, Daniel Morgan

The following data are the measurements from the Cone Calorimeter for each sample. They are given in the following order: heat release per unit area, mass loss rate, specific extinction area, extinction coefficient, and smoke production rate. The samples of the same composition are given on the same graph for comparison.

50 kW Test

Hetron with ATH Ratio 100:0

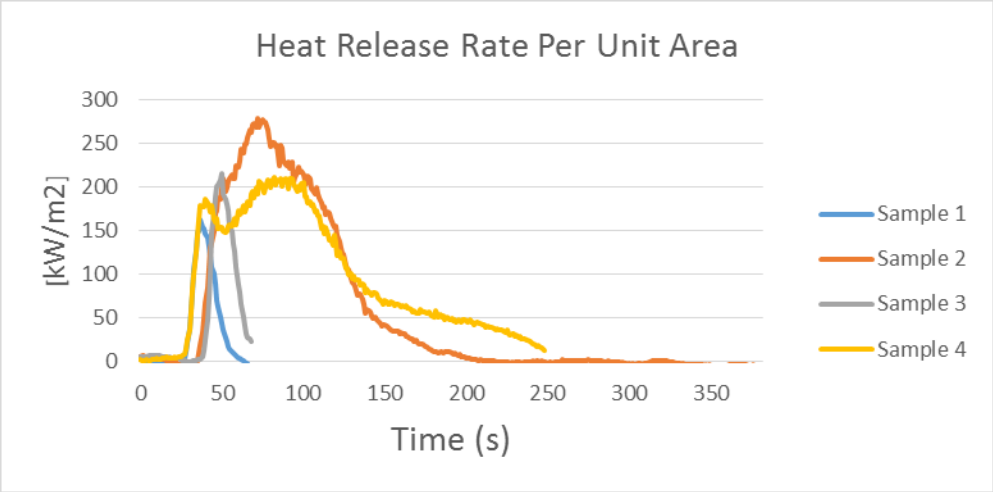

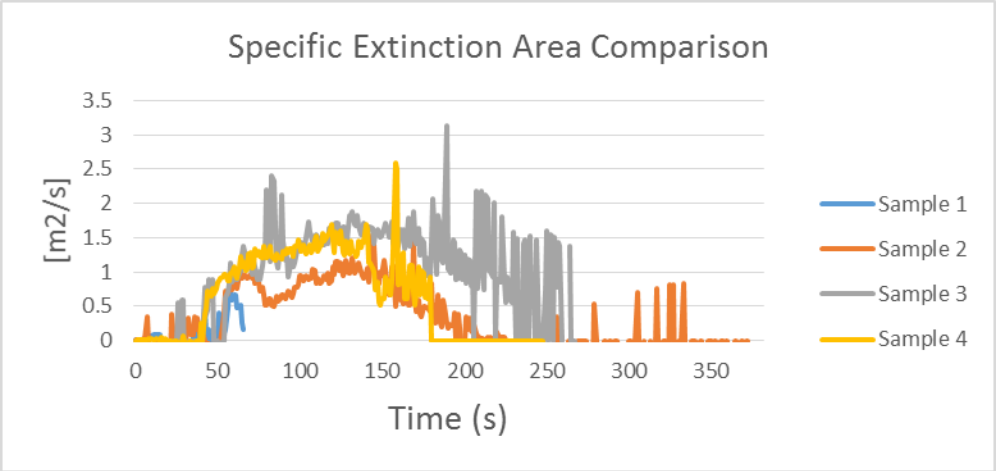
Specific Extinction Area Comparison
[m2/s]
3.5
3
2.5
2
1.5
1
0.5
0
0
50
100
150
200
250
300
350
Time (s)
Sample 1
Sample 2
Sample 3
Sample 4

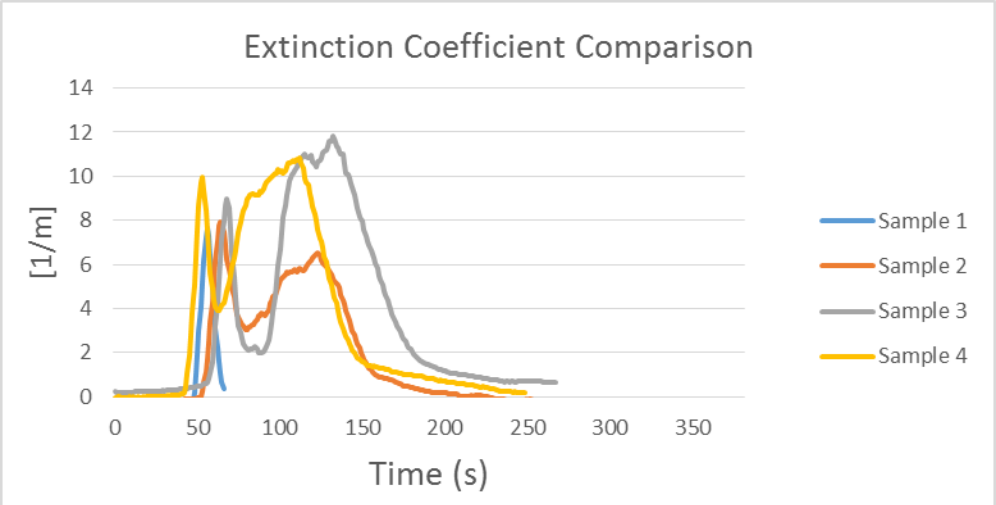
Extinction Coefficient Comparison
[1/m]
14
12
10
8
6
4
2
0
0
50
100
150
200
250
300
350
Time (s)
Sample 1
Sample 2
Sample 3
Sample 4

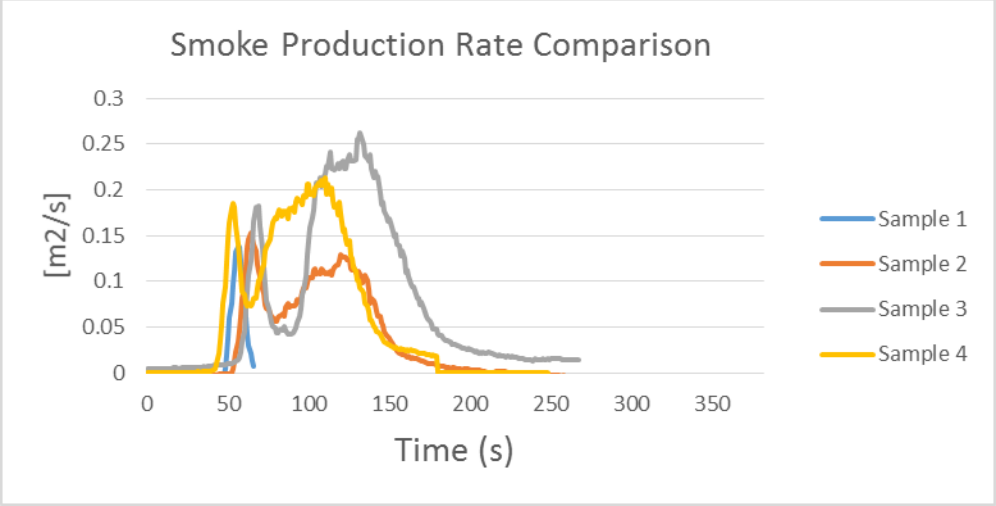
Smoke Production Rate Comparison
[m2/s]
0.3
0.25
0.2
0.15
0.1
0.05
0
0
50
100
150
200
250
300
350
Time (s)
Sample 1
Sample 2
Sample 3
Sample 4

Hetron with ATH Ratio 100:33

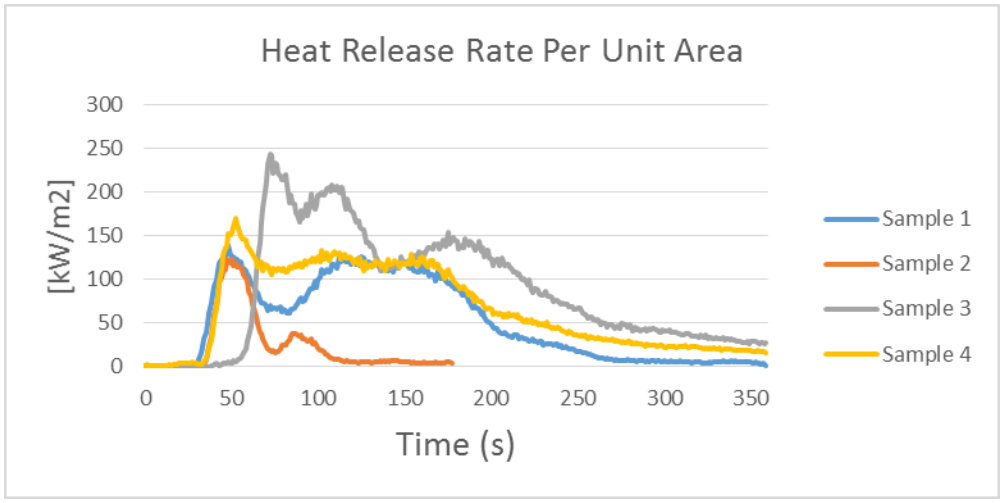

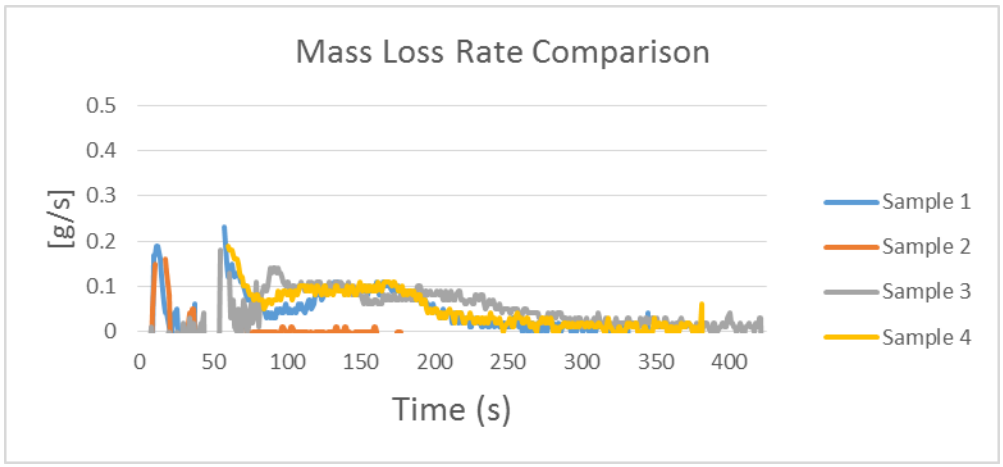

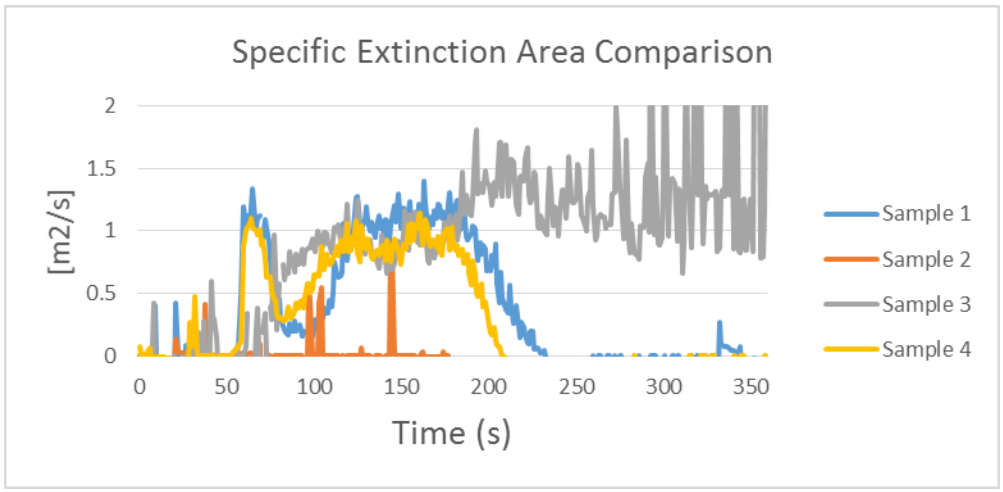

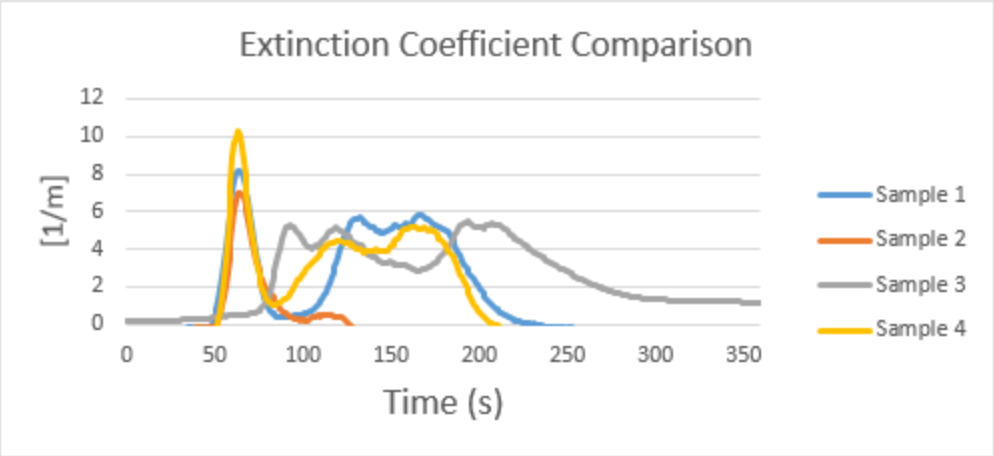

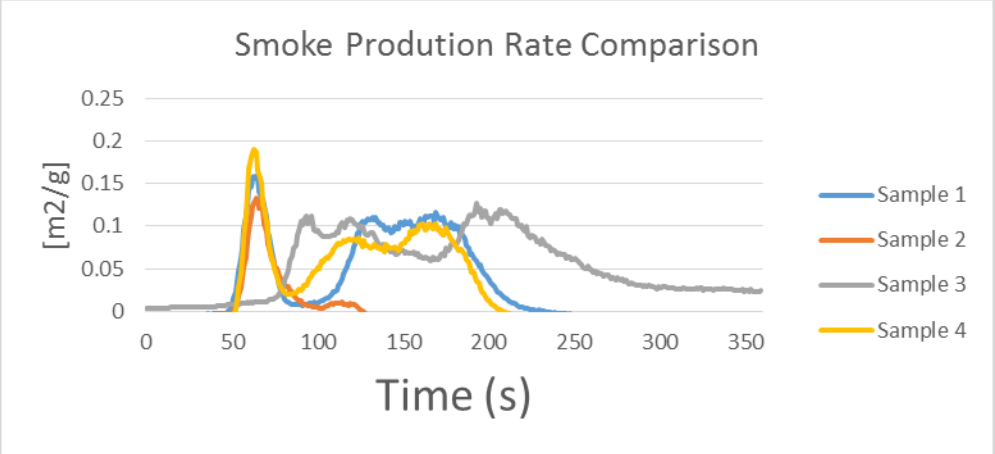

Hetron with ATH Ratio 100:66

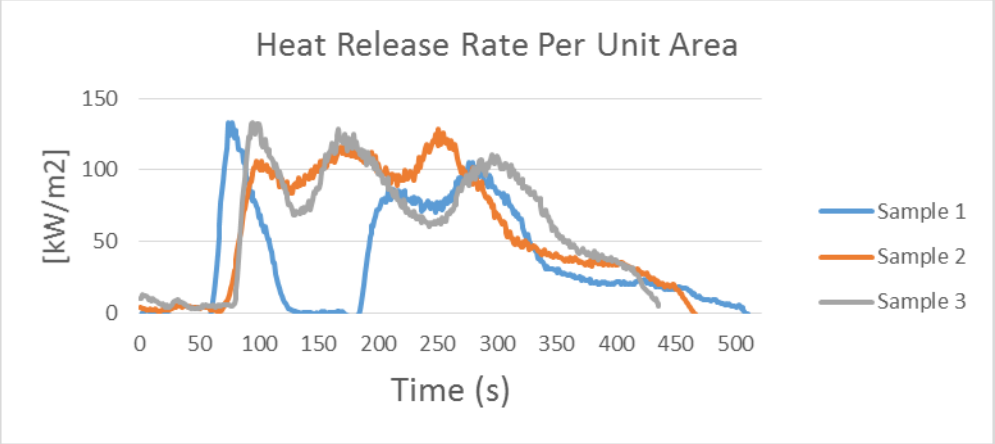

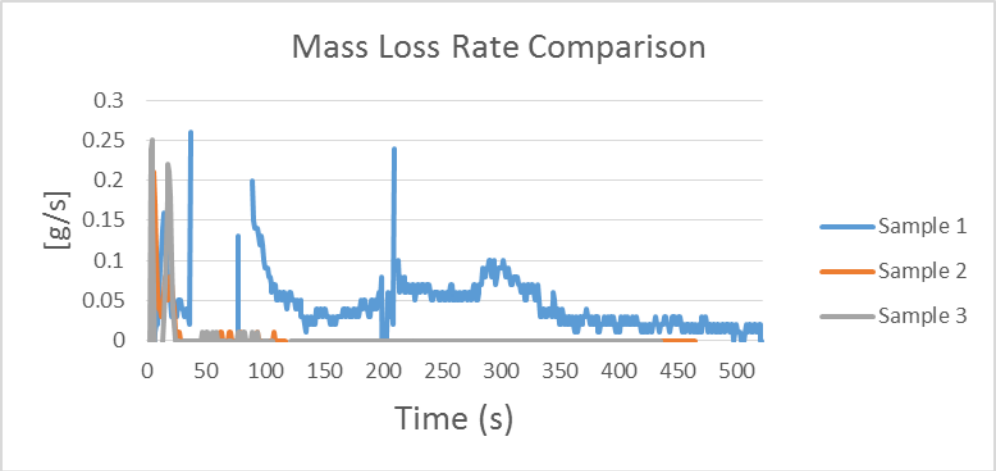
Mass Loss Rate Comparison
[g/s]
0.3
0.25
0.2
0.15
0.1
0.05
0
0 50 100 150 200 250 300 350 400 450 500
Time (s)
Sample 1
Sample 2
Sample 3

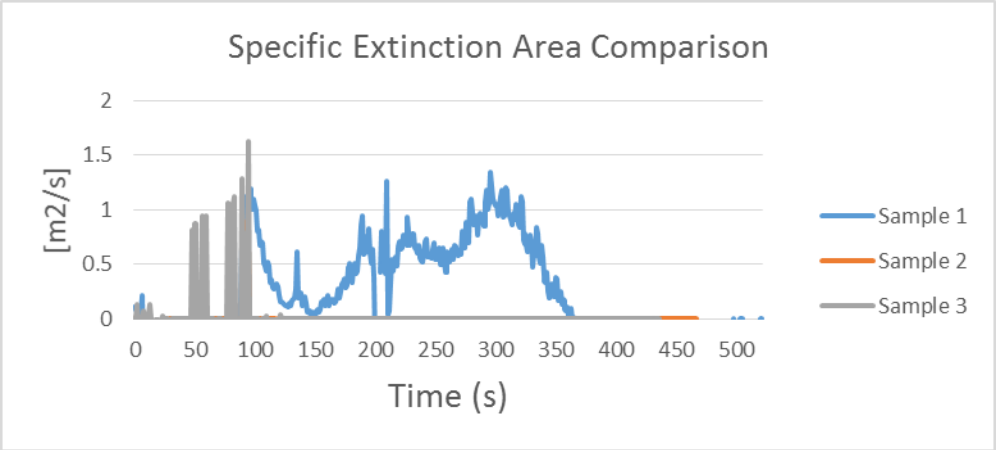
Specific Extinction Area Comparison
[m2/s]
2
1.5
1
0.5
0
0 50 100 150 200 250 300 350 400 450 500
Time (s)
Sample 1
Sample 2
Sample 3

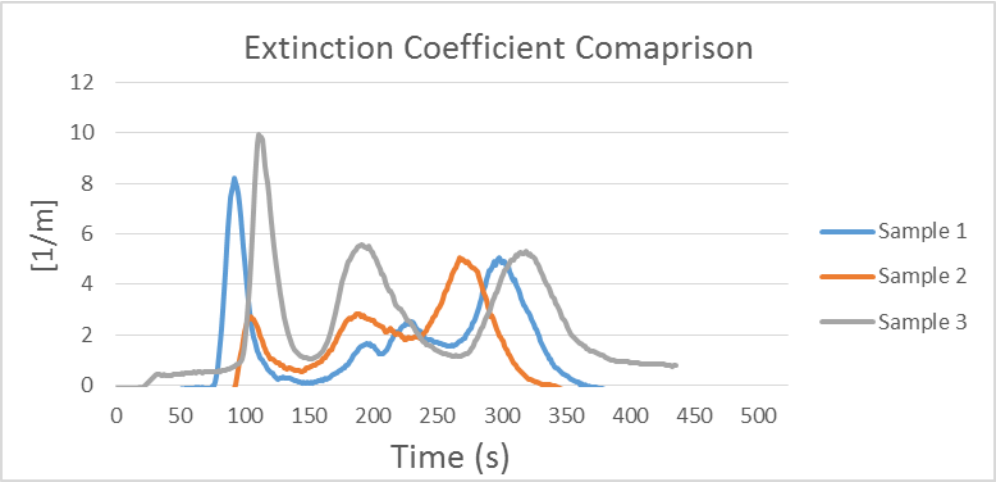
Extinction Coefficient Comaprison
[1/m]
12
10
8
6
4
2
0
0 50 100 150 200 250 300 350 400 450 500
Time (s)
Sample 1
Sample 2
Sample 3

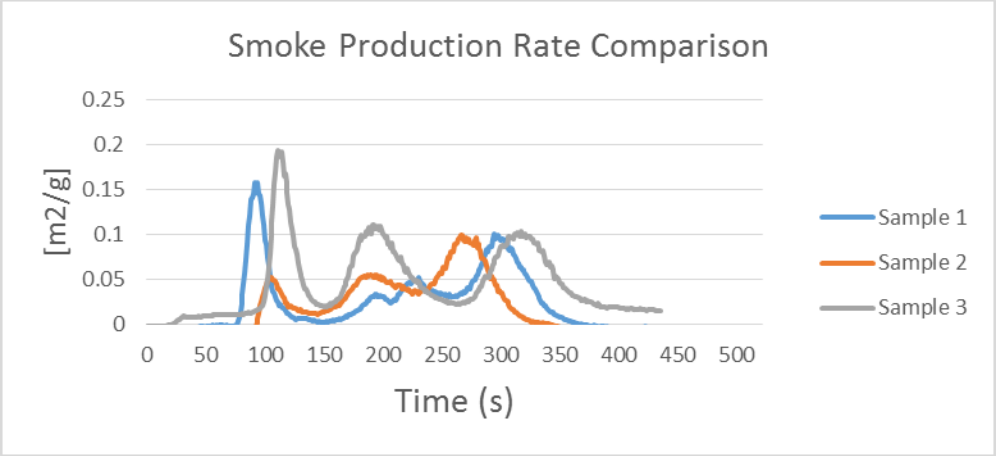

Hetron with ATH Ratio 100:100

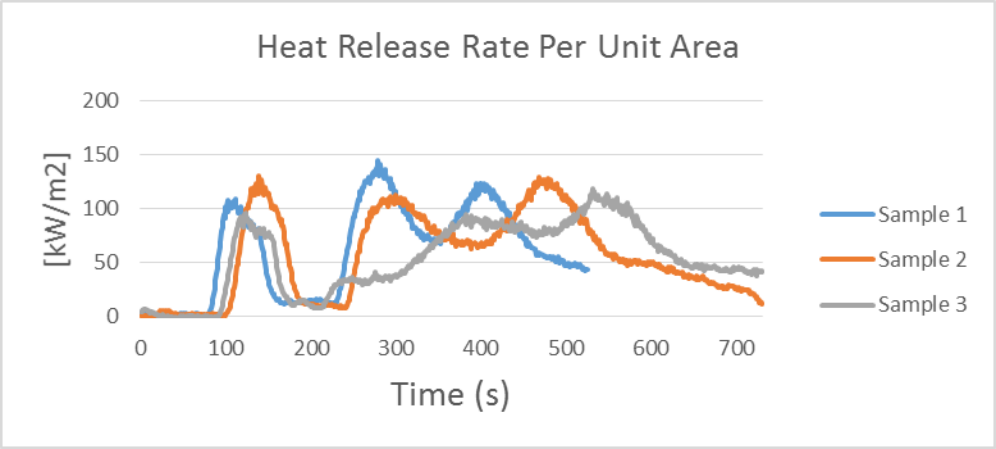

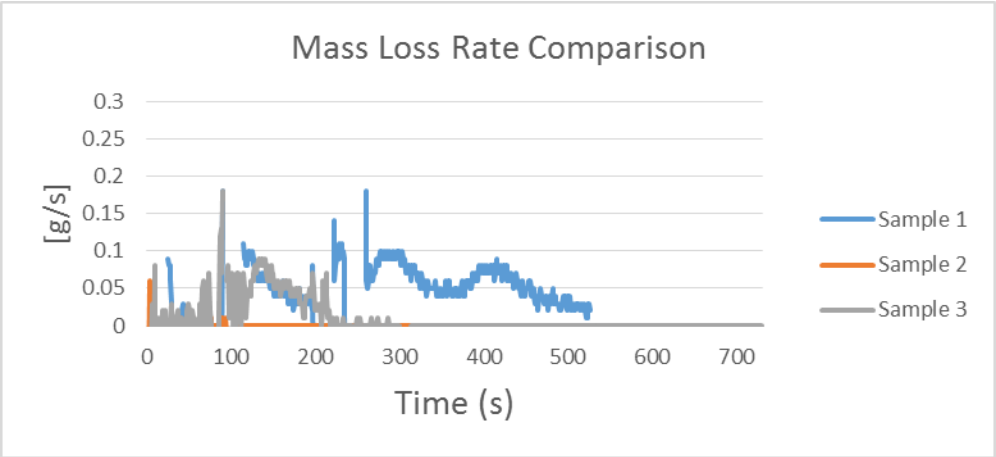

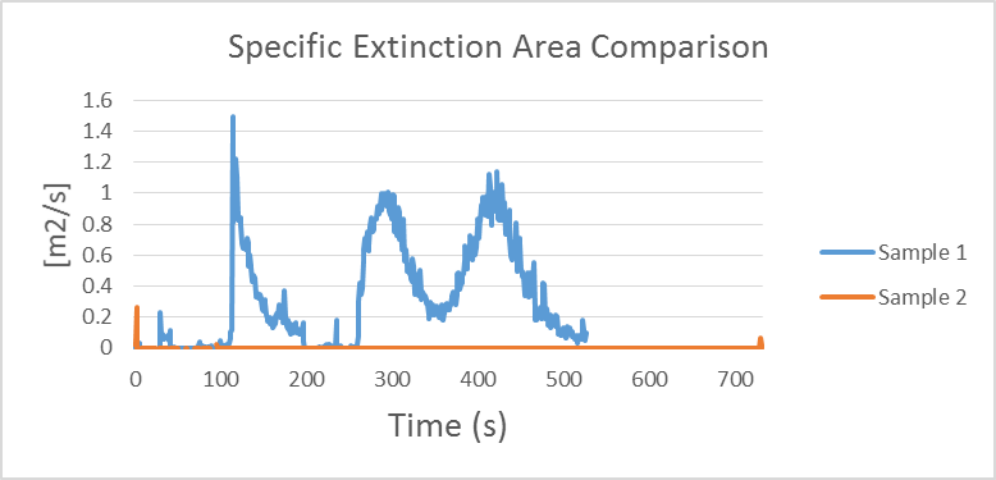
Specific Extinction Area Comparison
[m2/s]
1.6
1.4
1.2
1
0.8
0.6
0.4
0.2
0
0
100
200
300
400
500
600
700
Time (s)
Sample 1
Sample 2

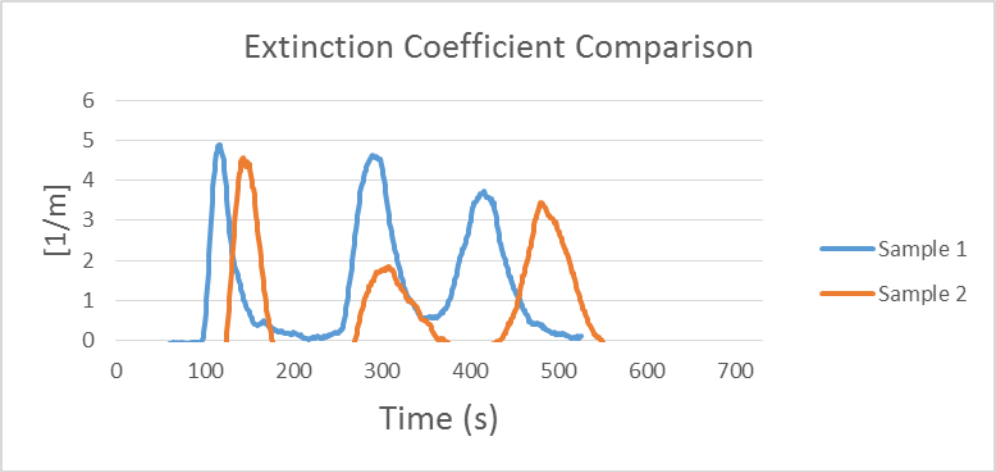
Extinction Coefficient Comparison
[1/m]
6
5
4
3
2
1
0
0
100
200
300
400
500
600
700
Time (s)
Sample 1
Sample 2

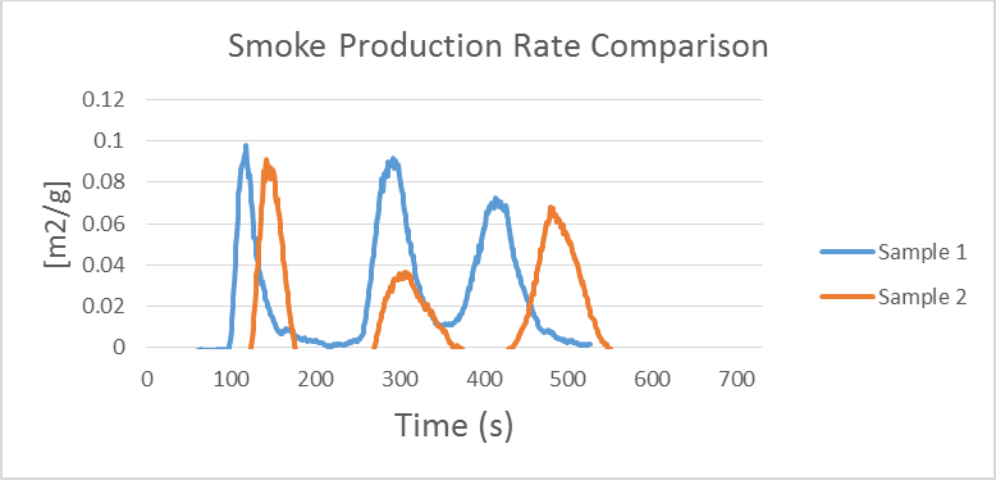
Smoke Production Rate Comparison
[m2/g]
0.12
0.1
0.08
0.06
0.04
0.02
0
0
100
200
300
400
500
600
700
Time (s)
Sample 1
Sample 2

Hetron with ATH Ratio 100:130

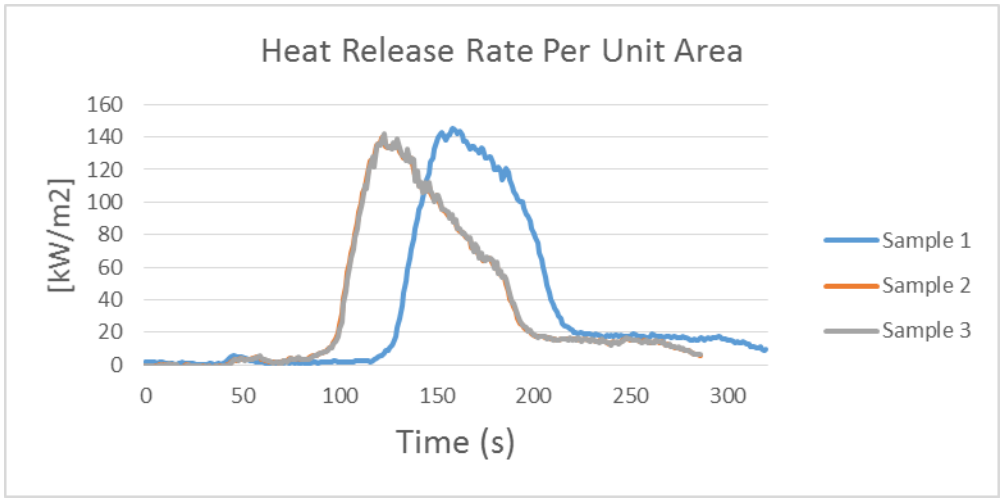

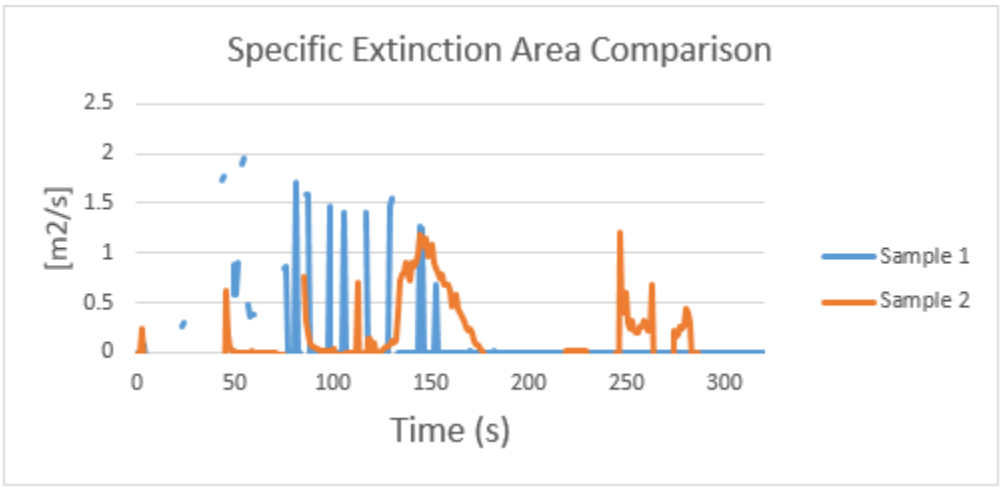

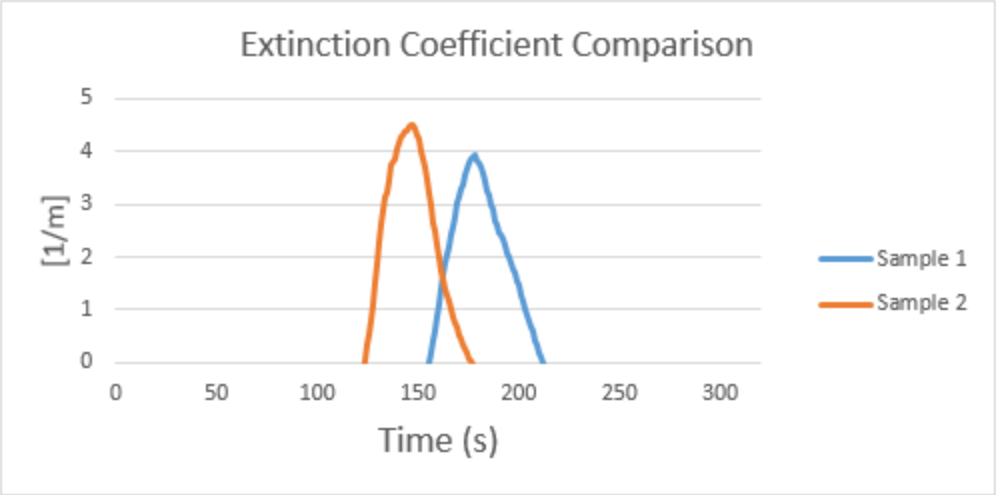

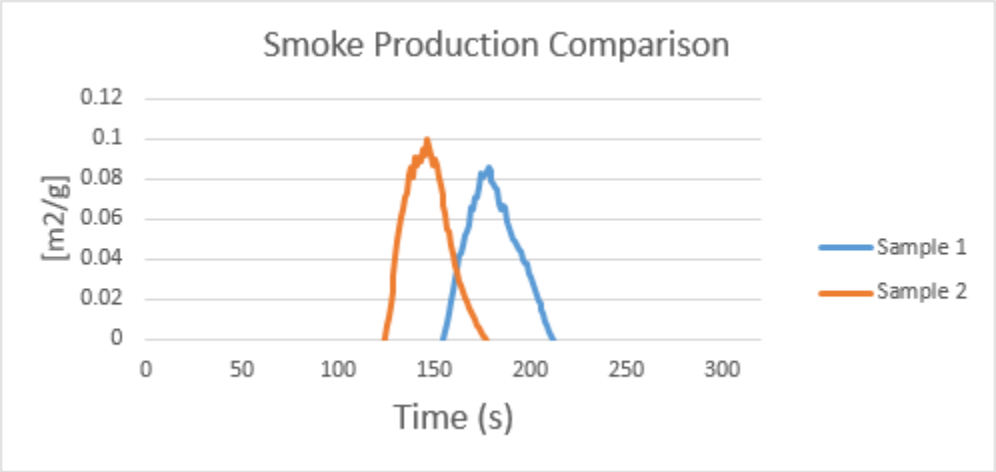

Fireblock with Sand Ratio 100:0

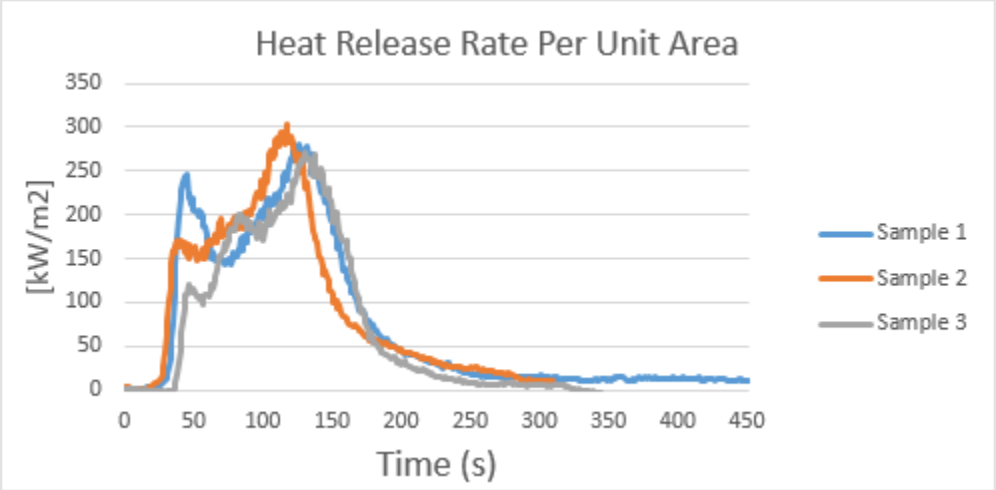

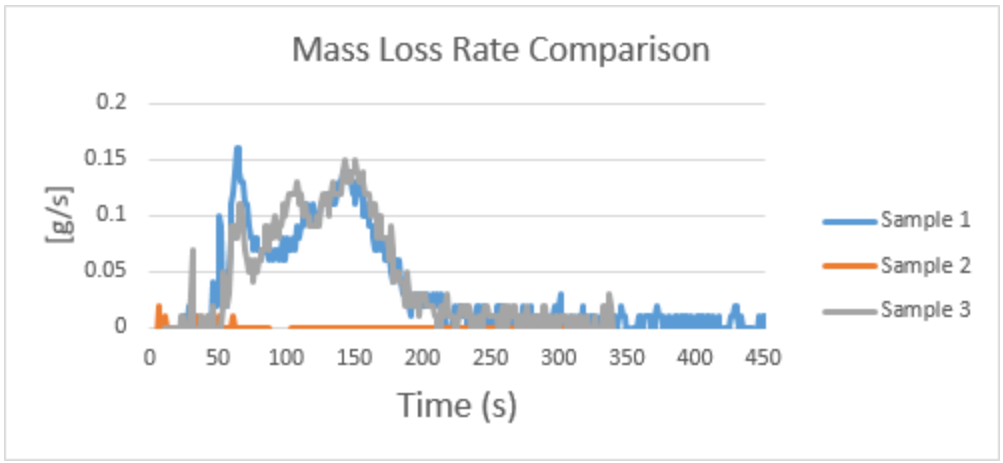
Mass Loss Rate Comparison
0.2
0.15
0.1
0.05
0
[g/s]
0
50
100
150
200
250
300
350
400
450
Time (s)
Sample 1
Sample 2
Sample 3

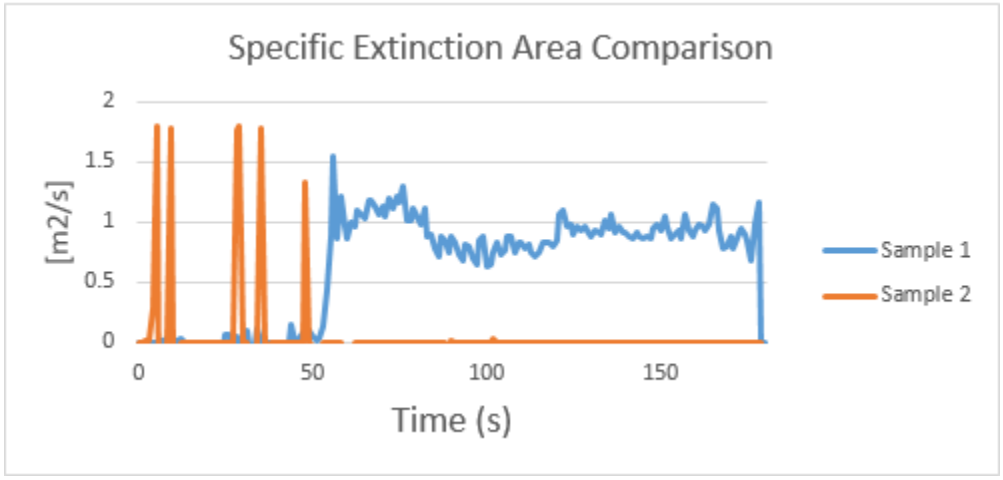
Specific Extinction Area Comparison
2
1.5
1
0.5
0
[m2/s]
0
50
100
150
Time (s)
Sample 1
Sample 2

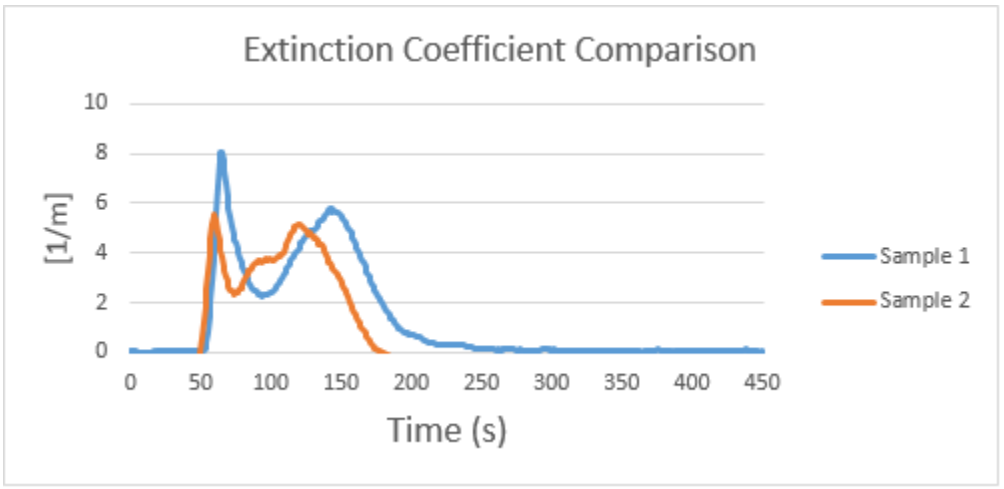
Extinction Coefficient Comparison
10
8
6
4
2
0
[1/m]
0
50
100
150
200
250
300
350
400
450
Time (s)
Sample 1
Sample 2

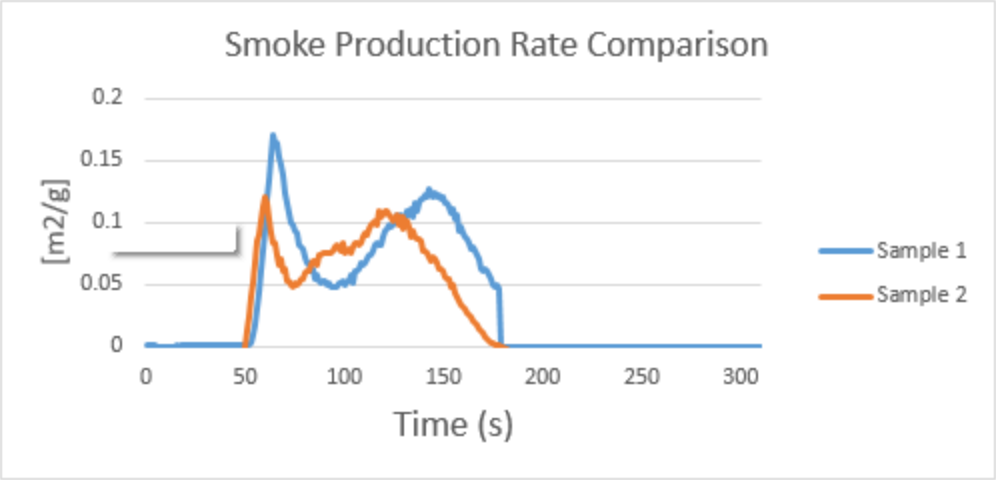

Fireblock with Sand Ratio 70:30

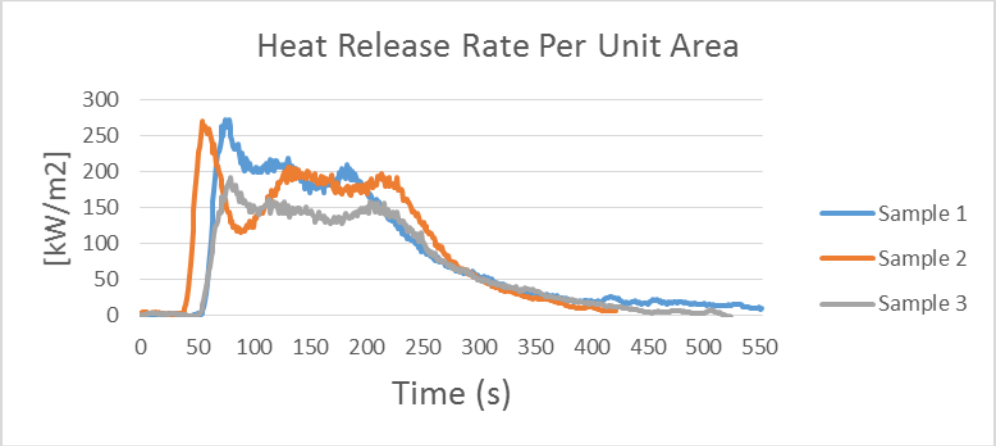

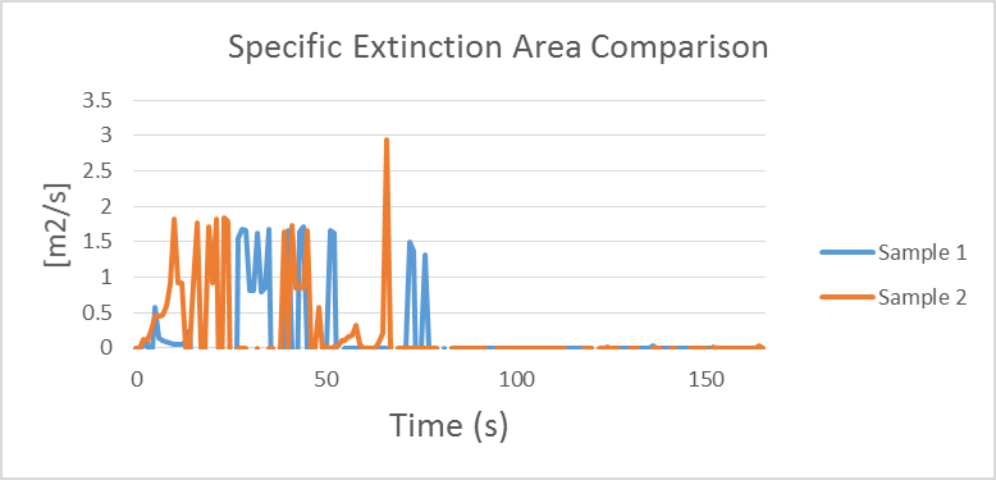
Specific Extinction Area Comparison
[m2/s]
3.5
3
2.5
2
1.5
1
0.5
0
0
50
100
150
Time (s)
Sample 1
Sample 2

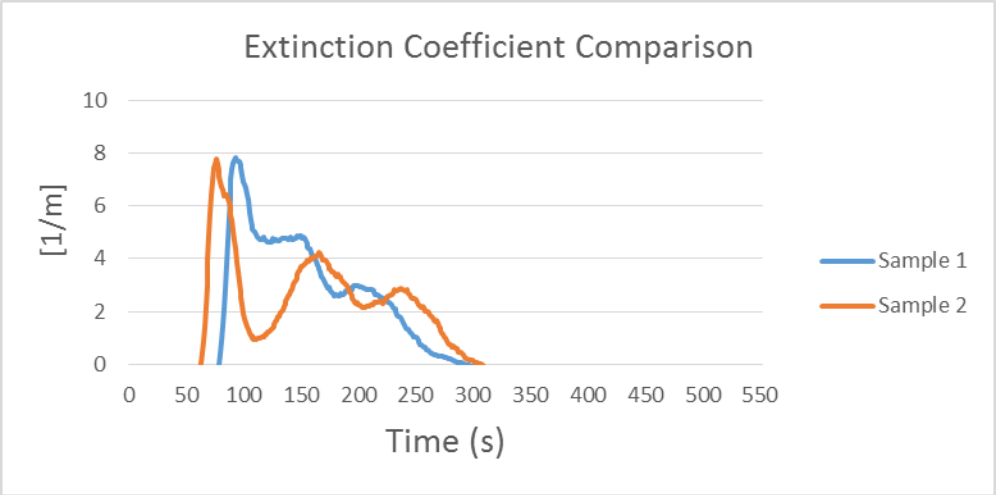
Extinction Coefficient Comparison
[1/m]
10
8
6
4
2
0
0 50 100 150 200 250 300 350 400 450 500 550
Time (s)
Sample 1
Sample 2

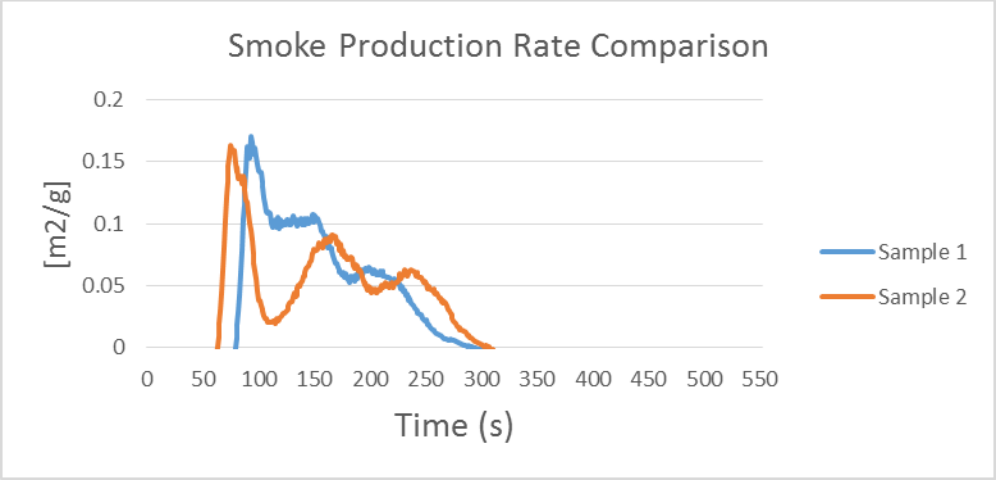
Smoke Production Rate Comparison
[m2/g]
0.2
0.15
0.1
0.05
0
0 50 100 150 200 250 300 350 400 450 500 550
Time (s)
Sample 1
Sample 2

Fireblock with Sand Ratio 60:40

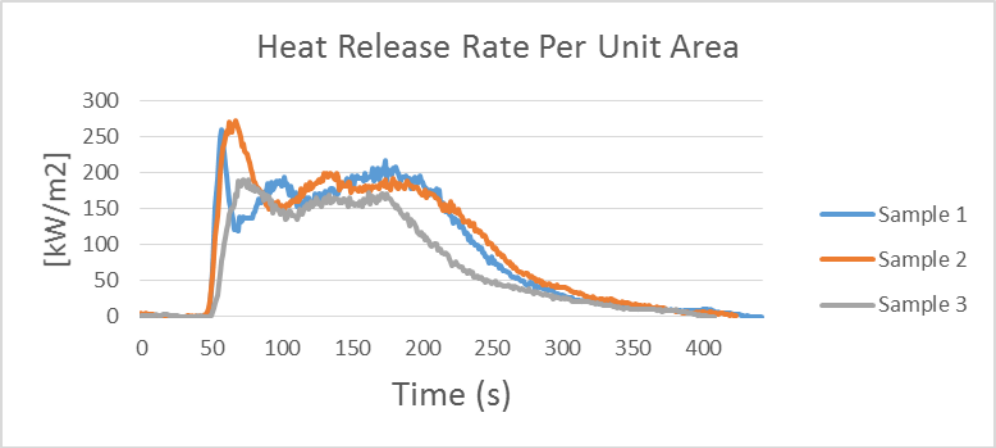

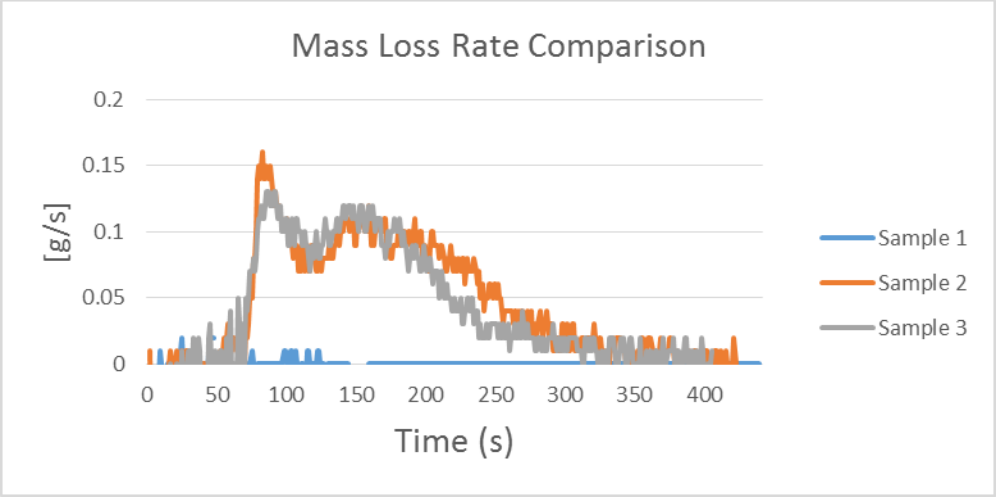

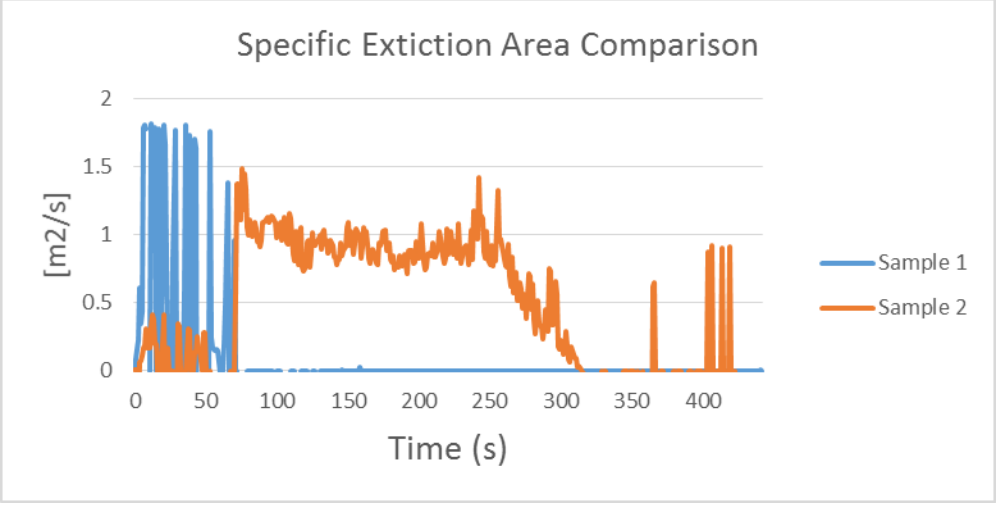

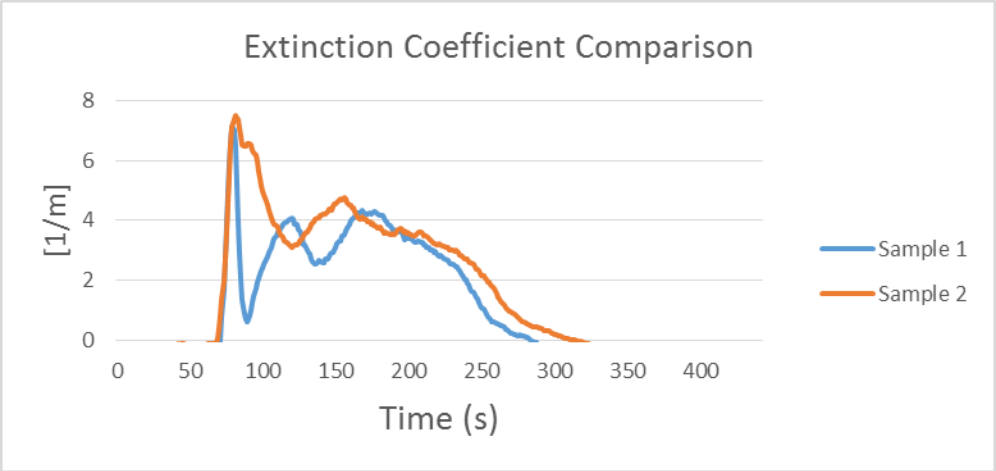

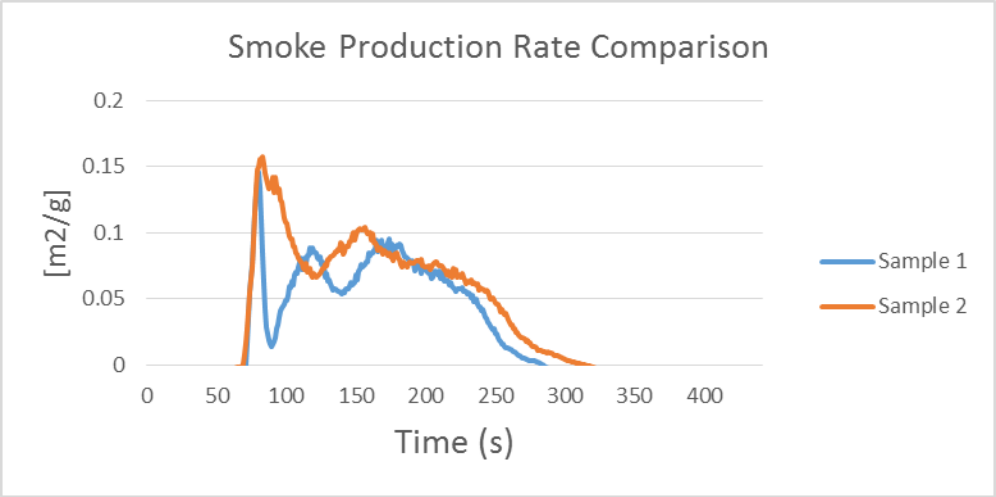

Fireblock with Sand Ratio 50:50

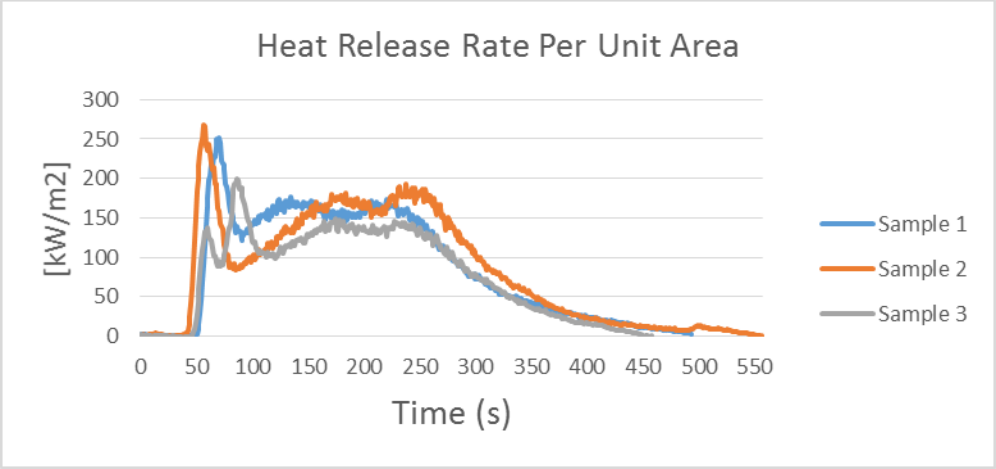

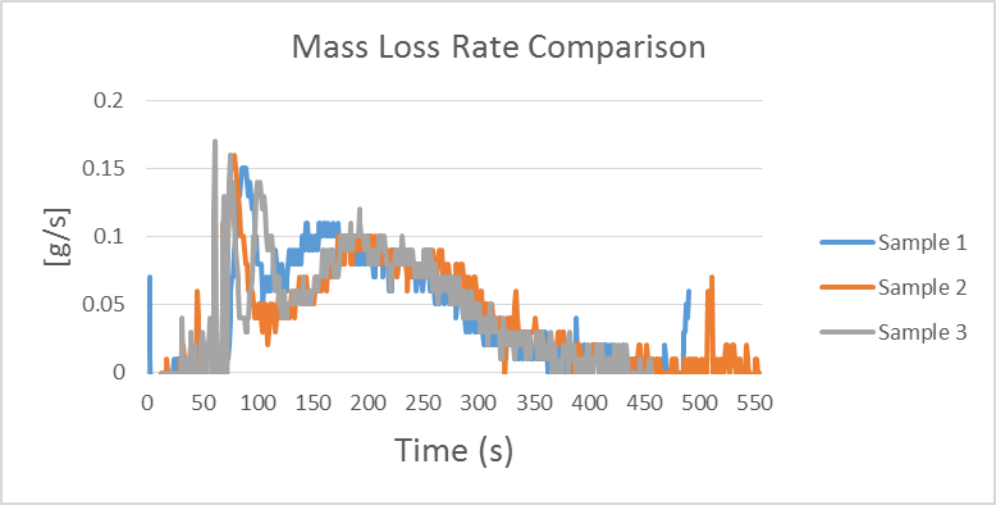
Mass Loss Rate Comparison
0.2
0.15
0.1
0.05
0
[g/s]
0 50 100 150 200 250 300 350 400 450 500 550
Time (s)
Sample 1
Sample 2
Sample 3

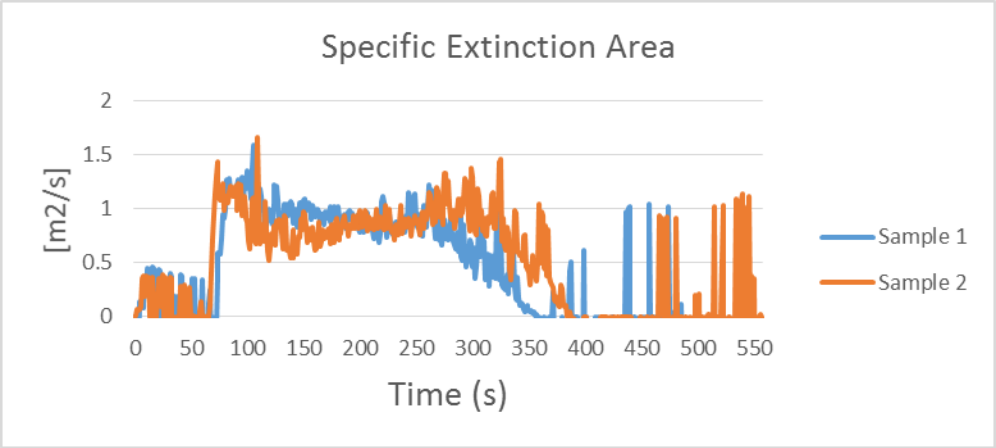
Specific Extinction Area
2
1.5
1
0.5
0
[m2/s]
0 50 100 150 200 250 300 350 400 450 500 550
Time (s)
Sample 1
Sample 2

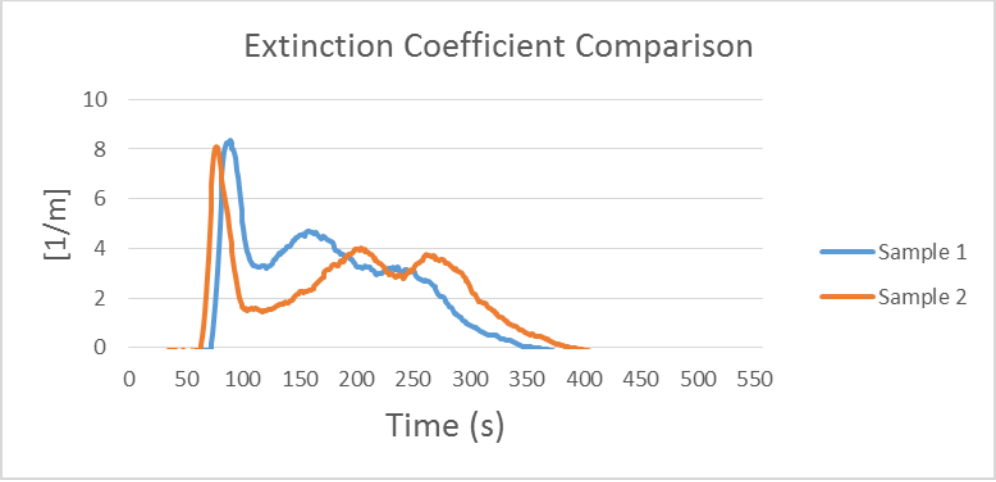
Extinction Coefficient Comparison
10
8
6
4
2
0
[1/m]
0 50 100 150 200 250 300 350 400 450 500 550
Time (s)
Sample 1
Sample 2

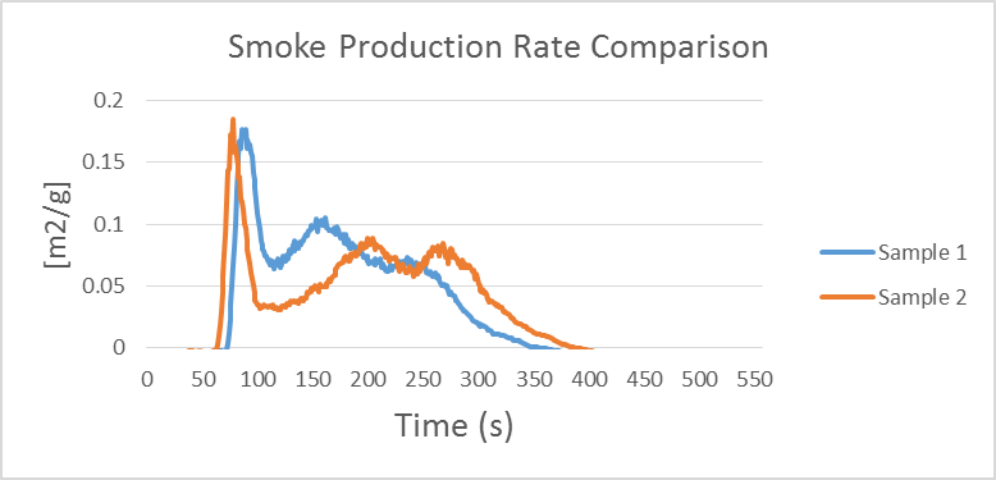

Fireblock with Sand Ratio 40:60

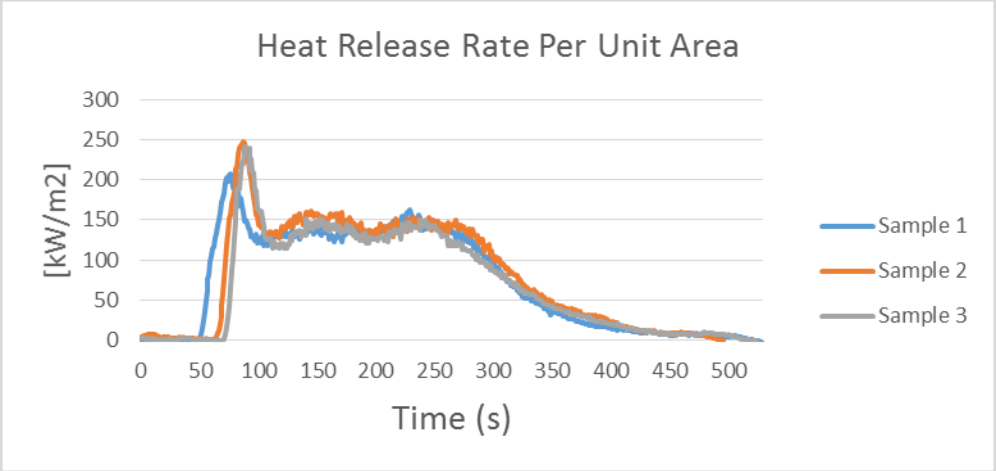

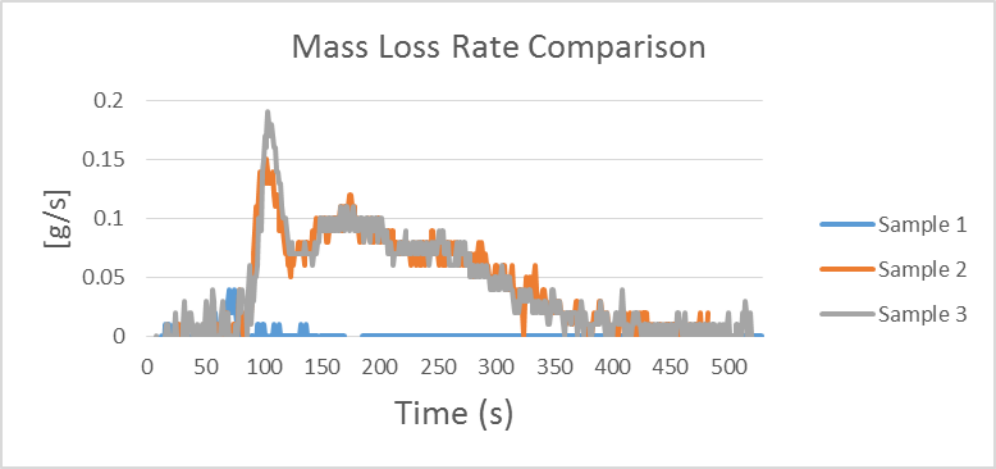

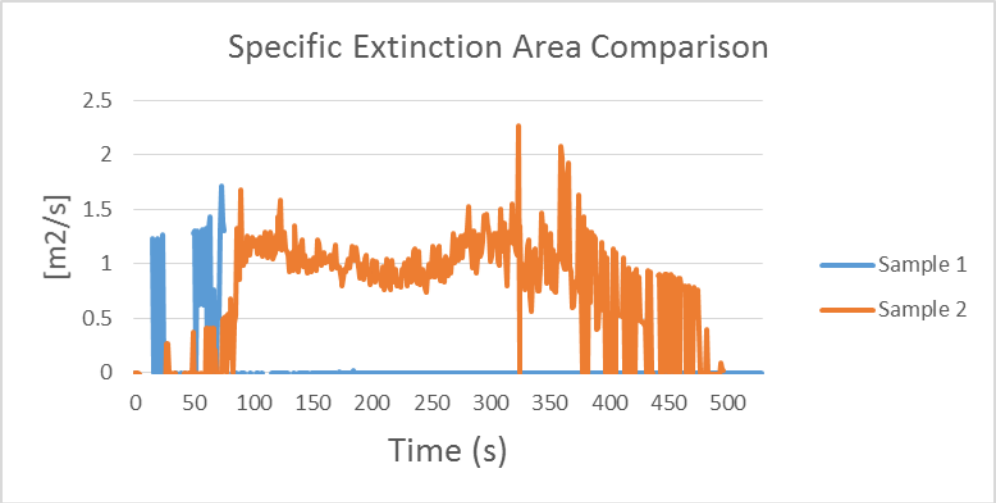
Specific Extinction Area Comparison
[m2/s]
2.5
2
1.5
1
0.5
0
0 50 100 150 200 250 300 350 400 450 500
Time (s)
Sample 1
Sample 2

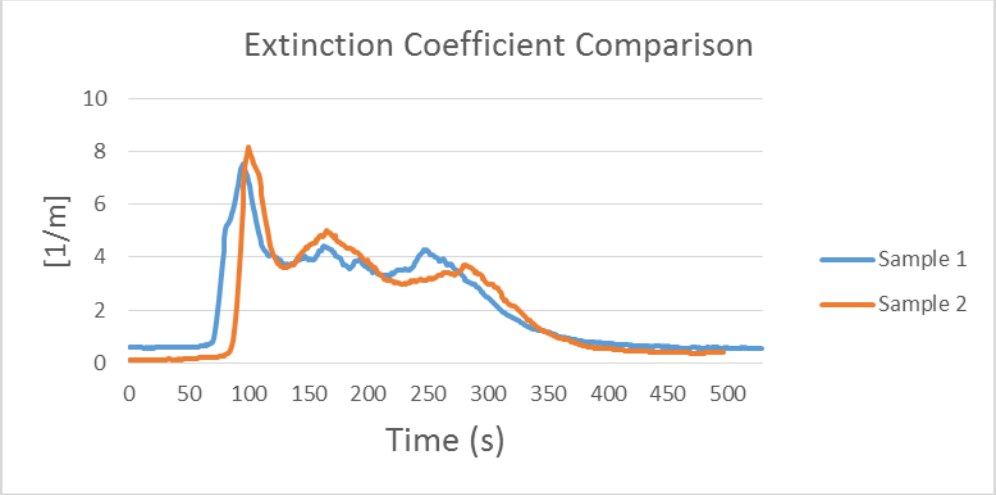
Extinction Coefficient Comparison
[1/m]
10
8
6
4
2
0
0 50 100 150 200 250 300 350 400 450 500
Time (s)
Sample 1
Sample 2

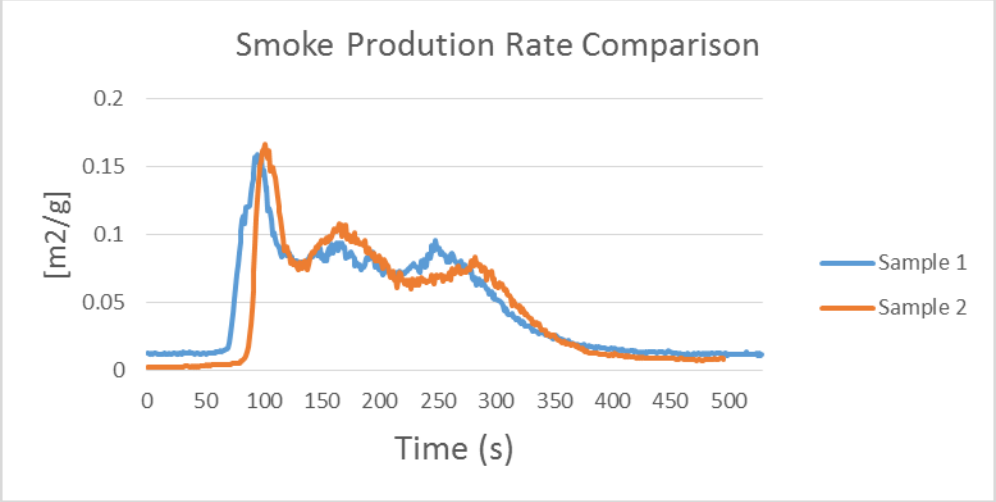
Smoke Prodution Rate Comparison
[m2/g]
0.2
0.15
0.1
0.05
0
0 50 100 150 200 250 300 350 400 450 500
Time (s)
Sample 1
Sample 2

Epoxy 100:0

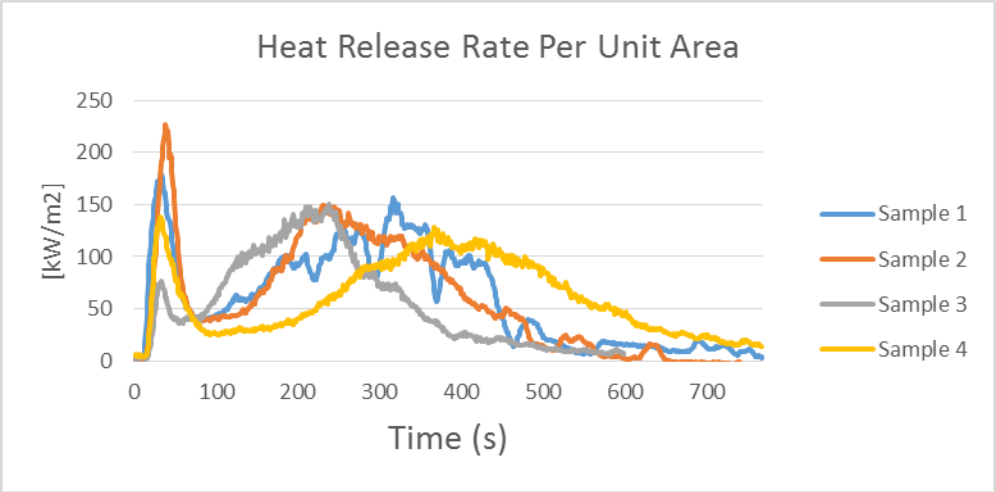
Heat Release Rate Per Unit Area
250
200
150
100
50
0
[kW/m2]
0
100
200
300
400
500
600
700
Time (s)
Sample 1
Sample 2
Sample 3
Sample 4


Mass Loss Rate Comparison
0.25
0.2
0.15
0.1
0.05
0
[g/s]
0
100
200
300
400
500
600
700
Time (s)
Sample 1
Sample 2
Sample 3
Sample 4

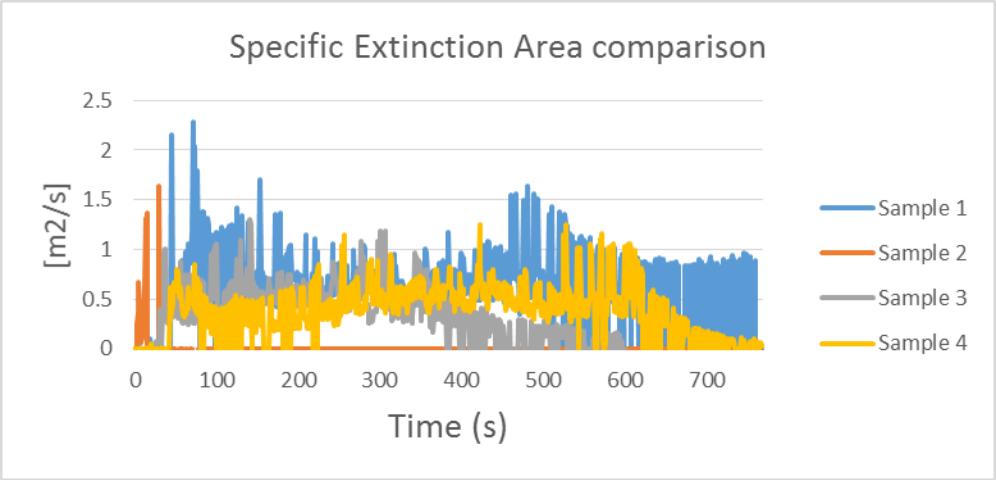
Specific Extinction Area comparison
2.5
2
1.5
1
0.5
0
[m2/s]
0
100
200
300
400
500
600
700
Time (s)
Sample 1
Sample 2
Sample 3
Sample 4

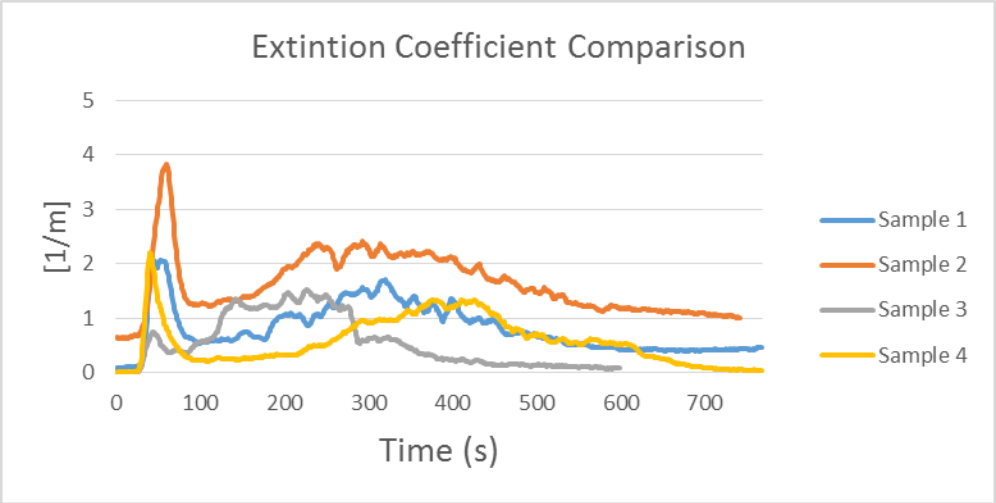

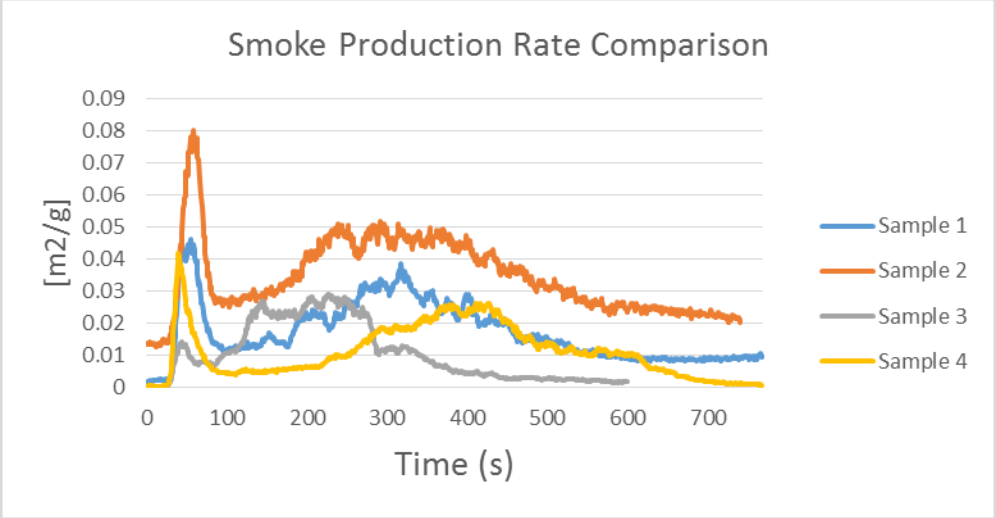

25 kW Heat Flux Test

Hetron with ATH Ratio 100:0

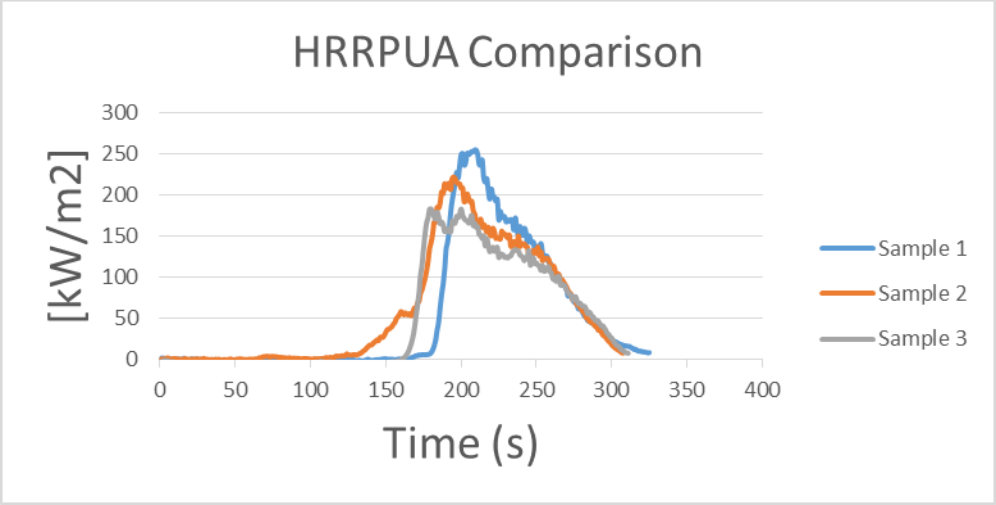

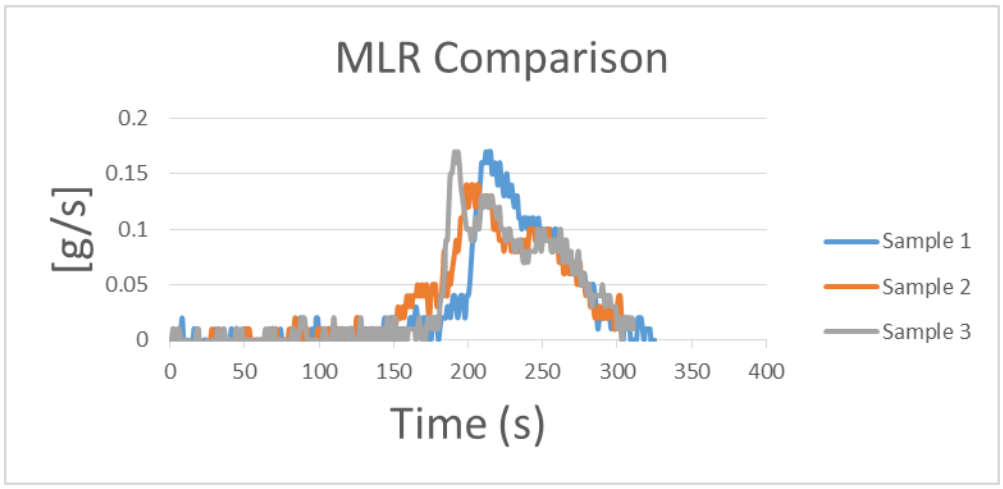
MLR Comparison
[g/s]
0.2
0.15
0.1
0.05
0
0
50
100
150
200
250
300
350
400
Time (s)
Sample 1
Sample 2
Sample 3

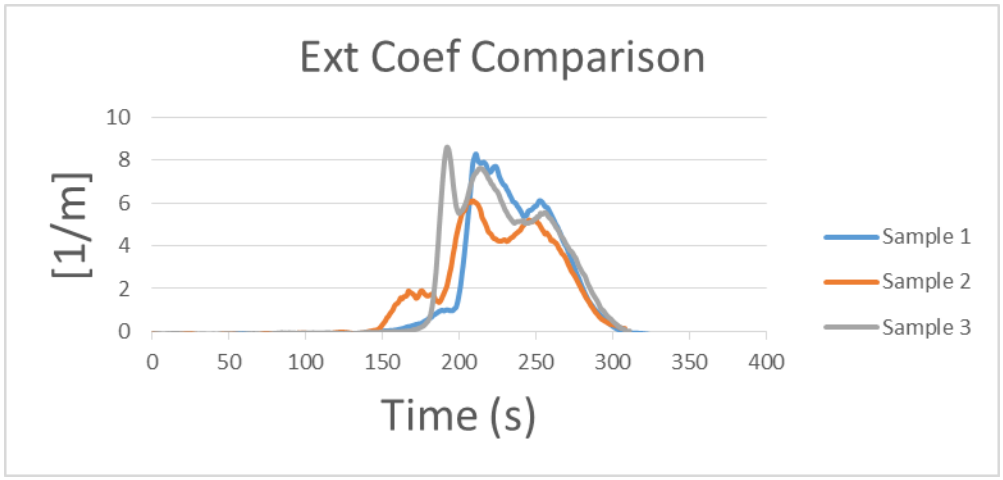
Ext Coef Comparison
[1/m]
10
8
6
4
2
0
0
50
100
150
200
250
300
350
400
Time (s)
Sample 1
Sample 2
Sample 3

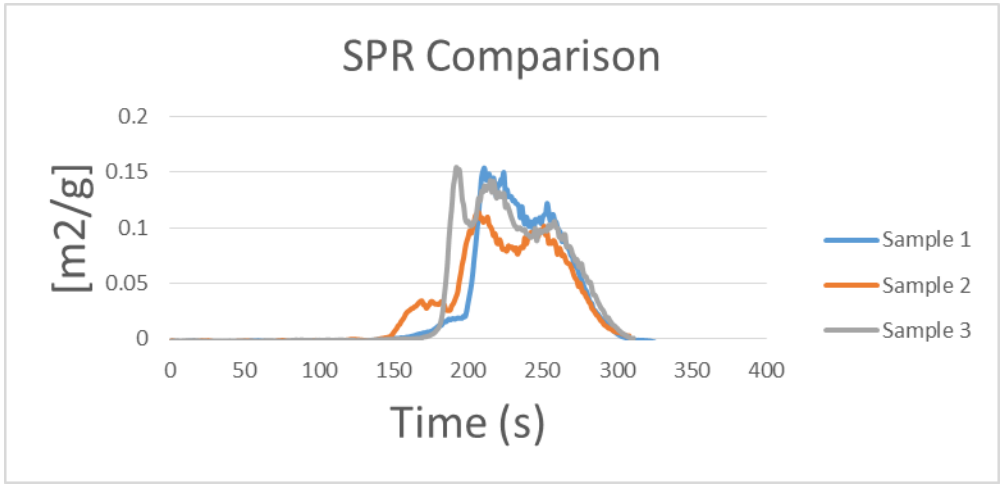
SPR Comparison
[m2/g]
0.2
0.15
0.1
0.05
0
0
50
100
150
200
250
300
350
400
Time (s)
Sample 1
Sample 2
Sample 3

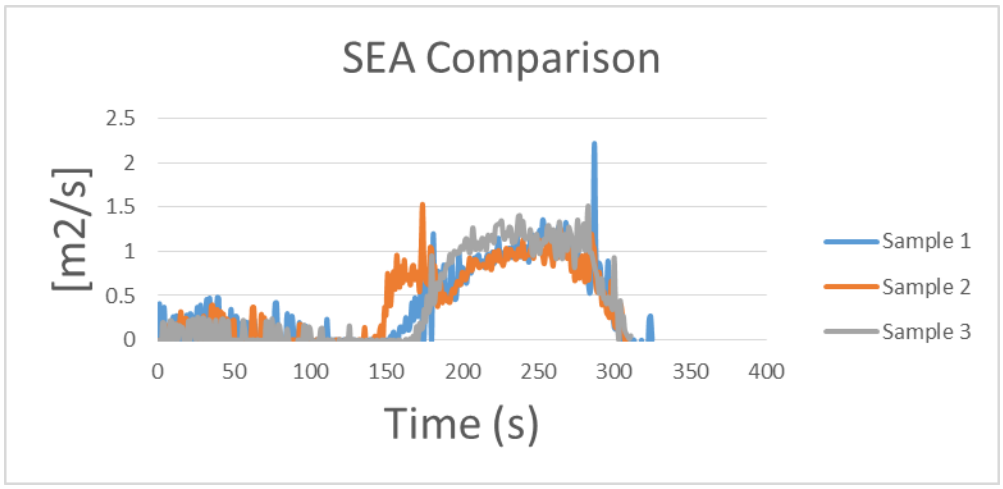

Hetron with ATH Ratio 100:100

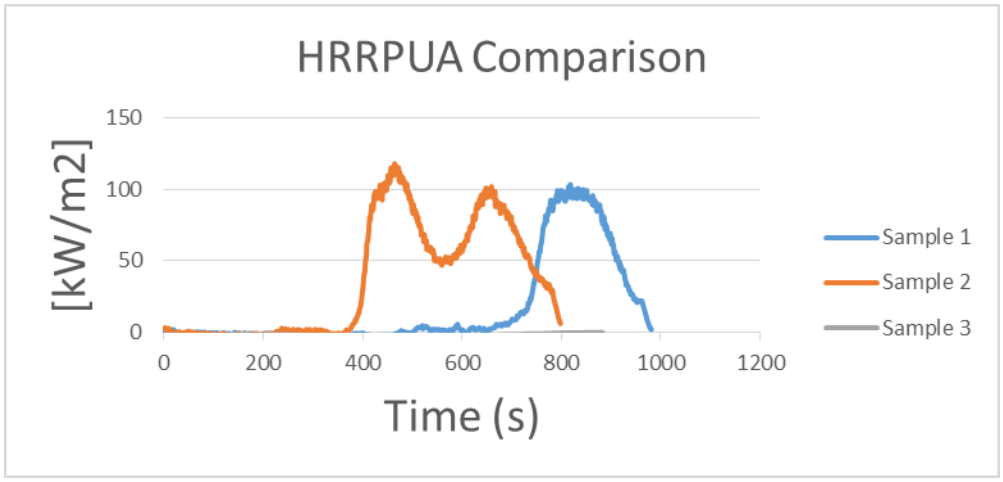

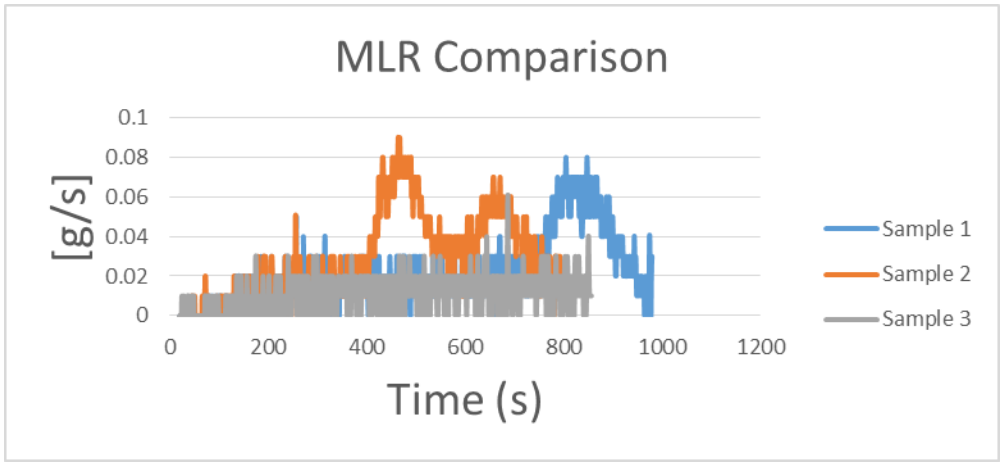

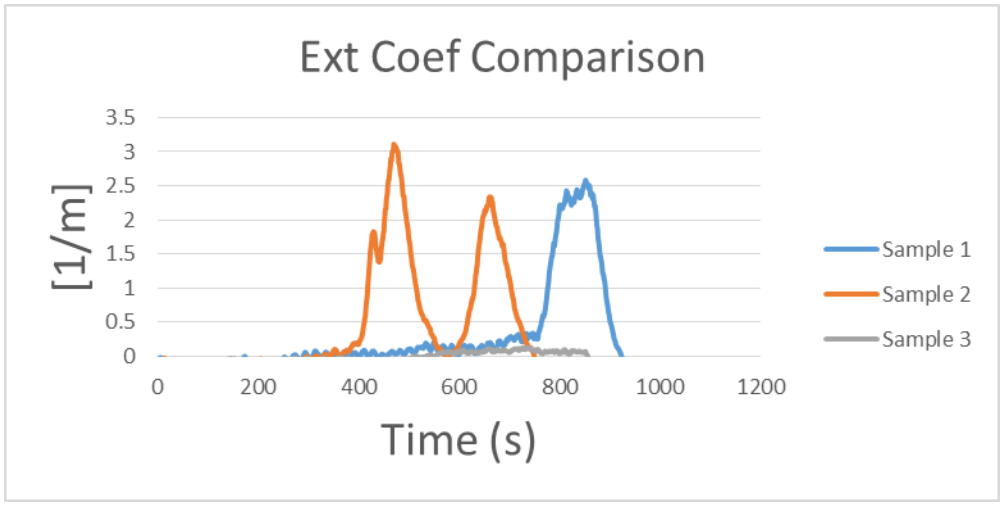
Ext Coef Comparison
[1/m]
3.5
3
2.5
2
1.5
1
0.5
0
0
200
400
600
800
1000
1200
Time (s)
Sample 1
Sample 2
Sample 3

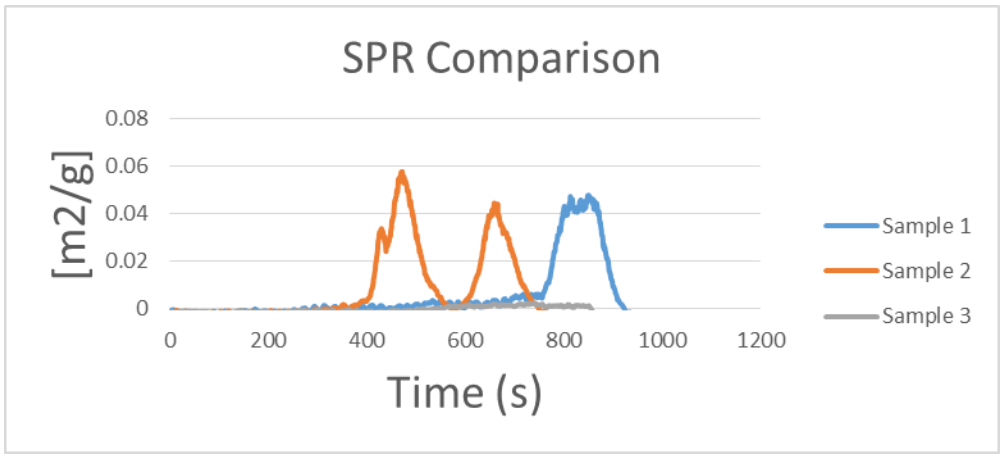
SPR Comparison
[m2/g]
0.08
0.06
0.04
0.02
0
0
200
400
600
800
1000
1200
Time (s)
Sample 1
Sample 2
Sample 3

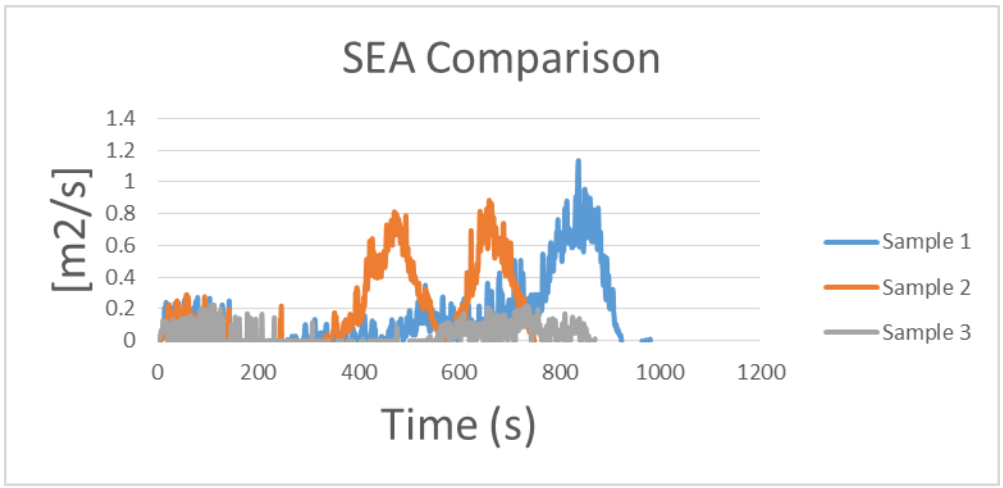
SEA Comparison
[m2/s]
1.4
1.2
1
0.8
0.6
0.4
0.2
0
0
200
400
600
800
1000
1200
Time (s)
Sample 1
Sample 2
Sample 3

Hetron with ATH Ratio 100:130

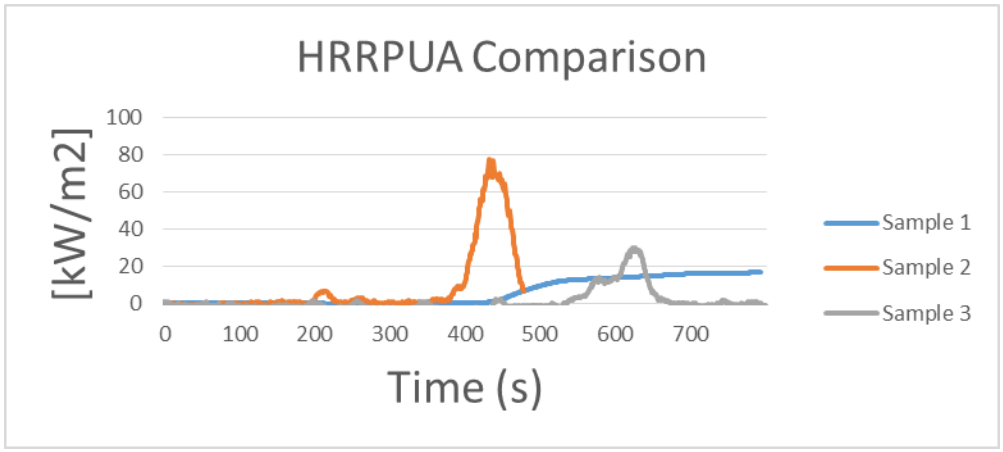

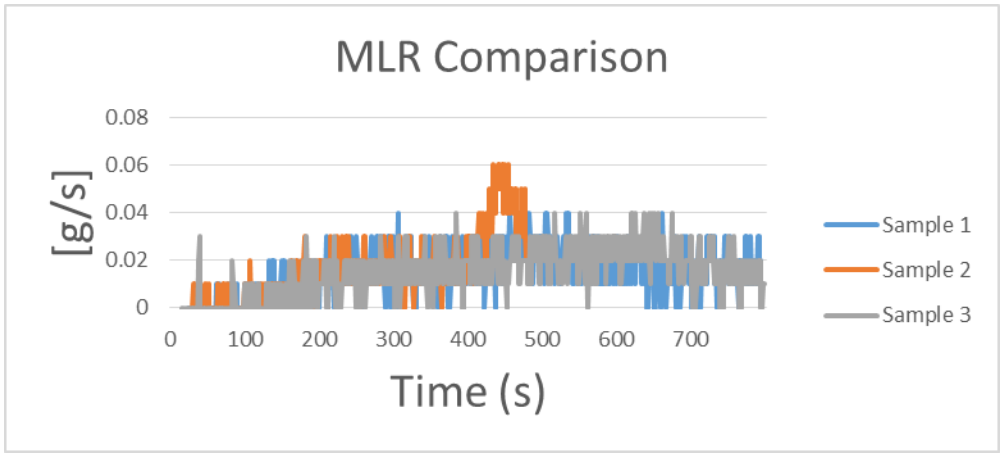

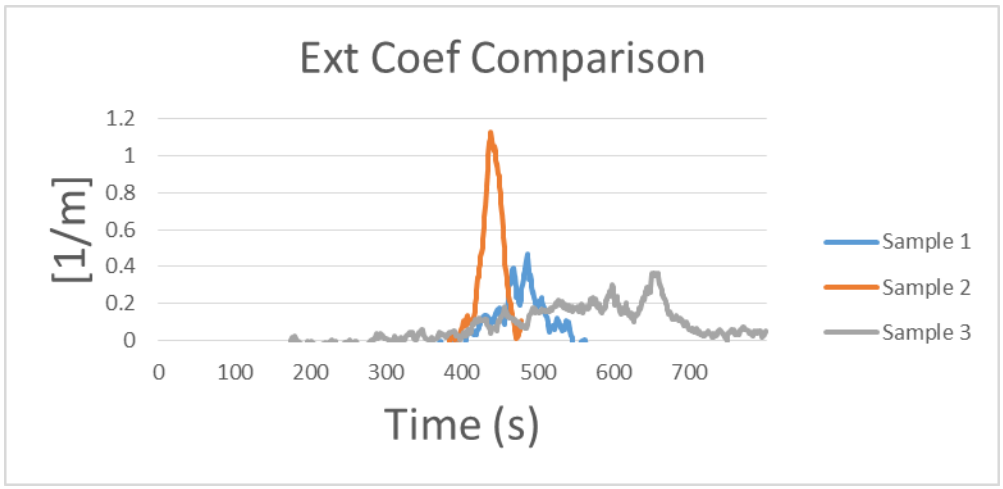

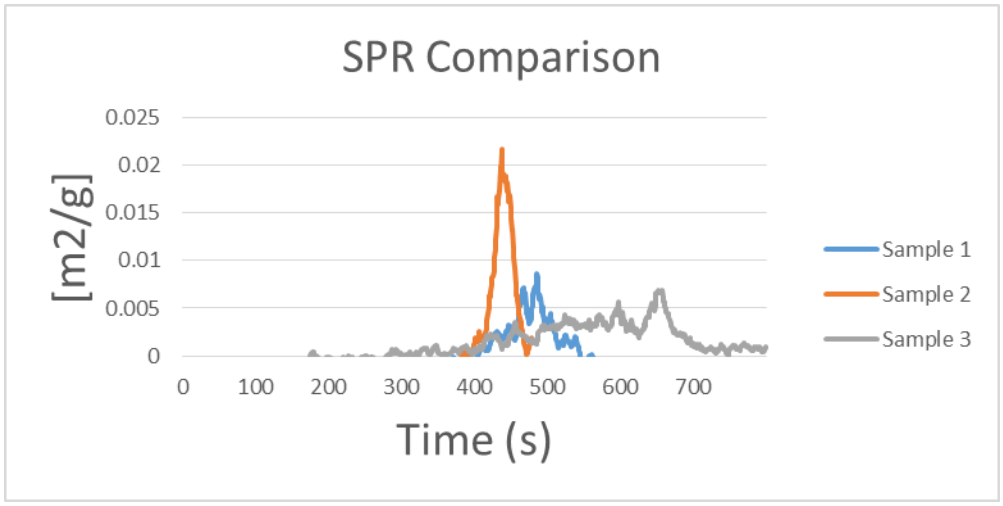

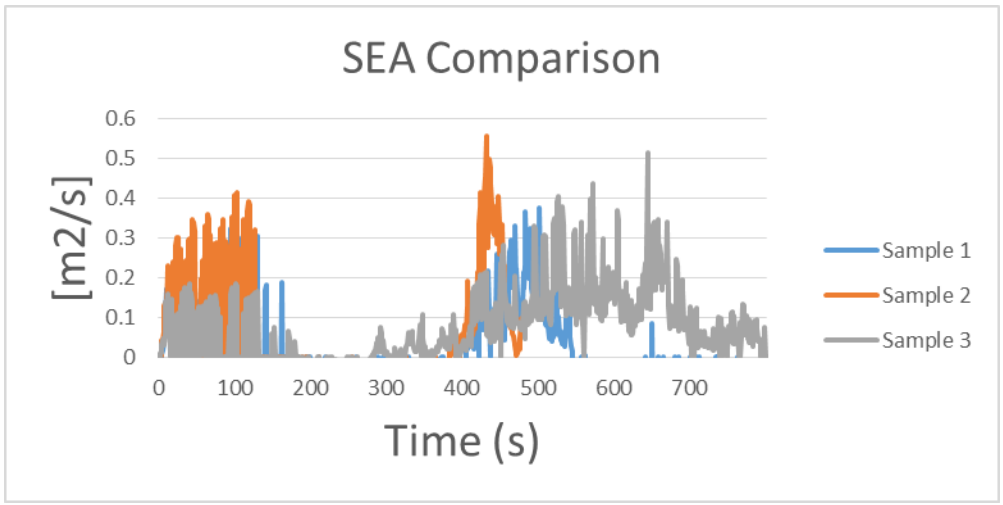

Fireblock with Sand Ratio 100:0

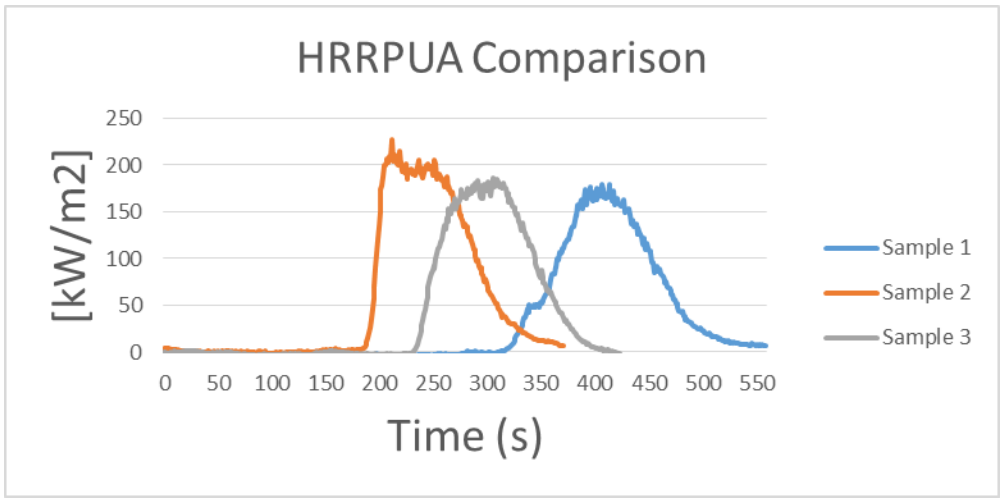

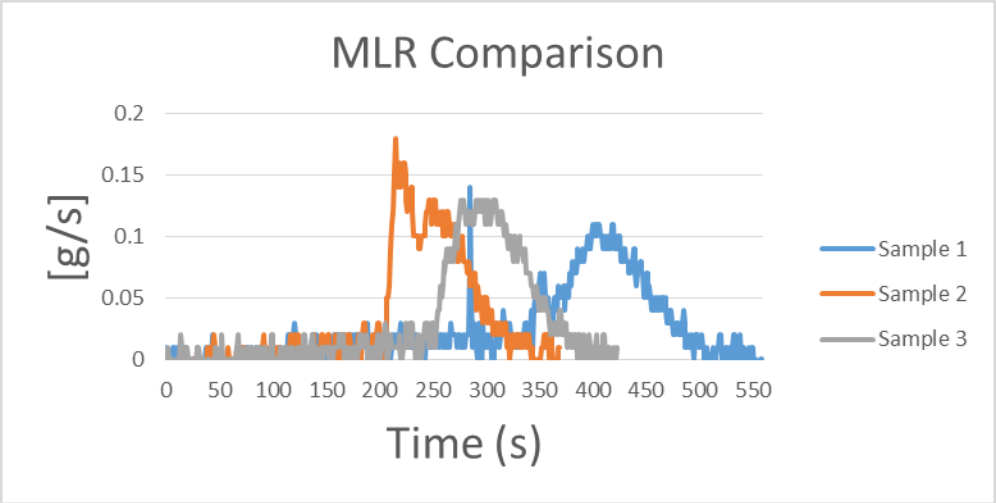
MLR Comparison
[g/s]
0.2
0.15
0.1
0.05
0
0 50 100 150 200 250 300 350 400 450 500 550
Time (s)
Sample 1
Sample 2
Sample 3

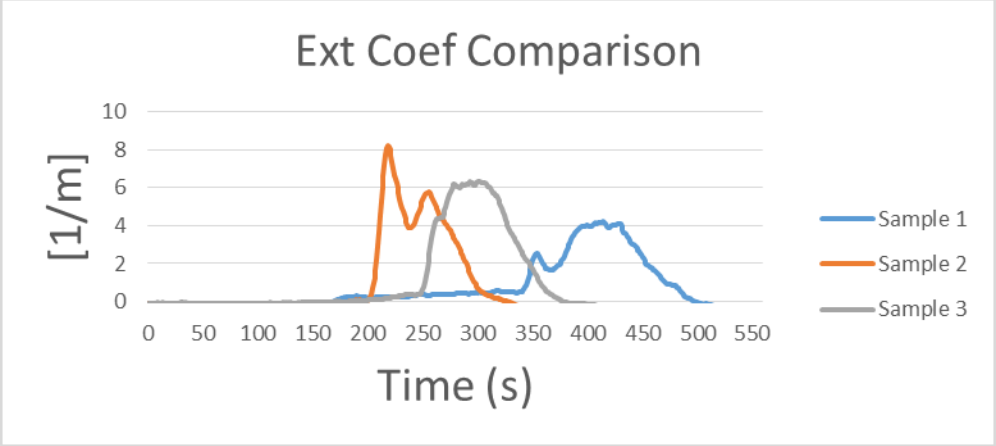
Ext Coef Comparison
[1/m]
10
8
6
4
2
0
0 50 100 150 200 250 300 350 400 450 500 550
Time (s)
Sample 1
Sample 2
Sample 3

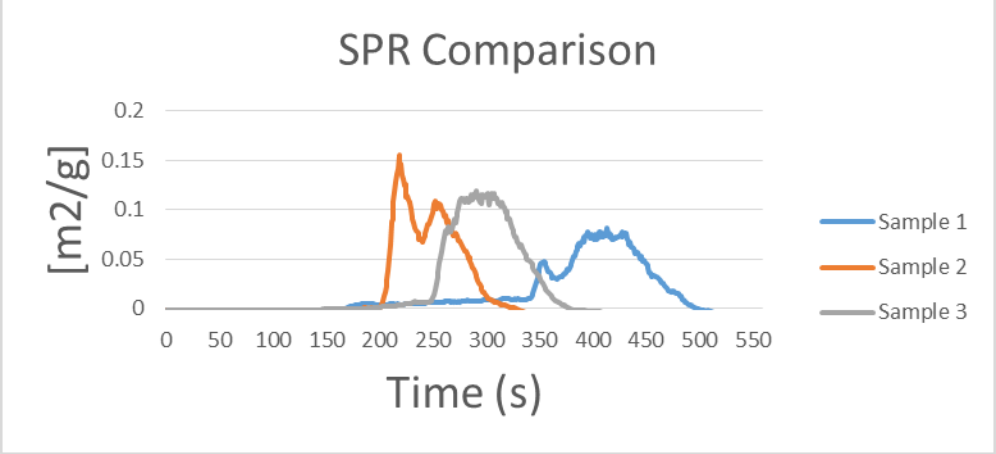
SPR Comparison
[m2/g]
0.2
0.15
0.1
0.05
0
0 50 100 150 200 250 300 350 400 450 500 550
Time (s)
Sample 1
Sample 2
Sample 3

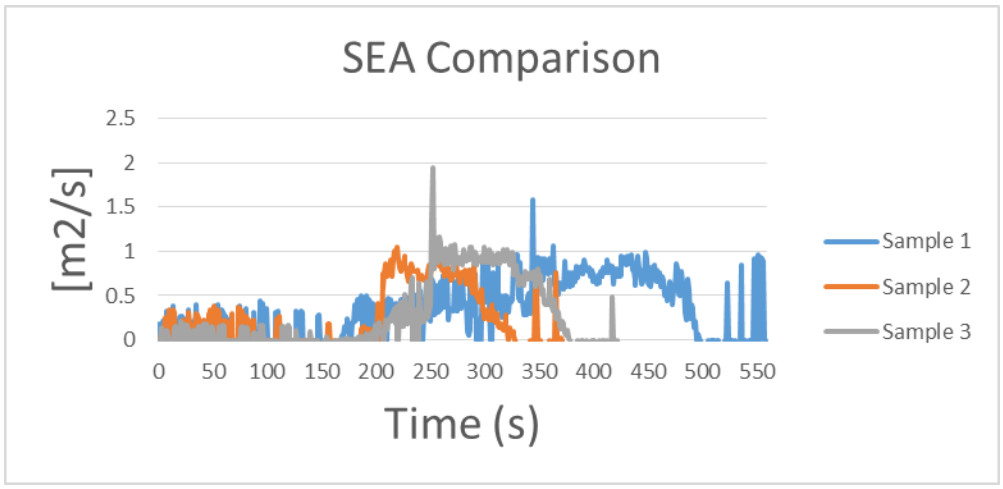

Fireblock with Sand Ratio 60:40

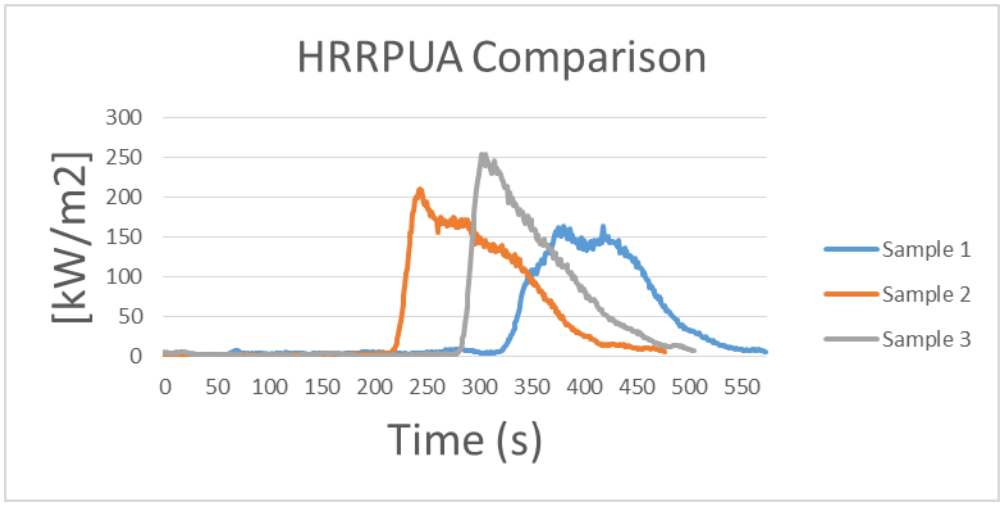

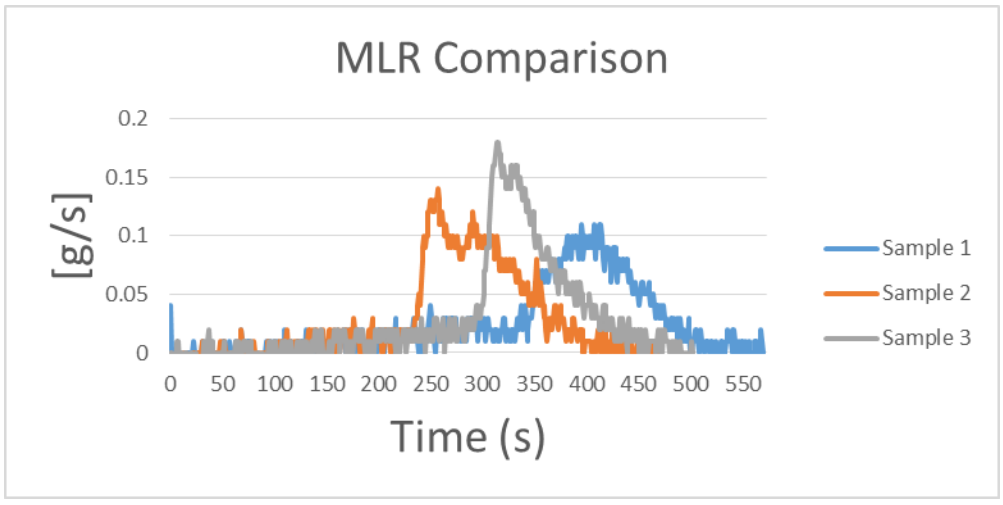

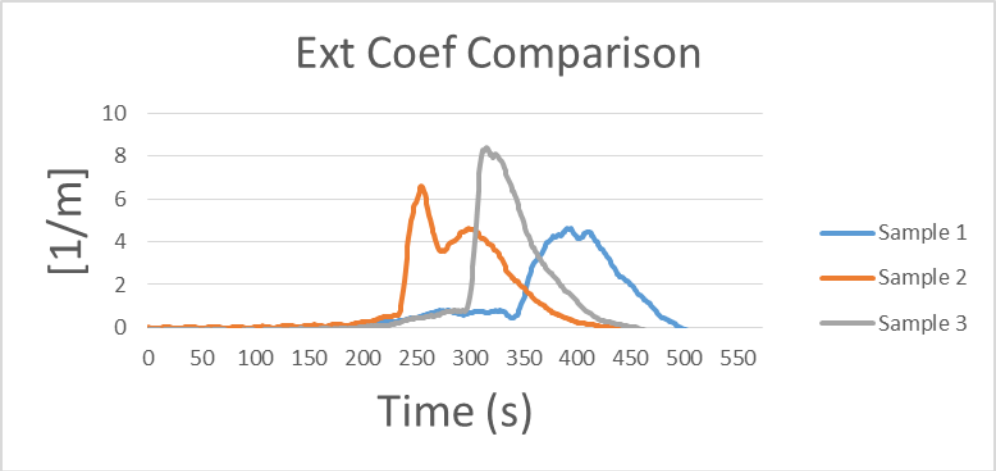
Ext Coef Comparison
[1/m]
10
8
6
4
2
0
0 50 100 150 200 250 300 350 400 450 500 550
Time (s)
Sample 1
Sample 2
Sample 3

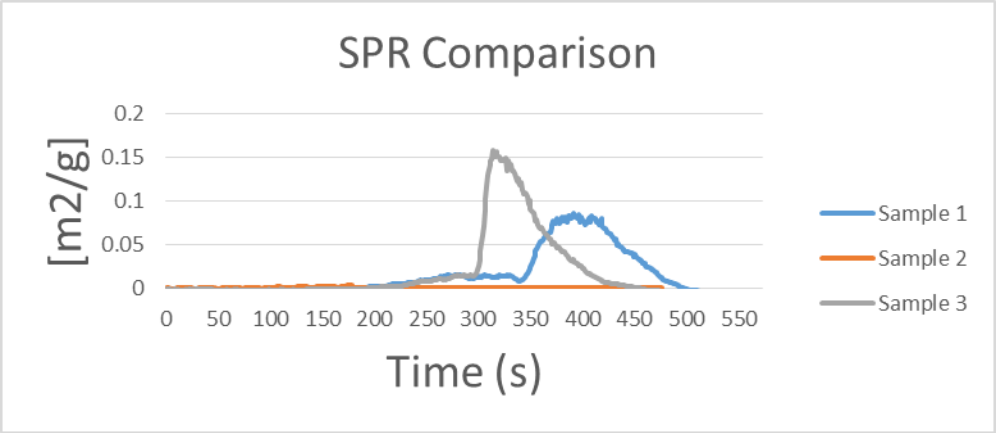
SPR Comparison
[m2/g]
0.2
0.15
0.1
0.05
0
0 50 100 150 200 250 300 350 400 450 500 550
Time (s)
Sample 1
Sample 2
Sample 3

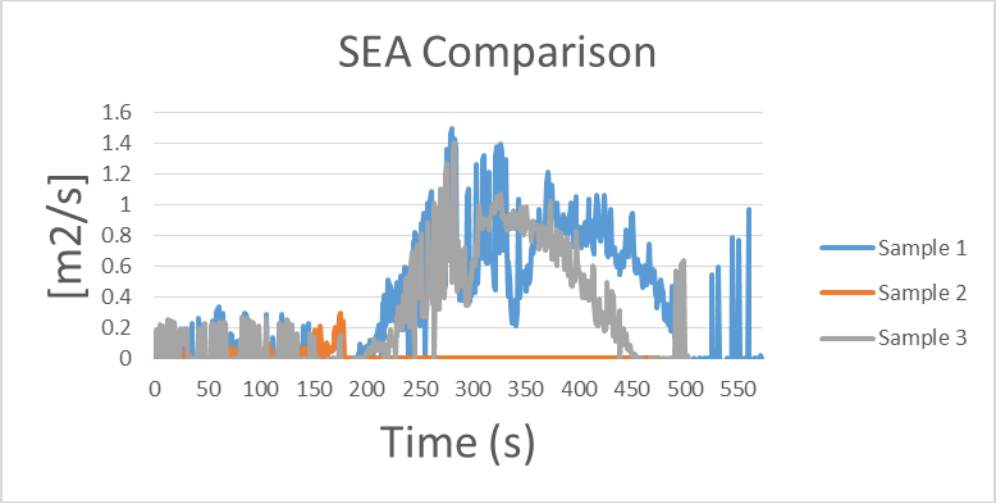
SEA Comparison
[m2/s]
1.6
1.4
1.2
1
0.8
0.6
0.4
0.2
0
0 50 100 150 200 250 300 350 400 450 500 550
Time (s)
Sample 1
Sample 2
Sample 3

Fireblock with Sand Ratio 40:60

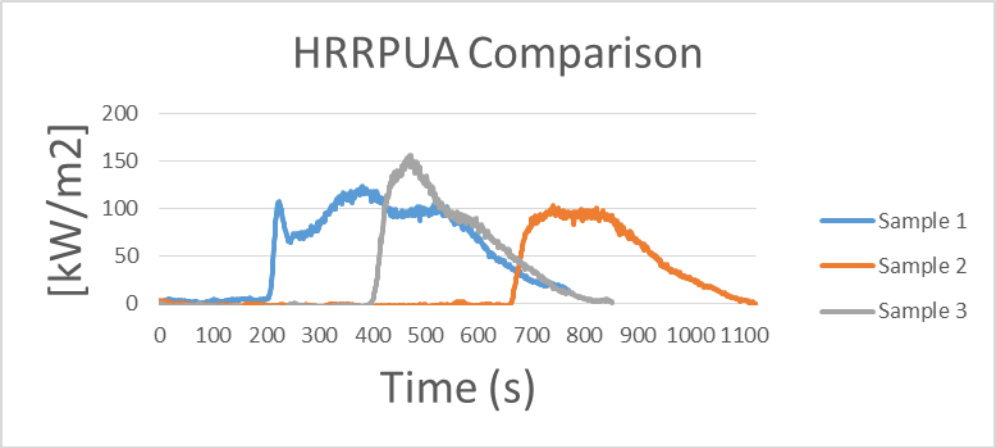

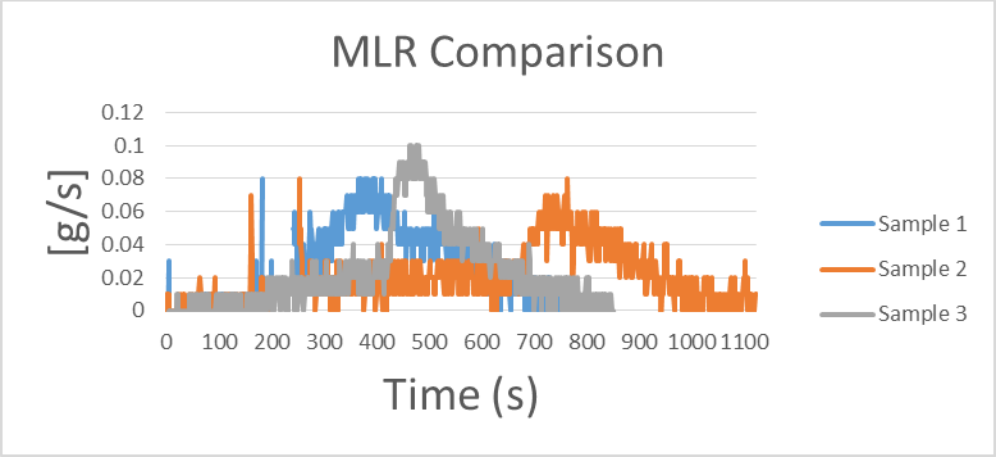

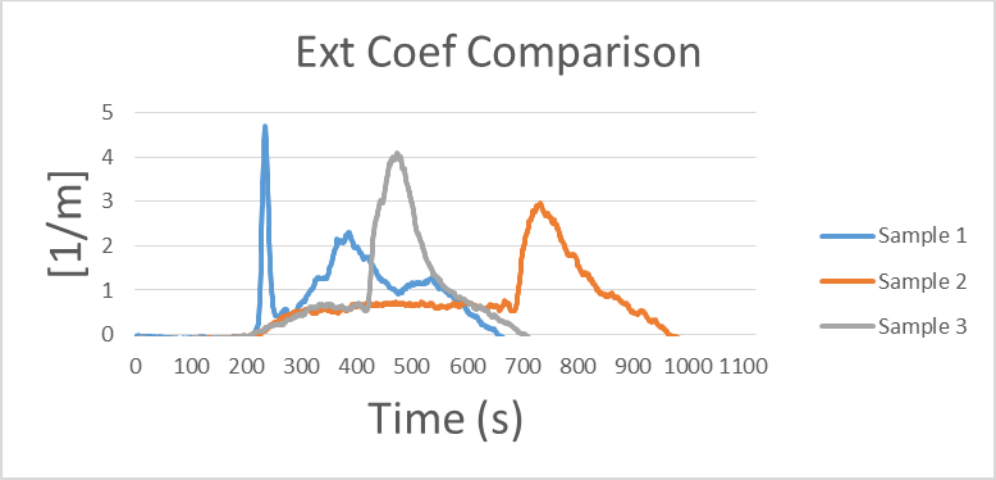

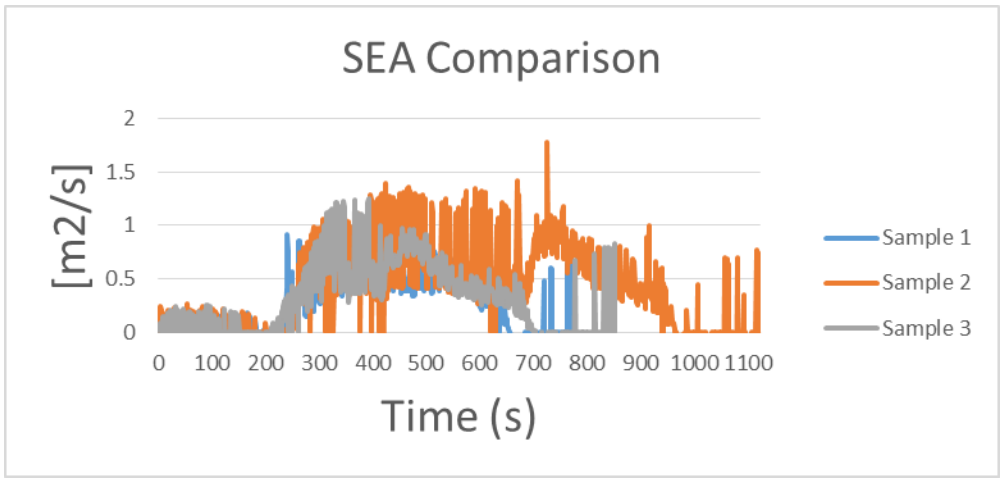

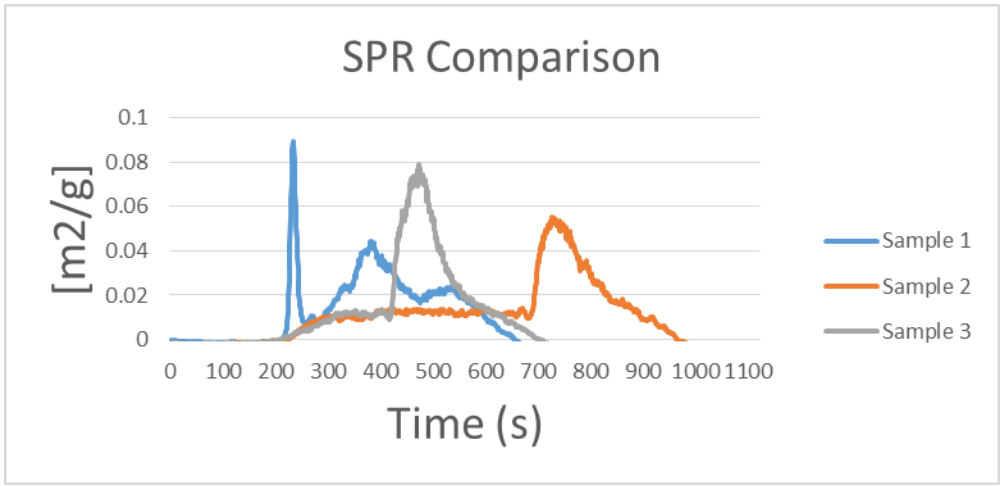

40 kW Heat Flux Test

Hetron with ATH Ratio 100:0

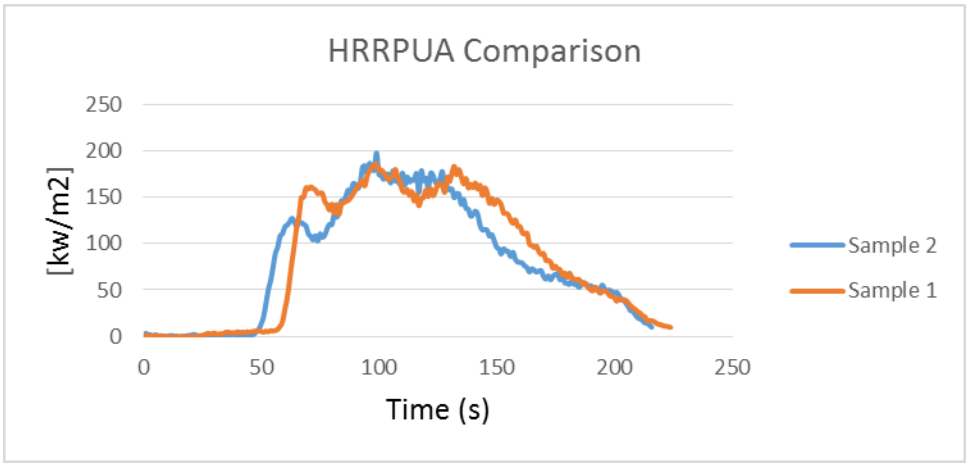

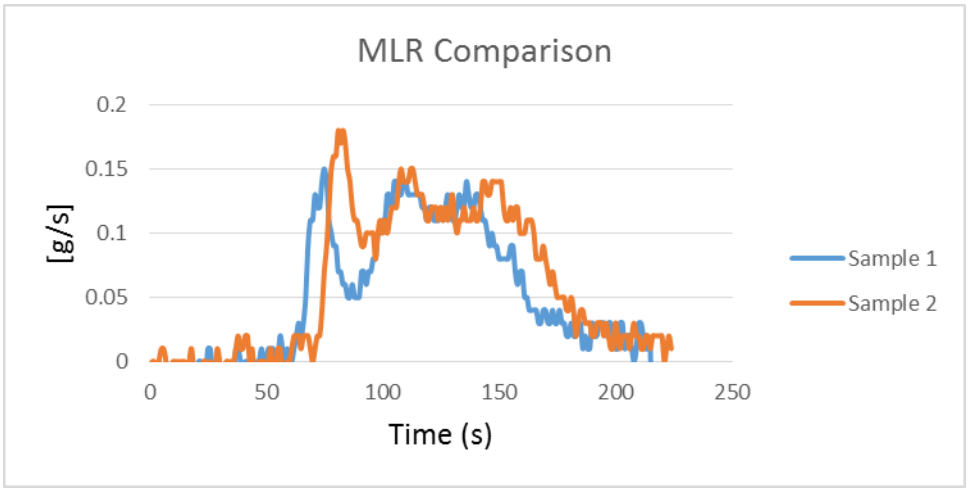
MLR Comparison
0.2
0.15
0.1
0.05
0
[g/s]
0
50
100
150
200
250
Time (s)
Sample 1
Sample 2

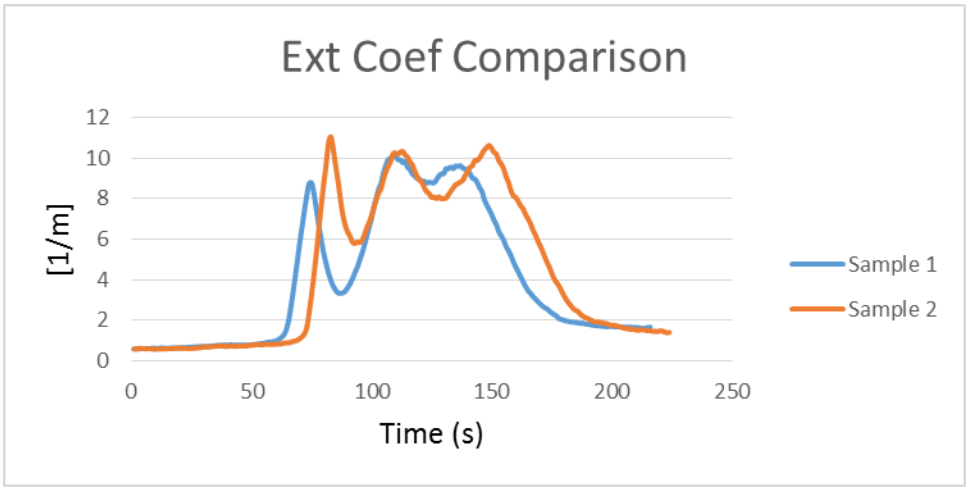
Ext Coef Comparison
12
10
8
6
4
2
0
[1/m]
0
50
100
150
200
250
Time (s)
Sample 1
Sample 2

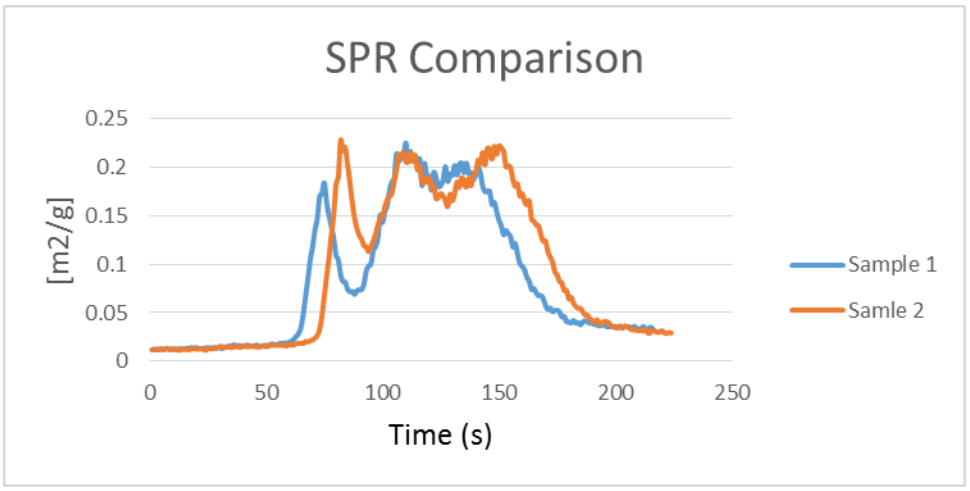
SPR Comparison
0.25
0.2
0.15
0.1
0.05
0
[m2/g]
0
50
100
150
200
250
Time (s)
Sample 1
Samle 2

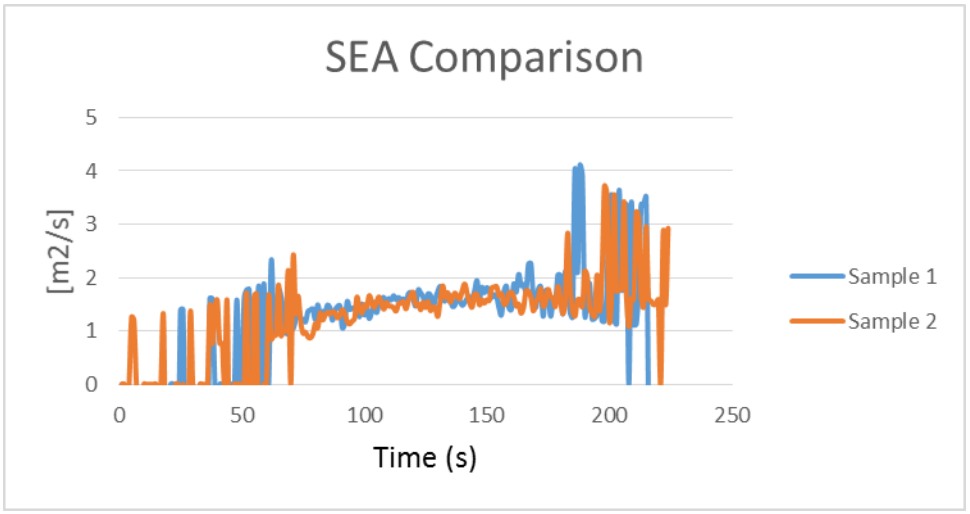

Hetron with ATH Ratio 100:100

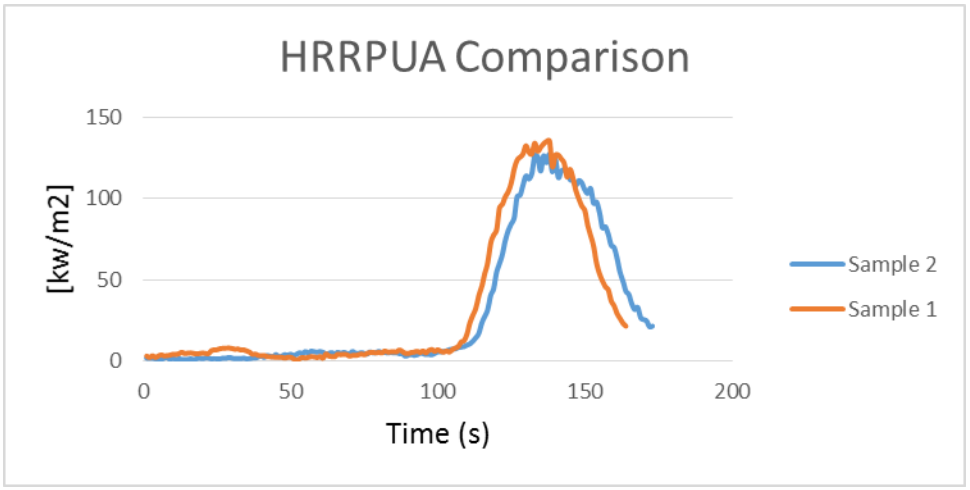

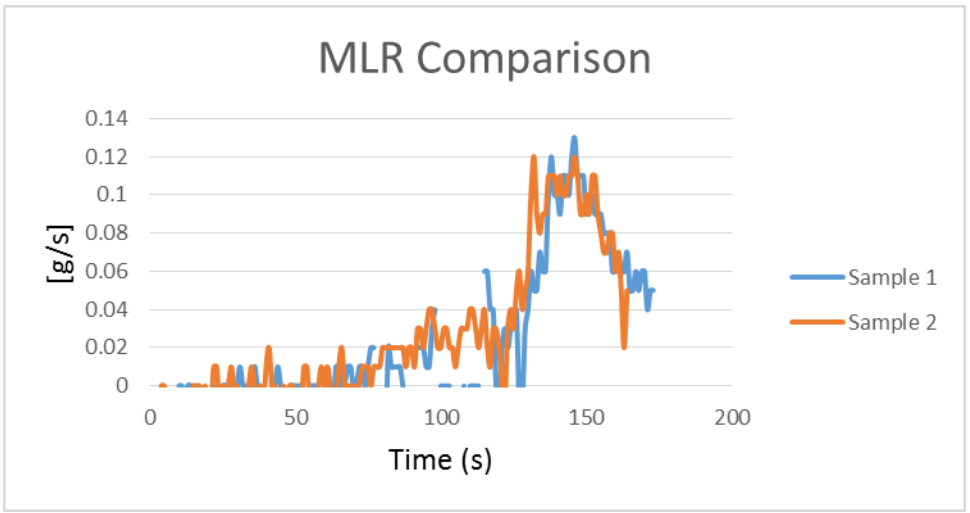

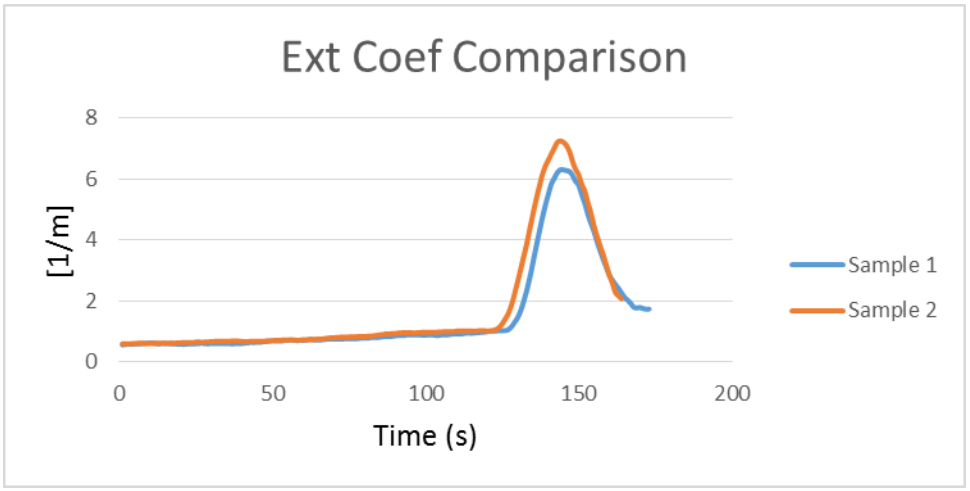
Ext Coef Comparison
[1/m]
8
6
4
2
0
0
50
100
150
200
Time (s)
Sample 1
Sample 2

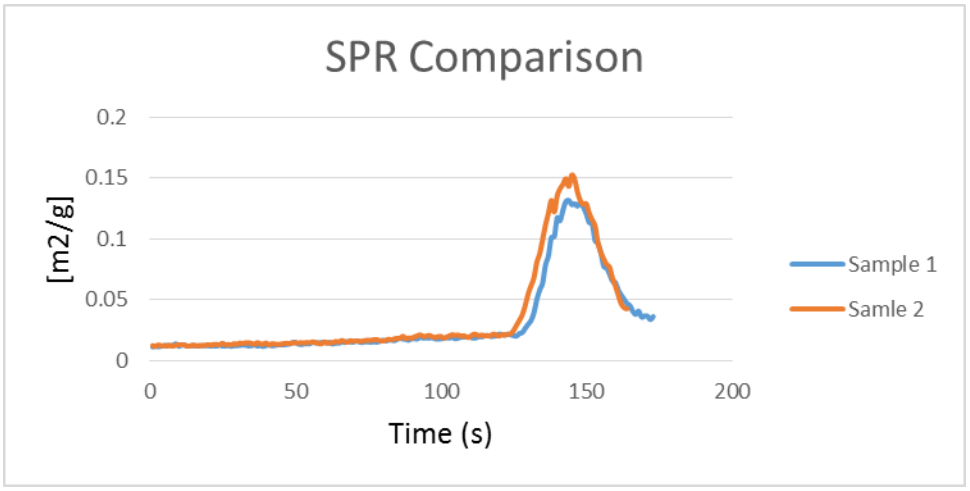
SPR Comparison
[m2/g]
0.2
0.15
0.1
0.05
0
0
50
100
150
200
Time (s)
Sample 1
Samle 2

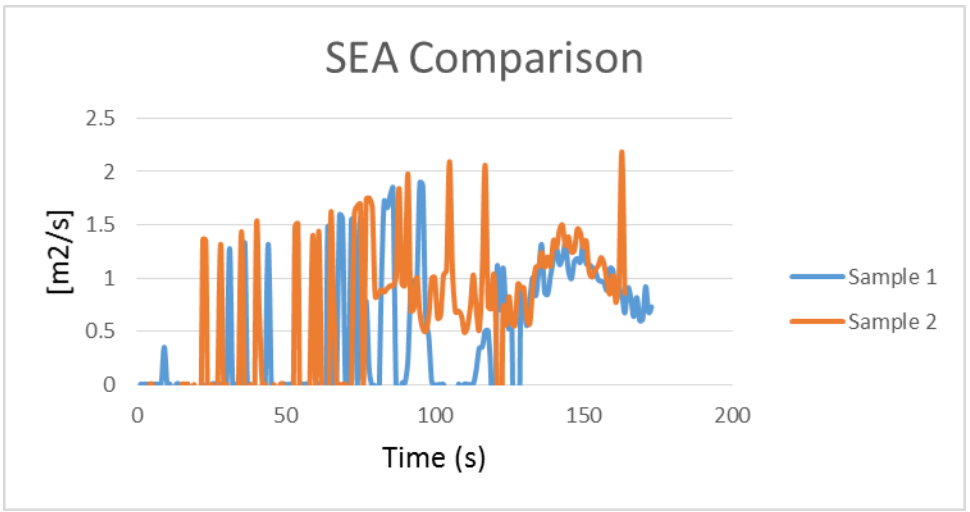
SEA Comparison
[m2/s]
2.5
2
1.5
1
0.5
0
0
50
100
150
200
Time (s)
Sample 1
Sample 2

Hetron with ATH Ratio 100:130

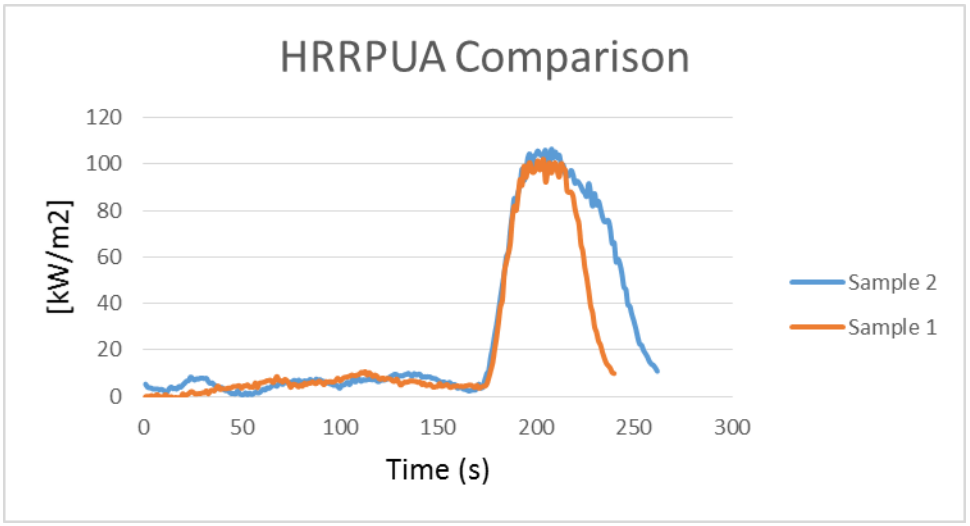

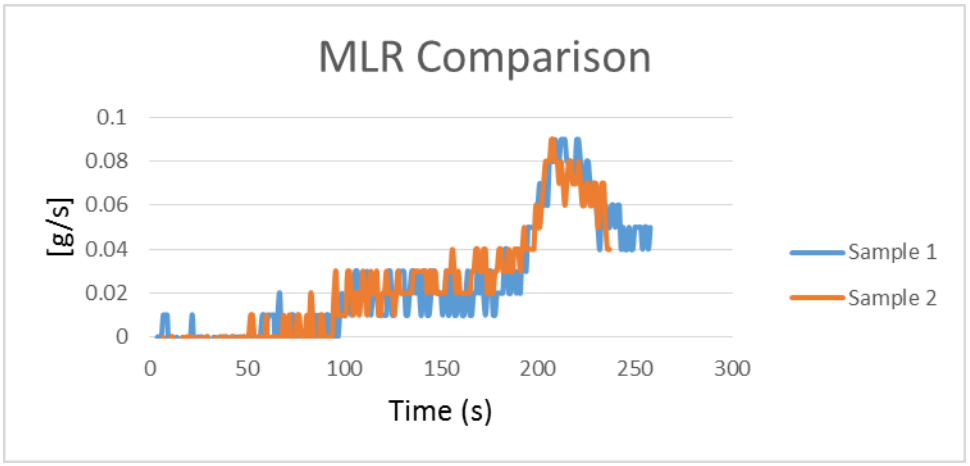

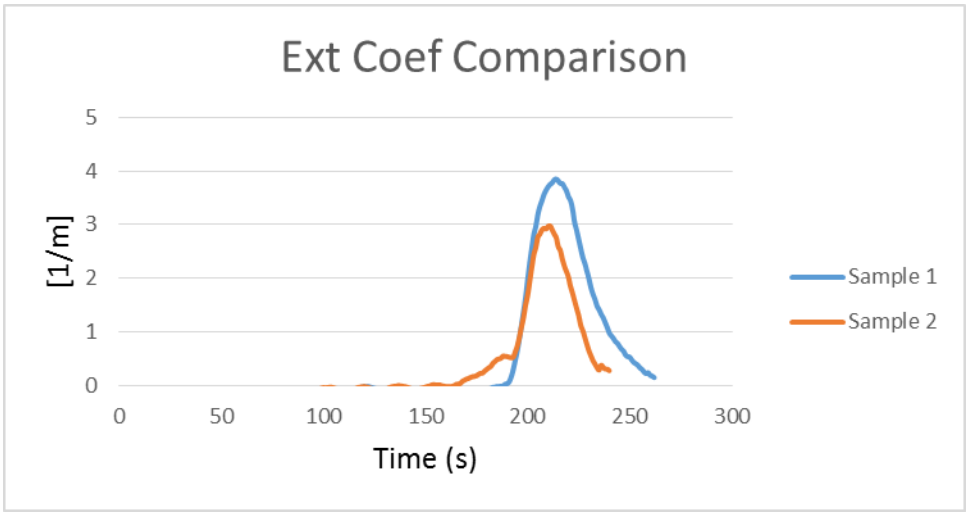

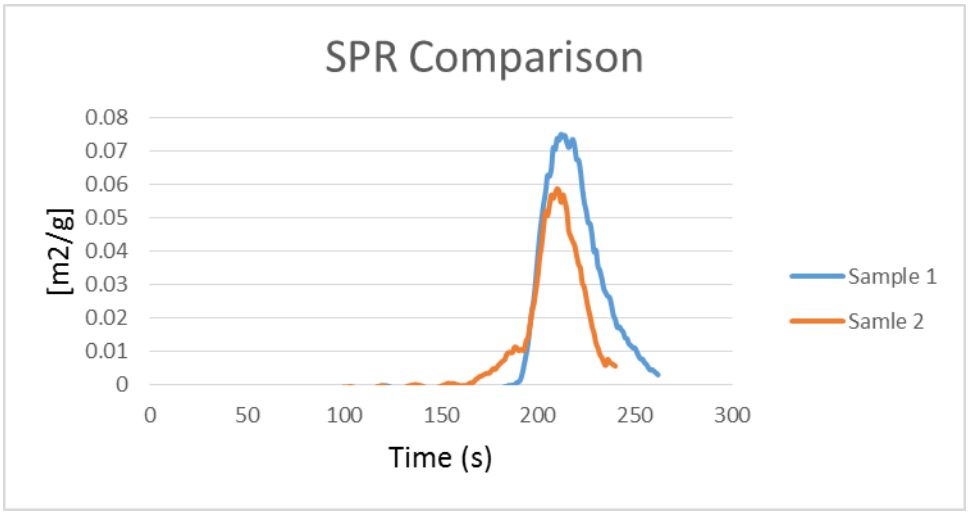

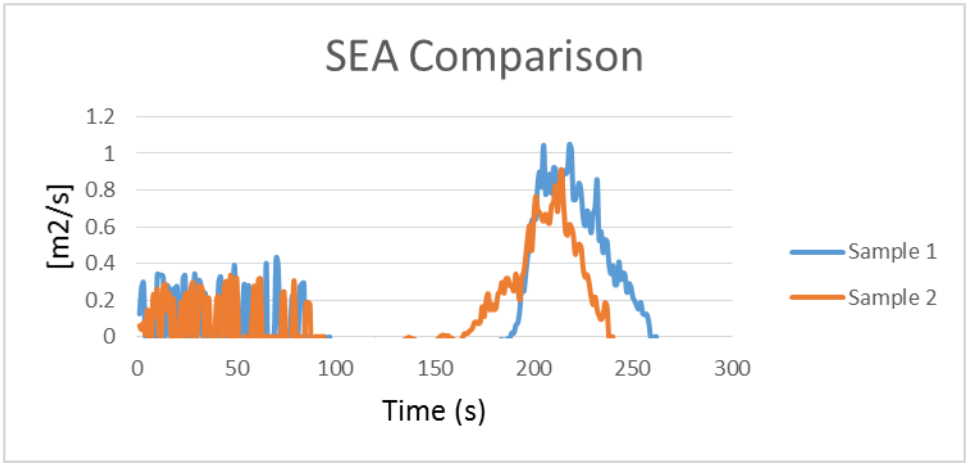

Fireblock with Sand Ratio 100:0

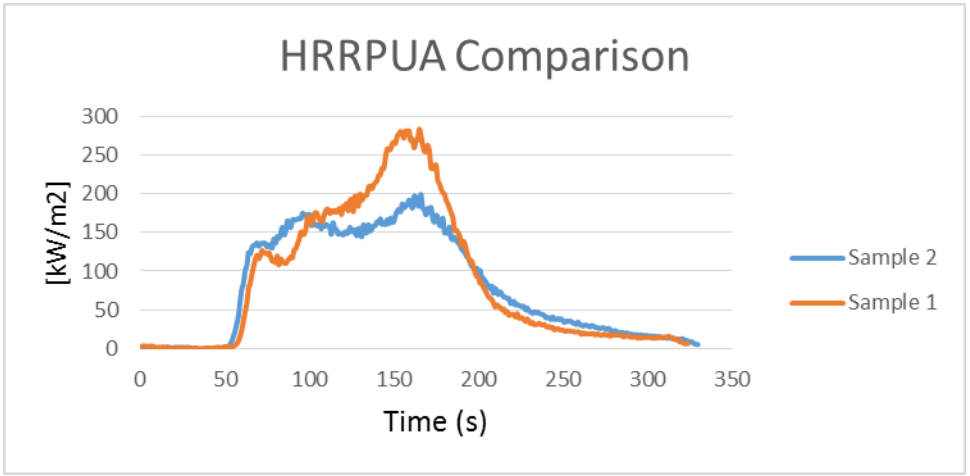

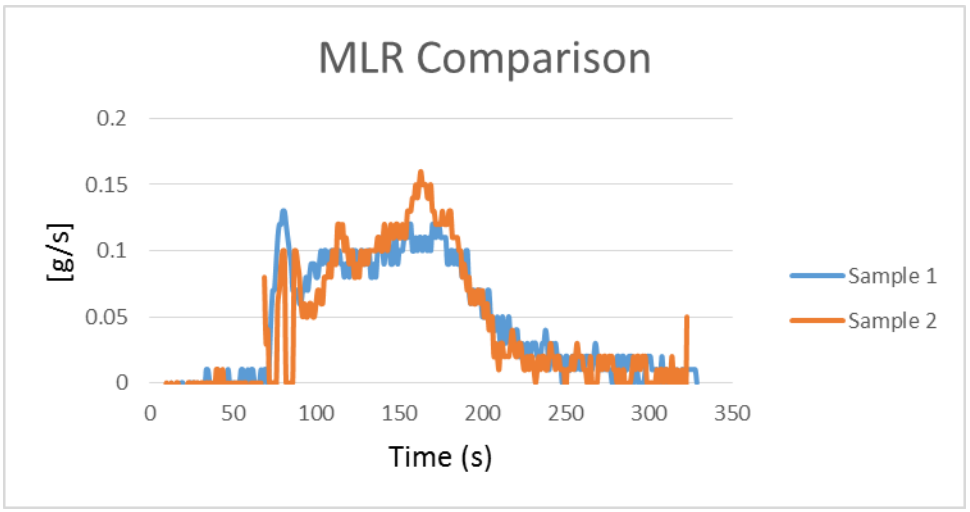
MLR Comparison
0.2
0.15
0.1
0.05
0
[g/s]
0
50
100
150
200
250
300
350
Time (s)
Sample 1
Sample 2

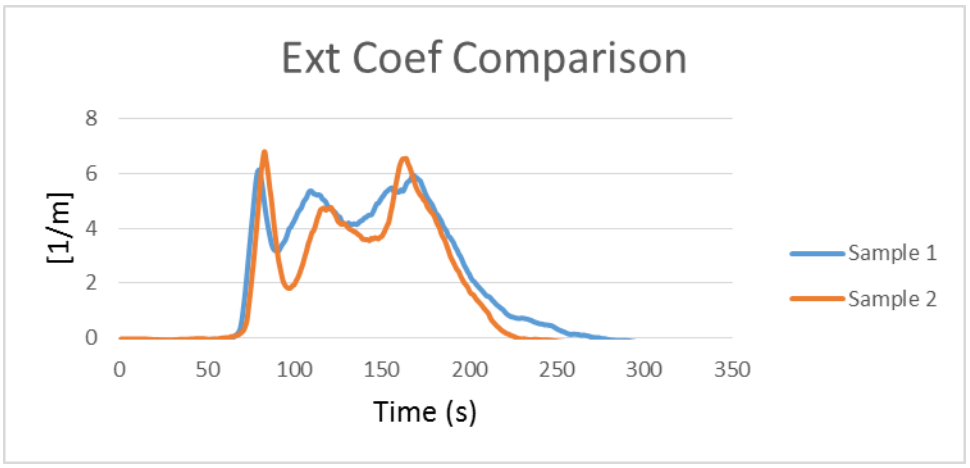
Ext Coef Comparison
8
6
4
2
0
[1/m]
0
50
100
150
200
250
300
350
Time (s)
Sample 1
Sample 2

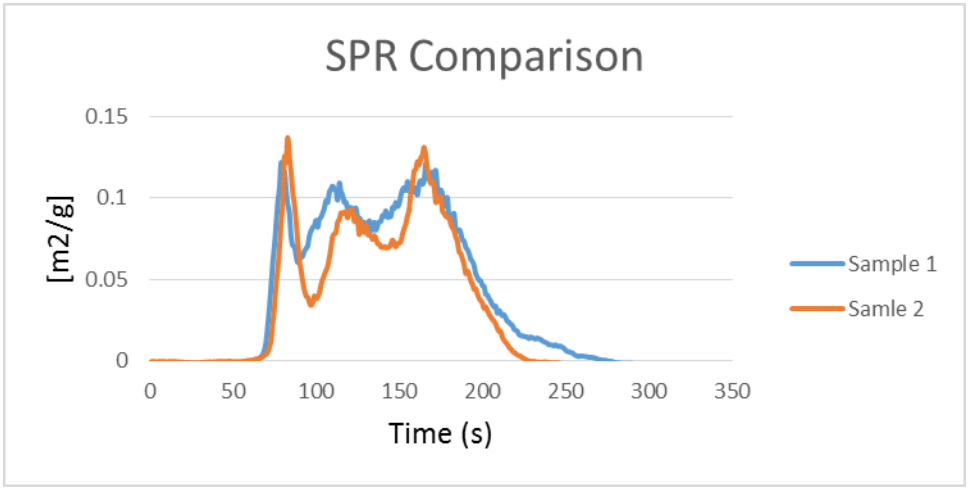
SPR Comparison
0.15
0.1
0.05
0
[m2/g]
0
50
100
150
200
250
300
350
Time (s)
Sample 1
Samle 2

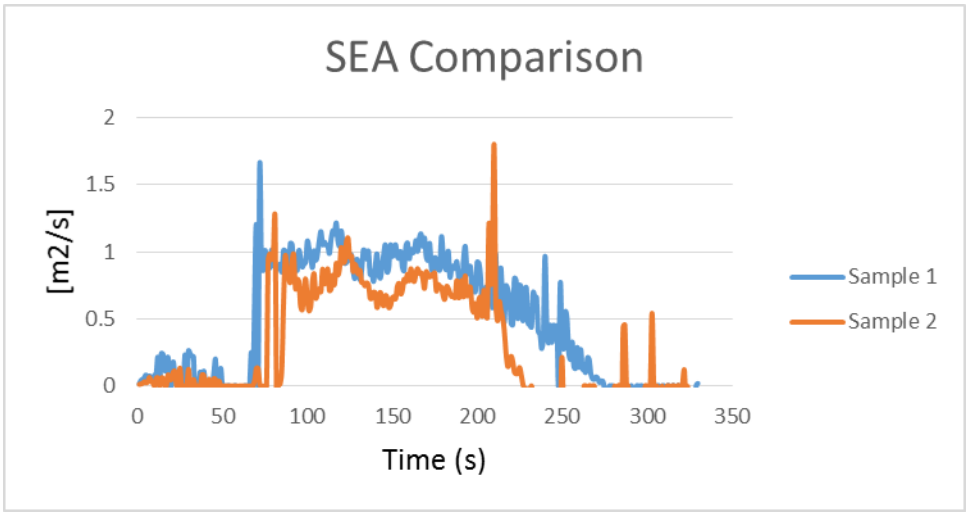

Fireblock with Sand Ratio 60:40

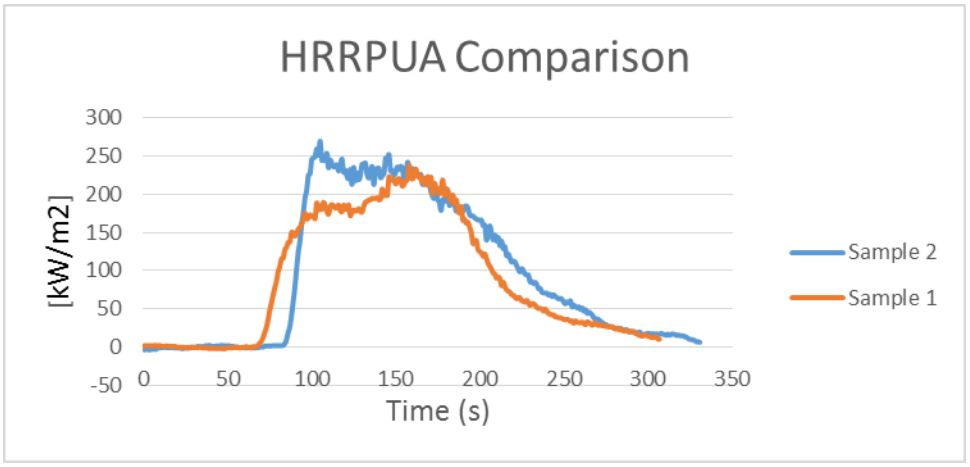

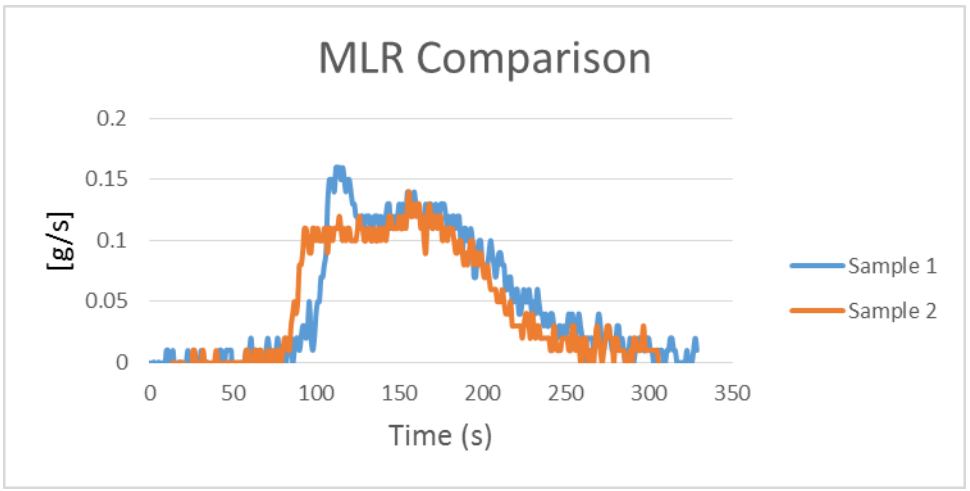

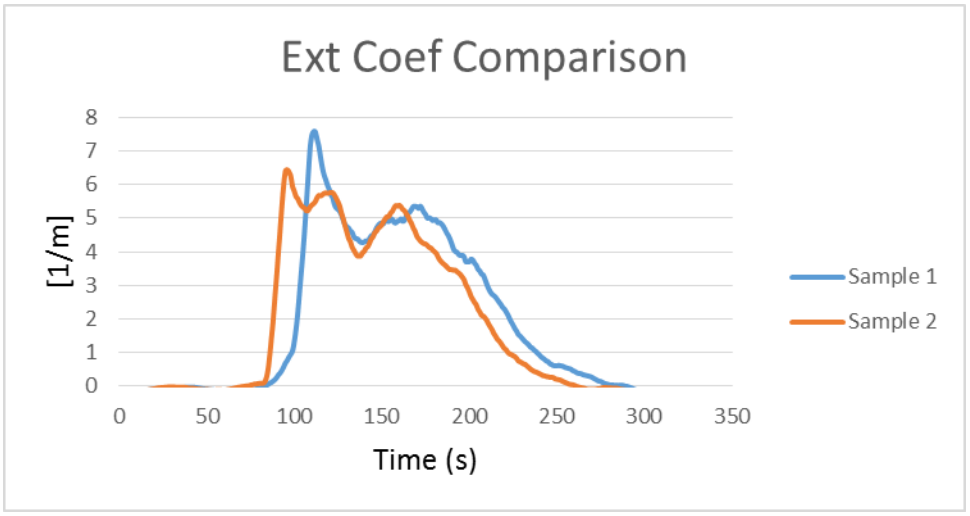
Ext Coef Comparison
[1/m]
8
7
6
5
4
3
2
1
0
0
50
100
150
200
250
300
350
Time (s)
Sample 1
Sample 2

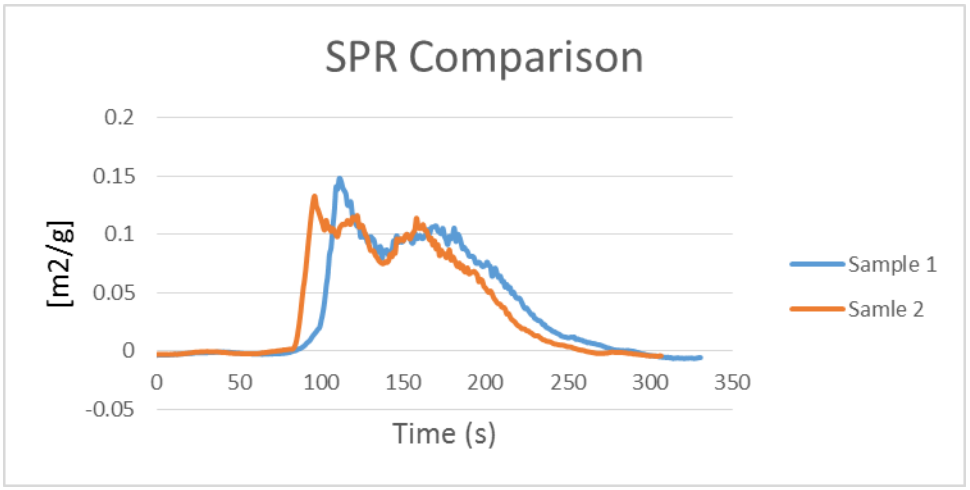
SPR Comparison
[m2/g]
0.2
0.15
0.1
0.05
0
-0.05
0
50
100
150
200
250
300
350
Time (s)
Sample 1
Samle 2

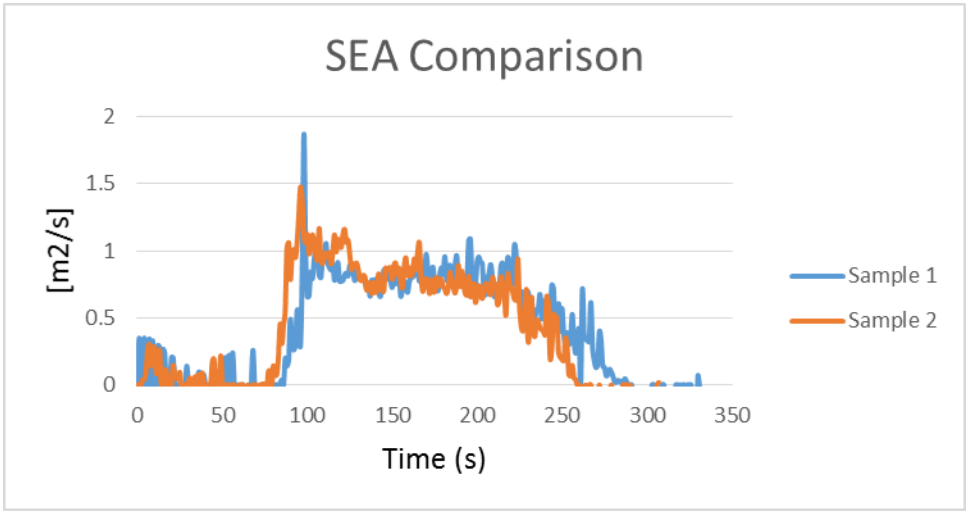
SEA Comparison
[m2/s]
2
1.5
1
0.5
0
0
50
100
150
200
250
300
350
Time (s)
Sample 1
Sample 2

Fireblock with Sand Ratio 40:60

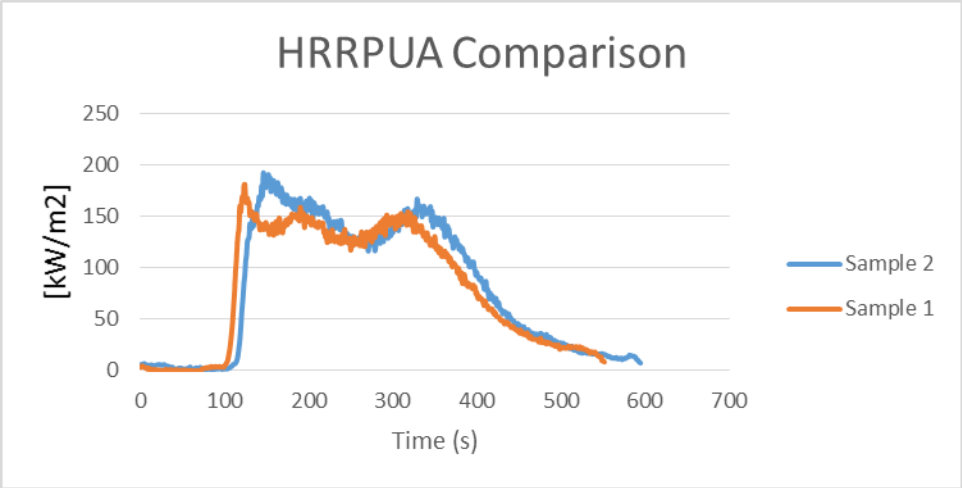

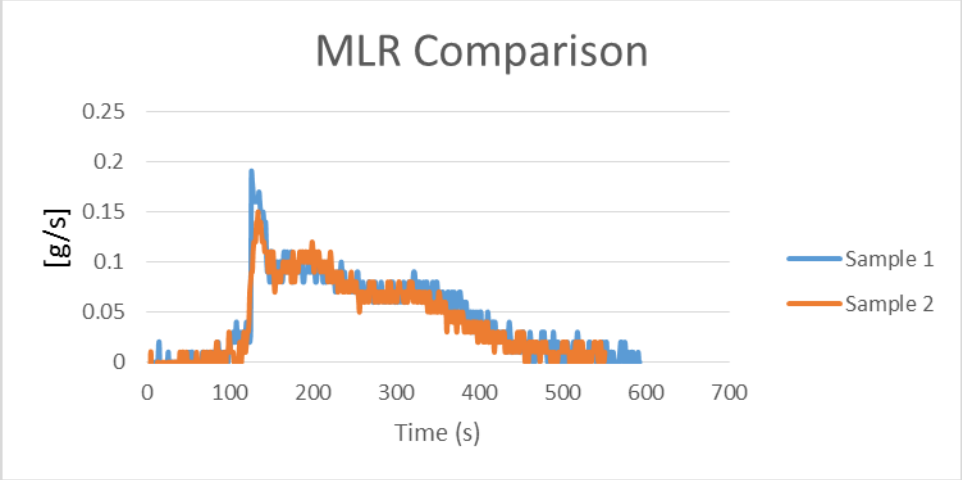

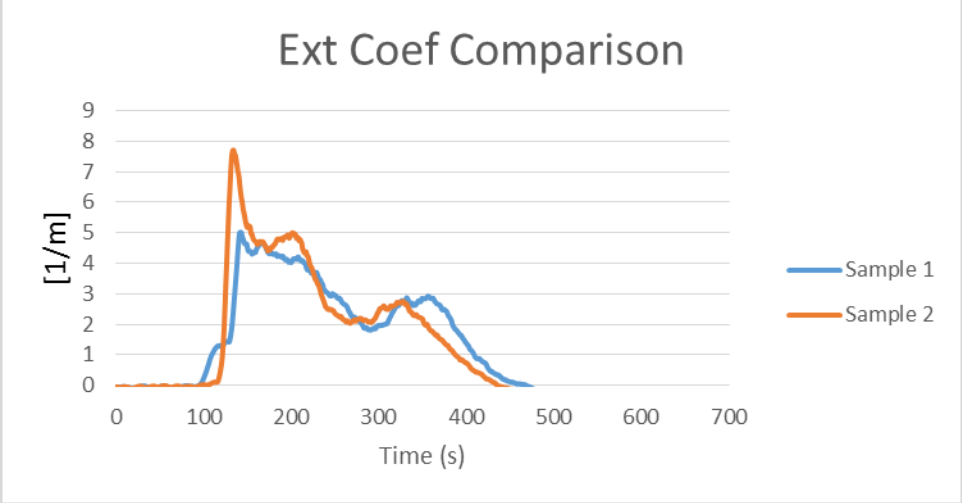

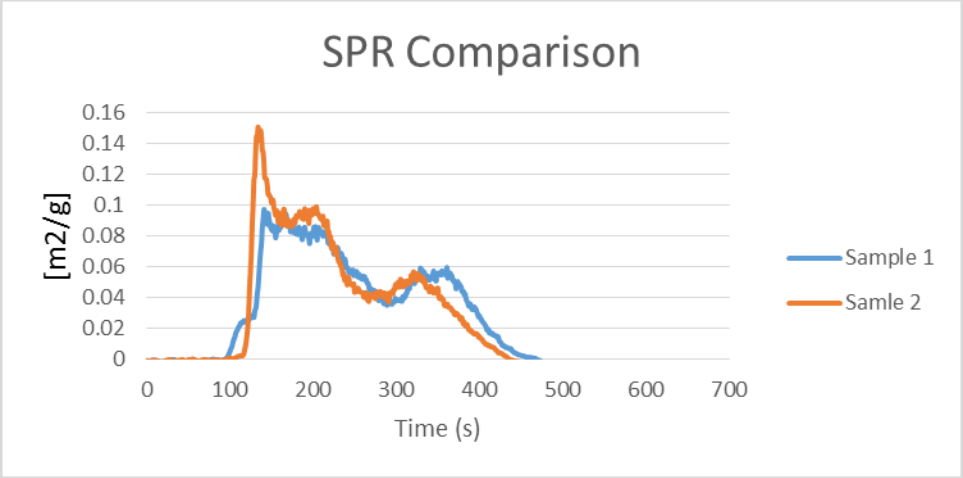

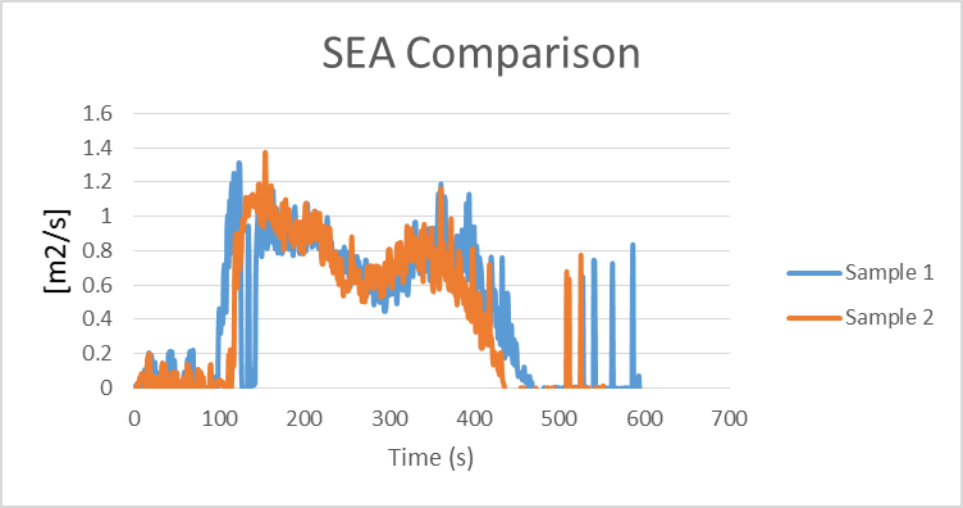

75 kW Heat Flux Test

Hetron with ATH Ratio 100:0

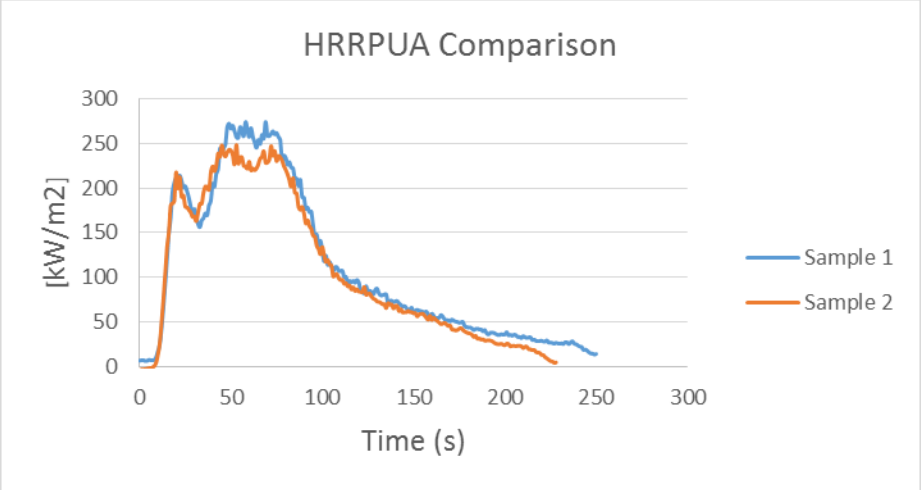

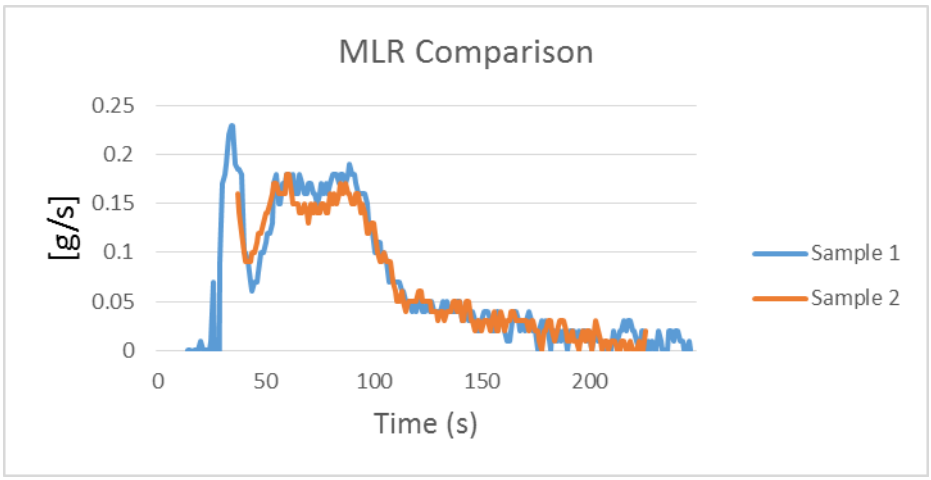
MLR Comparison
[g/s]
0.25
0.2
0.15
0.1
0.05
0
0
50
100
150
200
Time (s)
Sample 1
Sample 2

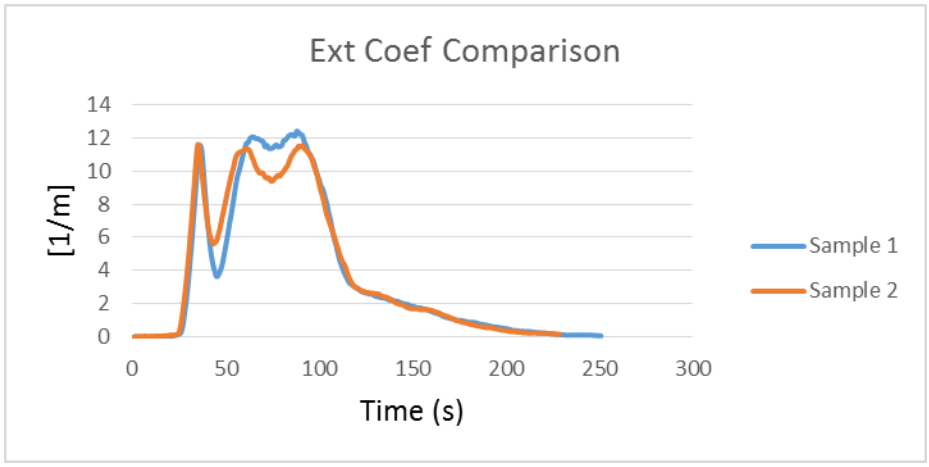
Ext Coef Comparison
[1/m]
14
12
10
8
6
4
2
0
0
50
100
150
200
250
300
Time (s)
Sample 1
Sample 2

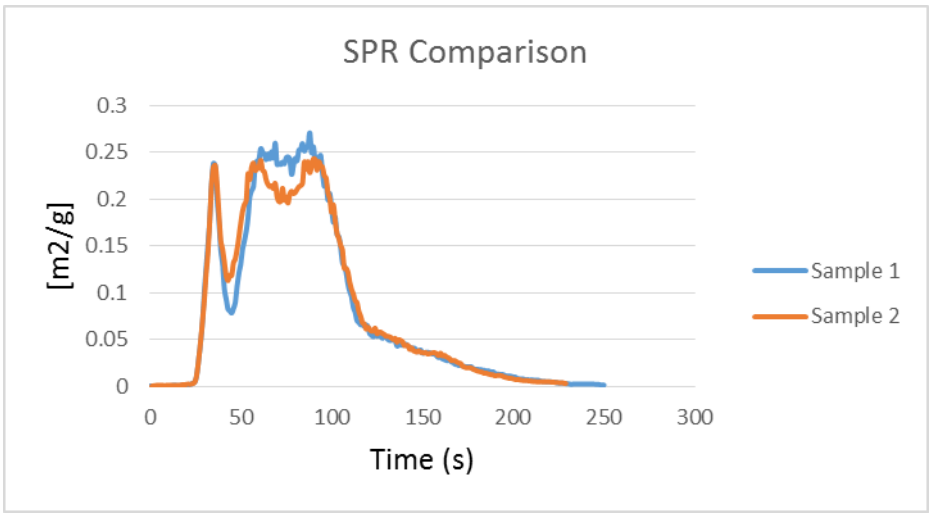
SPR Comparison
[m2/g]
0.3
0.25
0.2
0.15
0.1
0.05
0
0
50
100
150
200
250
300
Time (s)
Sample 1
Sample 2

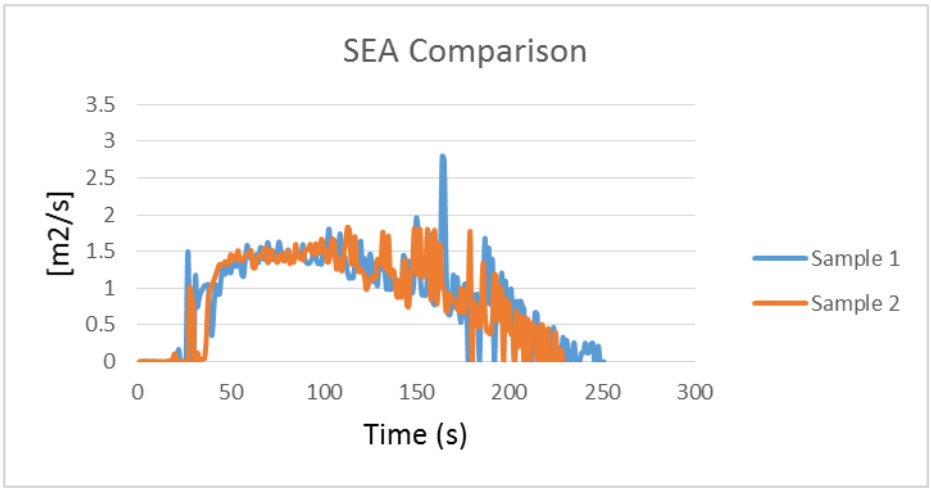

Hetron with ATH Ratio 100:100

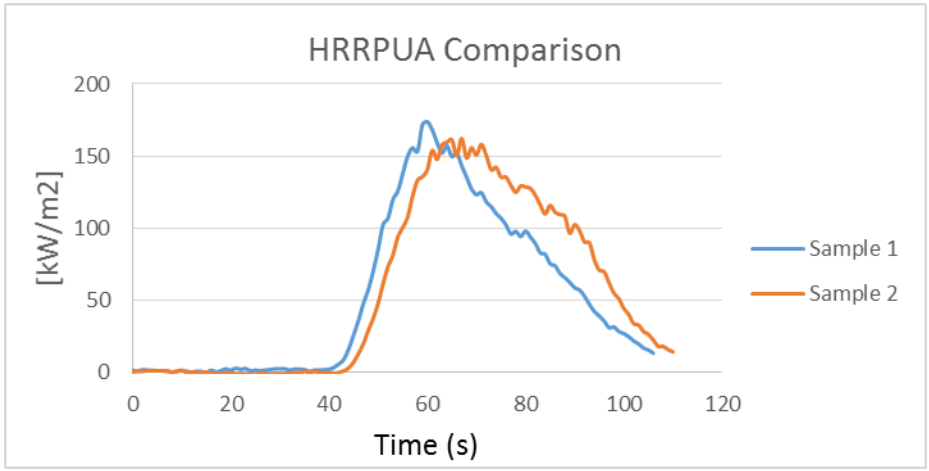

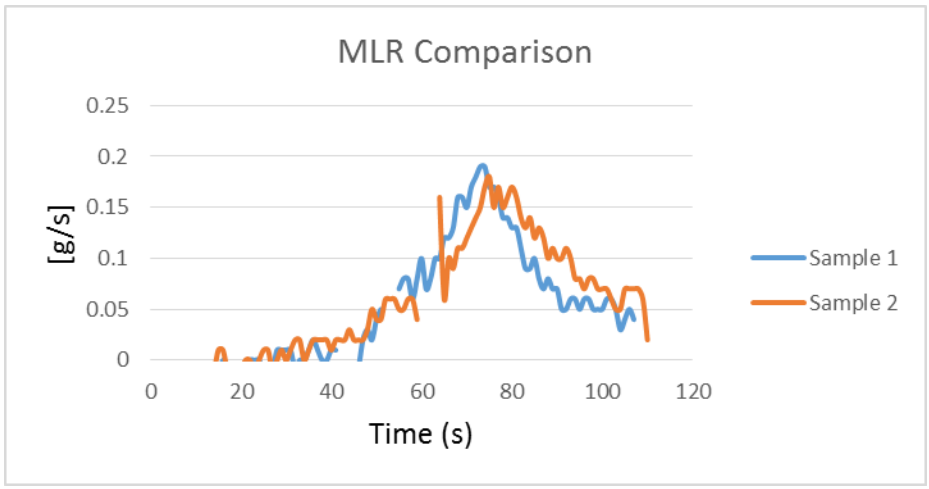

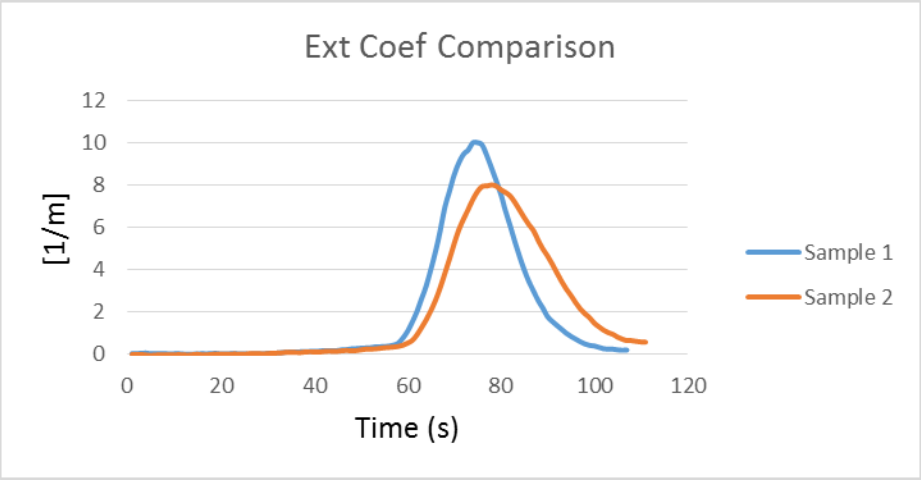
Ext Coef Comparison
12
10
8
6
4
2
0
[1/m]
0
20
40
60
80
100
120
Time (s)
Sample 1
Sample 2

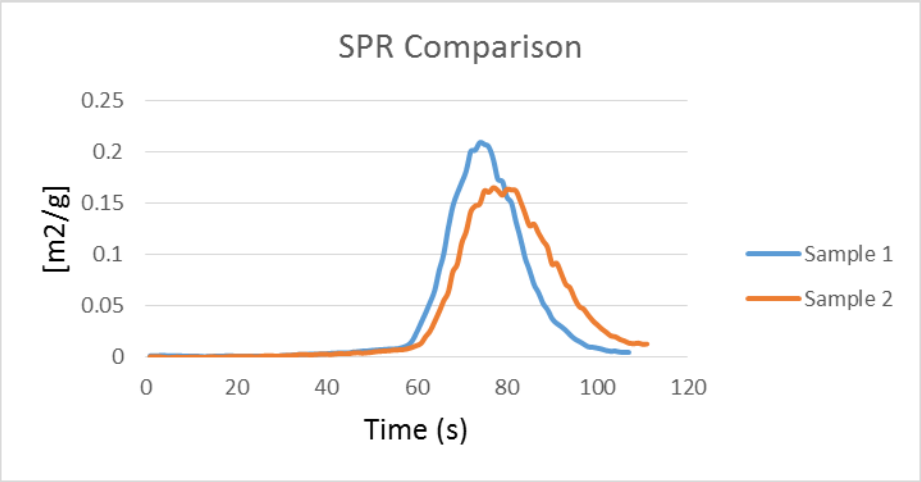
SPR Comparison
0.25
0.2
0.15
0.1
0.05
0
[m2/g]
0
20
40
60
80
100
120
Time (s)
Sample 1
Sample 2

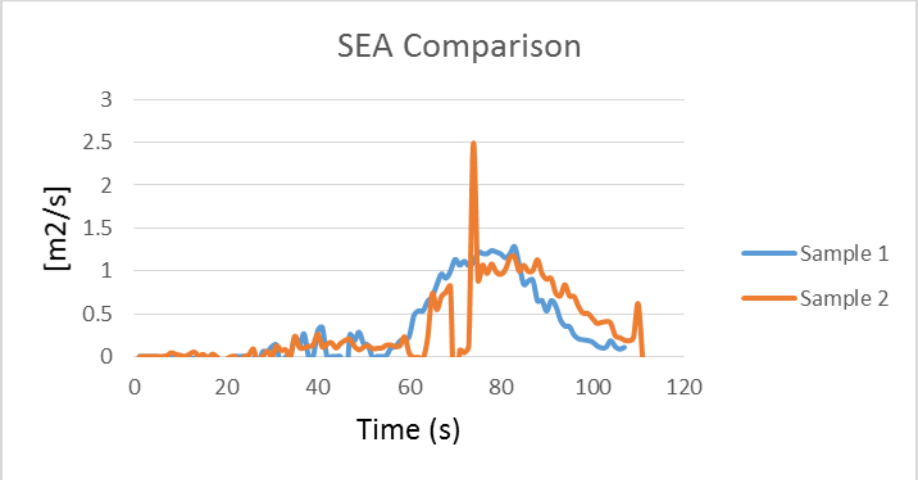
SEA Comparison
3
2.5
2
1.5
1
0.5
0
[m2/s]
0
20
40
60
80
100
120
Time (s)
Sample 1
Sample 2

Hetron with ATH Ratio 100:130

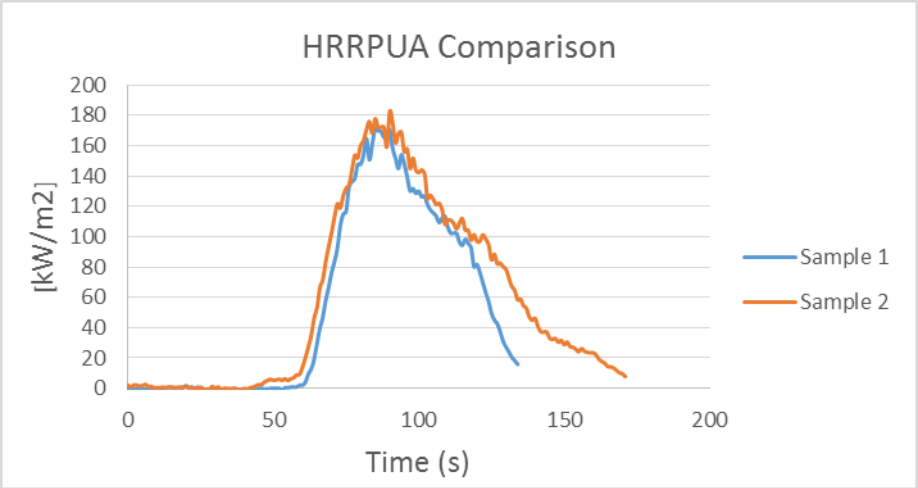

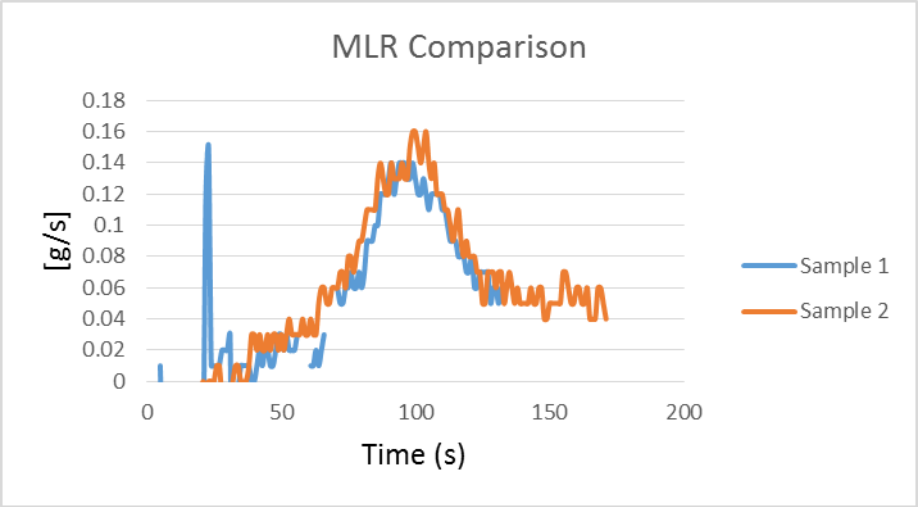

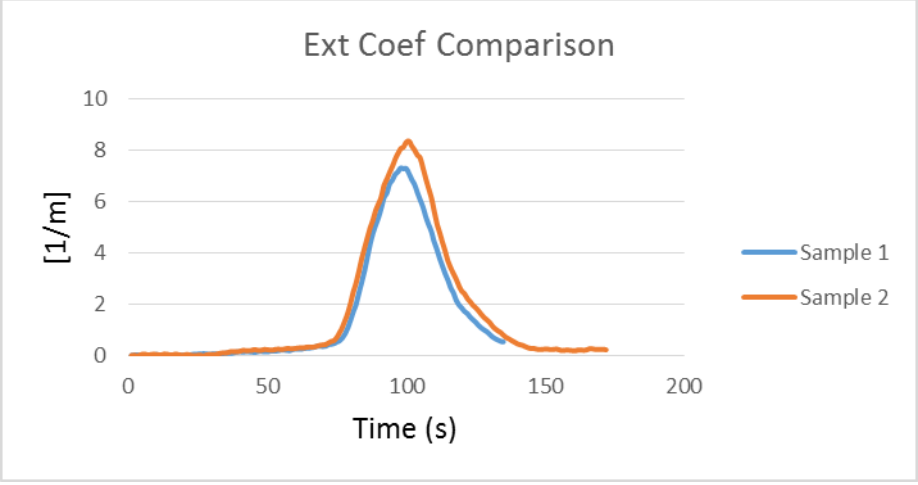

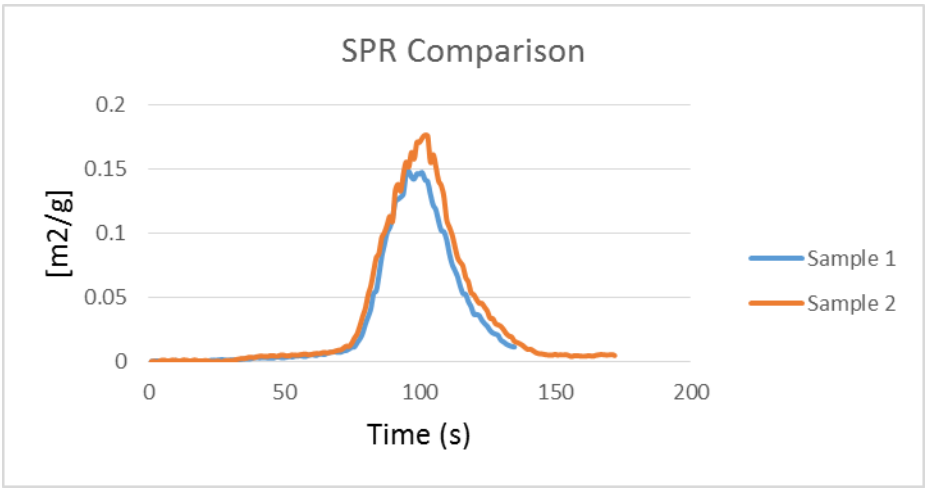

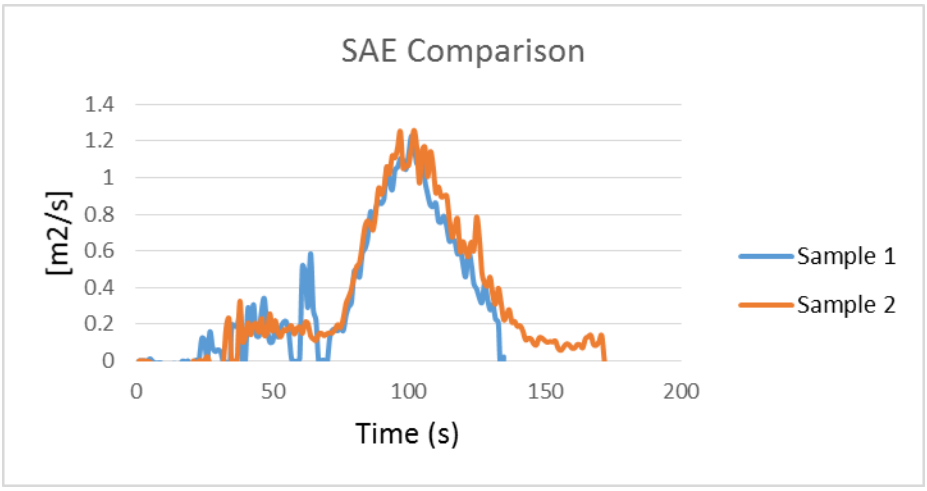

Fireblock with Sand Ratio 100:0

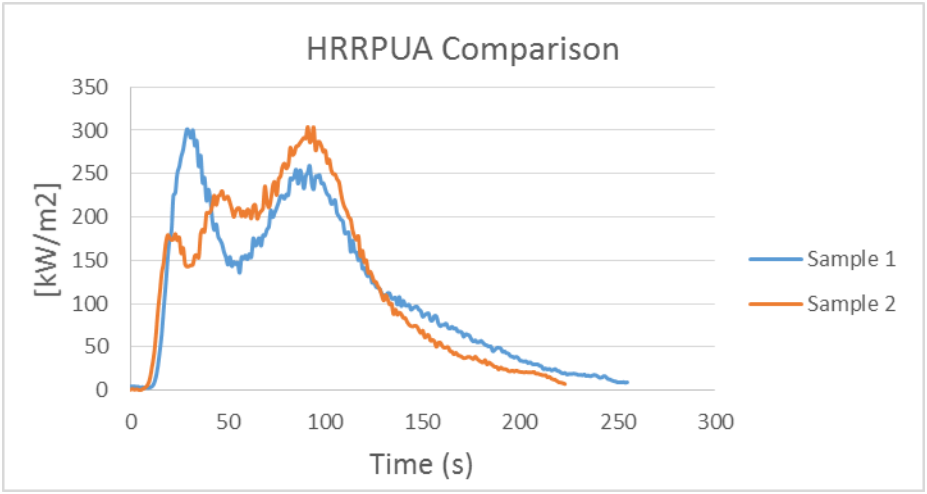

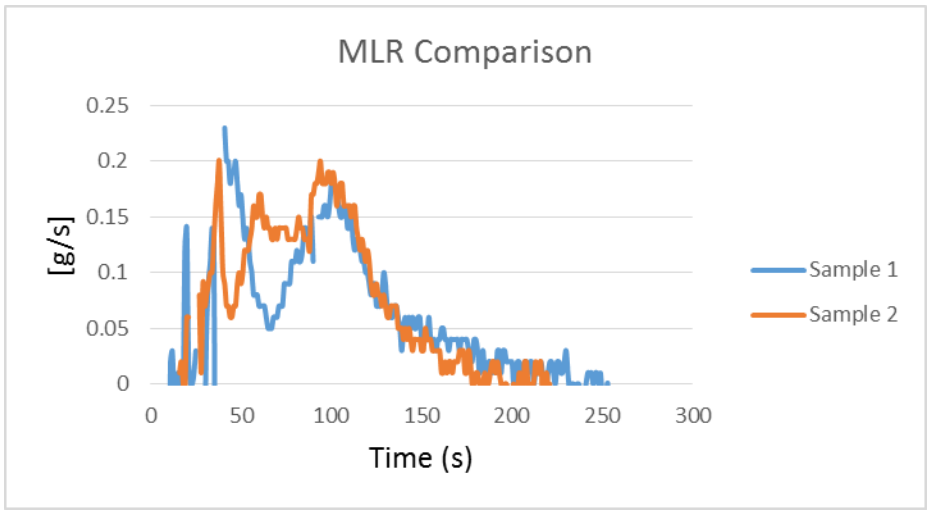
MLR Comparison
0.25
0.2
0.15
0.1
0.05
0
[g/s]
0
50
100
150
200
250
300
Time (s)
Sample 1
Sample 2

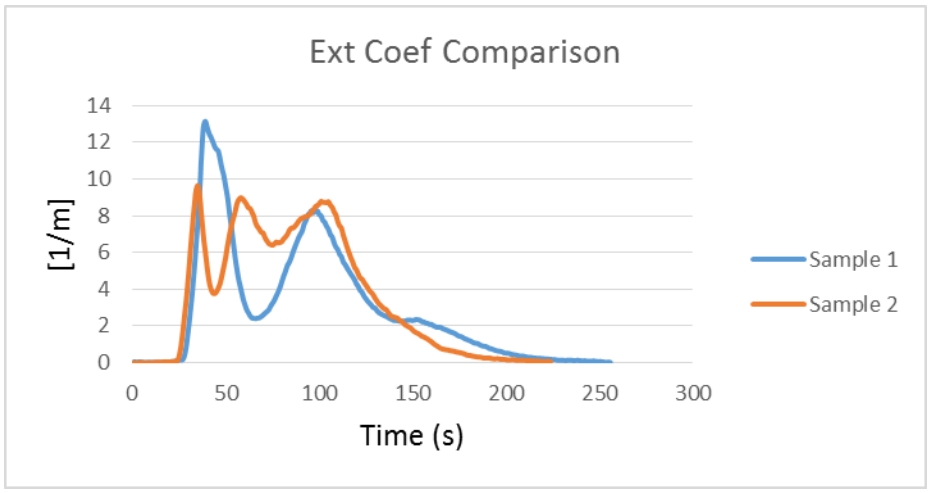
Ext Coef Comparison
14
12
10
8
6
4
2
0
[1/m]
0
50
100
150
200
250
300
Time (s)
Sample 1
Sample 2

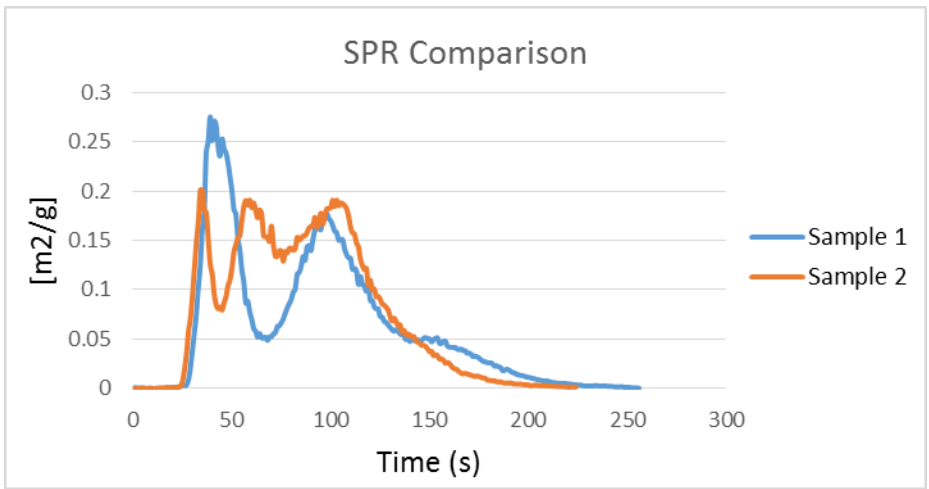
SPR Comparison
0.3
0.25
0.2
0.15
0.1
0.05
0
[m2/g]
0
50
100
150
200
250
300
Time (s)
Sample 1
Sample 2

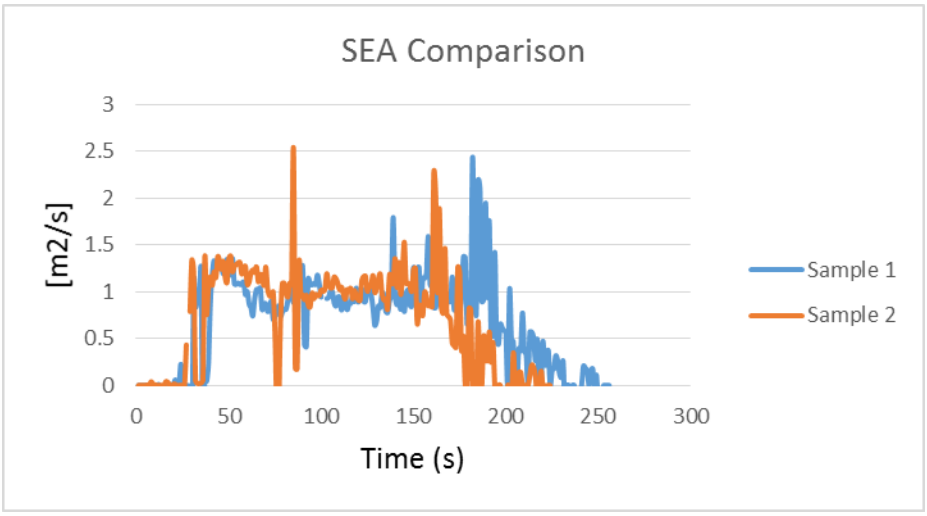

Fireblock with Sand Ratio 60:40

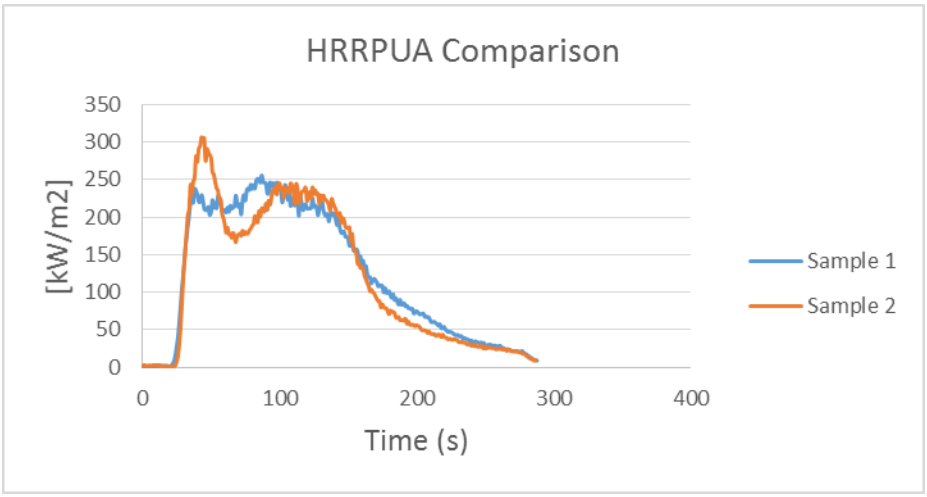

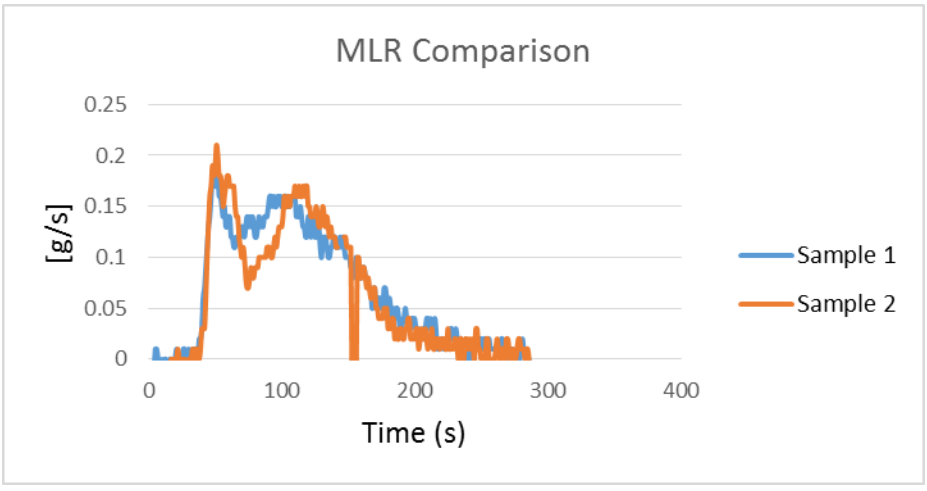

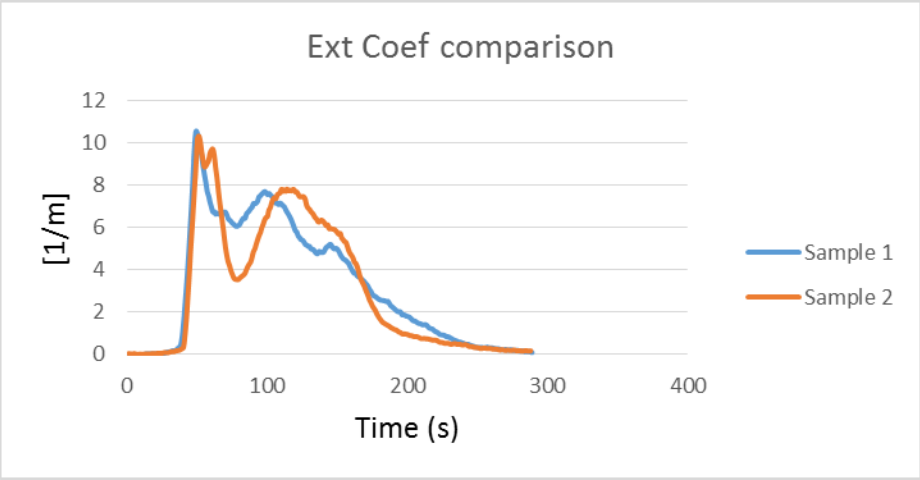
Ext Coef comparison
12
10
8
6
4
2
0
[1/m]
0
100
200
300
400
Time (s)
Sample 1
Sample 2

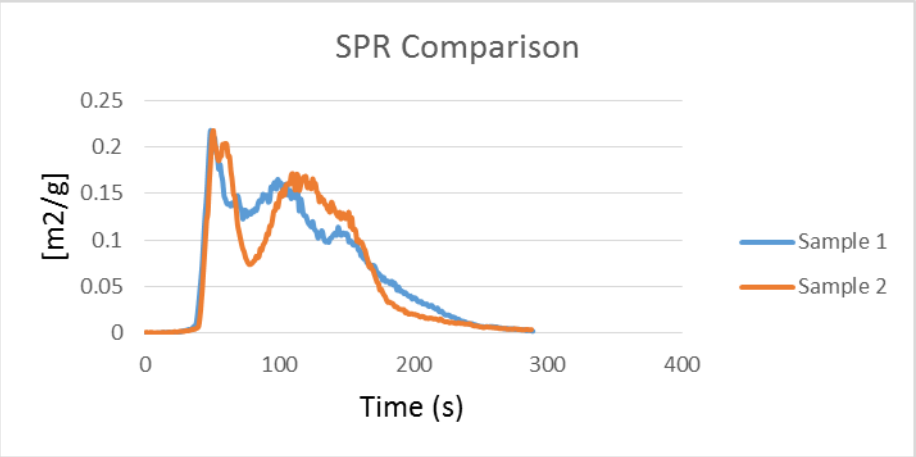
SPR Comparison
0.25
0.2
0.15
0.1
0.05
0
[m2/g]
0
100
200
300
400
Time (s)
Sample 1
Sample 2

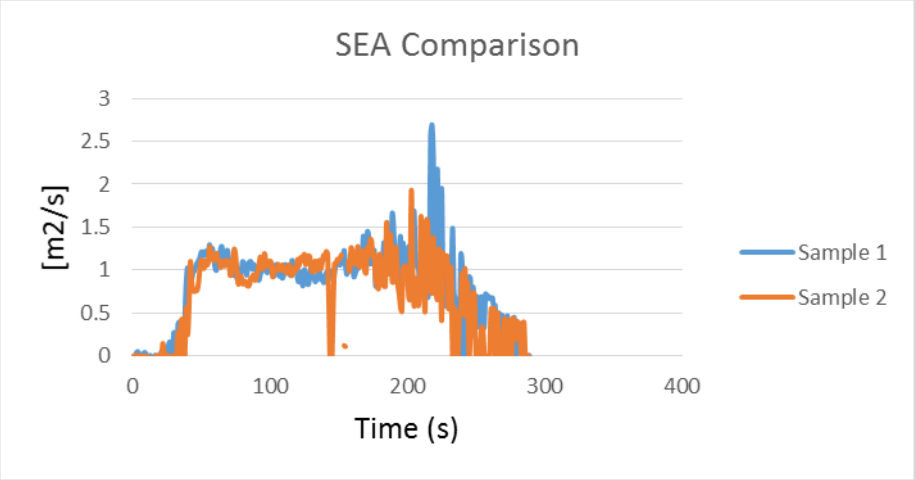
SEA Comparison
3
2.5
2
1.5
1
0.5
0
[m2/s]
0
100
200
300
400
Time (s)
Sample 1
Sample 2

Fireblock with Sand Ratio 40:60

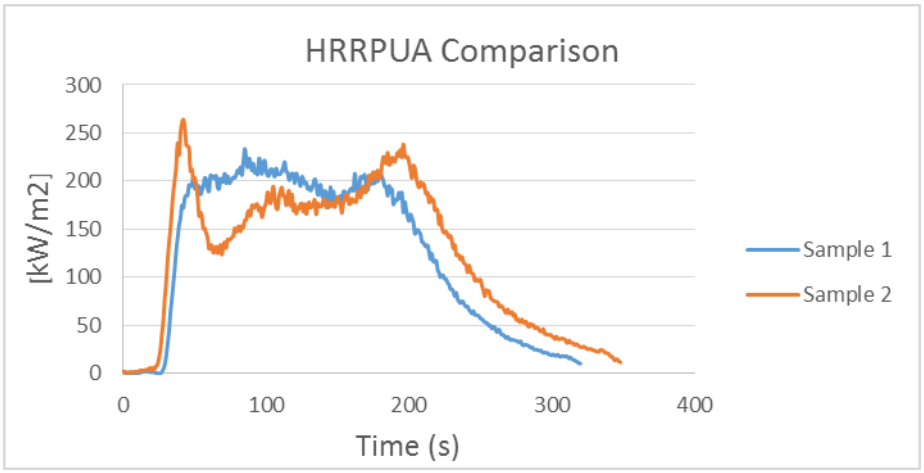

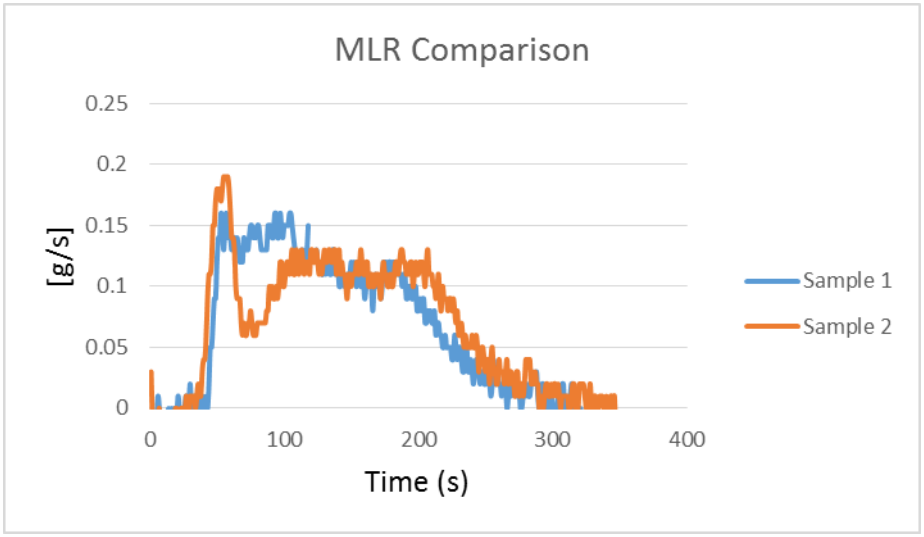

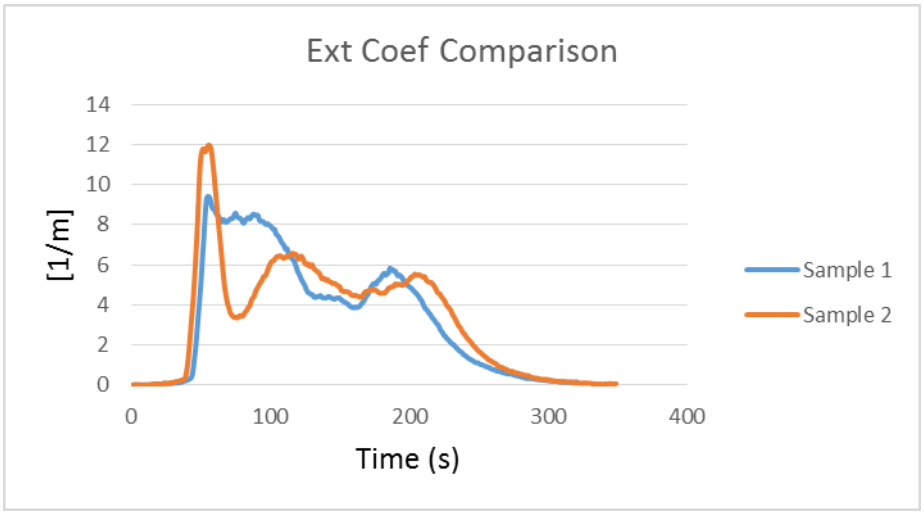

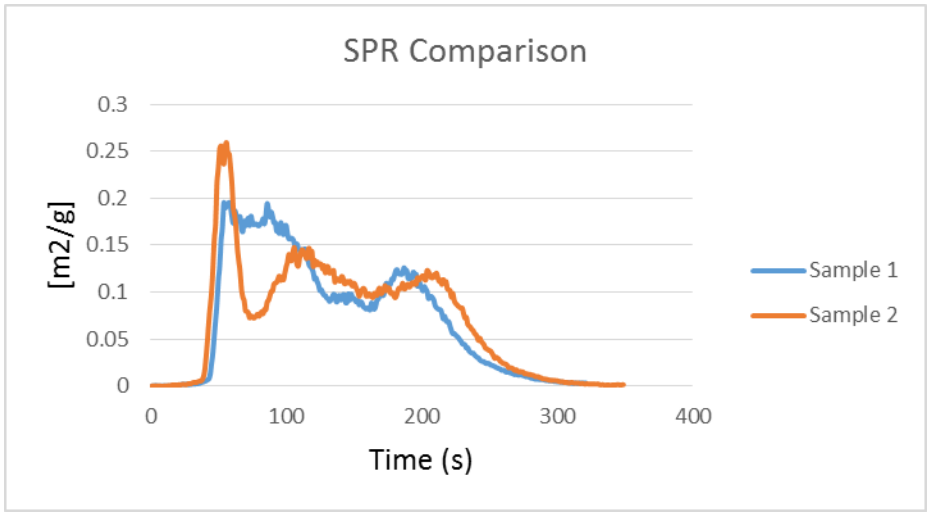
SPR Comparison
0.3
0.25
0.2
0.15
0.1
0.05
0
[m2/g]
0
100
200
300
400
Time (s)
Sample 1
Sample 2

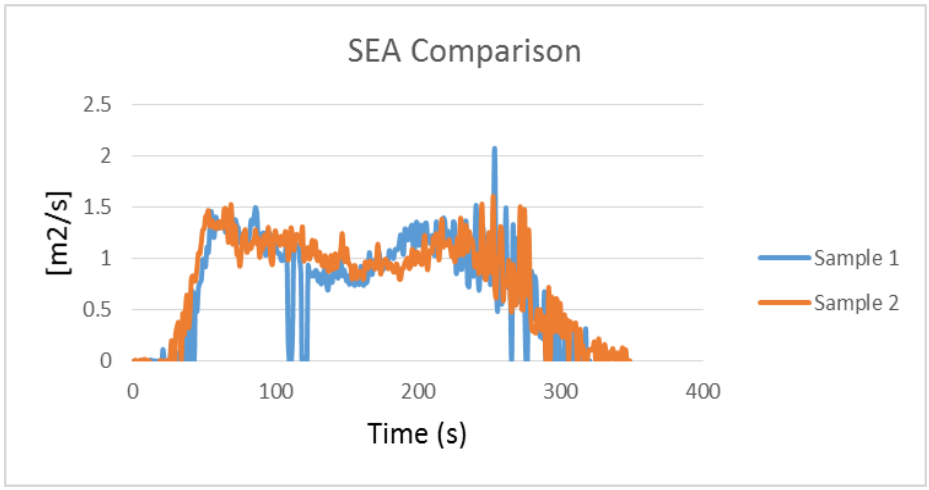
SEA Comparison
2.5
2
1.5
1
0.5
0
[m2/s]
0
100
200
300
400
Time (s)
Sample 1
Sample 2

Appendix- Flammability Parameter (FP)

Primary Author-Cristina Herrera

Secondary Author-None

This is a simple model of upward flame spread for thin interior materials. The analysis uses Cone Testing information and data points to describe a model with specific parameters to predict pyrolysis front propagation. The model takes into account the pyrolysis front at ignition time and the burnout front that starts afterwards. The proposed theory describes the key parameters controlling the flame spread process based on the upward flame spread model developed by Cleary and Quintiere[1]. The schematic modelling in shown in Figure 24.

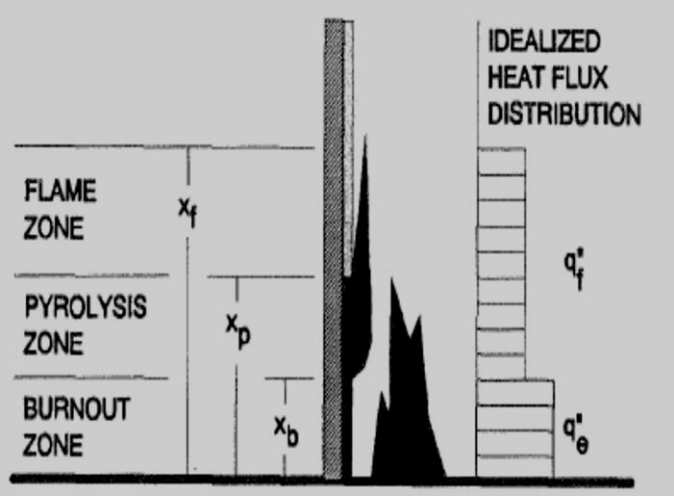

Figure 24: Schematic of Flame Spread Model[2]

According to Mowrer and Williamson[2] and based on the above model, the net rate flame propagation equals the difference between the pyrolysis front velocity and the burnout front velocity.

In this way, the rate of pyrolysis front advance is defined by:

$$(1) \qquad V_p = \frac{dx_p}{dt} = \frac{x_p(t + t_{f)} - x_p(t)}{t_f} = \frac{x_f(t) - x_p(t)}{t_f}$$

Model flame spread time calculated for heating inert wall with constant properties

$$(2) \qquad t_f = k\rho c \left[\frac{(T_{ig} - T_s)}{\dot{q}''}\right]^2$$

Where:

$k\rho c = thermal\ inertia$

$\dot{q''} = heat\ flux$

Likewise, the rate of fuel burnout is defined by the following equation:

(3) $$V_b = \frac{dx_b}{dt} = \frac{x_b(t + t_{bo}) - x_b(t)}{t_{bo}} = \frac{x_p(t) - x_b(t)}{t_{bo}}$$

At this point, Mowrer and Williamson made a distinction between the flame length before and after burnout commences. Flame length before burnout commences is defined by the ratio of the flame zone and the pyrolysis zone:

(4) $$\frac{x_f}{x_p} = k_f \dot{Q}''$$

Where:

$\dot{E}'' = energy\ release\ per\ unit\ area$

On the other hand, after burnout begins, flame length becomes:

(5) $$\frac{(x_f - x_b)}{(x_p - x_b)} = k_f \dot{Q}''$$

It is possible to assign a known value to the flame length parameter (k_f) as an assumption from Cleary and Quintiere, which is:

(6) $$k_f = 0.01\ \frac{m^2}{kW}$$

By using equation (6), the flame length equation before burnout, the rate of pyrolysis becomes:

(7) $$\frac{dx_p}{dt} = \left(k_f \dot{Q''} - 1\right)\frac{x_p}{t_f}$$

At the same time, it can be integrated with the following limits:

$x = x_{po} \quad when \quad t = 0$

$x = x_p \quad when \quad t = t$

(8) $$\int_{x_{po}}^{x_p} \frac{dx_p}{dt} = \int_0^t \left(k_f \dot{Q''}\right) \frac{dt}{t_f}$$

(9) $$\ln x_p - \ln x_{po} = \left(k_f \dot{Q''}\right) \frac{t}{t_f} - 0$$

(10) $$\ln \frac{x_p}{x_{po}} = \left(k_f \dot{Q''}\right) \frac{t}{t_f}$$

(11) $$\frac{x_p}{x_{po}} = \exp\left(k_f \dot{Q''}\right) \frac{t}{t_f}$$

The result becomes:

(12) $$x_p = x_{po} \exp\left[\frac{\left(k_f \dot{Q''} - 1\right)t}{t_f}\right]$$

Before burnout, the flame spread rate will be acceleratory if $x_f > x_p$ and deceleratory if $x_f < x_p$ if $k_f \dot{Q''} < 1$ when: $t > t_b$

The net rate of flame propagation can be expressed as the difference between the pyrolysis front velocity and the burnout front velocity.

(13) $$V_p(t) - V_b(t) = \frac{d}{dt}\left(x_p - x_b\right) = \frac{\left(x_f - x_p\right)}{t_f} - \frac{\left(x_p - x_b\right)}{t_{bo}}$$

Using the dimensionless flame length from equation (5):

(14) $$x_f = k_f \dot{Q''}\left(x_p - x_b\right) + x_b$$

(15) $$\frac{d}{dt}\left(x_p - x_b\right) = \frac{k_f \dot{Q''}\left(x_p - x_b\right) + x_b - x_p}{t_f} - \frac{\left(x_p - x_b\right)}{t_{bo}}$$

(16) $$\frac{d}{dt}\left(x_p - x_b\right) = \left(x_p - x_b\right)\left[\frac{k_f \dot{Q''} - 1}{t_f} - \frac{1}{t_{bo}}\right]$$

(17) $$\frac{d}{dt}(x_p - x_b) = (x_p - x_b)\left[\frac{(k_f \dot{Q}'' - 1)t_{bo} - t_f}{t_f t_{bo}}\right]$$

It can be integrated with the following limits:

$(x_p - x_b) = (x_{p1} - x_{po})$ $when$ $t = t_b$

$(x_p - x_b) = (x_p - x_b)$ $when$ $t = t$

The equation becomes:

(18) $$\int_{x_{p1}-x_{po}}^{x_p - x_b} (d(x_p - x_b))\frac{1}{(x_p - x_b)} = \int_{t_b}^{t}\left[\frac{(k_f \dot{Q}'' - 1)t_{bo} - t_f}{t_f t_{bo}}\right]dt$$

(19) $$\ln(x_p - x_b) - \ln(x_{p1} - x_{po}) = \left(\frac{(k_f \dot{Q}'' - 1)t_{bo} - t_f}{t_f t_{bo}}\right)t - \left(\frac{(k_f \dot{Q}'' - 1)t_{bo} - t_f}{t_f t_{bo}}\right)t_b$$

(20) $$\ln\frac{(x_p - x_b)}{(x_{p1} - x_{po})} = \left(\frac{(k_f \dot{Q}'' - 1)t_{bo} - t_f}{t_f t_{bo}}\right)(t - t_b)$$

(21) $$(x_p - x_b) = (x_{p1} - x_{po})e^{\left(\frac{k_f \dot{Q}'' t_{bo} - t_{bo} - t_f}{t_f t_{bo}}\right)(t - t_b)}$$

(22) $$(x_p - x_b) = (x_{p1} - x_{po})e^{\left(k_f \dot{Q}'' - \frac{t_f}{t_{bo}} - 1\right)\left(\frac{t - t_b}{t_f}\right)}$$

As result, the potential for acceleratory spread depends on three major parameters:

- Heat release rate per unit area $\dot{Q}''$
- Flame spread time t_f
- Burning duration t_{bo}

In this way, acceleratory spread is predicted when:

(23) $$k_f \dot{Q}'' - \frac{t_f}{t_{bo}} > 1$$

For simplicity, the above inequality can be represented and rearranged as:

(24) $$k_f \dot{Q}'' - \frac{t_f}{t_{bo}} - 1 > 0$$

t_f is the time that the material takes to heat to the point where ignition is possible, it is measured directly in the cone as the time when the test sample ignites under the imposed heat flux.

On the other hand, t_{bo} can be interpreted as the time during the test where burnout is clearly identified, it can be the time from ignition to the time of the peak heat release rate, or it can be calculated from the test data as:

(25) $$t_{bo} = \frac{E''}{\dot{E}''}$$

Where: E'' is the total energy released during the test.

As a result, Mowrer and Williamson found two main equations: one that represents the flame spread before burnout commences equation (12) and after burnout commences equation (22). Based in these derivations, an acceleratory flame spread behavior is predicted by equation (24) when the result yields positive numbers. This factor is also known as the B parameter used to interpret the flammability nature of the material.

Nomenclature:

$\mathrm{E} -$ Energy release (kJ)

$\dot{\mathrm{E}}'' -$ Energy release rate (kW)

$\mathrm{k\rho c} -$ Thermal inertia $\left(\frac{\mathrm{kW}}{\mathrm{m^2 - K^2}} - \mathrm{s}\right)$

$\mathrm{k} -$ Flame lenght parameter

$\mathrm{m} -$ Mass (Kg)

$\dot{\mathrm{q}}'' -$ Heat Flux $\left(\frac{\mathrm{kW}}{\mathrm{m^2}}\right)$

$\mathrm{t} -$ Time (s)

$\mathrm{T} -$ Temperature (K or C)

$\mathrm{V} -$ Velocity $\left(\frac{\mathrm{m}}{\mathrm{s}}\right)$

$\mathrm{x} -$ lenght parameter (m)

Subscripts:

b - Burnout zone
bo - Burning duration
e - External
f - Flame zone
ig - Ignition
p - Pyrolysis zone
s - Surface

Flammability Parameter References

1. Cleary, T., and J. Quintiere. "A Framework For Utilizing Fire Property Tests."Fire Safety Science 3 (1991): 647-56. Print
2. Mowrer, F., and R. Williamson. "Flame Spread Evaluation For Thin Interior Finish Materials."*Fire Safety Science* 3 (1991): 689-98. Print.

Appendix- Flammability parameter Average per composite (AVG)

Primary Author-Cristina Herrera

Secondary Author-None

Method one: Peak Heat Release Rate per Unit Area

The equation to find the flammability parameter or "B parameter" depends on three main factors, ignition time, burnout time and heat released rate based on the representation developed by Mowrer and Williamson[1]. The first approach for the heat releases rate is to use the value of the peak (maximum) HRRPUA during the test and the burnout time is the time between ignition and flame out (or burning duration),

Burnout time is defined as the time between ignition and edge burning (when possible) since that would be the total pyrolysis time of interest. When edge burning occurs, after that point, the data obtained from the cone is not useful for our analysis anymore since the cone works in just one dimension (x axis) and edge burning in principle occurs in three dimensions. The data obtained after edge burning will yield wrong information; therefore edge burning time was set as the time when burnout takes place. The procedure followed to obtain the flammability parameter using this approach is outlined as follows:

Procedure:

1. Identify the time of ignition from the cone data summary and subtract the time of shutter open to obtain a time from cero (when the sample was exposed to a heat flux) to the time where the sample hit ignition point.
2. Identify at what time edge burning occurs and record that time (subtracting the time at which the shutter opened) to have a reference point of where the burning (or the useful data from the cone) ends.
3. Find the maximum HRRPUA from the data summary page and identify at what time that peak occurred (again subtract the time at which the shutter was opened to be consistent and have a time from cero time when the sample was exposed to the heat flux)
4. Compare the time at which the peak occurred and the ignition time to verify that the peak heat released rate occurs after ignition. It is not physically consistent if

the peak happens before ignition. If there is any sample where the peak HRRPUA occurs before ignition, ignore that peak and take the next peak HRRPUA after ignition and before edge burning.

5. Record all the times and the maximum HRRPUA in a spreadsheet and solve for equation to compute the flammability parameter.
6. Compute the standard deviation for each composite.
7. Find the overall uncertainty for this method by using the pooled variance theory[2].

Results Method one: Peak HRRPUA

Table 10:Flammability parameter values method one

Composite	Average B parameter
Hetron 100:00	0.9628 ± 0.7773
Hetron 100:33	-0.043 ± 0.7740
Hetron 100:66	-0.0552 ± 0.0895
Hetron 100:100	-0.0627 ± 0.1273
Hetron 100:130	-1.7584 ± 1.2130
Fireblock 100:00	1.2302 ± 0.2948
Fireblock 70:30	0.2516 ± 0.1919
Fireblock 60:40	-0.2761 ± 0.4593
Fireblock 50:50	-0.2707 ± 0.4228
Fireblock 40:60	-0.7080 ± 0.0528

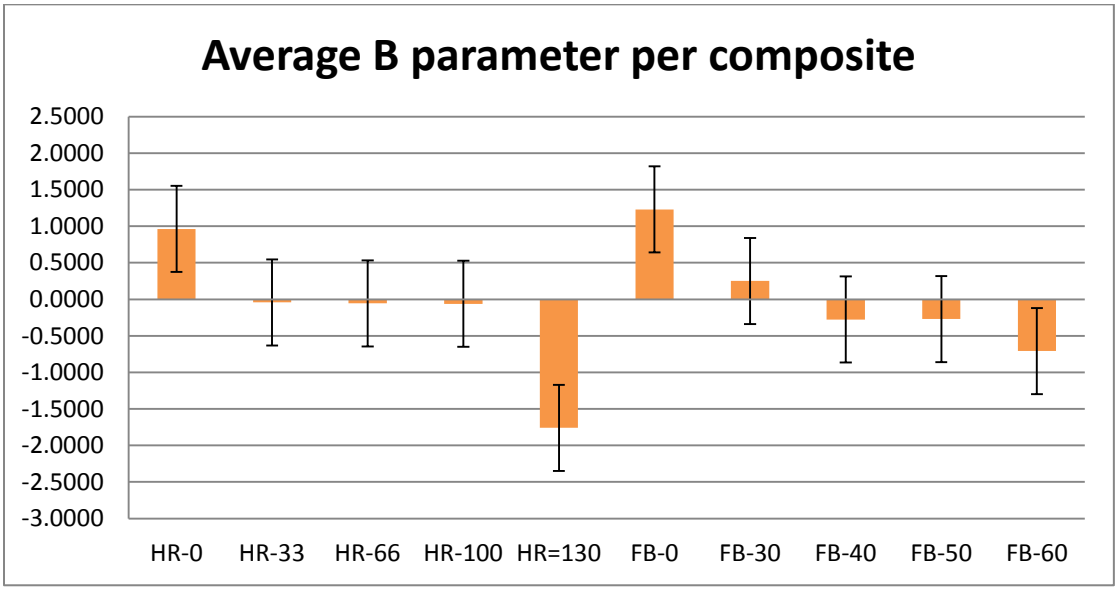

Figure 25: Flammability parameter method one

Since 3 and 4 trials were performed per composite to obtain systematic results, the standard deviation per composite was calculated as shown in Table 10. However, in order to better understand the uncertainty of method one, a method to estimate the overall standard deviation was used to find only one value that accounts for the error measurements. The pooled variance theory was applicable to this analysis because the data consists of different populations with different average values but the variance of these populations in assumed to be the same because it used the same instrumentation for all test (cone calorimeter) and the precision is assumed to be the same. The value obtained is the uncertainty for method one and in represented in Figure 25 in the error bars.

$$S_p{}^2 = \frac{(n_1 - 1){S_1}^2 + (n_2 - 1){S_2}^2 + \cdots + (n_k - 1){S_k}^2}{n_1 + n_2 + \cdots + n_k - k}$$

$$S_p{}^2 = \frac{3(0.7773)^2 + 3(0.7740)^2 + 2(0.0895)^2 + 2(0.1273)^2 + 2(1.2130)^2 + 2(0.2948)^2 + \cdots + 2(0.0528)^2}{4 + 4 + 3 + 3 + 3 + 3 + 3 + 3 + 3 + 3 - 10}$$

$$S_p{}^2 = \frac{7.6334}{22}$$

$$S_p{}^2 = 0.34697$$

$S_p{}^2$ is the pooled variance, and the square root of a pooled variance is the pooled standard deviation.

$$\boldsymbol{pooled\ standard\ deviation = 0.5890}$$

Method two: Average Heat Released Rate per Unit Area

The second method used to calculate the flammability parameter for all samples was really similar to the first method since both are derived from the same model. Instead of using the peak Heat Released Rate per Unit Area, the second method uses the average heat released rate from ignition to edge burning. The ignition time and the burnout time are the same as in method one; therefore, the procedure followed for method two is almost identical to the procedure of method one.

Procedure:

1. Identify the time of ignition from the cone data summary and subtract the time of shutter open to obtain a time from cero (when the sample was exposed to a heat flux) to the time where the sample hit ignition.
2. Identify at what time edge burning occurs and record that time (subtracting the time at which the shutter opened) to have a reference point of where the burning (or the useful data from the cone) ends.
   Calculate the average HRRPUA from ignition to edge burning.
3. Record all the times and the average HRRPUA in a spreadsheet and solve for equation to compute the flammability parameter.
4. Find the standard deviation for each composite.
5. Find the overall uncertainty of this method by using the pooled variance theory.

Results method two:

Table 11: Flammability Parameter method two

Composite	Average B parameter
Hetron 100:00	-0.4836 ± 0.7245
Hetron 100:33	-0.5919 ± 0.4583
Hetron 100:66	-0.5995 ± 0.1553
Hetron 100:100	-0.7192 ± 0.0524
Hetron 100:130	-2.2500 ± 0.9331
Fireblock 100:00	0.3313 ± 0.0233
Fireblock 70:30	-0.0493 ± 0.3539
Fireblock 60:40	-0.4574 ± 0.4610
Fireblock 50:50	-0.5308 ± 0.3401
Fireblock 40:60	-0.6568 ± 0.1639

Table 11 show average flammability parameter for each systems and the corresponding standard deviation.

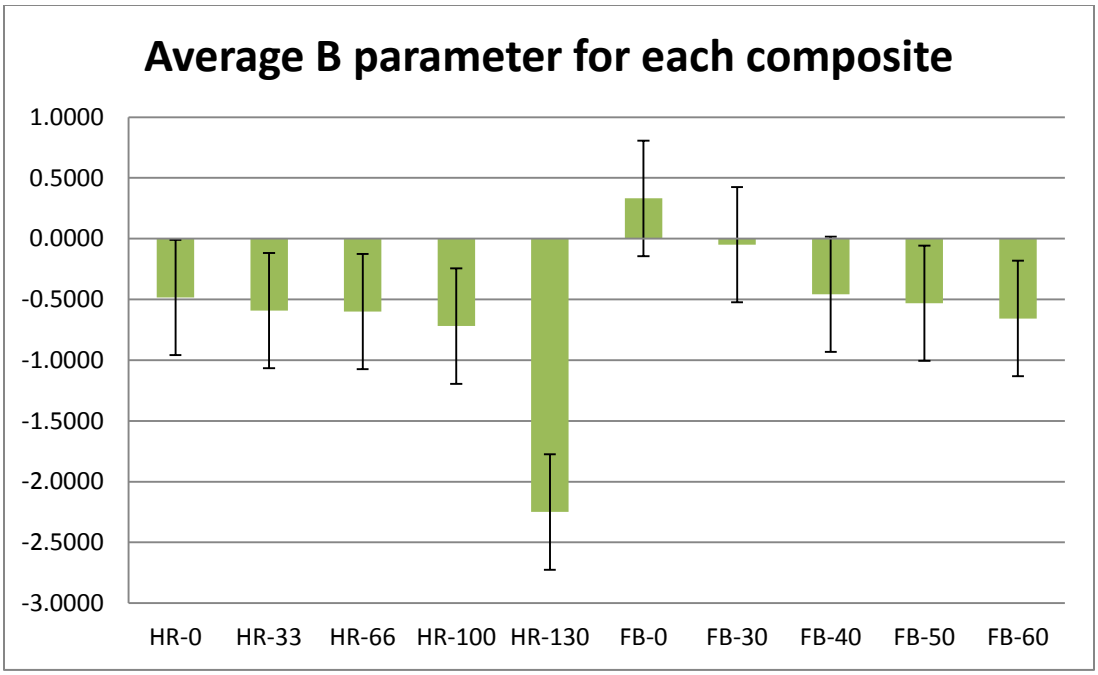

Figure 26: Flammability Parameter method two

$$S_p{}^2$$

$$= \frac{3(0.7245)^2 + 3(0.4583)^2 + 2(0.1553)^2 + 2(0.0524)^2 + 2(0.9331)^2 + 2(0.0233\ )^2 + \cdots + 2(0.1639)^2}{4 + 4 + 3 + 3 + 3 + 3 + 3 + 3 + 3 + 3 - 10}$$

$$S_p{}^2 = \frac{4.9616}{22}$$

$$S_p{}^2 = 0.2255$$

$S_p{}^2$ is the pooled variance, and the square root of a pooled variance is the pooled standard deviation.

$$\boldsymbol{pooled\ standard\ deviation = 0.4749}$$

Figure 26 shows the values obtained for each systems and the uncertainty of the method used is represented by the error bars.

Method three: calculated burnout time

The third method used to compute the flammability parameter is slightly different from the other two methods in the sense that this method calculates a burnout time instead of assume that the burn out time is when edge burning starts.

This last computation for the flammability parameter uses the average heat release rate and the ignition time that can be directly retrieved from the cone data summary. For the burnout time (t_{bo}) it applied the formula presented by Mowrer and Williamson[1] where:

$$t_{bo} = \frac{E''}{\dot{E}''}$$

E'' is the total energy released during the test in kJ and $\dot{E}''$ is the average energy release rate which is in kW.

By simplifying the units in this operation (Joules and Watts) the result obtained is seconds (s) which is the unit desired to correctly determine this value as the burnout time (time at which the sample was consumed).

$$\frac{kJ}{kW} = \frac{(1000)\left(\frac{Kg * m^2}{s^2}\right)}{(1000)\left(\frac{Kg * m^2}{s^3}\right)} = \frac{s^3}{s^2} = s$$

Procedure:

This analysis followed the same step by step computation has in method one and two:

1. Identify the time of ignition from the cone data summary and subtract the time of shutter open to obtain a time from cero (when the sample was exposed to a heat flux) to the time where the sample hit ignition.
2. Find the total heat release (kJ) during the entire test.
3. Find the average heat released rate (kW) for each test.
4. Solve for the burnout time.
5. Record all the values in a spreadsheet and solve for equation to compute the B parameter.
6. Find the standard deviation for each composite.
7. Find the overall uncertainty of this method by using the pooled variance theory.

Results method three: calculated burnout time

Table 12: Flammability Parameter method three

Composite	Average B parameter
Hetron 100:00	-0.3995 ± 0.6820
Hetron 100:33	-0.5298 ± 0.4051
Hetron 100:66	-0.5547 ± 0.1766
Hetron 100:100	-0.6126 ± 0.0461
Hetron 100:130	-0.7048 ± 0.2031
Fireblock 100:00	0.5495 ± 0.1262
Fireblock 70:30	0.2960 ± 0.2686
Fireblock 60:40	0.1654 ± 0.1816
Fireblock 50:50	-0.1329 ± 0.2372
Fireblock 40:60	-0.0342 ± 0.1208

Table 12 shows the average flammability parameter calculated with method three and the correspondent standard deviation.

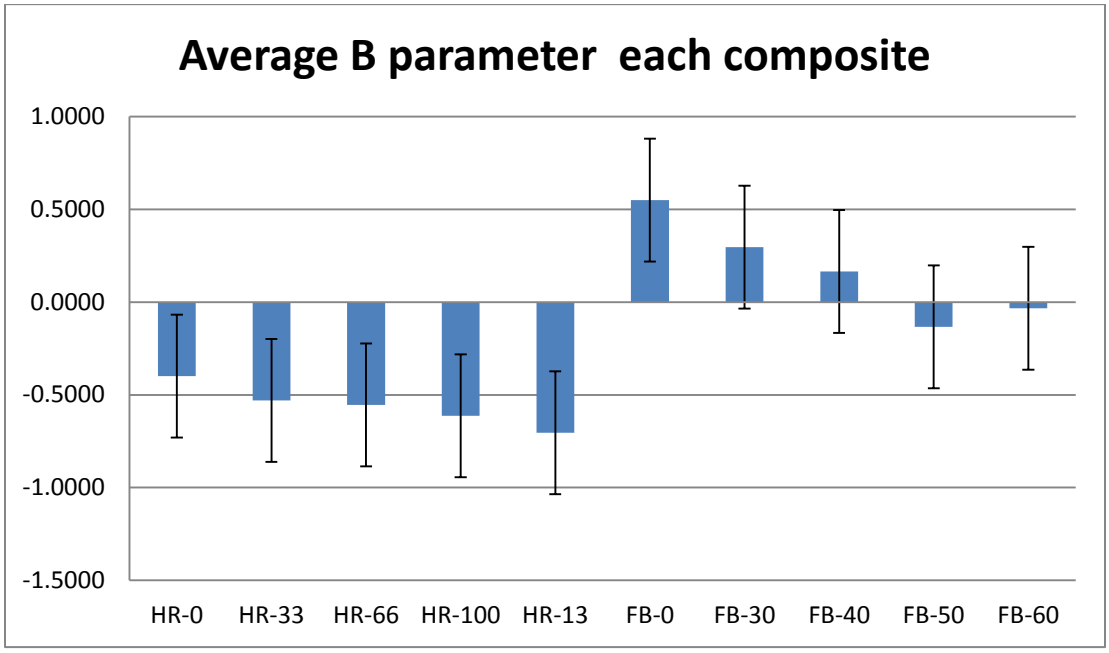

Figure 27: Flammability parameter method three

$$S_p{}^2$$

$$= \frac{3(0.6820)^2 + 3(0.4051)^2 + 2(0.1766)^2 + 2(0.0461)^2 + 2(0.2031)^2 + 2(\ 0.1262)^2 + \cdots + 2(0.1208)^2}{4 + 4 + 3 + 3 + 3 + 3 + 3 + 3 + 3 + 3 - 10}$$

$$S_p{}^2 = \frac{2.4206}{22}$$

$$S_p{}^2 = 0.1100$$

$S_p{}^2$ is the pooled variance, and the square root of a pooled variance is the pooled standard deviation.

$$\boldsymbol{pooled\ standard\ deviation = 0.3317}$$

The uncertainty for method three is represented in Figure 27 with the error bars.

The burnout time calculated in each test is slightly higher than the time we recorded as edge burning time (the time at which edge burning was visually evident, and this marked the end of the test). Therefore, if the burnout time is higher than the time we took as the end of term some inconsistency might alter the final results for the flammability parameter.

Nevertheless, the values obtained with this approach are more sound but they do vary slightly with the flammability parameter values computed with method one and method two. This visible difference can be explained by some factors in the data acquisition and data interpretation.

The visually assumption of edge burning tome might not be completely accurate, something that is expected in an experimental procedure such as the cone calorimeter testing.

The values for energy released rate (kW) sometimes register negative values, something that is physically inconsistent

Error of the measurements devices and the calibration process might have some influence in those negative values that are idiosyncrasies of the machine and the process but those values do not mean that during that period of time no energy was released, when we used the numerical average of the energy release rate during the test those negative value might affect the total result. The same circumstance takes place with the measures of total energy released (kJ) where the summary page of the cone data have a column to display the heat released summed and it also takes into account the negative values recorded.

Average flammability parameter of the three methods

After computing the average flammability parameter using three different methods, method two and method three yield similar results, while method one yields values very different specially for Hetron Samples (Fireblock samples are more volatile regardless the method used) as shown in Table 13. The fact that method two and method three yield closer values can be justified by the fact that both method use the average heat release rate per unit area while method one uses the peak HRRPUA. At this point it is important to highlight that using a peak value for HRRPUA might not be the most suitable model for the type of graphs obtained for HRRPUA, where there is not a distinctive peak. In some cases the peak HRRPUA happened before or right at ignition time, which made the calculations more difficult. On the other hand, method two and three are more consistent and their calculations did not any major problem.

Table 13: Summary Table Flammability Parameter

Composite	Peak HRRPUA	Average HRRPUA	Burnout time
Hetron 100:00	0.963	-0.484	-0.399
Hetron 100:33	-0.043	-0.592	-0.529
Hetron 100:66	-0.055	-0.599	-0.555
Hetron 100:100	-0.063	-0.719	-0.613
Hetron 100:130	-1.758	-2.25	-0.705
Fireblock 100:00	1.230	0.331	0.549
Fireblock 70:30	0.252	-0.049	0.296
Fireblock 60:40	-0.276	-0.457	0.165
Fireblock 50:50	-0.271	-0.531	-0.133
Fireblock 40:60	-0.708	-0.657	-0.034

Given this discrepancy between method one and the other two methods, and in order to provide a final flammability parameter value for each composite, an average was obtained from method two and method three as shown in Table 14:

Table 14: Averaged Flammability Parameter

Composite	Average B parameter
Hetron 100:00	-0.441
Hetron 100:33	-0.561
Hetron 100:66	-0.577
Hetron 100:100	-0.666
Hetron 100:130	-1.477
Fireblock 100:00	0.440
Fireblock 70:30	0.123
Fireblock 60:40	-0.146
Fireblock 50:50	-0.332
Fireblock 40:60	-0.345

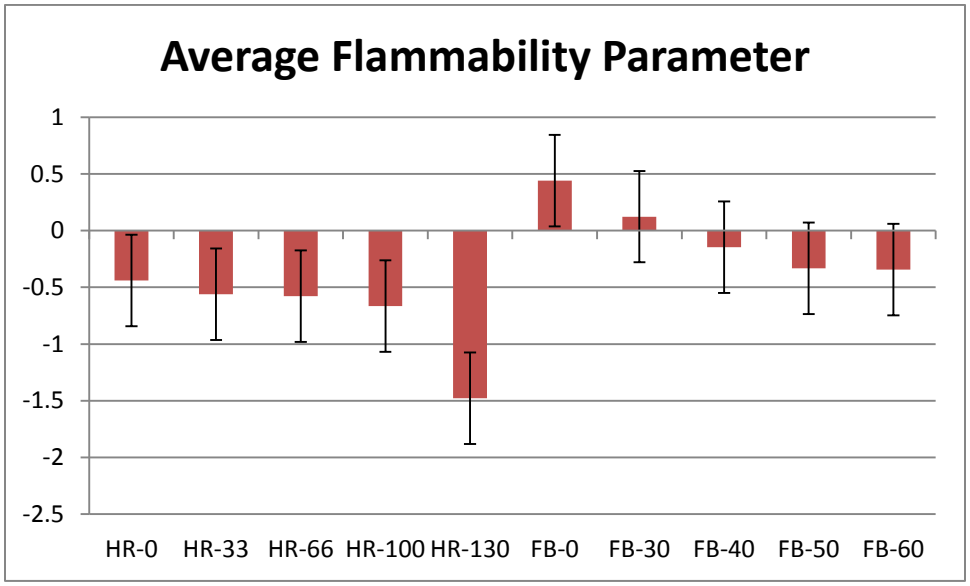

Figure 28: Averaged Flammability Parameter

As shown in *Figure **28**: Averaged Flammability Parameter*Figure 28, according to the negative values for the flammability parameter, all Hetron samples are not expected to have an acceleratory flame spread behavior while two Fireblock samples registered positive values which might suggest an acceleratory flame spread behavior; however, those positive values are really small, they are closer to zero than to 1 so in general terms we can say that Sand samples are not expected to have an acceleratory flame spread behavior either.

Looking at the data for Hetron samples, the flammability parameter values for Hetron 100:00 to Hetron 100:100 are really close values while for Hetron 100:130 it increases to more than twice the value. A ratio of ATH greater than 130 definitely makes a significant different in the composite, for ratios below that there is no a significant change in the behavior of the material overall.

On the other hand, Fireblock samples do not shown a visible trend in terms of what happen when the ratio of Sand decreases. At Fireblock 50:50 it seems that the flammability parameter reaches a steady value of -0.7.

The overall uncertainty for these values was calculated to be ±0.4033 which is represented by the error bars.

References

1. Mowrer, F., and R. Williamson. "Flame Spread Evaluation For Thin Interior Finish Materials."*Fire Safety Science* 3 (1991): 689-98. Print.
2. Gravetter, Frederick J., and Larry B. Wallnau. Essentials of Statistics for the Behavioral Sciences. Australia: Wadsworth, Cengage Learning, 2014. Print.

Appendix- Flame length screening tool (FLST)

Primary Author-Cristina Herrera

Secondary Author-None

The model developed by *Acosta et al.* used the idea of static concurrent flame lengths; this means that the pyrolysis zone (burn area) does not change as the specimen burns and the flame is extending in the direction in which the air is moving. This statement is assumed to be correct because limited pyrolysis movement is a characteristic of specimens with a flame spread rating of less than 25 (Class A materials). All the samples analyzed in this project (Hetron and Fireblock systems) are assumed to be Class A because they were developed as fire retardant and thermal resistance composites. Nevertheless, this assumption will be verified or re-stated after computing the flame spread index for all samples.

Since this model was developed to correlate cone calorimeter data with tunnel test performance, the second assumption states that "there is an imposed air flow in the tunnel test of 1.25 m/s in the direction which the flame propagates."[1]. The final model developed is described by the following equation:

$$L_f = (\beta + \gamma) * \dot{Q}'^n$$

The basic assumption for this model states that the heat release rate of the specimen and the burners in the tunnel act as a line fire point source that also accounts for a point source that moves as the specimen burns in the tunnel. Gama and beta are the constants that accounts for these two basic assumptions. Beta (β) would be the constant responsible for creating a flame length of 4.5 feet (when the burners are on), and Gama (γ) represents the fire scenario after ignition by using an ignition delay from the cone test. Similarly, $\dot{Q}'$ is the heat release rate per unit width of the heat generated by the sample plus the heat generated by the burners. Finally, n is a constant that correlates different models to predict the flame length in the tunnel.

Based on this model, two set of equations were developed for flame length screening tool, one that uses multiple incident heat fluxes and one that uses a single incident heat flux. The first model is an accurate representation of the tunnel test environment using heat release rate from the cone calorimeter. The incident flux at which the sample is exposed in the tunnel is not constant, and according to William Parker[2], the incident heat flux changes as the distance and the time increase. Therefore, the total length of the tunnel is divided into three main areas that

represent three different scenarios along the tunnel. The tunnel schematic is represented in Figure 29.

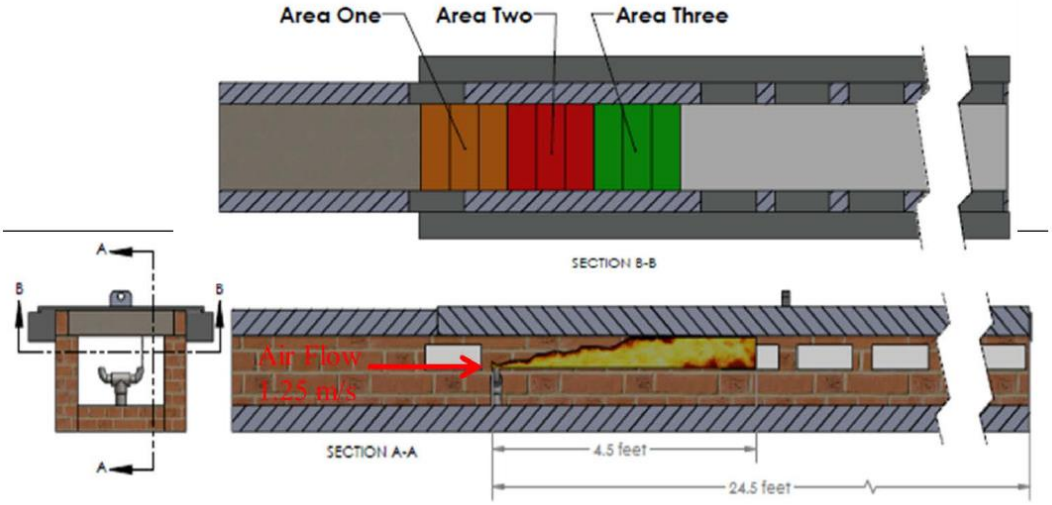

Figure 29: Tunnel Schematic-Areas from Acosta et al.

Cone tests were performed with three incident heat fluxes (20 kW/m^2, 30 kW/m^2, 40 kW/m^2) to better describe the thermal environment along the tunnel.

Model for multiple incident heat fluxes

After some readjustments, the final model is driven by the two main equations that have the same physical interpretation but are applicable to two different cases (coated and non-coated FRPs):

$$(1) \quad Case\ stone\ coating\ L_f = \left(0.2211 * \left(\dot{Q}' + 204.47\right)^{0.6709}\right) - 4.5$$

$$(2) \quad Noncoated\ FRPs\ L_f = \left(0.1647 * \left(\dot{Q}' + 204.47\right)^{0.6709}\right) - 4.5$$

This equation yields the flame extension at the tunnel test (after the 4.5 foot generated by the burners), where $\dot{Q}'$ is an aggregate heat release rate per unit width (compound of the three HRR curves from the three different heat fluxes)

The width of the Steiner tunnel is known to be 0.43 m.

In other to find the compound heat release per unit width it is necessary to combine all the heat release rate curves obtained for each trial of the same composite by:

- Averaging the heat release rate per unit area if there is more than one trial per sample for each incident heat flux (for each second of the test).

- Taking into account that the total length of 4.5 is divided in three equal areas, each heat release rate per unit area curve is only applied to the section of the burn area that is affected by that incident heat flux. This means that the heat release rate needs to be multiplied by 0.20 m^2 which is the pyrolysis area.
- Adding all the three heat release rate curves will yield the total HRR.
- Multiplying HRR by 0.43m to obtain the heat release rate per unit width.
- 204.47 kW/ m^2 is added to account for the heat generated by the burners (also expressed as HRR per unit width).

This model applies a flame extension of zero before the ignition time.

Single incident heat flux model:

Governed by the same previous model, another set of equations is derived for a simplest case where just one incident heat flux is used. After some rearrangements to the model to account for air velocity, ignition delay, and flame lengths according to several correlations, the final model seems to be less accurate than the first model presented but it can be applicable as a quick screening of how the specimen would perform in tunnel testing. The best incident heat flux was found to be 40 kW/m^2. Following the same analysis as before, the two new equations are:

$$(3) \quad Gelcoat\ Concrete\ Polymer\ L_f = \left(0.2322 * \left(\frac{0.6\dot{Q}'' + 88}{0.43}\right)^{0.6494}\right) - 4.5$$

$$(4) \quad Noncoated\ Hetron\ L_f = \left(0.1574 * \left(\frac{0.6\dot{Q}'' + 88}{0.43}\right)^{0.6494}\right) - 4.5$$

Where $\dot{Q}''$ is heat release rate per unit area from the cone data (therefore it needs to be multiplied by 0.6 which would represent the pyrolysis area at the tunnel because with this model does not divide the length of the tunnel into sub-area; instead, it takes 4.5 foot as the total pyrolysis length since there is just one representative incident heat flux)
The constant 88 (kW) accounts for the heat release by the burners.
Similar to the first set of equations, this model applies a flame extension of zero before ignition.
For the purpose of this project, case stone coating will predict the behavior of gel-coat Fireblock samples. On the other hand, the equation for non-coated FRPs will predict the behavior of Hetron samples (unsaturated polyester).

After obtaining the flame extension for the specimen using either of the two set of equations, that data can be used to obtain the flame spread index by using the following equation presented in the ASTM E84[3] standard for tunnel test:

$$(3) \quad FSI = 0.515 * A_T \; for \; an \; area \; \leq \; 97.5$$

$$(4) \quad FIS = \frac{4900}{195 - A_T} \; for \; an \; area > 97.5$$

Where A_T is a single value equal to the total area under the curve of flame extension versus time.

Data interpretation:

This analysis used the single incident heat flux model as a quick screening to predict how Hetron and Fireblock samples would behave at tunnel testing under an incident heat flux of 50 kW/m^2 for all 10 systems, and under an incident heat flux of 40 kW/m^2 for selected systems. The analysis method followed is outlined step by step in the following list:

- Average the heat release rate per unit area (HRRPUA) of all the trials per composite to obtain a single representative value for HRRPUA.
- Use HRRPUA values from ignition until edge burning. Recall that before ignition, the flame extension is zero according to the model. Similarly, edge burning is the limit of useful data from the cone.
- Use equation (3) to solve for the flame extension for Hetron samples or use equation (4) for Fireblock samples, both equations assume a flame extension of zero before ignition.
- Based on the flame extension obtained, analyze whether or not the values obtained are sound. For example, it is not physically consistent if the flame extension obtained as time increases is smaller than the flame extension obtained at ignition. It is not possible that the flame shrinks at any point after the test started. Therefore, if this seems to be the case, use an "if condition" in the spreadsheet to ensure that the next value for flame length is not smaller than the one obtained previously.
- Plot the graph of flame extension versus time to obtain the area under the curve, A_T.
- Use the trapezoid rule for approximating integrals.

Figure 30 and 32 show the flame extension curves obtained for Hetron Systems at an incident heat flux of 50 kW/m^2 and 40 kW/m^2 respectively. Figure 31 and 33 show the flame extension for Fireblock Systems at an incident heat flux of 50 kW/m^2 and 40 kW/m^2 respectively.

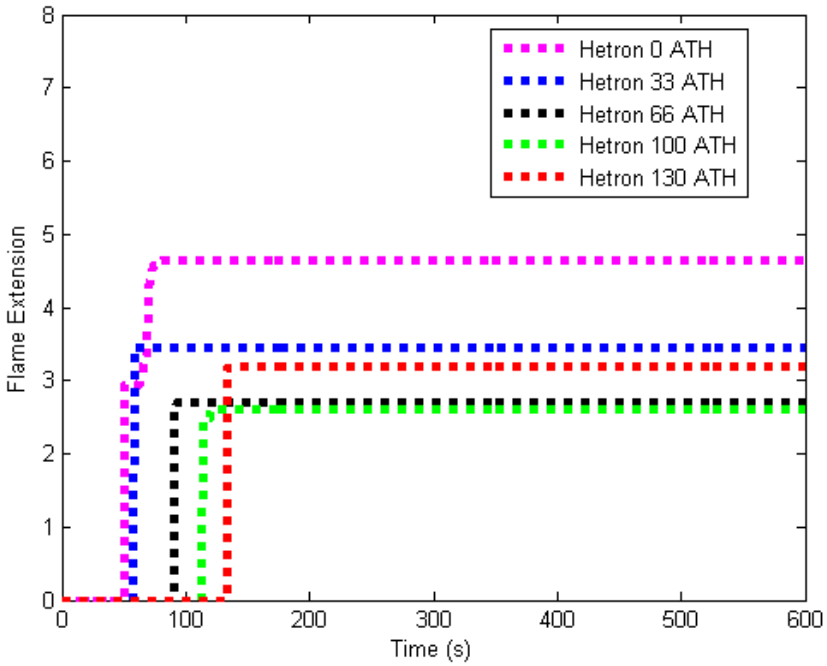

Figure 30: Flame extension Hetron Samples an IHF of 50 kW/m^2

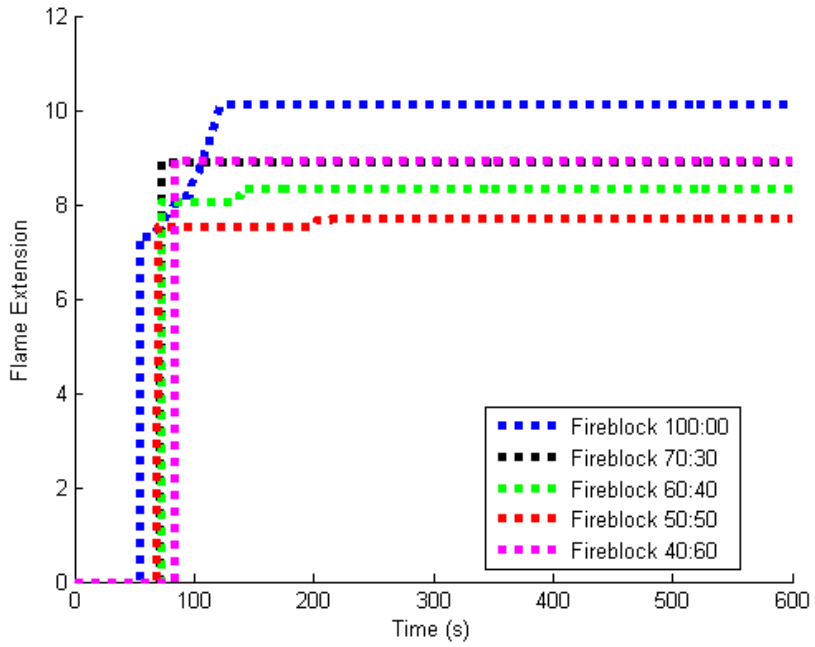

Figure 31: Flame extension Fireblock Samples an IHF of 50 kW/m^2

Figure 30 and Figure 31 show the flame extension for Hetron and Fireblock samples at an incident heat flux of 50 kW/m^2 where Fireblock samples tends to exhibit a larger flame extension compared to Hetron samples, it is almost twice the value of Hetron flame extension. As the ATH ratio increases in Hetron samples, the flame extension decreases but at a ratio of 130 ATH is increases again. On the other hand, for Fireblock samples there is no a visible trend of the flame extension as the sand ratio varies.

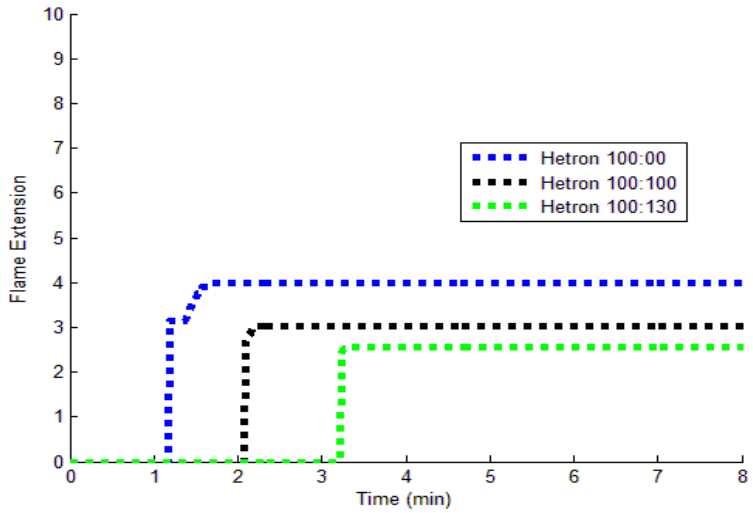

Figure 32: Flame Extension of Hetron Samples at IHF of 40 kW/m^2

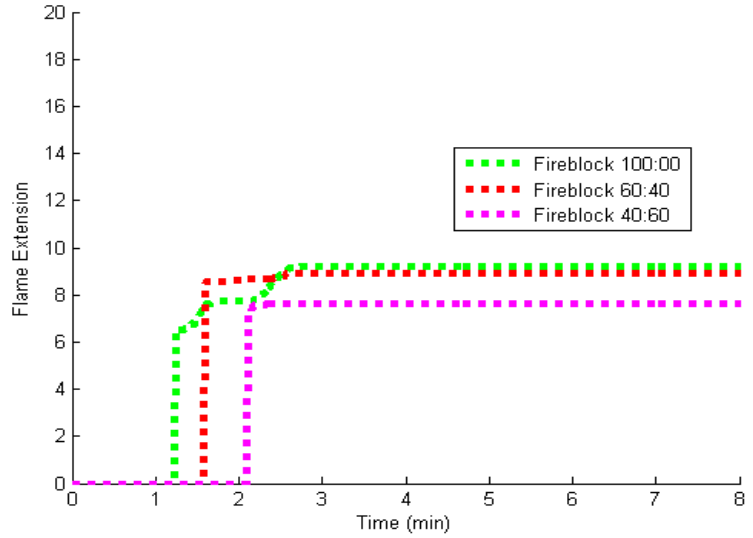

Figure 33: Flame Extension for Fireblock Samples at IHF of 40 kW/m^2

Figure 32 and 33 show the flame extension of Hetron and Fireblock at an incident heat flux of 40 kW/m^2 where there is a more visible influence of the additive ratio in both composites. As the ATH ration increases in Hetron samples, the flame extension tends to decrease. A similar behavior is observed for Fireblock samples, as the sand ratio increases the flame extension decreases. The influence of ATH is more perceptible than the influence of sand because the flame extension in Fireblock samples decreases by a very little amount.

References

1. Acosta, C., Mahoney, S., Nava, N. and Wright, W. (2013). "Evaluation of Fiber Reinforced Polymer Bench Scale Specimen Sizes and Prediction of Full Scale Flame Spread Testing for Building Applications". (Undergraduate Major Qualifying Project No. NAD FM12).
2. Parker, William. "An Investigation of the Fire Environment in the ASTM E 84 Tunnel Test." National Bureau of Standards technical note 945 (1977): 28. Print.
3. ASTM Standard e-84,2013, "Standard Test Method for Surface Burning Characteristics of Building Materials," ASTM International, West Conshohocken, PA, 2013 DOI : 10.1520/E0084-12A, www.astm.org.

Appendix- Smoke developed Index (SDI)

Primary Author-Cristina Herrera

Secondary Author-None

In order to be able to use the heat release rate obtained from the cone in a model that predict the smoke developed index in the tunnel test some correlations need to be done. First, the main variables from the cone are described as:

1. Heat release rate per unit area (kW/m^2):

$$(5) \quad \dot{q''}_{(t)} = \frac{\dot{Q}_{(t)}}{A_s} = \left[\frac{kW}{m^2}\right]$$

2. Specific extinction area (m^2/g):

$$(6) \quad SEA = \frac{\dot{V} k \Delta t}{m_1 - m_2} = \frac{k\dot{V}}{\dot{m}} = \frac{SPR}{\dot{m}}$$

$$\left[\frac{\frac{m^3}{s} * \frac{1}{m} * s}{g}\right] = \left[\frac{m^2}{g}\right] = \left[\frac{\frac{1}{m} * \frac{m^3}{s}}{\frac{g}{s}}\right] = \left[\frac{m^2}{g}\right] = \left[\frac{\frac{m^2}{s}}{\frac{g}{s}}\right] = \left[\frac{m^2}{g}\right]$$

3. Extinction coefficient (1/m):

$$(7) \quad k = \frac{1}{L} \ln \frac{l_o}{l}$$

Where:

- L=extinction beam path, m.
- l= actual beam intensity
- lo= beam intensity with no smoke

4. Effective heat of combustion (kJ/g):

$$(8) \quad h_{eff} = \frac{\dot{Q}_{(t)} \Delta t}{m_1 - m_2} = \left[\frac{kW * s}{g}\right] = \left[\frac{kJ}{g}\right]$$

Rearranging this expression:

$$\frac{(m_1 - m_2)}{\Delta t} * h_{eff} = \dot{Q}_{(t)}$$

$$\dot{m} * h_{eff} = \dot{Q_{(t)}}$$

$$(9) \quad h_{eff} = \frac{\dot{Q}_{(t)}}{\dot{m}} = \left[\frac{kW}{\frac{g}{s}}\right] = \left[\frac{kJ}{g}\right]$$

With these same parameters it is possible to relate the smoke production rate in the tunnel in terms of the heat release rate predicted in the tunnel and the cone data:

$$(10) \quad SPR_{tunnel} = \frac{\dot{Q}_{tunnel} * SEA_{cone}}{h_{eff}}$$

Where the predicted heat release rate in the tunnel is described by the following equation:

$$(11) \quad \dot{Q}_{tunnel} = \left(0.6 * \dot{Q''}_{cone}\right) + 88$$

The previous equation describes a transformation of the heat released rate per unit area from the cone into a heat release rate per unit width, by multiplying the $\dot{Q''}$ by 0.6 which is the exposed pyrolysis area in the tunnel, in a two dimensions representation. This term was then added to 88 kW to account the heat generated by the burners at the tunnel.

This analysis leads to a relation between the extinction coefficient and the SPR in the tunnel:

$$SPR_{tunnel} = k\dot{V}$$

Where:

$$k = \frac{SPR_{tunnel}}{\dot{V}}$$

Now, using Janssens' model[1]:

$$(12) \quad T\%_{(t)} = 100/\exp\left(\frac{293 \times SPR_{(t)} \times D}{\dot{V}_a T_{e\,(t)}}\right)$$

The light transmission at the tunnel can be compute after obtaining the SPR at the tunnel and rearranging Janssens' model:

$$(13) \quad T\%_{(t)} = 100/\exp\left(\frac{293 * k * 0.076}{T_{e\,(t)}}\right)$$

Where Te is the temperature in the exhaust duct and can be computed using the following equation from Parker's analysis[2]:

$$(14) \qquad T_e = 31 + 2.5\left[0.43 * \dot{Q}_{tunnel}\right]$$

The transmission percentage equation can be rearranged as:

$$(15) \qquad T\%_{(t)} = \frac{100}{\exp\left(\frac{293 * k * 0.076}{31 + 2.5\left(0.43 * (0.6 * \left(\dot{Q'}_{cone} + 88\right)\right)}\right)}$$

Then, the transmission percentage is a measurement based on two independent variables: k and Qcone

$$(16) \qquad T\%_{(t)} = \frac{100}{\exp\left(\frac{22.268 * k}{(0.645 * Q_{cone}) + 125.6}\right)}$$

Finally, from the ASTM E84[3] the smoke developed index is a ratio of the area under the curve of the light transmission versus time of the sample being tested and a standard reference of red oak light transmission:

$$(17) \qquad SDI = \frac{\left(\int_0^{10\ min}(100 - T\%)dt\right)_{Test\ specimen}}{\left(\int_0^{10\ min}(100 - T\%)\right)_{Red\ Oak}} \times 100$$

By applying the light transmission equation and the SDI presented in the standard, a quick screening to determine the smoke index of Hetron and Fireblock samples was computed following a step by step procedure outlined as:

- Clean all noise from the data obtained from the cone.
- Average the heat release rate per unit area of all the trials corresponding to same sample to create a composite Heat Released Rate.
- Average the extinction coefficient of all the trials corresponding to the same sample. At this point make sure that all extinction coefficient data points are sound values, this means, do not consider any negative value. In case the raw data yields negative extinction coefficient values, assumed they are zero. It is safe to assume them to be zero because a negative value for the extinction coefficient means that the Beam intensity with smoke is greater than the beam intensity without smoke, and since the beam intensity without smoke is assumed to be an intensity of 100%, a negative value means that our beam intensity with smoke is somehow greater than 100%, which is physically inconsistent. An

extinction coefficient of zero will represent an obscuration percentage of zero, assuming that there is no smoke produced.

- Convert the HRRPUA into a heat release rate representative of the tunnel environment by using equation 11.
- Use all the data collected up to this point to solve for the temperature in the exhaust duct of the tunnel by applying equation 14.
- Use equation 13 to find the light transmission of each sample.
- Finally, apply equation 17 to solve for the smoke developed index for each sample.

The reference point in equation 17 corresponds to the obscuration percentage of Red Oak. From the graph of red oak in the ASTM E84 standard, a reproduction of the obscuration versus time graph is shown in the following graph:

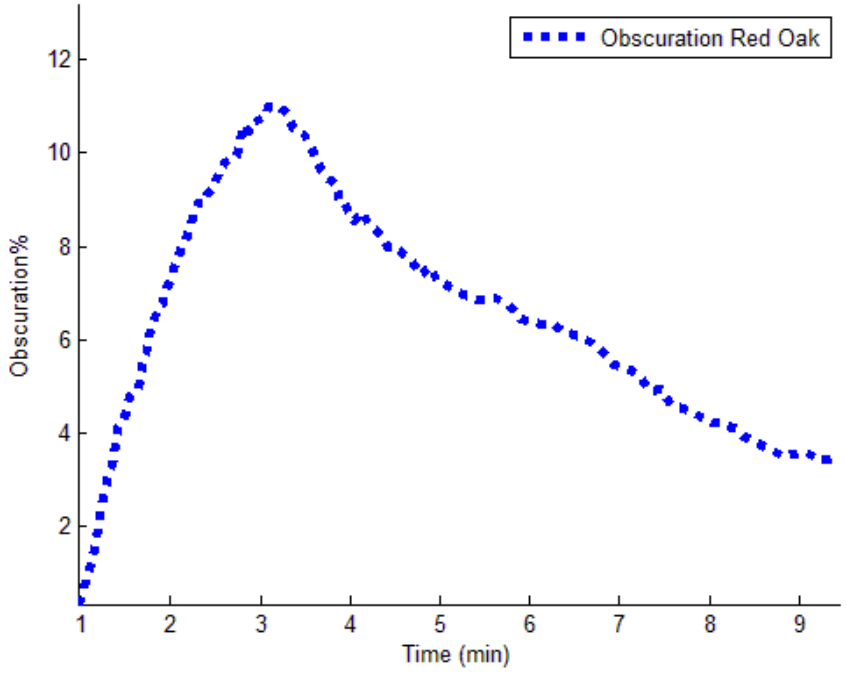

Figure 34: Obscuration Percentage Red Oak

The above graph shows the obscuration percentage of Red Oak, from which after applying the trapezoidal rule for approximating integral in a Matlab program, the area under the curve was found to be 54.07. After obtaining this constant and by applying equation (15), the obscuration percentage was found for each sample under an incident heat flux of 50 kW/m2 and for selected

samples under an incident heat flux for 40 kW/m2. Figure ***35***35 and Figure ***36***36 show the results obtained for Hetron systems, while Figure ***37***37and Figure ***38***38 show the results obtained for Fireblock samples under two different incident heat fluxes.

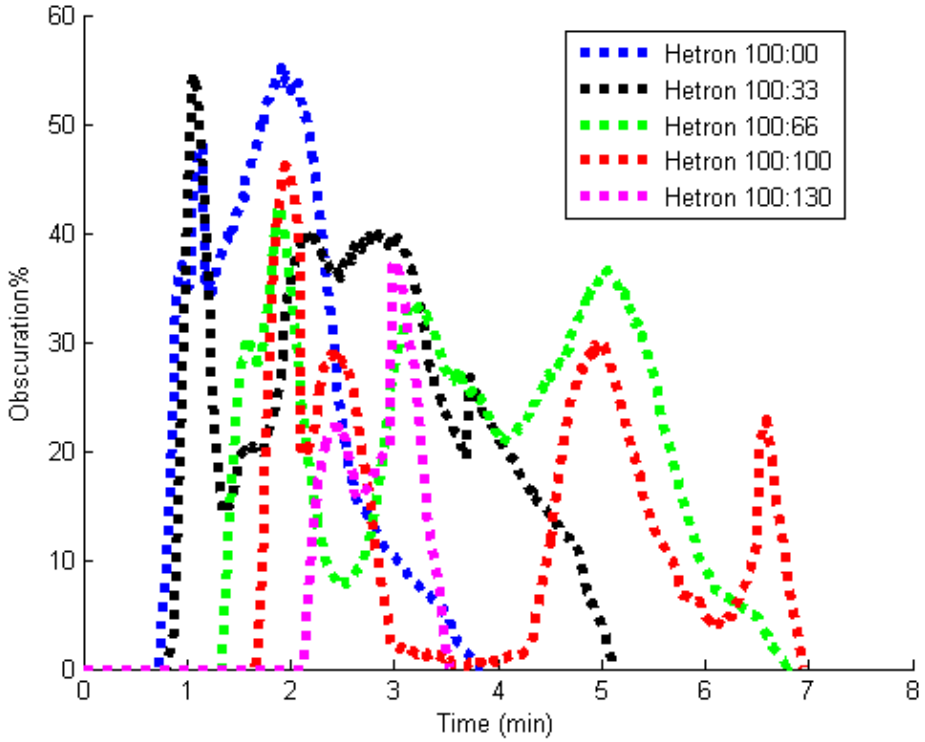

Figure 35: Obscuration Percentage Hetron Samples under an IHF of 50 kW/m2

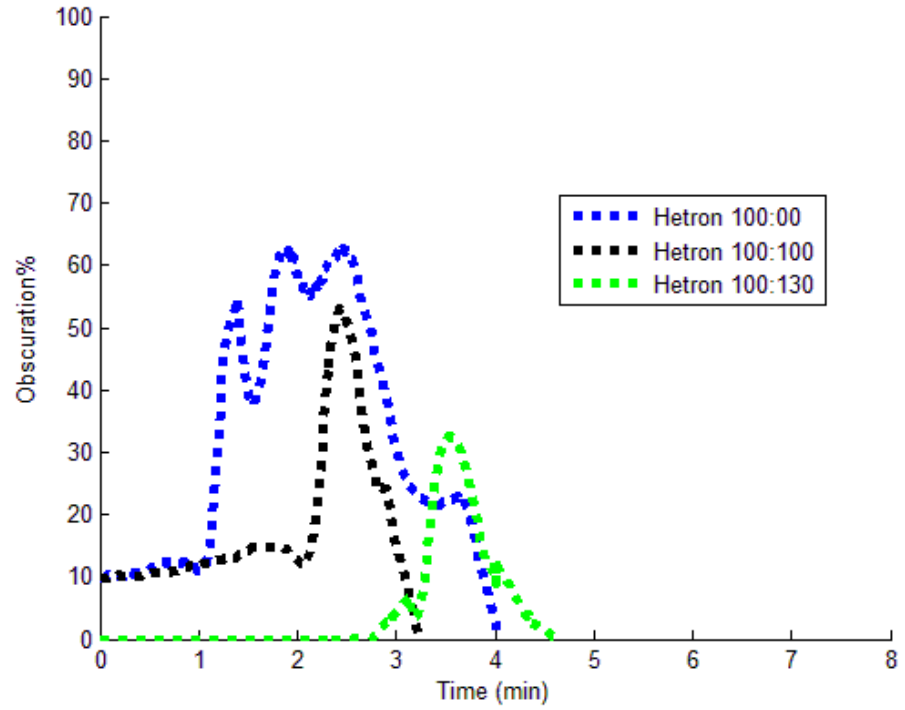

Figure 36: Obscuration Percentage Hetron Samples under an IHF of 40 kW/m2

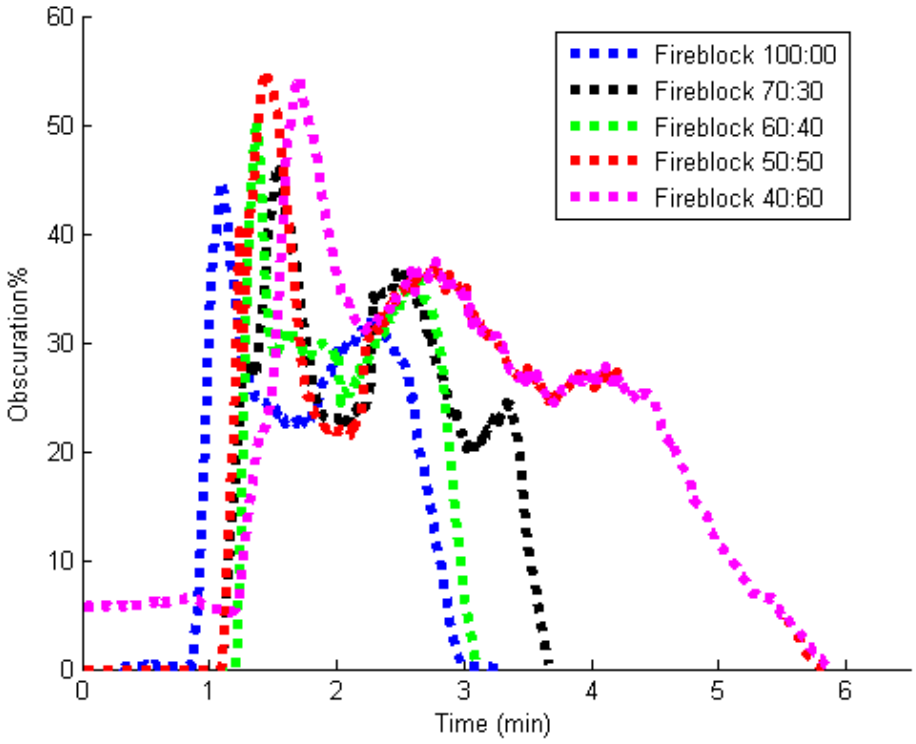

Figure 37: Obscuration Percentage for Fireblock Samples under an IHF of 50 kW/m2

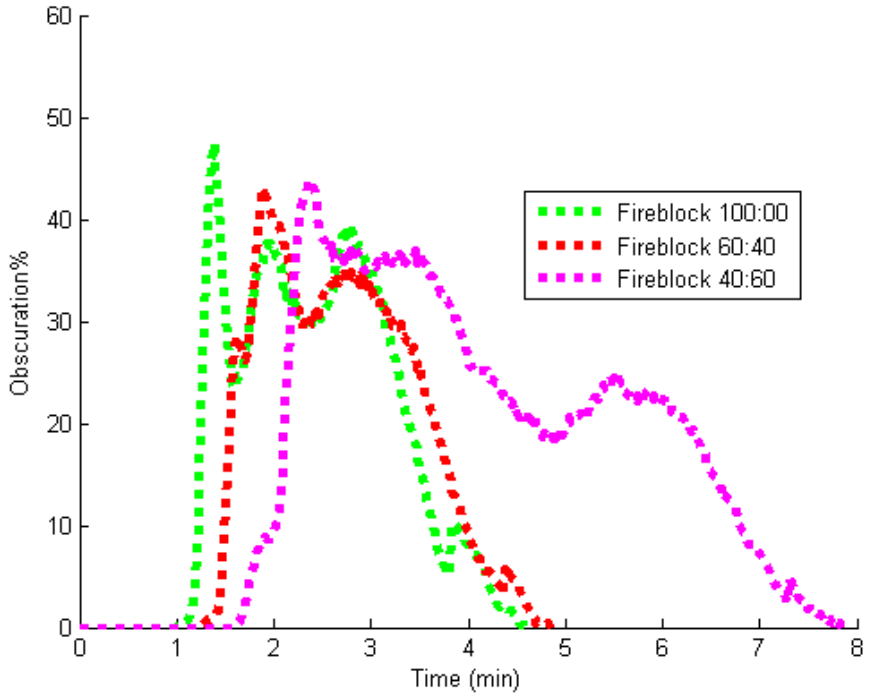

Figure 38: Obscuration Percentage for Fireblock samples under an IHF of 40 kW/m2

By looking at Figure ***35***35 and Figure 37, it is clear in both graphs that the time of duration of the tests was not until 10 min as the ASTM E84 standard requires, because the variables used in this model were obtained from the cone calorimeter test where the test last until flame out no matter how long it takes. Even though the ASTM E84 test is supposed to for 10 min, it is not recommendable to propagate the data until 10 min because the each system recorded a very different last value for the obscuration percentage. If the last point is taken to be constant until the end of the test (10 minutes) that would overestimate the value obtained for smoke developed index and that would make it unsound to compare all systems based on overestimated results.

The best option to predict the thermal behavior of each system in the tunnel test was to assume that the values for obscuration would hit zero following the same decreasing profile obtained in the last seconds of each test. Therefore, after obtaining the last value for obscuration percentage, 20 seconds were added to the each system to allow the data to reach zero. Equation 15 was applied even though the integral limit for time was not 10 minutes in any case; in fact, the time limits for each test were different as all four graphs show. All integrals were solved based

on the data available and using the same mathematical approach in an attempt to mitigate any discrepancy in the data interpretation.

Table 15:Smoke Developed Index for Hetron and Fireblock Samples under 50 and 40 kW/m2

Composite	Obscuration % 50 IHF	SDI 50 IHF	Obscuration % IHF	SDI 40 IHF
Hetron 100:00	83.759	153	128.240	243
Hetron 100:33	109.973	201	----------	---------
Hetron 100:66	118.872	217	----------	---------
Hetron 100:100	70.898	130	57.595	105
Hetron 100:130	26.484	48	21.668	40
Fireblock 100:00	52.336	96	79.432	145
Fireblock 70:30	66.788	122	----------	---------
Fireblock 60:40	53.447	98	76.649	140
Fireblock 50:50	116.662	213	----------	----------
Fireblock 40:60	123.457	226	132.358	242

As **Error! Reference source not found.** shows, the smoke released from Hetron samples decreases as the ATH ratio increases while for Fireblock samples the smoke released tends to increase as the sand ratio increases.

References

1. Janssens, M., Huczek, J. and Sauceda, A. "Development of a Model of the ASTM E 84 Steiner Tunnel Test." *Fire Safety Science* 9 (2008): 279-89. Print.
2. Parker, William. "An Investigation of the Fire Environment in the ASTM E 84 Tunnel Test." National Bureau of Standards technical note 945 (1977): 28. Print.
3. ASTM Standard e-84,2013, "Standard Test Method for Surface Burning Characteristics of Building Materials," ASTM International, West Conshohocken, PA, 2013 DOI : 10.1520/E0084-12A, www.astm.org

Appendix- Uncertainty for the Smoke Developed Index (UNC)

Primary Author-Cristina Herrera

Secondary Author-None

Since the model this paper uses to estimate the transmission percentage and the smoke developed by each composite is based on the experimental measurements of the cone testing, it is assumed that the results yield a "true value" that falls within a range that take into account random fluctuations that might took place during data acquisition. In order to account for this discrepancy, the uncertainty in the measurements of a large collection of data points can be calculated using the standard deviation:

$$\sigma_x = \sqrt{\frac{\sum(x - \bar{x})^2}{n - 1}}$$

Where:

$\bar{x} = mean\ value\ of\ x$

$n = number\ of\ measurements$

It is important to highlight that all the data points obtained from the cone tests correspond to data at each second while the sample was burning. Therefore, at each trial, data points are usually above 300 data points which are enough to describe the data as large populations.

Since the obscuration percentage is a measurement in terms of two independent variables: heat released rate per unit area and the extinction coefficient, the individual uncertainty of each term is needed to find the uncertainty of the transmission percentage using the law of propagation of uncertainty, which is defined by the following equation:

$$\Delta R^2 = \left(\frac{\partial f}{\partial x}\right)^2 (\Delta x)^2 + \left(\frac{\partial f}{\partial y}\right)^2 (\Delta y)^2 + \left(\frac{\partial f}{\partial z}\right)^2 (\Delta z)^2$$

Where:

$\Delta x, \Delta y,\ and\ \Delta z$ are the individual uncertainties of each variable, which can be represented as the standard deviation of each variable.

The equation for transmission percentage is defined by:

$$T\%_{(t)} = 100/\exp\left(\frac{293 * k * 0.076}{T_{e_{(t)}}}\right)$$

Where the term Te is dependent of the heat released rate in the tunnel test, which is defined as:

$$T_e = 31 + 2.5\left[0.43 * \dot{Q}_{tunnel}\right]$$

At the same time, the heat released rate (Q) in the tunnel can be obtained by the following equation that uses the heat release rate obtained from the cone:

$$\dot{Q}_{tunnel} = \left(0.6 * \dot{Q''}_{cone}\right) + 88$$

Taking into account these relations, the transmission percentage equation can be rearranged as:

$$T\%_{(t)} = \frac{100}{\exp\left(\frac{293 * k * 0.076}{31 + 2.5\left(0.43 * (0.6 * \left(\dot{Q'}_{cone} + 88\right)\right)}\right)}$$

Then, the transmission percentage is a measurement based on two independent variables: k and Qcone

$$T\%_{(t)} = \frac{100}{\exp\left(\frac{22.268 * k}{(0.645 * Q_{cone}) + 125.6}\right)}$$

In order to apply the propagation of law, let's set the extinction coefficient (k) as x and the heat release rate (Q) as y for simplicity in the partial derivatives computations,

$$f(x,y) = \left(\frac{100}{\exp\left(\frac{22.268x}{(0.645y) + 125.6}\right)}\right)$$

Where the partial derivatives are:

$$\frac{\partial f}{\partial x} = \frac{-3452.4e^{\left(\frac{-34.524x}{y+194.729}\right)}}{y + 194.729}$$

$$\frac{\partial f}{\partial y} = \frac{3452.4xe^{\left(\frac{-34.524x}{y+194.729}\right)}}{(y + 194.729)^2}$$

Finally, the propagation of uncertainty is defined by:

$$\Delta R^2 = \left(\frac{\partial f}{\partial x}\right)^2 (\Delta x)^2 + \left(\frac{\partial f}{\partial y}\right)^2 (\Delta y)^2$$

$$\Delta R^2 = \left(\frac{-3452.4e^{\left(\frac{-34.524x}{y+194.729}\right)}}{y + 194.729}\right)^2 (\Delta x)^2 + \left(\frac{3452.4xe^{\left(\frac{-34.524x}{y+194.729}\right)}}{(y + 194.729)^2}\right)^2 (\Delta y)^2$$

By applying the previous equation to all the sets of data obtained from cone testing corresponding to the 10 composite systems analyzed throughout the paper, the uncertainty for the transmission model was found for each composite as the following table shows:

Table 16: Uncertainty values for Hetron and Fireblock Systems

Composite	Coeff. (X)	HRR (Y)	error X	error Y	R^2	Uncertainty
Hetron 100:00	2.944743	91.98126	2.947684	76.31081	663.733	25.7630167
Hetron 100:33	2.322324	75.47866	1.710902	42.12931	275.8028	16.6073113
Hetron 100:66	1.664159	59.01628	1.284545	31.98523	199.392	14.1206243
Hetron 100:100	0.970806	53.07076	1.228257	41.08733	227.2655	15.0753291
Hetron 100:130	0.691896	41.53556	1.076879	45.706	205.4095	14.3321138
Fireblock 100:00	2.264548	141.7811	1.902473	85.34508	261.1937	16.1614887
Fireblock 70:30	2.480783	139.9463	1.943675	77.3902	261.9598	16.1851733
Fireblock 60:40	2.293132	123.8909	2.128662	84.35112	349.986	18.7079131
Fireblock 50:50	2.447957	115.0955	1.81644	58.8425	252.9758	15.905214
Fireblock 40:60	2.4784	90.02738	2.281076	73.02219	451.9064	21.2580904

As this table shows, the uncertainty obtained for each composite yield between 15% to 20% for all samples except for the first system which has an uncertainty of 26%. This outlier corresponds to Hetron 100:100 system; let's recall that this was the very first system to be tested so a larger uncertainty is expected due to lack of practice with the equipment used. In order to find a combined uncertainty for the entire model, the best that can be done taking into account that the individual uncertainties are in a relatively close range, the average of all the 10 uncertainties was computed to serve as the uncertainty of the transmission percentage. In this way, the approximated final uncertainty is ±%17. It is possible to average all the uncertainties of each sample since all measurements and variables were taken using the same equipment (cone calorimeter), and the model used to define the transmission percentage was the same for all samples.

Appendix- Pool Fires (POOL)

Primary Author-Daniel Morgan

Secondary Author-None

In order to be able to compare our cone calorimeter data to the NFPA 285 standard, we need a way to determine the height of the flame against a wall. The problem with that is that vary little research has been done for smaller flames on walls, especially those below 100 kilowatts per meters squared. Fortunately, pool fires have been research much more at lower heat release rates. By using the information learned from pool fires, a relation pool fires to wall fires, which can be used estimate how a wall fire will react at lower values of heat release rates.

Research on pool fires for smaller heat release rates has been done by several people, the most notable of which are Heskestad, Zukoski, and Wood et al. These three groups of people and their respective research are where we focused our attention. The measure that most the pool fire research has been done was using the quantity, $\dot{Q}_D^*$ *or* $\dot{Q}^*$. This quantity is the dimensionless Froude number defined as:

$$\dot{Q}_D^* = \frac{\dot{Q}}{(\rho_o)(c_p)(T_o)(g * D^5)^{0.5}}$$

The first paper that was researched was the paper "Characteristics of Pool Fire Burning" by Anthony Hamins, Takashi Kashiwagi, and Robert Burch for the National Institute of Standards and Technology[1]. This paper brought together the workings of Heskestad and Zukoski and the relations to flame heights that each of the correlated. The first flame height correlation that was shown was Heskestad correlation. The Heskestad correlation was correlated to a power law in the terms of $N(\dot{Q})$ is defined as:

$$\frac{z_f}{D} = -1.02 + 15.6 * N\left(\dot{Q}\right)^{0.2}$$

Where $N(\dot{Q})$ is defined as:

$$N\left(\dot{Q}\right) = \left[\frac{c_p(T_o)}{\left(\frac{H}{r}\right)}\right]^3 * \left(\dot{Q}_D^*\right)^2$$

Since the focus was more on the smaller flames, we need to define a point at which the pool fire is considered small. The paper mentioned above defined three points where various researchers considered the pool fire small.

$$\frac{Z_f}{D} \propto \left(\dot{Q}_D^*\right)^2;\ \ for\ small\ fires\ of\ \dot{Q}_D^* < 0.1,\ \ N(\dot{Q}) < 10^{-5},\ \ or\ \frac{Z_f}{D} < 0.5$$

$$\frac{Z_f}{D} \propto \left(\dot{Q}_D^*\right)^{\frac{2}{3}};\ \ for\ imtermediate\ fires\ of\ \dot{Q}_D^* > 0.1$$

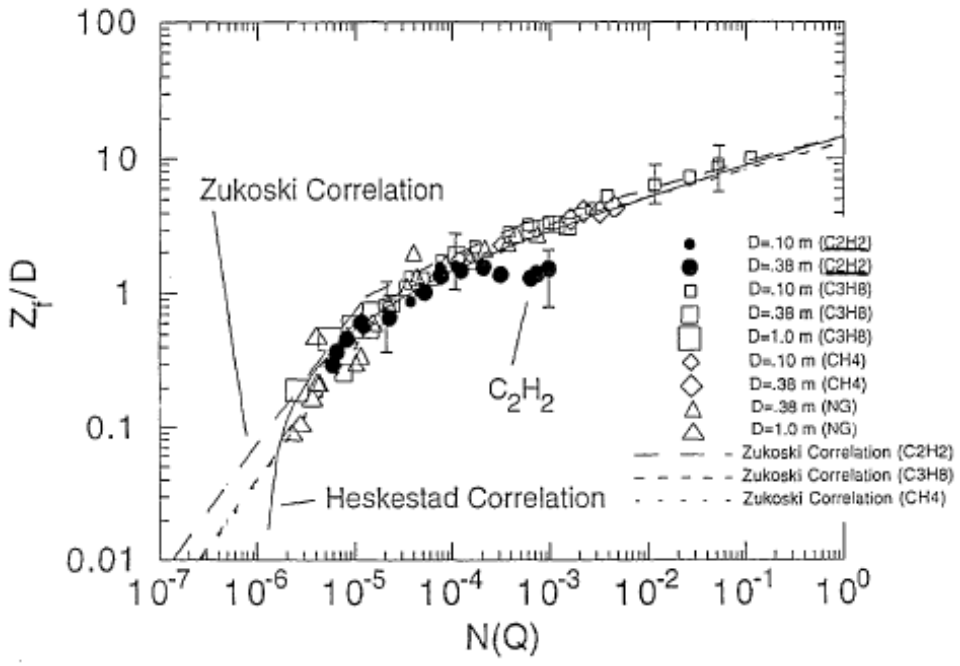

Figure 39: Heskestad Correlation

In the above graph (*Figure **39**: Heskestad Correlation*Figure 39), the normalized flame height is shown for a range of $N(\dot{Q})$ at differing pool diameters, ranging from 0.1m to 1.0 m. Four different correlations are added to the graph, three of which are from Zukoski and one is from Heskestad. The Heskestad correlation is the closest fit to the flame length data, except for C2H2 at higher values of $N(\dot{Q})$. The four correlations are a close match when the $N(\dot{Q})$ is above a value of 10^-4. However, at lower $(\dot{Q})$ values, the Zukoski correlations falls off while Heskestad follows the data.

Examining the Heskestad correlation and the way the data reacts, it seems that as the pool fires becomes small, the flame height seems to drop off more rapidly. Using that information, if we can determine that the flame heights of wall fires act in a similar way, it can assume that the wall flames will also experience a similar drop off the flame height as it becomes small.

The next correlation that was made using the same data field as shown in Figure 39 was done by Zukoski. He attempted to split the data field up into three separate sections, one for large pool fires, a one for intermediate fires, and one for the small fires. Zukoski then correlated a two flame height equations for the large and intermediate pool fires.

$$Z_f/D = 3.3 \cdot (\dot{Q}_D^*)^{(2/3)} \text{ for } \dot{Q}_D^* < 1$$

$$Z_f/D = 3.3 \cdot (\dot{Q}_D^*)^{(2/5)} \text{ for } \dot{Q}_D^* \geq 1$$

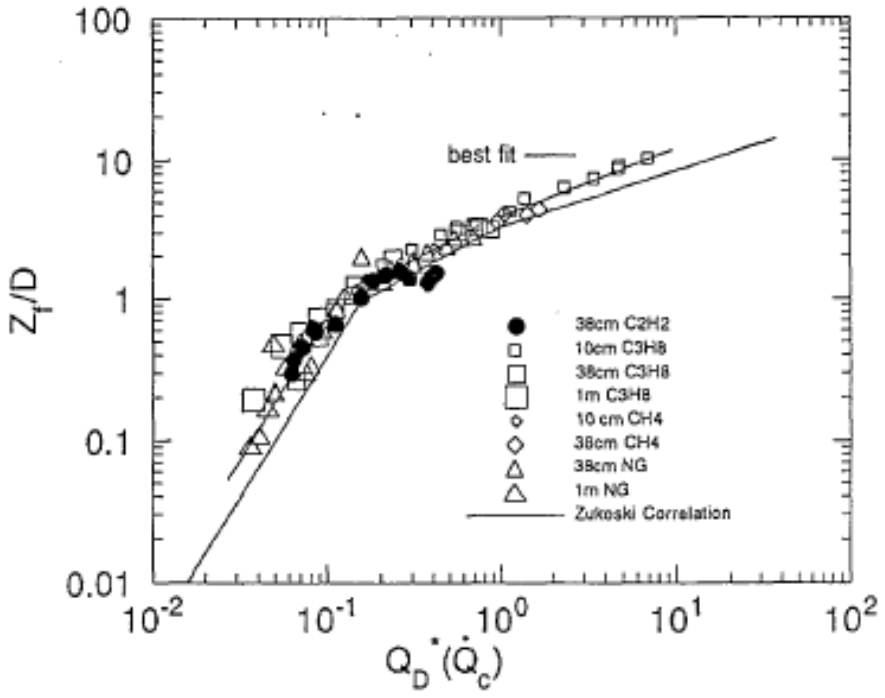

Figure 40: Zukoski Correlation

Figure 40 shows the Zukoski correlation that was mentioned above, along with a best fit curve. From examining the above graph, we can see that the Zukoski Correlation does not fit very well with the data. The best fit curve does fit the data relatively well. This best fit curve was not mentioned in detail in the paper, so we need to curve fit it to be able to determine what the equation is. This will be done later on along with several others as well.

The next place that was researched was a paper by Zukoski named "Fluid Dynamic Aspects of Room Fires" from the First Symposium of Fire Safety Science. In part of this paper, Zukoski breaks down the Flame height versus fuel flow rate into five sections. The five sections are shown in Figure 41 below.

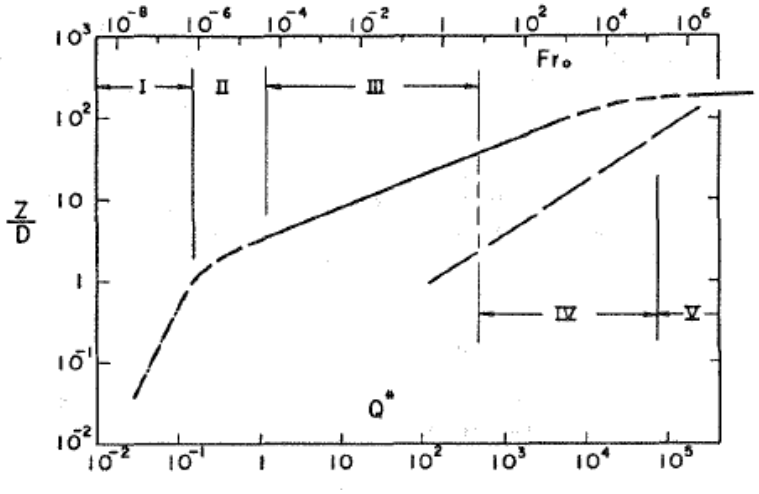

Figure 41: Flame height vs. Fuel flow rate

The regime that we are focused on is the first regime. This first regime represents the area where the small pool fires occur. In this regime, Zukoski observes that the flamelets roughly become independent of the diameter of the fire and is dependent on the heat release rate per unit area. Unlike the first paper, Zukoski proposes an equation that represents the flame height for the small pool fires. The equation he proposes is defined as:

$$\frac{z_f}{D} = (constant) * (Q^*)^2$$

By using the data from three different sources, Zukoski determines that the constant for the above equation is equal to either 40 or 15. The constant of 40 comes from the data of Wood et al[2], while the constant of 15 comes from the data of Cox and Chitty[3]. The difference between

the two constants is not certain, but Zukoski is much fonder of the constant of 40 from Wood et al. One reason behind this difference is that the constant determine by Cox and Chitty only go down to a $\dot{Q}_D^*$ value of 0.13, while other sets of data go as low as 0.037.

From Zukoski paper in the First Symposium, he collected several sets of data from a range of $\dot{Q}_D^*$ from 0.02 to 10. The data he used were taken from papers by Wood et al (1971), Cetegen et al (1985), and Alvarez (1985). Using the data, Zukoski set two different curves, one representing higher values of $\dot{Q}_D^*$, greater than about 0.2, and the other curve for $\dot{Q}_D^*$ of less than 0.2. The data sets that are involved with the first curve are mostly from Wood et al. The figure below shows the collection of data and the two curves. Although the data is more spread apart from the curve, it is a relatively good representation of the data.

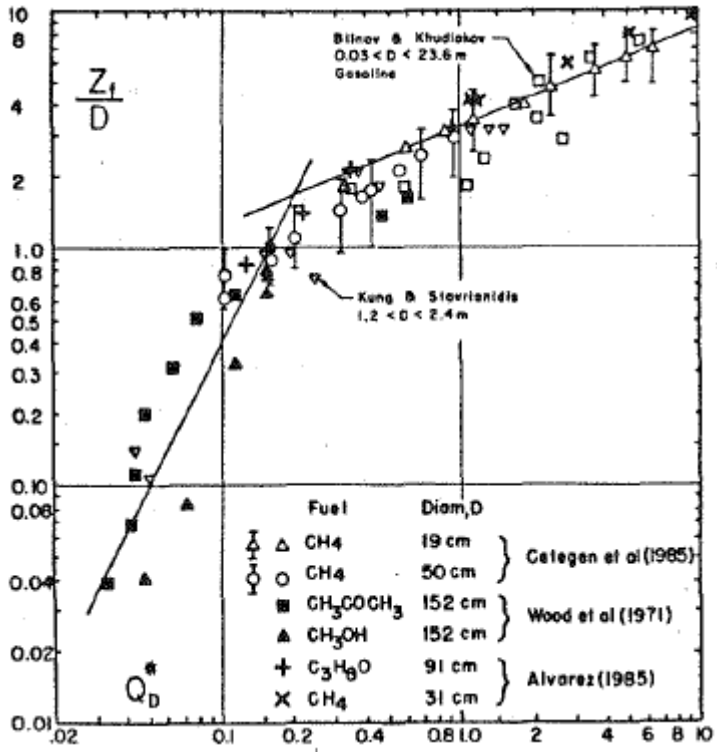

*Figure 42: Flame lengths for small Q**

Curve Fitting

For the figures (Figures 39-42) above that show the correlations, a curve fit was desired for all of the small pool fire regions to not only verify that the correlation that each person or group made was correct, but to determine some of the curves that were not given in the

respective papers. The first graph that was curve fitted was the graph of the Heskestad Correlation (Figure 39). This was curve fitted using a free curve fitting software since getting an accurate curve fit using excel was troublesome.

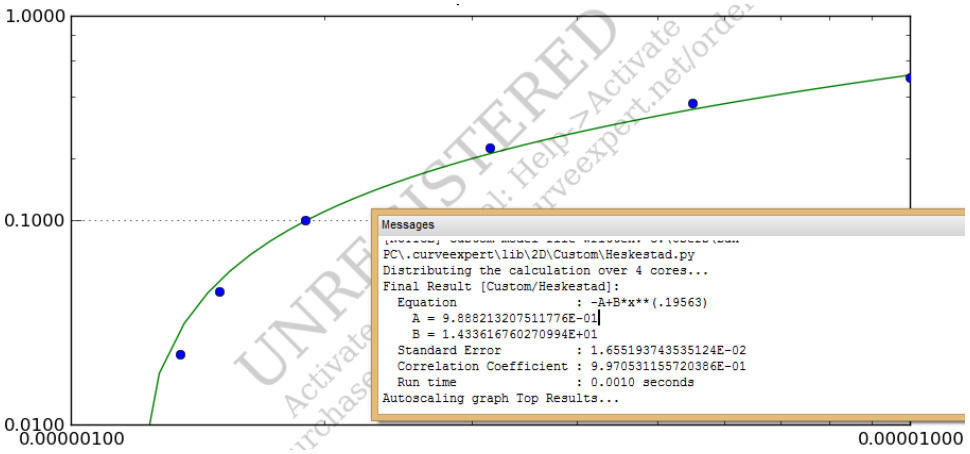

Figure 43: Heskestad Curve Fit

From the message box in the above figure, the Flame height equation that we curve fit was:

$$\frac{Z_f}{D} = -.988 + 14.336 * N(Q)^{0.19563}$$

Comparing this to the actual Correlation that was shown earlier, the curve fit equation is very close to the correlated one.

The second figure that was curve fit to determine the equation was that from Zukoski. The part of the graph that is shown below is for the region that is $\dot{Q}_D^*$ of less than 0.1, the point at which pool fire become small. The curve fit from this graph is being compared to the constants that Zukoski determined from the first symposium[4]. One thing to note is that since the points being put into excel where determined by looking at the graph, any inaccuracies that arise from this can have a large impact on the curve fit equation.

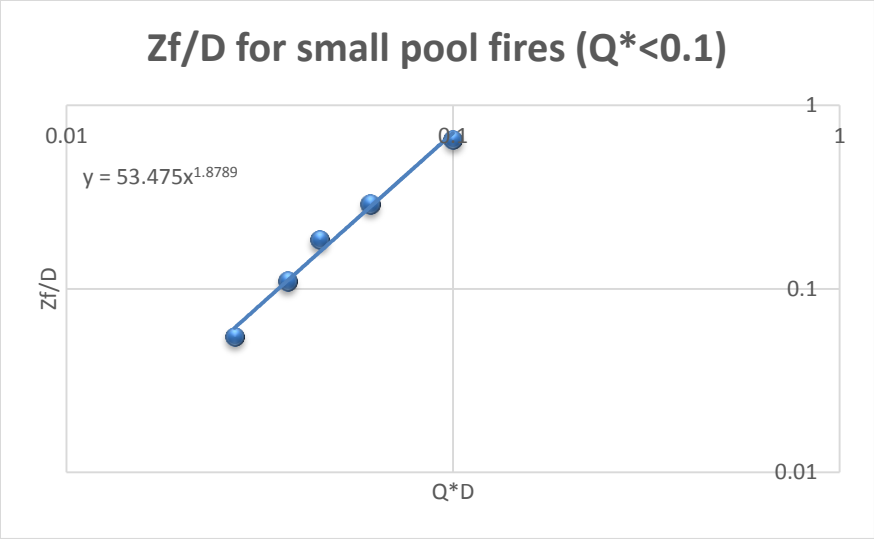

Figure 44: Zukoski Small Pool Fires

From examining the above curve fit, the equation that was determined to be:

$$\frac{Zf}{D} = 53.475 * \dot{Q}_D^{*\,1.8789}$$

Comparing this to the constant that Zukoski proposed in the First Symposium (ref), is it somewhat close to the 40 that he suggested, but more proof is needed before we can say that the constant is indeed 40.

The next figure that was curve fit was Figure 41 from Zukoski in the First Symposium[4]. In this figure, we only focused on the first Regime. This is the area that represents small pool fires and the curve fit should resemble the one shown above. The curve fit from the first regime is:

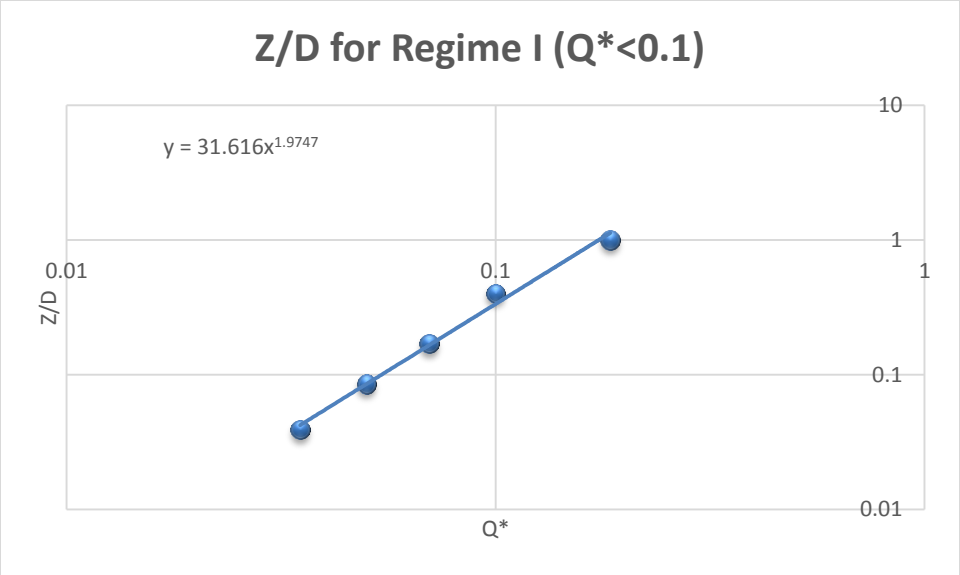

Figure 45: Regime I from Zukoski First Symposium

From the curve fit, the equation for the First Regime is:

$$\frac{Zf}{D} = 31.616 * \dot{Q}_D^{*\,1.9747}$$

Comparing the curve fit to both Figure 45 curve fit and what Zukoski suggest as the constant, it looking much more certain that the constant is 40. However, this is only two cases by the same person, so we need to compare the final figure to see what the curve fit is.

The final figure that was curve fit was Figure 42. This figure was a collection of data from a couple a sources. All of the separate points were plotted all of the separate points that were used for the curve fitting that Zukoski did, which was all points lower than $\dot{Q}_D^*$ of about 0.12. A curve fit was applied to the data and this was the result:

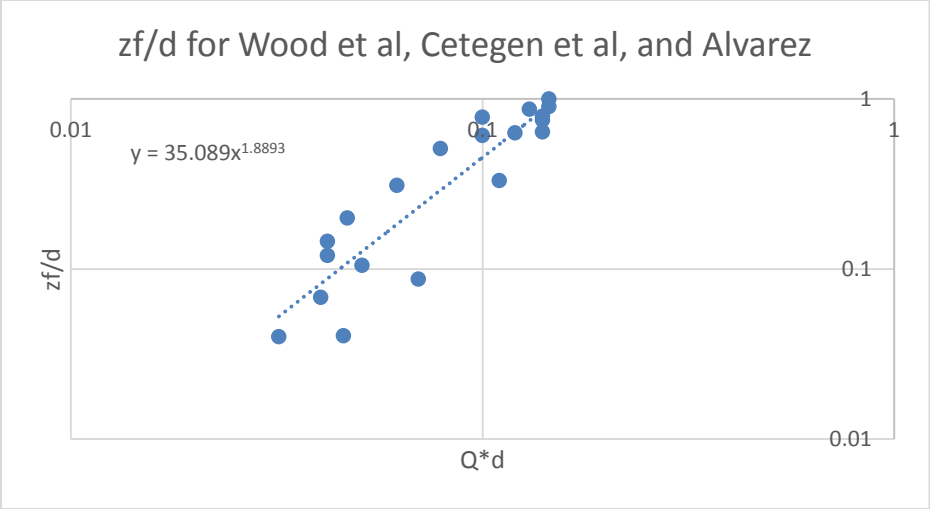

Figure 46: Curve fit for Wood et al, Cetegen et al, and Alvarez data.

From the curve fit for the above figure, the equation is:

$$\frac{Zf}{D} = 35.089 * \dot{Q}_D^{*\,1.8893}$$

Compiling all of the curve fits shown above with that from figures 44, 45, and 46, it is shown that the constant seems that it is very reasonable that the constant should be about 40. All of the curve fits done above seem to agree with Zukoski suggestion that the constant should be 40.

Results

From doing all of the research and curve fitting all of the graphs, shown below is a system of equations that can represent the flame height of a pool fires ranging in all sizes.

$$\frac{Zf}{D} = 40 * \dot{Q}_D^{*\,2}; for\ \dot{Q}_D^* < 0.1$$

$$\frac{Zf}{D} = 3.3 * \dot{Q}_D^{*\frac{2}{3}}; for\ \dot{Q}_D^*\ between\ 0.1\ and\ 1$$

$$\frac{Zf}{D} = 3.3 * \dot{Q}_D^{*\frac{2}{5}};\ \ for\ \dot{Q}_D^*\ of\ greater\ than\ 1$$

Relation to our Data

In order to be able to relate the correlations and the equations to the data that was collected from the cone calorimeter, a relation was needed to be able to relate the $\dot{Q}_D^*$ equations to the heat release rate per unit area that is given from the cone. The way to relate $\dot{Q}_D^*$ to our data is to convert that equation to use a heat release rate per unit area, instead of a heat release rate. The way we converted it is as follows:

$$Step\ 1: \quad \dot{Q}_D^* = \frac{\dot{Q}}{(\rho_o)(c_p)(T_o)(g * D^5)^{0.5}}; \quad \dot{Q} = \dot{Q}'' * A_p \ and \ A_p = \pi D^2/4$$

$$Step\ 2: \quad \dot{Q}_D^{*''} = \frac{\dot{Q}'' * \pi D^2/4}{(\rho_o)(c_p)(T_o)(g * D)^{0.5}(D^2)}$$

$$Step\ 3: \quad \dot{Q}_D^{*''} = \frac{\dot{Q}''(\pi)}{(\rho_o)(c_p)(T_o)(g * D)^{0.5}(4)}$$

The first step that was taken was to define all equations and define the heat release rate and the area of the pool. The second step was to substitute the values into the $\dot{Q}_D^*$ equation and to pull out the D^2 from under the square root. The final step was to cancel all similar quantities and simplify the equation as much as possible.

Another Important part that was needed was to know the range of heat release rate per unit area that our small pool fire equations is valid for. To do this, the values in the equations needed to be defined and also needed to be rearranged the equation to solve for the heat release rate. The method that was used is shown below:

$$\dot{Q}_D^* = \frac{\dot{Q}}{\rho_o c_p T_o (gD^5)^{0.5}}; \quad \dot{Q} = \dot{Q}'' * A_D; \quad 0.037 < \dot{Q}_D^* < 0.1$$

$$\rho_o = 1.2041 \frac{kg}{m^3}, \quad D = .1m, .38m, and\ 1m$$

$$c_p = 1000 \frac{J}{kgK}, \quad T_o = 20℃, \quad g = 9.8 \frac{m}{s^2}$$

$$\dot{Q} = \dot{Q}_D^* * (\rho_o c_p T_o (gD^5)^{0.5})$$

- **Upper Limit**

$$\dot{Q} = (.1) * \left((1.2041)(1000)(293)(9.8 * (1)^5)^{0.5}\right) = 110\ kW$$

$$\dot{Q}^{"} = \frac{\dot{Q}}{\frac{\pi * (D)^2}{4}} = \frac{110}{\frac{\pi * (1)^2}{4}} = 140\frac{kW}{m^2}$$

- **Lower Limit**

$$\dot{Q} = (.037) * \left((1.2041)(1000)(293)(9.8 * (.1)^5)^{0.5}\right) = .129\ kW$$

$$\dot{Q}^{"} = \frac{\dot{Q}}{\frac{\pi * (D)^2}{4}} = \frac{110}{\frac{\pi * (.1)^2}{4}} = 16.42\frac{kW}{m^2}$$

The first thing that was done was to define the values from the equation and reordering the equation to solve for the heat release rate. The properties were determined at the ambient temperature of 20 degrees Celsius, while the pool fire diameter was given in the charts. Once the properties and diameters were defined, the values were plugged into the equations and solved for the heat release rate. To then solve for the heat release rate per unit area, we then divided the heat release rate determined earlier by the area of the pool to get the heat release rate per unit area. This process was repeated for the lower limit. The range of heat release rate per unit area of small pool fires is from a minimum of about $16.5\frac{kW}{m^2}$ to a maximum of $140\frac{kW}{m^2}$.

References

1. Hamins, Anthony, Takashi Kashiwagi, and Robert R. Burch. Characteristics of Pool Fire Burning. Rep. N.p.: n.p., n.d. Fire.nist.gov. National Institute of Standards and Technology. Web. Jan.-Feb. 2014.
2. Blackshear, Perry L., and E. R. G. Eckert. "Mass Fire Model: An Experimental Study of the Heat Transfer to Liquid Fuel Burning from a Sand-Filled Pan Burner." Combustion

Science and Technology. By Byard D. Wood. Vol. 4. N.p.: Gordon and Breach Science Publications, 1971. 113-29. Print.

3. Chitty, R. "Some Source-Dependent Effects of Unbounded Fires." Combustion and Flame. By G. Cox. Vol. 60. N.p.: n.p., n.d. 216-32. Print.
4. Zukoski, E.E. "Fluid Dynamic Aspects of Room Fires." Fire Safety Science-Precedings of the First International Symposium. Hemisphere, New York: N.p., 1984. Print.

Hasemi, Yuiji, and Mitsuru Nishihata. "Deterministic Properties of Turbulent Diffusion Flames From Low Q* Fires." N.p., n.d. Web. Spring 2014. <https://www.jstage.jst.go.jp/article/fst/7/2/7_2_2_27/_article>.

Heskestad, Gunnar. "Fire Plumes, Flame Height, and Air Entrainment." SFPE Handbook of Fire Protection Engineering. Quincy, MA: National Fire Protection Association, 2002. 2-1--16. Print.

Kung, Hsiang-Cheng, and Paraskevas Stavrianidis. "Bouyant Plumes of Large-Scale Pool Fires." Nineteenth Symposium (International) on Combustion: At the Technion-Israel Institute of Technology, Haifa, Israel, August 8-13, 1982. Pittsburgh: Combustion Institute, 1982. 905-12. Print.

Appendix- Wall Fire Model (WALL)

Primary Author-Daniel Morgan

Secondary Author-None

Since very little information is known about wall fires that are at lower HRRPUA values, it is hard to predict what the flame height will be when it gets small. Fortunately, pool fires have been studied at lower HRRPUA ranges. We will assume that wall fires at lower ranges will act similarly to that of the pool fires. From pool fires research, there are three outlining flame height equations that can be used. These equations are as follows:

(1) $\frac{Zf}{D} = 40 * \dot{Q}_D^{*\,2}; for\ \dot{Q}_D^* < 0.1; for\ small\ pool\ fires$

(2) $\frac{Zf}{D} = 3.3 * \dot{Q}_D^{*\frac{2}{3}}; for\ \dot{Q}_D^*\ between\ 0.1\ and\ 1; for\ intermediate\ pool\ fires$

(3) $\frac{Zf}{D} = 3.3 * \dot{Q}_D^{*\frac{2}{5}};\ \ for\ \dot{Q}_D^*\ of\ greater\ than\ 1; for\ large\ pool\ fires$

From Delichatsios[1] and Ming-Mon Tu[2], both of their flame height equations that they calculated resulted in an exponent of 2/3. If both of their data sets appear to have a drop off as their heat release rate decreases similar to what is experience with pool fires, it can be assumed that the exponent for a wall fire with a low heat release rate is 2. It can also be assumed that the wall fires will become cellular at a similar point as they do in pool fires. So it is assumed that at a value of $\dot{Q}_{xp}^{\prime *}$ of about 0.1, the heat release rate for wall fires will be small. The constant can be determined from the data sets of Delichatsios and King-Mon Tu. In order to compare the two data sets together, both need data sets need to be in the same units for comparison. To do this, all heat release rates were converted to a dimensionless heat release rate similar to the form from Yuan and Cox[3]. The dimensionless heat release rate form is shown below in equation (4).

(4) $\dot{Q}_{xp}^{\prime *} = \frac{\dot{Q}'}{\rho_0 C_p T_0 \sqrt{g} X p^{3/2}}$

Once both of the data sets were converted to a form similar to the Yuan and Cox form, both data sets where plotted together on the same graph and a curve fit was applied to determine the constant of the wall fire equation. The graph and message box below in Figure 47 are the

curve fit for the combination of the two data sets. The equation for wall fires with higher heat release rates is shown below.

(5) $\frac{X_f}{X_p} = 6 * \left(\dot{Q}'^{*}_{xp}\right)^{\frac{2}{3}}; For\ \ \dot{Q}'^{*}_{xp} > 0.1\ (Large\ Wall\ Fires)$

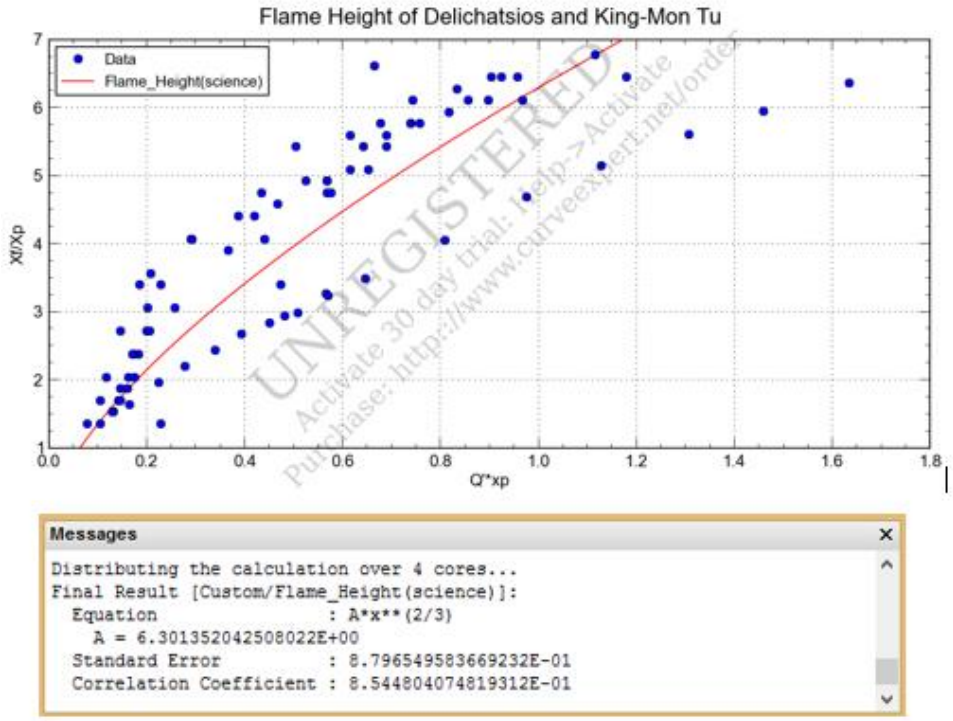

Figure 47: Combination of Delichatsios and King-Mon Tu Data sets

From the graph above, towards the end of the data sets nearing about 0.1, there appears to be a slight drop off in the data sets. By assuming that the data would in fact drop off when the dimensionless heat release rate goes below 0.1, it can be assumed that the exponent for a wall fire equation for low values of the dimensionless heat release rate will be 2. To determine the constant for the small wall fire equation, the large wall fire equation (equation 5) was set equal to the small wall fire equation format at a dimensionless heat release rate of 0.1 to solve for the constant.

(6) $6\left(\dot{Q}'^{*}_{xp}\right)^{\frac{2}{3}} = A\left(\dot{Q}'^{*}_{xp}\right)^{2} \rightarrow\ 6(0.1)^{\frac{2}{3}} = A(0.1)^{2} \rightarrow A = 130$

Now that the constant for the small wall fire equation is solved for, the system of equations for wall fires of all sizes is shown below in equations (7) and (8).

(7) $\frac{X_f}{X_p} = 6\left(\dot{Q}'^{*}_{xp}\right)^{\frac{2}{3}}; For\ \ \dot{Q}'^{*}_{xp} > 0.1\ (Large\ Wall\ Fires)$

(8) $\frac{X_f}{X_p} = 130\left(\dot{Q}'^{*}_{xp}\right)^{2}; For\ \ \dot{Q}'^{*}_{xp} < 0.1\ (Small\ Wall\ Fires)$

The above system of equations was plotted to determine that there was no discontinuity between the two equations and that the drop off as the dimensionless heat release rate gets smaller is similar to that from pool fires.

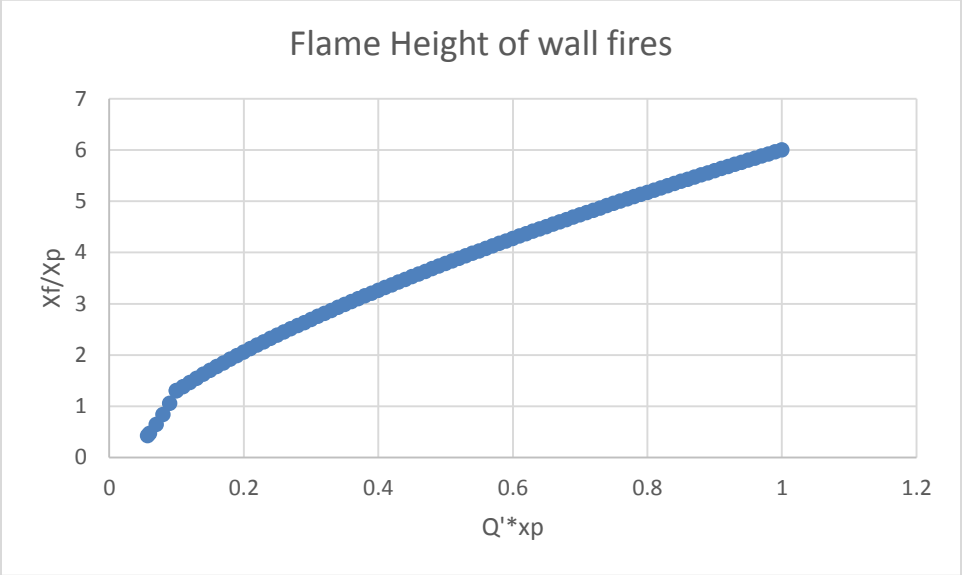

Figure 48: Flame heights of wall fires

Once it was determined that the system of equations that were developed would work, the equations where then adapted to determine the flame height in the NFPA 285 Standard.

The wall fire equations are limited on the allowable range of heat release rates per unit area that they work in. While there is no foreseeable upper limit on the heat release rate from the research, there are however limits on the lower heat release rates. The lowest limit of the allowable heat release rate per unit is based on the fact that from Mowrer and Williamson[28] Model, the flame height must be greater than or equal to the pyrolysis length. This is because the overall flame height measurement includes the pyrolysis length. So if the value of the flame height over the pyrolysis length becomes less than 1, the model fails. To solve for the lower limit of the model, the small wall fire equation was used to determine what value of the dimensionless heat release rate would result in a value of $\frac{X_f}{X_p}$ equal to one.

(9) $\frac{X_f}{X_p} = 130 * \left(\dot{Q}'^{*}_{xp}\right)^2 ; For\ \dot{Q}'^{*}_{xp} < 0.1\ (Small\ Flames)$

(10) $1 = 130 * \left(\dot{Q}'^{*}_{xp}\right)^2 \rightarrow \dot{Q}'^{*}_{xp} = 0.088$

Using the lowest value of dimensionless heat release rate which was about 0.088, we can calculate the lowest value of HRRPUA at differing pyrolysis lengths where the Mowrer and Williamson[28] form will not be applicable. Using values of pyrolysis length of 0.1 m, 0.5 m, 1 m, 1.5 m, and 2 m, the lowest value of the heat release rate per unit area can be determined.

(1) $\dot{Q}'^{*}_{xp} = \frac{\dot{Q}''X_p}{\rho_o c_{po} T_o \sqrt{g} X_p^{\frac{3}{2}}}; \quad solving\ for\ the\ HRRPUA$

(2) $\dot{Q}'' = \left(\dot{Q}'^{*}_{w}\right)(\rho_o c_{po} T_o \sqrt{g}\sqrt{X_p}) \rightarrow \dot{Q}'' = (.088)\left((1.21)(1000)(293)(9.8)^{\frac{1}{2}}(.1)^{\frac{1}{2}}\right)\left(\frac{1\ kJ}{1000\ J}\right)$

(3) $\dot{Q}'' = 30.88 \frac{kW}{m^2}$

Repeating the above steps, we get values for the rest of the Pyrolysis Lengths shown below:

Xp (m)	HRRPUA (kW/m2)
0.1	30.88507787
0.5	69.06113361
1	97.66719178
1.5	119.6173922
2	138.1222672

References

1. Delichatsios M. "Flame Heights in Wall Fires: Effects of Width, Confinement and Pyrolysis Length." *The Sixth International Symphosium* (n.d.): 729-40. Web.
2. Tu, King-Mon, and James G. Quintiere. "Wall Flame Heights with External Radiation." Fire Technology 27.3 (1991): 195-203. Print.
3. Yuan, Li-Ming, and G. Cox. "An Experimental Study of Some Line Fires." Fire Safety Journal 27.2 (1996): 123-39. Print.

Appendix- Runge-Kutta 4th Order Method Process (RK4)

Primary Author-Daniel Morgan

Secondary Author-None

Once the wall flame height equations were verified that they are continuous and experienced a drop off similar to pool fires, it is then applied to the NFPA 285 standard to determine the flame height. To do this, the wall fire equations needed to be converted to a form that can easily be dynamically solved for using the Runge-Kutta 4th order method. The wall fires equations were converted to the form from Mowrer and Williamson shown below in equation (1).

(1) $\frac{dX_p}{dt} = \frac{X_f - X_p}{t_{ig}}$

The first step that was taken was to rewrite each of the wall flame height equations into the Mowrer and Williamson form was to fully define the dimensionless heat release rate variable $\dot{Q}'^{*}_{xp}$.

(2) $\frac{X_f}{X_p} = 6 * \left(\frac{\dot{Q}'' X_p}{\rho_o c_{po} T_o \sqrt{g} X_p^{\frac{3}{2}}} \right)^{\frac{2}{3}}$

The next step was to simplify both sides of the equation and to rearrange the left side of equation so that X_f is by itself. The final wall flame height equation can be seen in equation (5).

(3) $\frac{X_f}{X_p} = 6 * \left(\frac{\dot{Q}'' X_p^{-\frac{1}{2}}}{\rho_o c_{po} T_o \sqrt{g}} \right)^{\frac{2}{3}}$

(4) $\frac{X_f}{X_p} = (6)\left(\rho_o c_{po} T_o \sqrt{g}\right)^{-\frac{2}{3}} \left(\dot{Q}''\right)^{\frac{2}{3}} \left(X_p\right)^{-\frac{1}{3}}$

(5) $X_f = (6)\left(\rho_o c_{po} T_o \sqrt{g}\right)^{-\frac{2}{3}} \left(\dot{Q}''\right)^{\frac{2}{3}} \left(X_p\right)^{\frac{2}{3}}$

The above process of rearranging the equation was repeated for the small wall fire equation. Equation (6) below is the small fire equation rearranged. One thing to note for the small wall fire equation is that when it is rearranged, the pyrolysis length drops out due the exponent being two.

(6) $X_f = (130)\left(\rho_o c_{po} T_o \sqrt{g}\right)^{-2}\left(\dot{Q}^{"}\right)^2$

The final step was the plug in equations (5) and (6), into equation (1). The resulting equations are in the final Mowrer and Williamson[28] form.

(7) $\frac{dX_p}{dt} = \frac{X_f - X_p}{t_{ig}} \rightarrow \frac{dX_p}{dt} = \frac{(6)\left(\rho_o c_{po} T_o \sqrt{g}\right)^{-\frac{2}{3}}\left(\dot{Q}^{"}\right)^{\frac{2}{3}}(X_p)^{\frac{2}{3}} - (X_p)}{t_{ig}}$

(8) $\frac{dX_p}{dt} = \frac{X_f - X_p}{t_{ig}} \rightarrow \frac{dX_p}{dt} = \frac{(130)\left(\rho_o c_{po} T_o \sqrt{g}\right)^{-2}\left(\dot{Q}^{"}\right)^2 - (X_p)}{t_{ig}}$

Once both of the equations were reformatted into the Mowrer and Williamson, both equations (7) and (8) were run through a Runge-Kutta 4th order method that allowed for the dynamic solving of the flame height and change in pyrolysis length throughout each test. The first step in running the Runge-Kutta 4th order method was to arrange equation (7) into the Runge-Kutta form. The Runge-Kutta form for the large wall fires is shown below in equation (9). The Runge-Kutta form for the small wall fires is shown below in equation (10).

(9) $\frac{dX_p}{dt} = f(X_p) = \frac{C1(C2)^{-\frac{2}{3}}(C3)^{\frac{2}{3}}(X_p)^{\frac{2}{3}} - (X_p)}{C4}$

(10) $\frac{dX_p}{dt} = f(X_p) = \frac{C1(C2)^{-2}(C3)^2 - (X_p)}{C4}$

Where the values of C1, C2, C3 and C4 are

$C1 = Wall\ fire\ Constant, either\ 6\ or\ 130\ depending\ on\ which\ equation\ is\ being\ used$

$C2 = \rho_o c_{po} T_o \sqrt{g}, all\ values\ are\ for\ ambient\ air$

$C3 = Heat\ Release\ Rate\ per\ unit\ area$

$C4 = Time\ to\ Ignition$

The next step is to break down equation (9) into the four k values shown in equations (11), (12), (13) and (14).

(11) $k1X_p = \left[\frac{C1(C2)^{-\frac{2}{3}}(C3)^{\frac{2}{3}}(X_p)^{\frac{2}{3}} - (X_p)}{C4}\right] dt$

(12) $$k2X_p = \left[\frac{C1(C2)^{-\frac{2}{3}}(C3)^{\frac{2}{3}}\left(X_p+\frac{k1X_p}{2}\right)^{\frac{2}{3}}-\left(X_p+\frac{k1X_p}{2}\right)}{C4}\right]dt$$

(13) $$k3X_p = \left[\frac{C1(C2)^{-\frac{2}{3}}(C3)^{\frac{2}{3}}\left(X_p+\frac{k2X_p}{2}\right)^{\frac{2}{3}}-\left(X_p+\frac{k2X_p}{2}\right)}{C4}\right]dt$$

(14) $$k4X_p = \left[\frac{C1(C2)^{-\frac{2}{3}}(C3)^{\frac{2}{3}}(X_p+k3X_p)^{\frac{2}{3}}-(X_p+k3X_p)}{C4}\right]dt$$

The previous steps were repeated for the small fire equation (10), and the resulting k values are shown below in equations (15), (16), (17) and (18).

(15) $$k1X_p = \left[\frac{C1(C2)^{-2}(C3)^{2}-(X_p)}{C4}\right]dt$$

(16) $$k2X_p = \left[\frac{C1(C2)^{-2}(C3)^{2}-(X_p+\frac{k1X_p}{2})}{C4}\right]dt$$

(17) $$k3X_p = \left[\frac{C1(C2)^{-2}(C3)^{2}-(X_p+\frac{k2X_p}{2})}{C4}\right]dt$$

(18) $$k4X_p = \left[\frac{C1(C2)^{-2}(C3)^{2}-(X_p+k3X_p)}{C4}\right]dt$$

Once all k values have been defined, it is possible to solve for the value of the pyrolysis length at each time step using equation (19) below.

(19) $$X_p = \frac{1}{6}(k1X_p + 2(k2X_p) + 2(k3X_p) + k4X_p)$$

Now that all of the Runge-Kutta equations have been defined above, the equations can now be solved for. In order to be able to solve the Runge-Kutta equations, a set of initial parameters and a "switch" had to be set up to switch from the large fire equations to the small fire equations. The initial parameters that are needed for the solving of the Runge-Kutta equations is the time to ignition of the sample and the heat release rate per unit area. The time to ignition was determined to be the average time to ignition between all of the sample tests at a certain additive ratio. As for the heat release rate per unit area, the average value of the heat release rate per unit area was used because if the heat release rate per unit area at each time step

is used, the pyrolysis area is being counted twice at each time step, which would result in false values.

The last item that was addressed before the equations were solved for was to develop a "switch", where the solution would be changed from large wall fire equation to small fire equation. The "switch" was based off of the dimensionless heat release rate $\dot{Q}'^{*}_{xp}$. The equation for $\dot{Q}'^{*}_{xp}$ is shown below in equation (20).

(20) $$\dot{Q}'^{*}_{xp} = \frac{\dot{Q}''X_p}{\rho_o c_{po} T_o \sqrt{g} X_p^{\frac{3}{2}}}$$

From the pool fire model in Appendix POOL, the dimensionless heat release rate where pool fire changes from intermediate to small fires is 0.1. After looking at the data sets from both Delichatsios and King-Mon Tu, the lowest values of their dimensionless heat release rates is in fact close to 0.1. This was the point at which it was assumed that wall fires would change from larger fires to smaller fires, and thus changing from equation (9) to equation (10). With the heat release rate per unit area being assumed to be constant, the "switch" is based solely on the pyrolysis length. With the "switch" and the initial parameters are defined, equations (11) through (19) were solved for each of the different additive ratios at both the incident heat flux of 50 kW/m2 and 40 kW/m2.

Results

The below figures show the resulting dynamic solution of the flame height and the pyrolysis length. For the samples of Hetron 100:66 and Hetron 100:100, the average heat release rate per unit area is lower than the lowest allowable heat release rate per unit area, so both of those graphs make no physical sense.

Results from testing at Incident Heat Flux of 50 kW/m^2

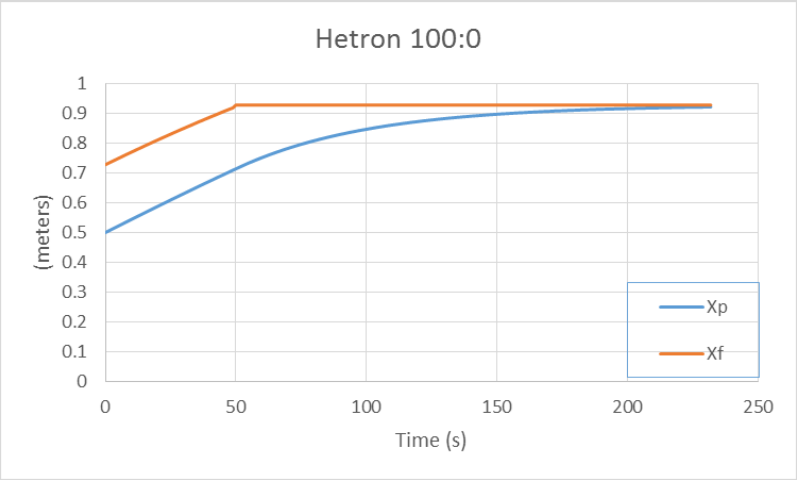

Figure 49: Hetron 100:0 at IHF of 50kW/m^2

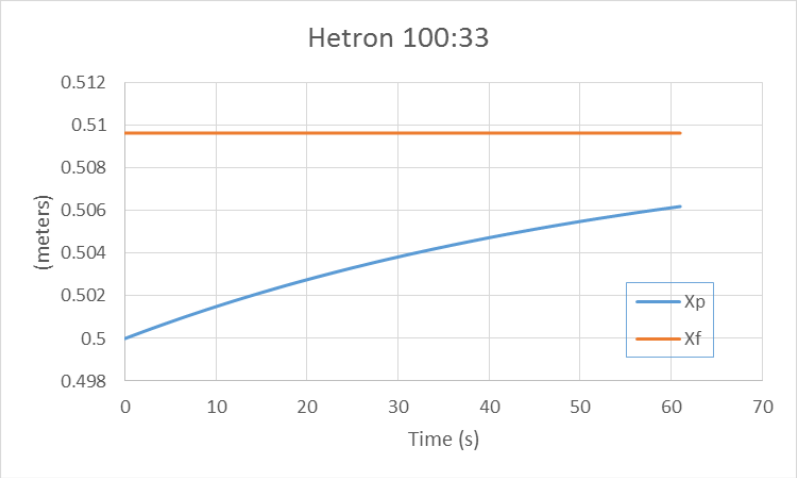

Figure 50: Hetron 100:33 at IHF of 50kW/m^2

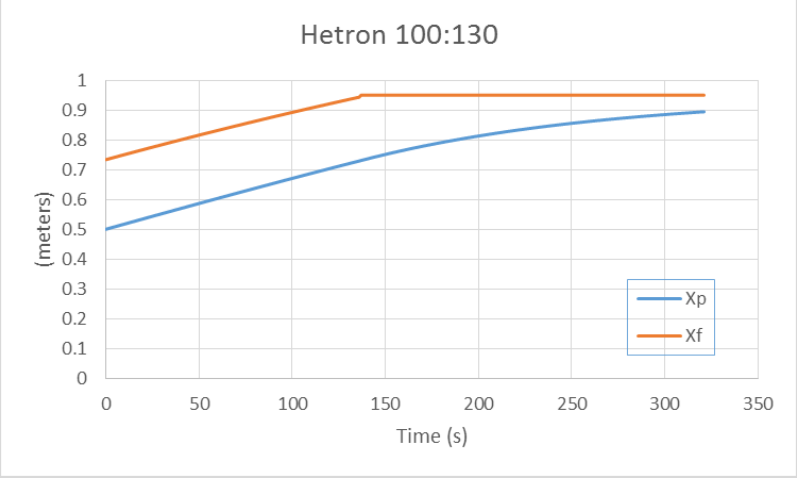

Figure 51: Hetron 100:130 at HF of 50 kW/m^2

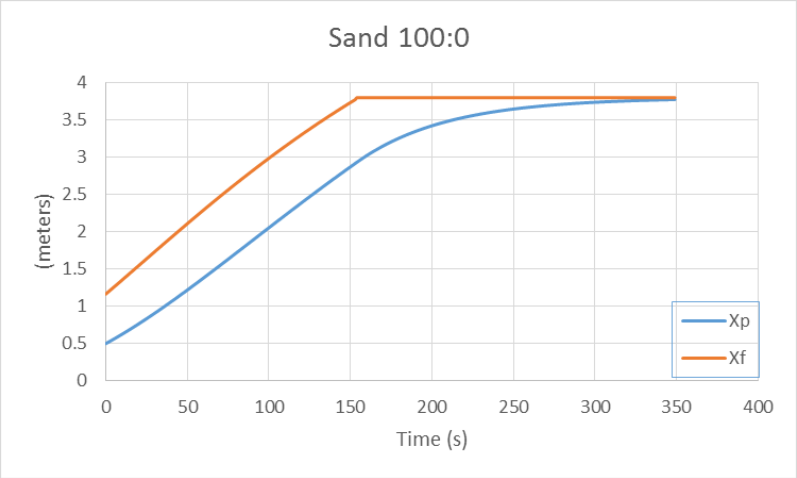

Figure 52: Fireblock 100:0 at IHF of 50 kW/m^2

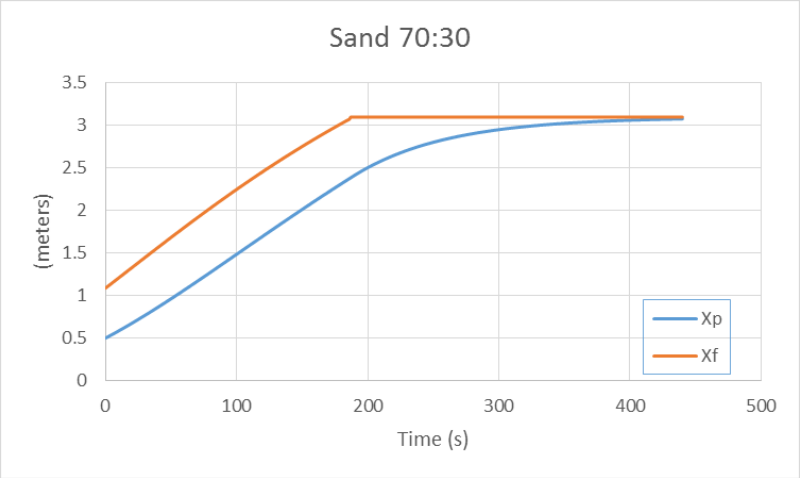

Figure 53: Fireblock 70:30 at IHF of 50 kW/m^2

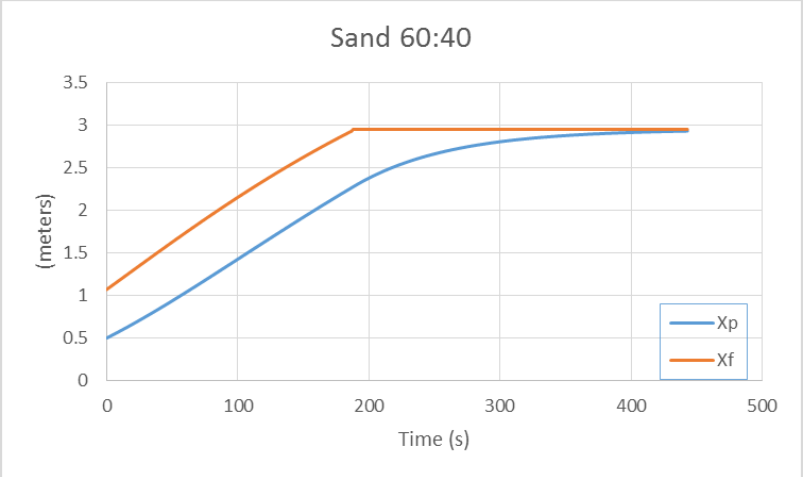

Figure 54: Fireblock 60:40 at IHF of 50 kW/m^2

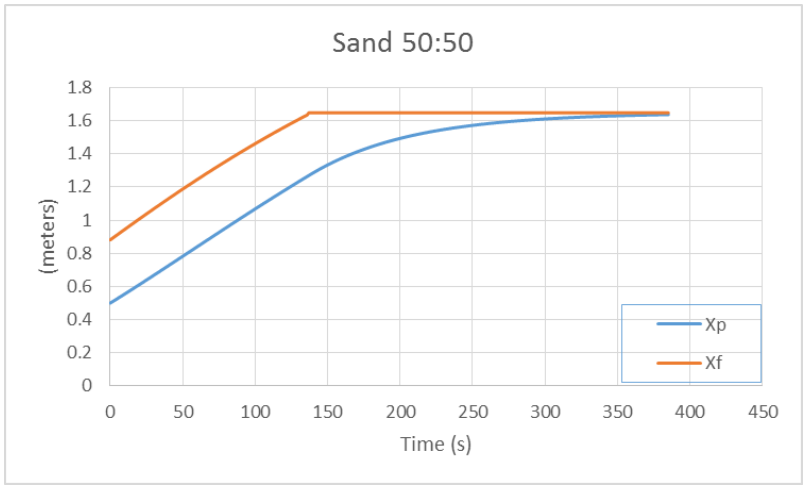

Figure 55: Fireblock 50:50 at IHF of 50 kW/m^2

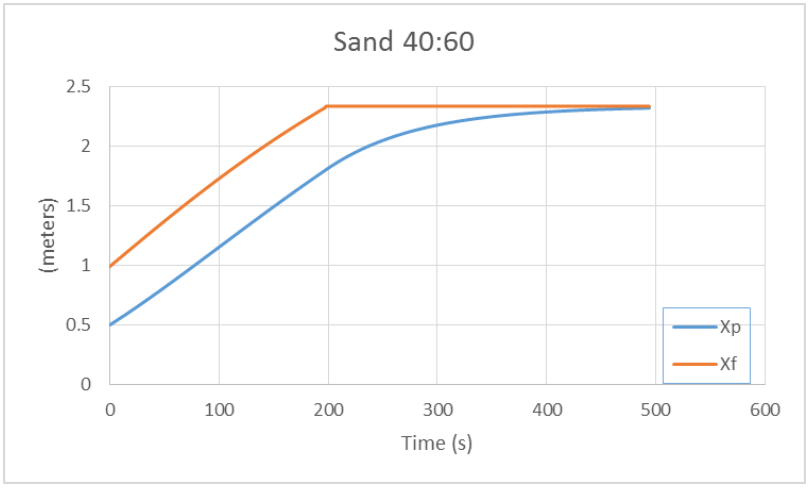

Figure 56: Fireblock 40:60 at IHF of 50 kW/m^2

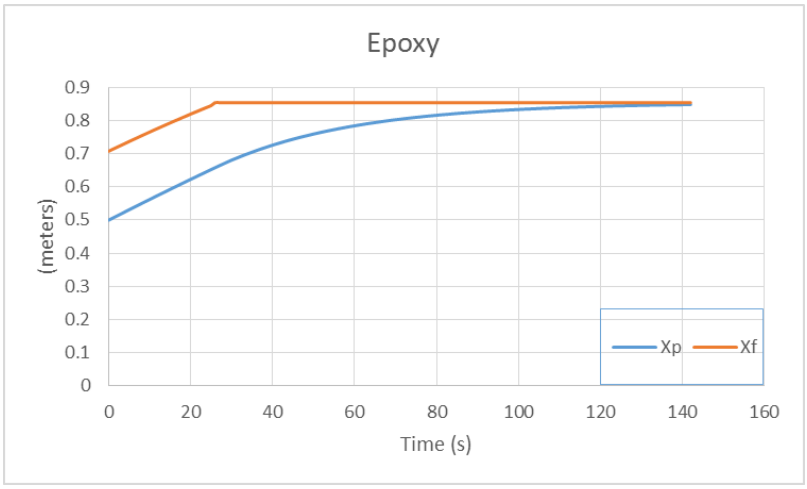

Figure 57: Epoxy at IHF of 50 kW/m^2

Results from Testing at Incident Heat Flux of 40 kW/m^2

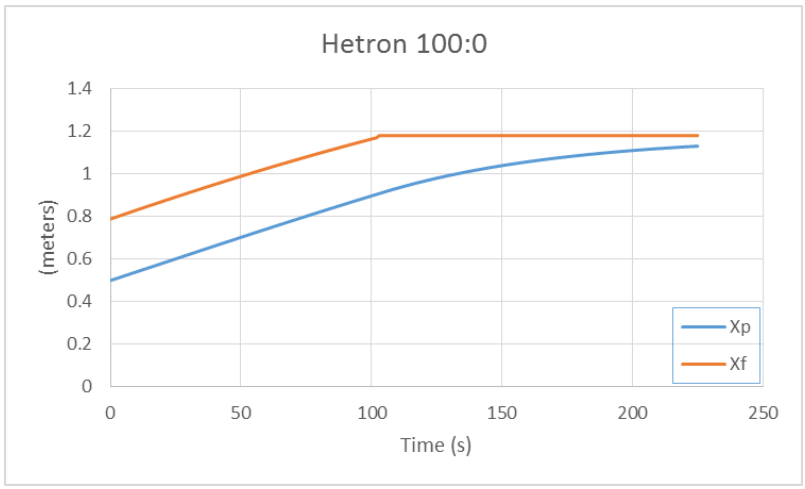

Figure 58: Hetron 100:0 at IHF of 40 kW/m^2

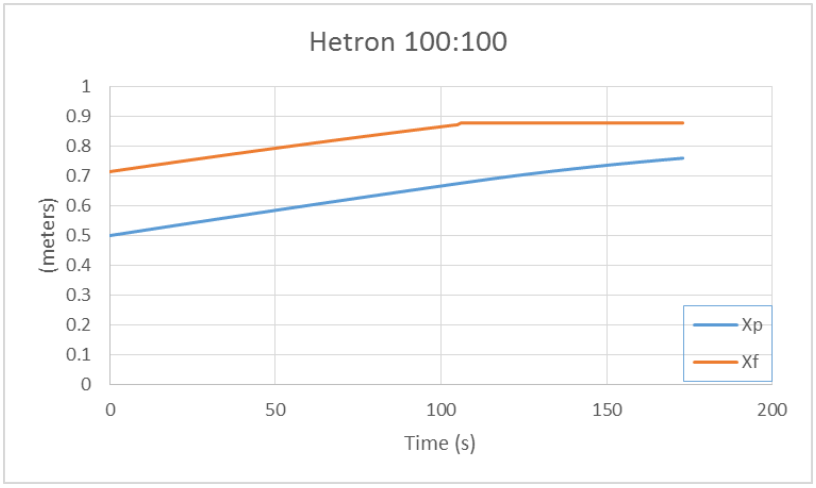

Figure 59: Hetron 100:100 at IHF of 40 kW/m^2

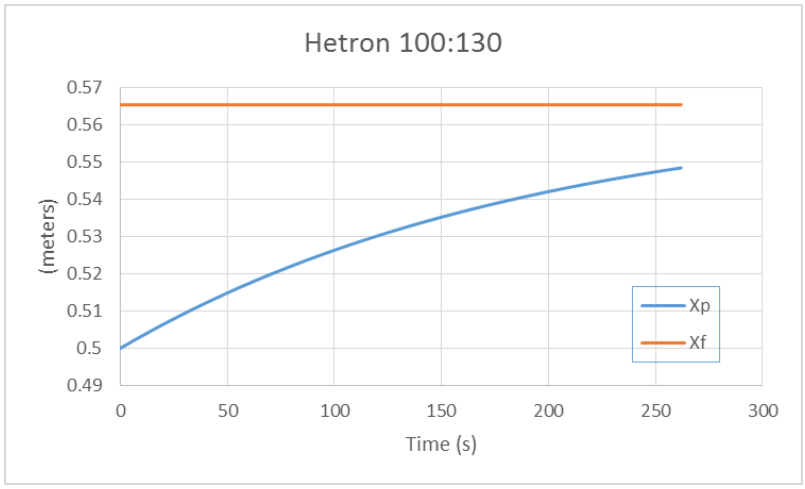

Figure 60: Hetron 100:130 at IHF of 40 kW/m^2

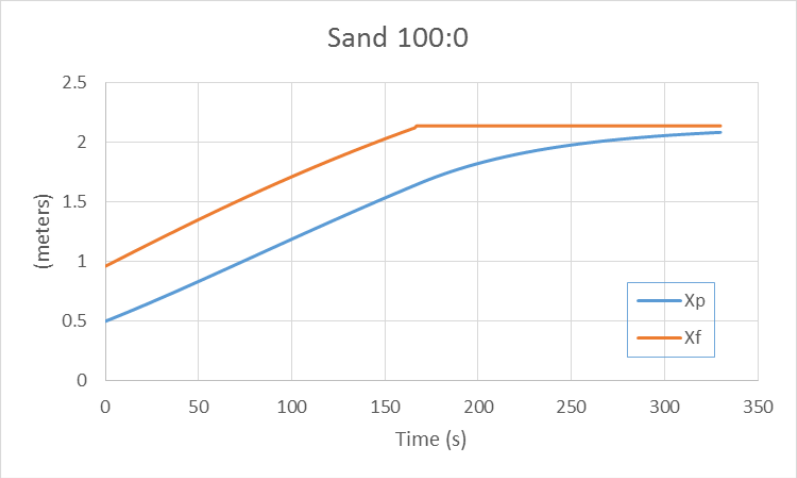

Figure 61: Fireblock 100:0 at IHF of 40 kW/m^2

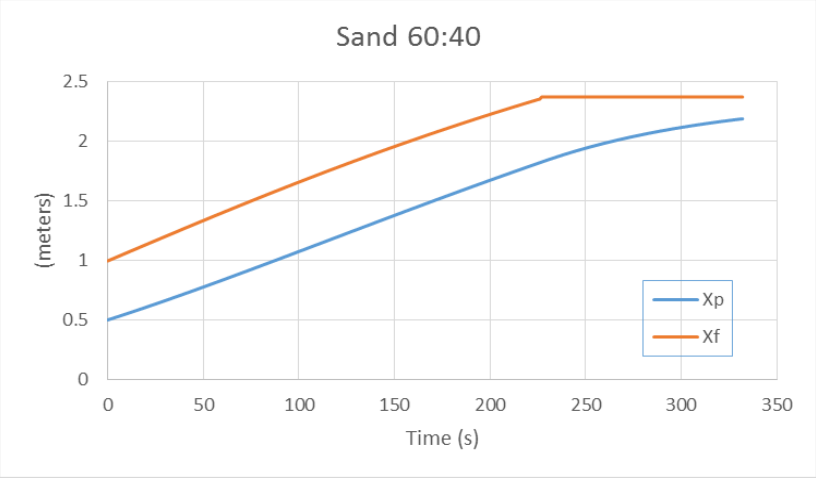

Figure 62: Fireblock 60:40 at IHF of 40 kW/m^2

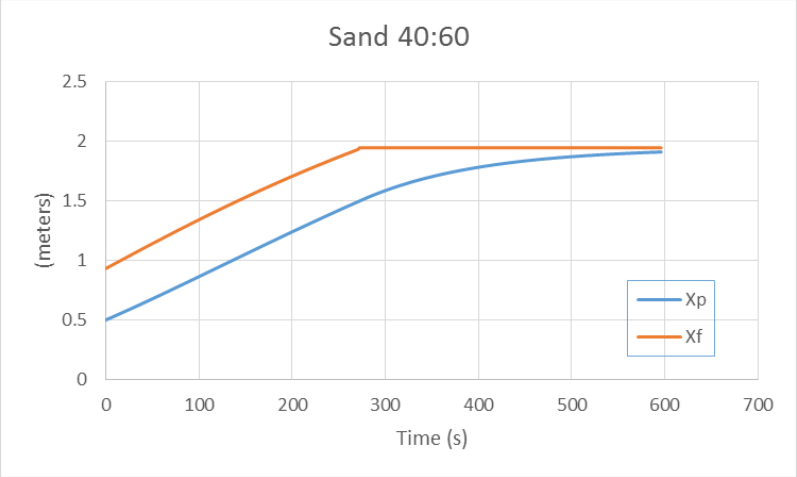

Figure 63: Fireblock 40:60 at IHF of 40 kW/m^2